

**"Shape Memory Polymers and Their Composites: Towards Field  
Applications via Production, Characterization and Modelling"**

by

Irina Tatiana Garces Arguello

A thesis submitted in partial fulfillment of the requirements for the degree of

Doctor of Philosophy

Department of Mechanical Engineering

University of Alberta

© Irina Tatiana Garces Arguello, 2021

# Abstract

Shape Memory Polymers (SMP) and Shape Memory Polymer Composites (SMPCs) can be used in field applications to replace mechanical actuators. They offer lightweight, ease of part manufacturing, reduced energy losses due to elimination of friction between components and a wide range of mobility. The present work focuses on production, characterization and modelling of SMPs and their composites with the ultimate goal to obtain controlled field applications. Firstly a detailed work on the properties of thermoplastic SMPs is put forward while looking at the capability to produce part manufacturing via Extrusion Based Additive Manufacturing (EBAM). To this end, a thorough characterization of different thermoplastic SMPs was done while looking at the effects of moisture on the material's mechanical performance and processability.

Modelling is crucial to understand the basic parameters needed for engineering design, such as the shape recovery ratio, shape recovery rate and shape recovery force. Hence, thorough literature review is provided on modelling techniques for thermoresponsive shape memory polymers. Although many great efforts have been made towards modelling, there is still a gap between modelling efforts and focus concerning engineering design. Specifically, it is necessary to provide models for the common types of loading in engineering applications. Many of the future applications for SMPs lie in soft robotics, unmanned aerial vehicles, self-assembly or self-folding structures, where bending is the most common type of load. The method of activation of the thermal shape memory effect must also be considered within engineering models. Furthermore, easy application and interpretation of models are required for first stage engineering design. Consequently, a model for SMPs under

bending applications, that can be later adapted to field heating conditions, is proposed to mitigate the mentioned knowledge gap. The proposed model is a transient viscoelastic model that can predict recovery properties for flexural applications. A methodology for parameter extraction via DMA has also been presented in this thesis to explain the change of material parameters with respect to time. This model can be easily adapted to different field activation methods of the SMPs.

Additive manufacturing of shape memory polymer composites was studied to acquire SMPCs, that can be easily formed into desired shapes and activated in out-of-laboratory conditions. As such, hybrid material SMPC structures manufactured by EBAM for field applications are proposed in this thesis. Fabrication, actuation, and characterization of the composite were done in this thesis. The proposed SMPC structure was easily manufactured and possessed great potential to be controlled and showed sensing capabilities in strain and temperature. This work has opened doors for SMPs to be used as self-sensing smart actuators in real life engineering applications.

# Preface

Some of the research reported in this thesis was conducted in collaboration with others.

Chapter 1 of this thesis shows the introduction, motivation, background and objectives proposed by I. T. Garces under the supervision of Dr. Cagri Ayranci.

Chapter 2 of this thesis is soon to be submitted to a journal for journal paper publication. The author contributed to literature collection, review analysis and manuscript preparation. Dr. Tian Tang provided modelling related insight and guidance to this work and provided input in editing the manuscript. Dr. Ayranci provided guidance and supervision to this part of the work in concept and experimental aspects and also provided input in editing the manuscript.

Chapter 3 of this thesis is accepted for publication in the "Rapid Prototyping Journal" as "I.T.Garces and C.Ayranci. Advances in Additive Manufacturing of Shape Memory Polymer Composite. The author provided with literature collection, analysis and manuscript preparation. Dr. Cagri Ayranci contributed to supervision and editing.

Chapter 4 of this thesis has been published as "I. T. Garces, S. Aslanzadeh, Y. Boluk, and C. Ayranci, "Effect of Moisture on Shape Memory Polyurethane Polymers for Extrusion-Based Additive Manufacturing," Materials 2, vol. 12, no. 2, p. 244, Jan. 2019". The author contributed to sample manufacturing, sample testing, data analysis, model application and manuscript preparation. Dr. Aslanzadeh participated in partial sample manufacturing and partial material characterization. Dr. Boluk provided insights into polymer science and manuscript editing. Dr. Ayranci was the supervisory author and was involved in the manuscript conceptualization and editing.

Chapter 5 of this thesis is soon to be submitted to a journal for journal publication. The author contributed to model transient adaptation, development of the model for constrained and free recovery as well as obtaining a procedure for material extraction. Model experimentation and experimental validation. Data collection, analysis and manuscript preparation. Xiaong Ma contributed with initial model development for bending. Dr. Tian Tang provided insights into polymer science, modelling expertise, mechanical science and editing. Dr. Cagri Ayranci provided conceptualization,

experimental knowledge, and editing.

Chapter 6 of this thesis was published as "I. T. Garces and C. Ayranci, A view into additive manufactured thermally-active reinforced smart composite structures, *Manufacturing Letters*, vol. 16, pp. 1–5, Apr. 2018." The author contributed with experimentation, sample manufacturing, testing and manuscript preparation. Dr. Ayranci contributed to supervision and editing.

Chapter 7 of this thesis was published as "I. T. Garces and C. Ayranci, Active control of 4D prints: Towards 4D printed reliable actuators and sensors, *Sensors & Actuators: A. Physical*, vol. 301, p. 111717, Jan. 2020." The author contributed with idea conceptualization, sample preparation, characterization, equipment manufacturing, testing and experimentation and manuscript development. Dr. Ayranci provided with supervision and editing.

# Acknowledgements

I would like to gratefully acknowledge the University of Alberta and the Mechanical Engineering Department.

I am profoundly grateful to my supervisor Dr. Cagri Ayranci for his endless support and for helping me grow into the scientist I am today. I would also like to thank Dr. Tian Tang, from whom I have learnt the value of hard work and have received invaluable guidance. I want to thank Dr. David Nobes for his advice and support during my academic career and for providing valuable insight during our committee meetings.

I want to acknowledge the mechanical engineering shop and the technicians who have helped me, with a special mention to Andrew Campbell, Marc Maccagno, Daniel Mooney, Rick Conrad and Ereddad Kharraz from the agriculture department. To my friends and lab mates, Eyup Demir, Milad Rezvani, Yu Chen, Vinay Patel, and Rijesh Augustine, for providing advice and assistance whenever I needed it.

I would also like to thank my parents, Francisco and Elena, for their loving support and for giving me invaluable educational opportunities. To my siblings, Francisco, Elena and Tannia, for their warm encouragement throughout grad school. Finally, to my husband, Nicolas, for being a constant source of love and support, for encouraging me to dream big and for showing me that I can always count on him.

# Contents

<b>Preface</b>	<b>iv</b>
<b>Acknowledgements</b>	<b>vi</b>
<b>List of Tables</b>	<b>xi</b>
<b>List of Figures</b>	<b>xii</b>
<b>1 Introduction</b>	<b>1</b>
1.1 Background . . . . .	4
1.2 Objectives of the Thesis . . . . .	5
1.3 Overview of Content . . . . .	5
1.4 References . . . . .	7
<b>2 Literature Review on Modelling of Thermoresponsive Shape Memory Polymers</b>	<b>10</b>
2.1 Introduction . . . . .	11
2.2 Thermally Activated Shape Memory Polymers . . . . .	12
2.2.1 Thermal Shape Memory Effect . . . . .	17
2.2.2 Characterizing the Irrecoverable Strain . . . . .	18
2.3 Modelling Approaches . . . . .	21
2.3.1 Models based on Elastic and Viscous Elements . . . . .	22
2.3.2 Models based on Phase Change . . . . .	28
2.3.3 Hybrid Models . . . . .	33
2.4 Recent Modelling Techniques and Developments . . . . .	35
2.5 Discussion Points . . . . .	37
2.6 Conclusions . . . . .	39
2.7 References . . . . .	39

<b>3</b>	<b>A Literature review on Advances in Additive Manufacturing of Shape Memory Polymer Composites</b>	<b>51</b>
3.1	Introduction . . . . .	53
3.1.1	3D printing of Shape Memory Polymers vs. 4D printing . . . . .	55
3.1.2	Additive Manufacturing techniques used for SMP . . . . .	56
3.1.3	Overview of SMPC . . . . .	60
3.1.4	Conductive Carbon based SMPC . . . . .	63
3.2	Additive Manufacturing of SMPC . . . . .	64
3.2.1	Particle dispersed SMPC . . . . .	64
3.2.2	Long fibre reinforced SMPC . . . . .	72
3.3	Multi-Material SMPC . . . . .	75
3.4	Opportunities Ahead . . . . .	78
3.5	Conclusions . . . . .	81
3.6	References . . . . .	82
<b>4</b>	<b>Effect of Moisture on Shape Memory Polyurethane Polymers for Extrusion-Based Additive Manufacturing</b>	<b>99</b>
4.1	Introduction . . . . .	100
4.2	Raw Materials . . . . .	102
4.3	Methodology . . . . .	103
4.3.1	Ribbon Preparation, Compounding and Water Absorption . . . . .	103
4.3.2	Filament Preparation for EBAM . . . . .	104
4.3.3	EBAM Manufactured Samples . . . . .	104
4.4	Experimental Methodology . . . . .	104
4.4.1	Moisture Manufacturing Effects: Moisture Trapping . . . . .	104
4.4.2	Moisture on Manufactured Parts: Effect of Moisture by Plasticization . . . . .	105
4.5	Results and Discussion . . . . .	107
4.5.1	Moisture Manufacturing Effects: Moisture Trapping . . . . .	107
4.5.2	Moisture on Manufactured Parts: Effect of Moisture by Plasticization . . . . .	108
4.6	Conclusions . . . . .	121
4.7	References . . . . .	122
<b>5</b>	<b>A Viscoelastic Model for Shape Memory Polymers Under Bending</b>	<b>127</b>
5.1	Introduction . . . . .	128
5.2	Model . . . . .	130
5.2.1	Viscoelastic Model . . . . .	130
5.2.2	Bending Model . . . . .	133
5.2.3	Numerical Procedure . . . . .	135

5.3	Material Parameters Estimation . . . . .	139
5.4	Materials and Methods . . . . .	141
5.4.1	Materials . . . . .	141
5.4.2	Dynamic Mechanical Analysis (DMA) . . . . .	142
5.4.3	Flexural Testing and Shape Setting . . . . .	143
5.4.4	Constrained Recovery . . . . .	143
5.4.5	Free End Recovery . . . . .	144
5.5	Experimental Validation Results . . . . .	146
5.5.1	Material Parameters Estimation . . . . .	146
5.5.2	Software Logic Validation and Convergence . . . . .	149
5.5.3	Shape Setting . . . . .	150
5.5.4	Constrained Recovery . . . . .	153
5.5.5	Free End Recovery . . . . .	157
5.6	Discussion and Recommendations . . . . .	161
5.7	Future Case Study . . . . .	163
5.8	Conclusions . . . . .	164
5.9	References . . . . .	164
<b>6</b>	<b>A view into additive manufactured thermally actived-reinforced smart composite structures: Manufacturing viability</b>	<b>168</b>
6.1	Introduction . . . . .	169
6.2	Experimental Methods . . . . .	170
6.3	Results and Discussion . . . . .	172
6.4	Conclusions and Recommendations . . . . .	174
6.5	References . . . . .	175
<b>7</b>	<b>Active control of 4D prints: Towards 4D Printed reliable actuators and sensors</b>	<b>178</b>
7.1	Introduction . . . . .	179
7.2	Materials and Methods . . . . .	181
7.2.1	Materials . . . . .	181
7.2.2	Specimen Manufacturing . . . . .	182
7.2.3	Equipment . . . . .	184
7.2.4	Experimental Set-up and Methodology . . . . .	185
7.3	Results and Discussion . . . . .	190
7.3.1	Material Characterization . . . . .	190
7.3.2	Shape Memory Effect . . . . .	195
7.4	Conclusions and Recommendations . . . . .	198
7.5	References . . . . .	199

<b>8</b>	<b>Conclusions</b>	<b>202</b>
8.1	Recommendations for Future Work . . . . .	204
	<b>References</b>	<b>206</b>
	<b>Appendices</b>	<b>240</b>
A.1	Permissions Related to Chapter 2 . . . . .	241
A.1.1	Figure 5 . . . . .	242
	Appendices . . . . .	241
A.2	Permissions Related to Chapter 3 . . . . .	244
A.2.1	Figure 4 . . . . .	245
A.2.2	Figure 5 . . . . .	247
A.2.3	Figure 7 . . . . .	249
A.2.4	Figure 9 . . . . .	250
A.2.5	Figure 10 . . . . .	252
A.2.6	Figure 11 . . . . .	254
A.2.7	Figure 12 . . . . .	256
B.3	Supplementary Information Related to Chapter 4 . . . . .	258
B.4	Supplementary Information Related to Chapter 7 . . . . .	260
C.5	MATLAB CODE Related to Chapter 5 . . . . .	262

# List of Tables

2.1	Summary of irrecoverable strain functions . . . . .	20
2.2	Summary of frozen volume fraction function used, this has been adapted and completed from [111]. . . . .	32
3.1	Common fillers used for manufacturing SMPs . . . . .	62
4.1	Printing parameters used when 3D printing with each respective material (MM4520 and MM7520). . . . .	104
4.2	Bonding frequencies for dry materials. . . . .	111
4.3	Estimated coefficients for MM4520 elastic modulus with respect to immersion time in water. . . . .	118
5.1	Steps and initial conditions, where $\tau$ is the time at the end of the programming stage	137
5.2	Material Parameter fits . . . . .	147
5.3	Summary of the model validation with experiments for the shape setting stage . . .	152
7.1	Used Printing Parameters . . . . .	182
7.2	Dimensions for different sample configurations. Dimensions are in mm. . . . .	184
1	Estimated Parameters . . . . .	261

# List of Figures

1.1	Areas of research to be developed for the advancement of shape memory polymers for field applications . . . . .	2
2.1	Schematic of a self-deployable Kayak that can take the shape of a sleeping bag for transportation . . . . .	13
2.2	Description of the SME showing the different stages: (a) permanent shape, (b) setting of temporary shape, (c) temporary Shape (d) recovery, (e) recovered shape. Reference of structures for Class I [76] , Class II [55], Class III [118, 62], Class IV [34] . . . . .	16
2.3	Spring-Dashpot model representation of an SMP configuration before shape programming and later recovery . . . . .	23
2.4	(a) SLV model with friction element to describe the SME [89], and (b) is the schematic of a model capturing hard and soft segment behaviour from [53] . . . . .	25
2.5	Representation of a 1D version of Nguyen <i>et al.</i> 's [67] model. Where descriptions for equilibrium and non-equilibrium are represented by <i>eq</i> and <i>neq</i> . The figure shows, Kelvin and Maxwell elements coupled until the Nth element. Reprinted with permission of [67] . . . . .	26
2.6	Representation of a 1D version of Srivastava <i>et al.</i> 's [84] model. The figure shows the micromechanisms implemented in a spring-dashpot representation . . . . .	28
2.7	Representation of an SMP configuration before shape programming and later recovery	30
2.8	Model calculation flow chart. Figure adapted from [50]. . . . .	34
2.9	Spring-dashpot model representation of an SMP at the glassy initial phase. Figure adapted from [73] . . . . .	35
3.1	Schematic of a 3D printed structure. The difference in 3D vs 4D printing is shown. .	57
3.2	AM techniques for SMPs. Figure modified and adapted from [97] for the relevance of this chapter. (Open-source figure) . . . . .	61
3.3	Common AM techniques for different types of reinforcements . . . . .	64

3.4	Figure reprinted with the permission from [169] (a section of this figure has been used for the relevance of this chapter). The recovery of a 3D printed photo-responsive structure can be observed in the image. . . . .	66
3.5	3D printed structures printed with PLA/CNT filament in (a) a ply-angle oriented configuration and in a (b) braided configuration. This image was obtained and published with the permission of [92] . . . . .	67
3.6	a) is a photo of the programmed and b) the recovered 3D printed thermoset SMPC stent. (Open source article and images) [134] . . . . .	68
3.7	DWA manufacturing used for PLA-ferromagnetic SMPC and stents printed. Image reprinted with the permission of [162]. . . . .	69
3.8	DLP manufacturing of a SMPC reinforced with nanosilica particles. Images reprinted with permission of [23] . . . . .	71
3.9	Ink deposition of CNT. Image reprinted with the permission of [160] . . . . .	72
3.10	a) FDM Continuous fibre placement and (b) nozzle. (c) The 3D printing and shape memory storage of the process. (d) and (e) are examples of accomplished shape-shifting with the technology. All images were reprinted and with the permission of [158]. A section of two images from the publication have been joined in this figure for the relevance and purpose of this chapter. . . . .	74
3.11	Figure (a) is a photograph of a laminate with a high curvature after activation and b) is a laminate with small curvature. Images reprinted with the permission of [47] .	75
3.12	(a) shows the activation process of PACs, b) a self-folding application and the c) manufacturing of PACs. This image is reprinted with the permission from [40]. (In this image sections of two figures have been used for the purpose and relevance of this chapter) . . . . .	77
3.13	CAD model demonstrating the AM process in (a), followed by the activation of the shape change. (Open source article and image)[10] . . . . .	78
3.14	4D SMPC design framework. Image modified from [53] . . . . .	81
4.1	Examples of 3D-printed applications of Shape Memory Polyurethane (SMPU) by EBAM. (a) A photograph of an in-house 3D-printed generic stent and (b) 3D-printed kayak prototype based on reference [11]. . . . .	101
4.2	Schematic of the chemical formula of SMP MM series, provided by the manufacturer (www2.smp techno.com) . . . . .	103
4.3	Schematic showing the programming and shape recovery procedure of a Shape Memory Polymer ribbon, where (a) shows the original sample (b) and (c) the sample while and after shape programming, respectively and (d) the recovered sample. . . . .	107

4.4	Photographs showing the effects of moisture in filaments on EBAM manufactured parts. Figure (a1), (b1), (c1) and (d1) are images of MM4520 printed parts manufactured with filaments immersed in water for 0, 10 min, 5 h and 24 h. Figures (a1), (b2), (c2) and (d2) show zoomed-in views of the printed surfaces. Similarly (e1), (f1) and (g1) are images of MM7520 printed parts manufactured with filaments immersed in water for 0, 10 min and 24 h, the close-up versions are shown in (e2), (f2) and (g2).	109
4.5	TGA and DTGA curves of (a) and (c) MM4520; and (b) and (d) MM7520 after different immersion times in water . . . . .	110
4.6	(a) Ratio of water content to MM4520 and MM7520 after different immersion times in water (b) water Saturation with respect to Shape Memory Polyurethane $T_g$ series.	111
4.7	(a) Degree of phase separation with respect to different SMPU series (MM3520, MM4520 and MM7520) and (b) change in the degree of phase separation with respect to moisture absorption for MM4520 and MM7520. . . . .	113
4.8	Values of bond stretching for (a) N–H bond, (b) C=O and (c) C–O bonds. . . . .	114
4.9	Graph showing a change in $T_g$ with respect to immersion time in water for MM4520 and MM7520. . . . .	115
4.10	Graphs showing the mechanical behavior of both materials. (a) Describes the evolution in mechanical behavior while (b) shows the drop in elastic modulus with respect to immersion time in water. . . . .	116
4.11	Graph of elastic modulus ( $E_y$ )for MM4520 for (a) fitted model and (b) residuals. . .	117
4.12	Representation curves for strain recovery of (a) MM4520 at activation temperature $T = 50^\circ C$ and (b) MM7520 after different immersion times in water at activation temperature $T = 80^\circ C$ . . . . .	119
4.13	(a) Box plot showing recovery of MM4520 and MM7520 dried materials and (b) maximum recovery of MM4520 and MM7520 after water immersion. . . . .	120
4.14	(a) Recovery rate for MM4520 and MM7520 with respect to immersion times in water (b) Recovery time for MM4520 and MM7520 with respect to immersion times in water.	120
5.1	Graphic representation of the viscoelastic model used by Tobushi et al. [28] . . . . .	130
5.2	(a) Exaggerated schematic of a three point bending test, (b) Discretization of half the beam. The figure shows the neutral axis "N" in blue. . . . .	134
5.3	Flow Chart that describes the logic of the model . . . . .	138
5.4	Pictures of an injected sample before sanding . . . . .	142
5.5	Picture of a double cantilever mode DMA set-up . . . . .	142
5.6	Picture of a three point bending test of an SMP sample. . . . .	143
5.7	Programming and constrained recovery cycle, where (a) is the holding of the displacement and (b) is the response to temperature changes. . . . .	144

5.8	Picture of a free end recovery test. . . . .	145
5.9	(a)photographs of the initial, beginning of recovery and recovered state of a the beam (b)Trajectories detected at every single point in the beam . . . . .	145
5.10	Results from DMA using various amplitudes . . . . .	146
5.11	Material Parameters . . . . .	148
5.12	Comparisson between analytical solution for a strain relaxation test and the numerical model . . . . .	150
5.13	Convergence for shape setting . . . . .	150
5.14	Results of the programming stage where (a) are the result of the model prediction and experimental validation of the displacement with respect to time. (b) Effect of changing $\lambda(T_g)$ . (c) Effect of changing $\mu(T_g)$ . . . . .	151
5.15	fit of $\varepsilon_L(T)$ . . . . .	152
5.16	(a)Experimental esults of sample curves of the shape recovery force at different heating rates and (b) are model runs at different heating rates . . . . .	153
5.17	(a)Comparison between model and experimental data, the figure shows the regimes in which the model enters (b) Shape Recovery Force results and comparisson to experimental data at different heating rates . . . . .	154
5.18	(a) Changes in the magnitude quantity by increasing the values of $\lambda_0$ (c) Effect of material parameters using WLF equations . . . . .	155
5.19	(a)Recovery of the deflection with different heating rates (b) Model recovery with different heating rates . . . . .	157
5.20	(a)Recovery ratio with different heating rates (b) Model comparisson and experimental comparisson with different heating rates . . . . .	159
5.21	Changes in the recovery ratio with respect to $\lambda_0$ and (b) Comparisson of recovery ratio using WLF . . . . .	160
5.22	Render image of a robotic spider with reconfigurable SMPC legs . . . . .	163
6.1	Representation of Gcode manufacturing of samples. . . . .	171
6.2	a) Sample with an entire layer in between representing 30 <i>wt%</i> content of Graphene/-PLA b) Sample showing the surface of printed Graphene/PLA layer with 20 <i>wt.%</i> embedded Graphene/PLA and c) Sample showing the embedded printed Graphene/-PLA layer of 20 <i>wt.%</i> inside the SMP. . . . .	172
6.3	Recovering sequence of 3D printed SMPC laminate of size 15×50 mm. . . . .	173
6.4	a) Lamina showing a detail of the embedded Graphene-PLA lines showing an alteration of volume fraction by changing ratio between distances a and b. b) Laminate showing exploded delaminated view compounded of different angle oriented laminae. . . . .	174

6.5	a) Printed prototype of a kayak made of SMP deploying, b) concept of a 3D printed Kayak with graphene embedded polymer on a SMP matrix. CAD adapted from [6].	174
7.1	(a) 3D illustration of the proposed composite. The illustration shows a section view A-A at the bottom. (b) Schematic of the proposed unit cell to print.(c) Photograph of a manufactured sample (d) Picture of the 3D printing process of a sample[6]	183
7.2	Schematics of (a) Sample design with base dimensions and (b) sample configurations	184
7.3	Schematic modified from [6], where (a) is the design of the in-house built control unit where points A denote power input, SMPC denotes the conected sample at point B (WB), C is the signal amplifier, and D are the thermocouples. (b) Is the picture of the built control unit and (C) is the schematic of the control algorithm	187
7.4	Experimental setup for heating characterization	188
7.5	The programming process at the left (steps 1-4) and the two types of recovery at the right	188
7.6	(a) 3D printed SMPC sample programmed in the temporary shape and being activated to record its recovery force (b)3D printed SMPC sample programmed in the temporary shape and being activated, the software recognition of reference points to measure recovery angle and percentage its shown below	189
7.7	TGA of GPLA showing weight percentage drops	190
7.8	MDSC curves of SMP and GPLA for $T_g$ characterization	191
7.9	Plot of obtained volume resistance values for configuration 1 and 2	192
7.10	Data representation is shown for samples (a) C1.T1-S1, (b) C1.T2-S2 and (c) C1.T3-S1. On the first row, representation curves of sample transient heating with respect to power input are shown. At the bottom row, curves of resistance changes with respect to temperature readings can be seen.	193
7.11	(a) Heat distribution presented by samples C1.T1,C1.T2,C1.T3 when they reach the activation temperature $T_g$ ( $75^\circ C$ ) and (b) bar graph showing time to reach activation for all collected samples	194
7.12	(a) Shape memory programming cycle by increased ambient temperature (b) Sample activation C1.T1 and C1.T2 via resistive heating with 4 Watts	196
7.13	(a) Picture of sample C1.T1 recovering while 4 Watts are applied to the sample. (b) Graph of recovery angle percentage and resistance readings after the application of 4 Watts	197
1	Free Permission for Academic Purposes	249
2	Examples of DSC measurement for MM4520 and MM7520	258
3	FTIR spectrums for (a) MM4520 and (b) MM7520 with zoomed in at different bonds	259

4	(a) In-house built control unit with resistances for calibration and (b) Calibration fit to resistance measurements with graph of residuals at the bottom . . . . .	260
---	---	-----

# Chapter 1

## Introduction

Shape Memory Polymers (SMPs) offer advantages over mechanical actuators due to their lightweight, low cost, ease of part manufacturing, and optimization of energy due to the elimination of friction between components and can offer limitless and complex ways of motion. Thermosensitive SMPs are the most commonly studied materials since their temporary shapes can be stored and released via the application of heat. This activation method is convenient and has the potential to be fully controlled. Although SMPs show vast potential, there are still limitations that have held back their broader engineering applications. These limitations include uncharacterized behaviour to ambient conditions, difficulties in part manufacturing, motion predictability, and challenges when activating these in out-of-laboratory conditions. Overcoming the mentioned limitations can expand the applications of SMPs. Promising applications have been found in the biomedical area, i.e. active splints, sutures, cast devices, tissue engineering [16, 22, 10] and self deployable stents [3]. Other engineering applications include wings for aerial vehicle gliders, motion triggering switches, self-appearing QR codes, actuators for soft robotics, applications in the space industry such as antenna deployment, and in the consumer industry for toy development, sports equipment and furniture storage, among others [23, 9, 1, 20].

A few areas of study must be looked at in-depth to achieve all of the applications mentioned above. These areas are summarized in Figure 1.1 and include the manufacturing viability, understanding the effects of ambient conditions, modelling and predictability of the material's behaviour and the field activation. To manufacture with these materials, we must look at how repeatable the manufacturing process is; there must be ease for part manufacturing while keeping the manufacturing process cost-effective. For these materials to be used in field applications, we must understand the moisture and temperature effects on these materials while also predicting how they will behave

under such conditions. Moreover, understanding how the material will behave during programming and recovery is also crucial for mechanical devices and the engineering design of actuators. Models that describe the most common type of loading while predicting critical parameters for design, such as how fast, how much the material will recover and what force it will give off when recovering, are essential for designing with SMPs. Furthermore, tailorable models for different loading conditions and that are easily applicable to engineers and designers are essential to design with SMPs. Field activation of SMPs is perhaps one of the most critical aspects of applying these materials to real engineering applications. An activation method that is repeatable when manufacturing, that can be controlled and can provide feedback information, that is tailorable for heat application, and that does not impede the shape recovery characteristics is desired and optimal for the use of SMPs

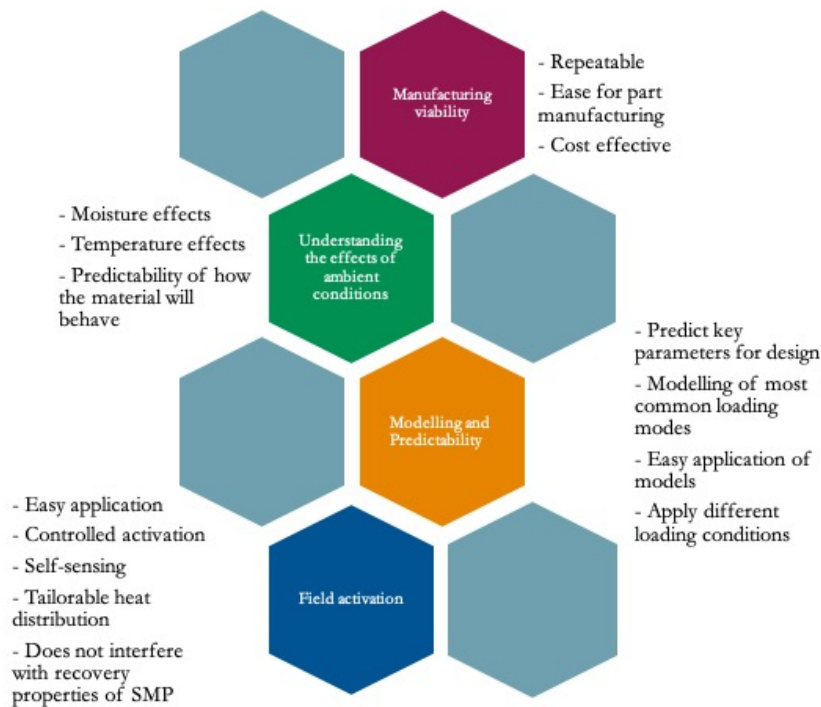


Figure 1.1: Areas of research to be developed for the advancement of shape memory polymers for field applications

With the mentioned areas in mind, this research's long-term goal is to prove the viability of shape memory polymers for engineering design and product development. The effect of environmental conditions on the materials' properties, such as on processability and field behaviour, needs to be performed as the first stepping stone into this goal while considering part manufacturing feasibility. Furthermore, modelling of SMPs is required for a first stage design of the developed

products. Field activation of these materials must be considered for any engineering applications with SMPs. Finally, to fully exploit these materials' potential, self-sensing and self-actuation need to be implemented and characterized within the material, which can be accomplished using composite materials (Shape Memory Polymer Composites (SMPCs)). This thesis contributes to the advancements made in the area of shape memory polymers for field applications. The thesis begins by providing a thorough literature review of the modelling of thermosensitive shape memory polymers. A knowledge gap on practical models for the first stage design was identified through this review (Chapter 2).

The recent advances in additive manufacturing have opened a gateway to multi-material capabilities. This area is particularly exciting since to create structures and composite materials with multi-functionalities such as self-actuation and sensing. A review of the advancements in additive manufacturing of shape memory polymer composites was done to investigate methods in which thermally active shape memory polymer composites could be created via additive manufacturing to activate these via joule heating. Several promising manufacturing techniques and areas of study were identified, among those the opportunity to develop smart self-actuating self-sensing shape memory polymer composites (Chapter 3).

Thermoplastic SMPs of the polyurethane type (SMPU) have been widely studied in recent years and have shown to possess a wide range of "activation temperatures." Therefore, two thermoplastic SMPU materials were characterized thoroughly to understand the effects of field conditions, such as moisture, on the materials' performance and processability for part manufacturing. A viable SMP of the SMPU class was identified in this study for field applications (Chapter 4).

Most SMP applications are subjected to bending (flexural) loads, specifically those in soft-robotics and self-folding structures. Hence, a transient model for shape memory polymers under bending for engineering design was proposed to fill the identified knowledge gap. The aforementioned SMPU material was used to validate this model (Chapter 5).

Field activation of shape memory polymers was recognized to be easily applied via joule heating while using a simple manufacturing technique that can be accommodated to manufacture complex parts. Activation of the Shape Memory Effect (SME) is proposed by embedding a conductive thermoplastic able to provide feedback data. The activation via additive manufacturing of shape memory polymer composites was published in this area, this showed the feasibility of achieving the necessary high temperature for activation (Chapter 6). Building on this work, a detailed study was done on the SME, including the material and thermal characterization and the proposed structure's self-sensing properties (Chapter 7). This thesis is one of the first stepping stones to relate shape memory polymers to real-life applications. There is still much work to be done in this area; hence questions and recommendations for future research are presented in this thesis (Chapter 8).

## 1.1 Background

The SME of thermo-sensitive SMPs is the response of the material to a series of thermomechanical loadings. These thermomechanical loadings include the programming and activation of the SME. The programming steps include:

1. Increase of temperature above the transition temperature.
2. Application of mechanical loading.
3. Cooling of the material below the transition temperature under the applied load or under a fixed mechanical constraint.
4. Activation of the SME by elevating the temperature to, or above, the transition temperature.

SMP can be thermoplastic (TP-SMPs) and thermoset (TS-SMPs). TP-SMPs have processability advantages over The SME in that they are easier to process, lower cost and recycle. Thermoplastic block copolymers SMPs functions through physical bonds (hydrogen bonding) [4]. Thermoplastics SMPUs are fabricated with hard-crystallized (urethane segments) and soft-amorphous segments (polyether segments). Soft segments have lower glass transition temperatures ( $T_g$ ) (the polymer's temperature at which it switches from glassy to rubbery) than hard segments. Because of a hard to soft segment ratio, a new  $T_g$  is developed for the polymer; such temperature is the SME's triggering temperature. Additionally, the thermodynamic incompatibility between hard and soft segments causes a microphase separation that contributes to the recovery characteristics of the SME [4, 26, 13]. Different ratios of hard to soft segments define the SMP's characteristics, namely their activation temperature, moisture sensitivity, shape recovery characteristics, and mechanical properties [24, 18, 15, 12, 21].

The SME of temperature-activated SMPCs can be done through different methods: increasing the surrounding ambient temperature or inserting elements that generate heat within the material. Although increasing the surrounding material's temperature is the most straightforward option for activation, one must consider that SMPs have a low heat conduction coefficient ( $k = 0.3W/mK$ ) (obtained from measured data) similar to that of a thermal insulator. Therefore heat conduction occurs from the outside surrounding into the material relatively slow. Alternatively, this can be done so that the heat distribution within the material is homogeneous, and therefore, controlled activation of the SME is achieved.

Studies have looked at nano-filler dispersion within the SMP matrix and the use of carbon black, graphene and carbon nanotubes as nano-filler particles to produce conductive materials to produce resistive Joule heating. To properly embed these particles in a TP-SMP matrix, melt extrusion processes need to acquire good particle dispersion and avoid filler agglomerations within the ma-

terial. The main disadvantage of this method is that high quantities of filler material are needed to acquire a good percolation threshold, which decreases the shape recovery properties of the SMP matrix [25, 28, 17]. These agglomerations also form unpredictable stress concentration factors and reduce the strength of the material. Other techniques have focused on adding heating material such as shape memory alloy wires, gold foil, and resistive metals to a SMP matrix [14, 19, 2, 11, 27]. At the moment, these techniques are complicated to mass-produce. Furthermore, there has been no attempt to fully study and control the activation of SMPs with any of the techniques mentioned.

## 1.2 Objectives of the Thesis

This thesis's objectives have been defined with the intention to significantly contribute to the fundamental understanding of shape memory polymers in characterization and modelling to enable their real-life engineering applications. The objectives of this thesis are proposed as follows:

1. To understand the effect of ambient conditions on the mechanical/thermomechanical properties and processability of the SMPU for part manufacturing.
2. To develop a transient model that is easy to apply and interpret, to predict the shape memory behaviour of SMPs under bending.
3. To develop a technology that will allow for proper field activation of shape memory polymers while keeping part manufacturing simple, repeatable and economically accessible.
4. To describe and explore the multifunctionality of thermally activated SMPCs via joule heating, including activation and sensing capabilities.

## 1.3 Overview of Content

Most of the work done as part of this thesis has been published in peer-reviewed journal publications and presented in international conferences, and published in conference proceedings. Some of the work is in the progress of being submitted to peer-reviewed journals.

- Chapter 2 is a comprehensive literature review on property modelling of shape memory polymers. An extensive classification of SMPs has been done, and a detailed review of the model development efforts up to date is presented. Additionally, a discussion portion for areas of research and applications is included. A version of this chapter is soon to be submitted to a peer-reviewed journal for publication.

- Chapter 3 presents a literature review about the advances in additive manufacturing of shape memory polymer composites to identify manufacturing techniques that will allow the manufacturing of SMPs and SMPCs that can be field activated. The review highlights the opportunities in the field of additive manufacturing of shape memory polymer composites, including embedding material sensors into smart shape-shifting structures. This review has been accepted for publication in the "Rapid Prototyping Journal" as seen in reference [7].
- Chapter 4 explores, in detail, the effects of moisture on thermoplastic SMP. The study centers on two materials from the same family with different activation temperatures. The study identifies the differences in these materials that ultimately lead to more defined plasticization or moisture trapping depending on the hard-to-soft segment ratio. Moreover, a model is used to predict the plasticization effect of these materials. Findings are used to guide the study to avoid increased difficulty due to moisture when extruding or 3D printing by Extrusion Based Additive Manufacturing (EBAM). This publication is published as see in reference [8].
- Chapter 5 presents a transient model for shape memory polymers under bending. The proposed model predicts parameters such as the shape recovery force and the shape recovery ratio necessary for understanding and designing with SMPs. A method for extracting SMP material parameters via DMA is also proposed in this section. This work is a crucial stepping stone towards a model that can be used for materials that are activated via joule heating. A version of this chapter is almost ready and will soon be submitted to a peer-reviewed journal for publication.
- Chapter 6 introduces the technology developed to additive manufacture thermally active shape memory polymer composites. An SMPC structure has been 3D printed with two different materials to achieve heating and activation of the shape memory effect. This work has been published as seen in reference [5].
- Chapter 7 builds on Chapter 6. Here a detailed work on the joule heating behaviour of a 3D printed SMPC structure is outlined and studied. Different ratios of conductive and SMP material are investigated. The heating behaviour of the structure is carefully characterized. An electronics and control system were developed to accurately measure resistance while providing a controlled current to produce heat and activate the shape memory effect. This system provides the control of a self-sensing mechanism, in which the smart structure can be controlled with respect to temperature and strain. This work was published as seen in reference [6].

## 1.4 References

- [1] Silvestro Barbarino, Onur Bilgen, Rafic M Ajaj, Michael I Friswell, and Daniel J Inman. A review of morphing aircraft. *Journal of Intelligent Material Systems and Structures*, 22(9):823–877, June 2011.
- [2] H A Bruck, C L Moore III, and T M Valentine. Bending actuation in polyurethanes with a symmetrically graded distribution of one-way shape memory alloy wires. *Experimental Mechanics*, 44(1):62–70, 2004.
- [3] Yu Chen, Irina Tatiana Garces, Tian Tang, and C. Ayranci. Cellulose nanocrystals reinforced shape memory polymer cardiovascular stent. *Rapid Prototyping Journal*, ahead-of-print(ahead-of-print):19, December 2020.
- [4] Bradley Finnigan, Darren Martin, Peter Halley, Rowan Truss, and Kayleen Campbell. Morphology and properties of thermoplastic polyurethane nanocomposites incorporating hydrophilic layered silicates. *Additive Manufacturing*, 45(7):2249–2260, March 2004.
- [5] I T Garces and C. Ayranci. A view into additive manufactured electro-active reinforced smart composite structures. *Manufacturing Letters*, 16:1–5, April 2018.
- [6] I T Garces and C. Ayranci. Active control of 4D prints: Towards 4D printed reliable actuators and sensors. *Sensors and Actuators, A: Physical*, 301:111717, January 2020.
- [7] I T Garces and C. Ayranci. Advances in additive manufacturing of shape memory polymer composites, January 2021.
- [8] Irina T Garces, Samira Aslanzadeh, Yaman Boluk, and C. Ayranci. Effect of Moisture on Shape Memory Polyurethane Polymers for Extrusion-Based Additive Manufacturing. *Materials*, 12(2):244, January 2019.
- [9] Lindsey Hines, Veaceslav Arabagi, and Metin Sitti. Shape Memory Polymer-Based Flexure Stiffness Control in a Miniature Flapping-Wing Robot. *IEEE Transactions on Robotics*, 28(4):987–990.
- [10] Alina-Maria Holban and Alexandru Grumezescu. *Materials for Biomedical Engineering: Nanobiomaterials in Tissue Engineering*. Elsevier, March 2019.
- [11] Chetan S Jarali, S Raja, and A R Upadhyaya. Constitutive modeling of SMA SMP multifunctional high performance smart adaptive shape memory composite. *Smart Materials and Structures*, 19(10):105029–10, September 2010.

- [12] F L Ji, J L Hu, and J P Han. Shape memory polyurethane-ureas based on isophorone diisocyanate. *High Performance Polymers*, 23(3):177–187, June 2011.
- [13] Hong-Yang Jiang and Annette M Schmidt. Shape-Memory Polymers and Multifunctional Composites. pages 1–43, May 2010.
- [14] C S Jithin, S Balasivanandha Prabu, and Ramachandran Velmurugan. Development of Shape Memory Alloy Polymer Composite and Influence of Material Parameters on Shape Memory. *Applied Mechanics and Materials*, 592-594:158–163, July 2014.
- [15] Andreas Lendlein and Steffen Kelch. Shape-Memory Polymers. John Wiley & Sons, Inc., Hoboken, NJ, USA, 2002.
- [16] YueJia Li, Fenghua Zhang, Yanju Liu, and Jinsong Leng. 4D printed shape memory polymers and their structures for biomedical applications. *Science China Technological Sciences*, 63(4):545–560, February 2020.
- [17] Fei Liang, Jihua Gou, He Shen, Yunjun Xu, and Bob Mabbott. Carbon fiber reinforced shape memory nanocomposites incorporated with highly conductive carbon nanopaper for electro actuation. In *ASME 2013 Conference on Smart Materials, Adaptive Structures and Intelligent Systems, SMASIS 2013*. University of Central Florida, Orlando, United States, January 2013.
- [18] J Dyana Merline, C P Reghunadhan Nair, C Gouri, G G Bandyopadhyay, and K N Ninan. Polyether polyurethanes: Synthesis, characterization, and thermoresponsive shape memory properties. *Journal of Applied Polymer Science*, 107(6):4082–4092, 2007.
- [19] D M Phillips and J W Baur. A microvascular method for thermal activation and deactivation of shape memory polymers. *Journal of Intelligent Material Systems and Structures*, 24(10):1233–1244, 2013.
- [20] S G Rauscher. Testing and analysis of shape-memory polymers for morphing aircraft skin application. 2008.
- [21] Christian Schuh, Kerstin Schuh, Maria C Lechmann, Louis Garnier, and Arno Kraft. Shape-Memory Properties of Segmented Polymers Containing Aramid Hard Segments and Polycaprolactone Soft Segments. *Polymers*, 2(2):71–85, June 2010.
- [22] Ward Small IV, Pooja Singhal, Thomas S Wilson, and Duncan J Maitland. Biomedical applications of thermally activated shape memory polymers. *Journal of Materials Chemistry*, 20(17):3356–11, 2010.
- [23] Wei Wang, Hugo Rodrigue, Hyung-Il Kim, Min-Woo Han, and Sung-Hoon Ahn. Soft composite hinge actuator and application to compliant robotic gripper. *Composites Part B: Engineering*, 98:397–405, August 2016.

- [24] Wenshou Wang, Peng Ping, Xuesi Chen, and Xiabin Jing. Biodegradable polyurethane based on random copolymer of L-lactide and  $\epsilon$ -caprolactone and its shape-memory property. *Journal of Applied Polymer Science*, 104(6):4182–4187, 2007.
- [25] Xin Wang, John Sparkman, and Jihua Gou. Electrical actuation and shape memory behavior of polyurethane composites incorporated with printed carbon nanotube layers. *Composites Science and Technology*, 141:8–15, March 2017.
- [26] Wei Xu, Ruoyu Zhang, Wei Liu, Jin Zhu, Xia Dong, Hongxia Guo, and Guo-Hua Hu. A Multiscale Investigation on the Mechanism of Shape Recovery for IPDI to PPDI Hard Segment Substitution in Polyurethane. *Macromolecules*, 49(16):5931–5944, 2016.
- [27] Kai Yu, David M Phillips, Jeffery W Baur, and H Jerry Qi. Analysis of shape-memory polymer composites with embedded microvascular system for fast thermal response. In *Journal of Composite Materials*, pages 1881–1893. The George W. Woodruff School of Mechanical Engineering, Atlanta, United States, January 2015.
- [28] L Zhu and R Pitchumani. Analysis of a process for curing composites by the use of embedded resistive heating elements. *Composites Science and Technology*, 60(14):2699–2712, November 2000.

## Chapter 2

# Literature Review on Modelling of Thermo-responsive Shape Memory Polymers

### **Abstract**

Shape Memory Polymers (SMPs) are a type of multifunctional material that has received much attention from academia and industry. There is a vast potential to use these materials as sensors and actuators, which could shift the view of engineering materials in design. Thermo-sensitive SMPs are the most commonly used type of SMPs because of their ease of activating the Shape Memory Effect (SME). As such, there is a need for models that describe the thermomechanical behaviour and shape memory properties of these materials. Specifically, the required traits of these materials needed for engineering applications are the shape recovery force, shape recovery ratio and shape recovery speed. Many great efforts have been made in the literature. This section seeks to review the most important models up to date in this area.

# Nomenclature

$\alpha$	Coefficient of thermal expansion	$\varepsilon_a$	Strain of the active phase
$\mathbf{F}^e$	Elastic Deformation Gradient	$\varepsilon_c$	Creep strain
$\mathbf{F}^m$	Mechanical Deformation Gradient	$\varepsilon_f$	Strain of the frozen phase
$\mathbf{F}^v$	Viscoelastic Deformation Gradient	$\varepsilon_{me}$	Mechanical strain
$\mathbf{F}^{th}$	Thermal Deformation Gradient	$\varepsilon_p$	Plastic strain
$\mathbf{F}$	Deformation Gradient	$\varepsilon_{str}$	Stored strain
$\mathbf{S}$	Stress Tensor	$\varepsilon_s$	Irrecoverable strain
$\lambda$	Retardation time	$\varepsilon_{th}$	Thermal strain
$\mu$	Viscosity	$\zeta$	Entropy
$\mu_h$	Viscosity of the hard segment	$E$	Elastic Modulus
$\mu_s$	Viscosity of the soft segment	$T$	Temperature
$\phi_a$	Active volume fraction	$T_f$	Final Temperature
$\phi_f$	Frozen volume fraction	$T_g$	Glass transition temperature
$\psi$	Helmholtz free energy	$T_h$	Upper bound of transition temperature
$\sigma$	stress		
$\sigma_c$	Creep stress	$T_L$	Lower bound of transition temperature
$\sigma_y$	Yield stress	$T_m$	Melting temperature
$\varepsilon$	strain	$T_{trans}$	Transition temperature
$\varepsilon_0$	Prescribed strain	$U$	Internal energy

## 2.1 Introduction

Smart materials can change their physical or chemical configuration in a controlled manner when subjected to triggering mechanisms. Among these, Shape Memory Materials (SMM) have the ability to store a temporary shape and recover their original (permanent) shape upon the application of a stimulus, such as a change in temperature, pH, UV-light and moisture [40]. The ability of these materials to recover their original shape is often referred to as the Shape Memory Effect (SME). Among common SMM, Shape Memory Polymers (SMPs) are among the most studied due to their promising applications in the biomedical [99, 81, 82, 46], consumer [70], oil and gas [68] and aerospace industries [56]. SMPs have many desirable traits such as their high strain recoverability ( $\sim 150\%$ ) and considerable lower density in comparison to Shape Memory Alloys

(SMA) and Shape Memory Ceramics (SMC), which have a recoverability of  $\sim 20\%$  and  $\sim 10\%$ , respectively [54, 47]. Additionally, polymers possess advantages over metals and ceramics such as their ease of manufacturing, potential recyclability, biodegradability, bio-compatibility and tailorability [58].

Thermal responsive SMPs have gathered the most attention in the field compared to other types of stimulus-driven materials due to the ease of activation (increase in temperature or heat application). For these reasons, the present review will only focus on thermal sensitive SMPs. Efforts have principally focused on characterizing these polymers experimentally [36], however in the recent decade, considerable modelling attempts have been made. Complete understanding of the shape memory behaviour is necessary to implement SMPs in the many potential future applications like in self-assembling structures [21, 94], self-deployable catheters [99], self-adjusting sutures [99], self appearing QR codes [112], and the like. Many of these applications will require SMPs to undergo large deformations and severe thermo-mechanical loadings, specifically during the programming and recovery cycles. Therefore, predictive models that accurately describe the recovery process are necessary for engineering design with these materials. Accurate and easy to apply models can allow engineers to push forward broader applications with SMPs.

Modelling the SME in polymers can be difficult to tackle due the complexity of the physical phenomena, and generalizing a procedure for these polymers can be problematic due to the different morphologies that they possess, i.e. amorphous and semi-crystalline [60, 36, 49]. The author looked at the different morphologies and has classified common SMPs for the relevance of the review. A classification of the modelling techniques of SMPs has also been put forward and is described into three different kinds, those composed of (a) Spring-Dashpot components (section 2.3.1), (b) Phase Change (section 2.3.2) and a (c) Hybrid modelling approach (section 2.3.3).

## 2.2 Thermally Activated Shape Memory Polymers

The SME in thermal responsive SMPs is a reaction of the material to specific thermo-mechanical loadings rather than an intrinsic material property [60]. Some of the proposed applications for these novel materials include micro-mechanical systems, rewritable data systems [84] such as Quick Response (QR) codes [112] and self-deployable structures, among them morphing origami-like structures [65], self actuated hinges [25], antenna for space applications [7, 104], wings for gliders [88] and sports equipments such as a self deployable kayak [24]. An example of the thermal activated SME applied to an application is illustrated in Figure 2.1. In the figure, a schematic of an SMP kayak is activated and can be stored in a temporary shape for transportation. In other fields, such as mechatronics and biomedical engineering, applications such as crawling robots [22, 23], surgical

stents, sutures, orthodontic devices, drug-delivery systems, self-adapting cast and splints [33, 80] have been proposed and studied. Some of the desired traits of SMPs that allow real applications to pass the prototyping stage are high recovery percentage, shape recovery speed, ratio and shape recovery force exerted by the material during recovery.

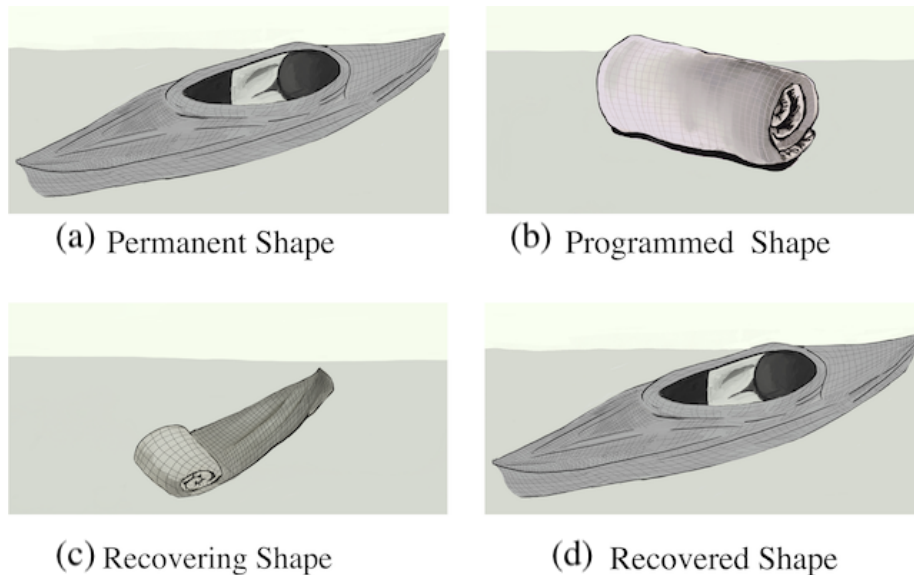


Figure 2.1: Schematic of a self-deployable Kayak that can take the shape of a sleeping bag for transportation

Although the SME is said to be a response of the material, different chemical structures provide a variety of SM properties. In general, SMPs can be either thermoplastics or thermosets, defined by physical or covalent cross-links, respectively. Generally, for amorphous polymers the transition temperature is the glass transition temperature and for crystalline polymers it is said to be the melting temperature  $T_m$  [47, 48]. For both types of polymers, the SME is the consequence of the phase change from crystalline or glassy, to rubbery [113]. Generally, soft segments (which can be cross linked chains or curing agents) are linked by netpoints that can be of covalent nature or crystalline segments. This particular chapter will focus on the one-way shape storing of SMPs, although there are multiple polymer microstructures that enable the ability of SMPs to store two-way or multiple-way shape change.

One of the most commonly referenced classification for SMPs is the one provided in the reviews of Liu *et al.* [54] and Nguyen *et al.* [67]. In the mentioned reviews, the authors classified temperature activated SMPs into four major classes as:

- I covalently (chemically) cross-linked glassy thermoset networks (amorphous networks)

$$(T_{trans} = T_g)$$

II covalently (chemically) cross-linked semi-crystalline networks (rubbers)

$$(T_{trans} = T_m)$$

III physically cross-linked glassy (amorphous) copolymers, or semicrystalline homopolymers

$$(T_{trans} = T_g \text{ or } T_m)$$

IV physically cross-linked semi-crystalline block-copolymers

$$(T_{trans} = T_m)$$

A general schematic representations of the internal structures of these polymers at different stages can be found in Figure 2.2. Notice that only the general mechanism behind the SME is illustrated in the figure, and the microstructure may differ for different polymers even within the same class. For instance polymers such as epoxy, and thermosetting PU are both considered to be class I although their microstructures differ [39]. The general shape memory mechanism works by setting their permanent shape by cross links and actuating their temporary shape by their sharp glass transition. In the figure, chemical cross-links are depicted by circles and are found in classes I and II, while physical cross-links, can be found in classes III and IV. Notice that physical crosslinks are not limited to these since they may appear in crystalline structures.

Just as for class I, the permanent shape of class II is set by the chemical crosslinks (depicted with circles) while the temporary shape is set by crystallization and hence crystals are formed in the form of organized structures depicted in the figure. Examples of these are Polyethylene (PE) and Polycaprolactone (PCL), among others [39]. When the temperature is increased above the transition temperature, these crystals melt and the secondary shape is set. During the cooling process, crystals can again reform.

The permanent shape for class III and IV is set by rigid segments. In the case of class III it is set by rigid amorphous domains (crystals), hydrogen bonding or ionic clusters. In the figure, the general structure with amorphous and hard segments is shown for a general representation. The permanent shape is set by these rigid segments while the temporary shape is set by amorphous or soft segments. Hence the activation temperature for class III is either  $T_g$  or  $T_m$  (depending on the structure) of the soft amorphous phase. A common material and an example of this class is PLA (Polylactic Acid) [39, 87].

Just as with class III, physical crosslinks set the permanent shape for class IV polymers. Physical crosslinks include, polar interactions, hydrogen bonding or crystallization which includes these types of physical bondings. In this type of SMPs, crystallization is the main cause for setting the temporary shape. Class IV includes one of the most studied SMPs often referred to as thermoplastic elastomers due to their physical crosslinking [18, 47], e.g. thermoplastic polyurethane (TPU) [39].

More examples of these classes include : (I) VeriFlex<sup>TM</sup> [61], II Poly( $\epsilon$ -caprolactone)[109], Liquid Crystal Elastomers and hydrogels [54], (III) Polyurethanes [108, 90, 38] and (IV) PCL diol/MDI/BD [37].

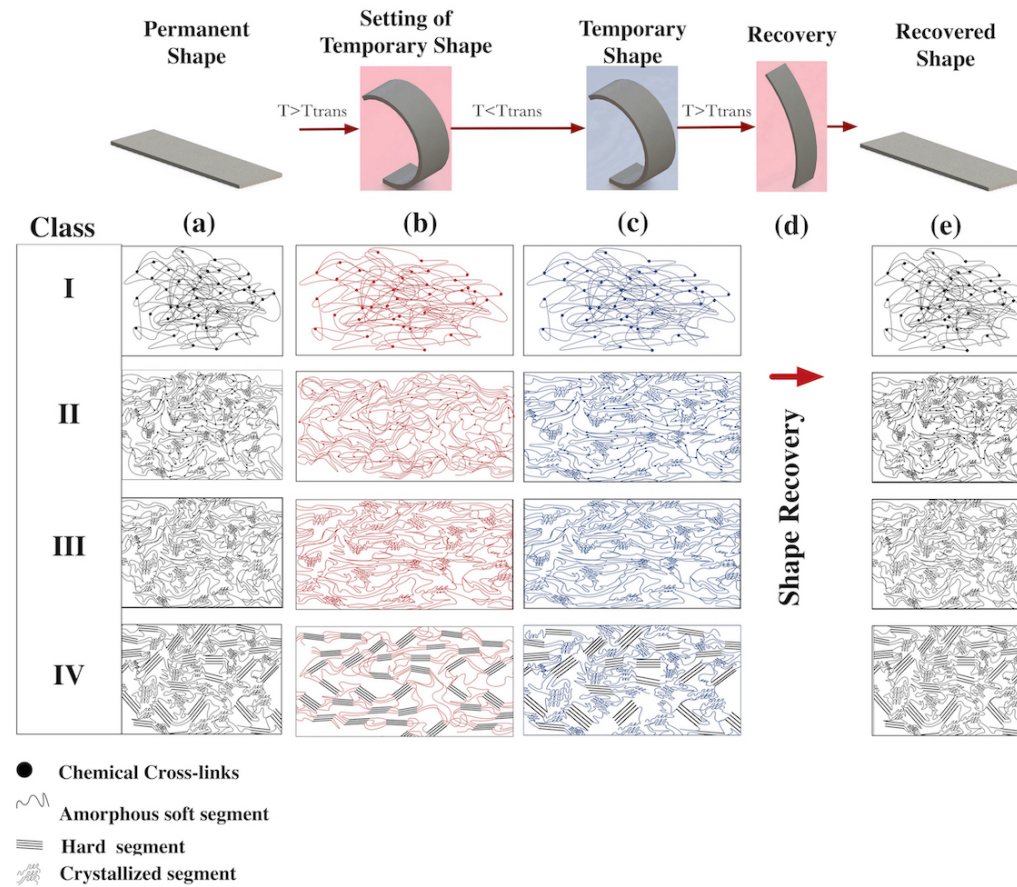


Figure 2.2: Description of the SME showing the different stages: (a) permanent shape, (b) setting of temporary shape, (c) temporary Shape (d) recovery, (e) recovered shape. Reference of structures for Class I [76], Class II [55], Class III [118, 62], Class IV [34]

### 2.2.1 Thermal Shape Memory Effect

The shape memory properties of thermally sensitive SMPs are closely dependent on temperature, time and load. When an SMP is heated, its elastic modulus can decrease several orders of magnitude. This particular property allows for the reconfiguration of the material and the retention of a temporary shape. Below the transition temperature,  $T_{trans}$ , the polymer behaves as an elastic-viscoplastic glassy material, meaning linear or nonlinear elastic behaviour coupled with time-dependent plasticity. When the temperature is within or above the transition range, the material changes to a viscoelastic rubber-like material [83]. A schematic of the SME cycle is seen in Figure 2.2, where a) represents the permanent/original shape (in black), b) represents the setting of the temporary shape c) the temporary shape, d) represents the recovery process and e) represents the recovered shape. From the described material behaviour, the programming cycle (from (a) to (c) in Figure 2.2) is as follows: i) increase the temperature above  $T_{trans}$ , ii) At  $T > T_{trans}$ , apply a load or strain, iii) while holding the applied load/strain, decrease the temperature below  $T_{trans}$ . The recovery of the original shape (Figure 2.2(d) to 2.2(e)) is acquired by increasing the temperature above  $T_{trans}$ . Notice that in the figure, the red colour represents an increase in temperature and blue, a decrease in temperature below the transition temperature  $T_{trans}$ .

At the microscopic scale, the polymeric structure of different classes of SMPs changes during thermal-mechanical loading to allow for the SME to take place. For instance, for the setting of the temporary shape, class I shows the movement of the chains as they reach a temperature above  $T_g$ , while the shape is conserved by the chemical cross-links anchoring the structure during cooling. Class II, on the other hand, has crystallizable amorphous chains. The crystallite structures melt away into amorphous chains when heated, and vitrification occurs during cooling, which sets the temporary shape. For thermoplastics class III, the setting of the temporary shape occurs by stretching the amorphous segment and anchor-points are created by physical cross-links between hard segments. Thermoplastics class IV show the setting of the temporary shape by melting the crystallites soft segments.

Although many polymers exhibit a thermal SME, specific characteristics allow certain SMPs to be used as sensors, actuators, or self-deployable structures. For a material to be used as actuators, a high recovery force, ratio and speed are usually desired. Intrinsic properties of the material, such as a narrower glass transition is also commonly desired to obtain a shorter recovery period [105]. Some of these material properties can be widely characterized by two different tests: the free recovery and the constrained recovery. The free recovery, as the name implies, allows the material to move freely during recovery. This test provides insight into the total recovery percentage and recovery speed. Contrarily, the recovery force can be obtained from the constrained recovery; for instance, both ends are constrained after programming during a uniaxial test [47]. After applying a prescribed strain,

$\varepsilon_0$ , and conducting a free or constrained recovery, parameters such as recovery speed, strain fixity, recovery strain and recovery stress ( $R_S$ ) can be quantified. Usual calculations include the total shape recovery ratio ( $R_r$ ) and the shape fixity ratio ( $R_f$ ) as well as the irrecoverable strain, ( $\varepsilon_s$ ), or the amount of strain that has not been recovered after the activation of the SME. Quantification of these values is often done by studying the viscoelastic properties of SMPs. These properties can be quantified from creep recovery, cyclic tensile tests and analysis of the viscoelastic behaviour through Dynamic Mechanical Analyzers (DMA). These tests are often useful to determine the degree of softening of the materials and can be correlated to the mentioned irrecoverable strain [116].

## 2.2.2 Characterizing the Irrecoverable Strain

### Modelling relationships

To be able to use SMPs in engineering applications, there is a need to understand and optimize the SME. A thorough investigation of the reminder non-recovered strain, also referred to as the irrecoverable strain, is necessary for SMP characterization and modelling to fully understand the material applicability. The amount of irrecoverable strain is greatly influenced by the intrinsic molecular structure of the polymers. For amorphous polymers, the remaining strain that is not recovered can be accredited to structural relaxation, which is a time-dependent process in which the polymer chains rearrange themselves to a new equilibrium position [67]. For semi-crystalline polymers, the irrecoverable strain could be correlated to the inelastic deformation of the crystalline part of the polymer, such as chain slip and twinning [86, 50]. The slippage mechanism is commonly assumed to be the dominant cause of the irrecoverable strain. Qi *et al.* [72] have also attributed the irrecoverable strain to breakage of hydrogen bonds in hard domains and possible interaction between hard/hard and hard/soft domains. Irrecoverable in cyclic loading has also been attributed to strain softening [72]. In rubbery materials, i.e. elastomers, strain-softening is referred to as the Mullins effect [72]. This phenomenon occurs when hard block sections re-orientate, which occurs when polymer chains are subjected to a strain that produces the hard segment to undergo breakage and reformation of hydrogen bonds.

The SME is the polymer's reaction to a shape memory training. Parameters such as programming temperature, strain/load rate, total applied load/strain, shape-holding time and recovery temperature affect the way irrecoverable strain evolves and sets through time. Resulting indicators that allow researchers to carefully look at the irrecoverable strain and correlate it with the SMP behaviour are the shape fixity, strain recovery rate, and strain recovery ratio. Strain fixity is measured by the rate between the applied programming strain and the existing experimental fixed

strain (equivalent to a spring-back in metals). Strain recovery rate is the rate per unit time at which the SMP recovers after the SME has been triggered [89, 50]. Shape programming methods by strain or load control are often used to determine the effects of experimental parameters on the SME. Among those interesting studies, it was found that for thermoset SMPs, the strain rate affects  $T_g$  and the activation temperature of the material [98].

Tobushi's *et al.* [89] described the ratio of recovery by relating the irrecoverable strain ( $\varepsilon_s$ ) observed after the shape recovery cycle with respect to the occurred creep strain during the programming stage,  $\varepsilon_c$ . This creep strain occurs in different amounts with respect to the applied temperature. This expression can be seen in equation 2.1. Tobushi *et al.* suggested that if large strains are applied then the same relationship may hold by implying that a plastic deformation,  $\varepsilon_p$  will occur as observed in equation 2.2 [93]. Later this irrecoverable ratio,  $S$ , was said to be the ratio between the irrecoverable strain,  $\varepsilon_s$ , and the holding strain,  $\varepsilon_h$  applied when shape programming ( $S = \frac{\varepsilon_s}{\varepsilon_h}$ ). As such, an empirical relationship that describes the irrecoverable ratio can be defined as a function of the loading and holding temperature,  $T_h$ , at which the SMP is programmed and its glass transition temperature  $T_g$  as seen in equation 2.3 [91, 92]. The authors proposed that the total irrecoverable ratio is a function of the maximum irrecoverable strain ratio that can occur,  $S_p$ , the time at which irrecoverable strain appears ( $t_s$ ) and a time constant  $c$ . From which,  $S_p$ ,  $t_s$  and  $c$  are all functions of the shape setting or holding temperature  $T_h$  and the glass transition temperature of the material ( $T_g$ ).

$$\varepsilon_s = S\varepsilon_c \quad (2.1)$$

$$\varepsilon_s = S(\varepsilon_c + \varepsilon_p) \quad (2.2)$$

$$S = S_p \left(1 - e^{-\frac{t_h - t_s}{c}}\right) \quad (2.3)$$

Balogun *et al.* [3, 4] have instead described the strain storage with respect to temperature to predict the Shape Memory (SM) behaviour and therefore estimate the irrecoverable strain. The authors introduced a binding factor using a similar method as Xiao *et al.* [107, 105, 106]. This factor, is an approximation that relates temperature and viscosity at high and low temperatures defined as  $\mu_h, \mu_l$ , respectively. The expression is defined in equation (2.4), and therefore the stored strain  $\varepsilon_{str}$  can be described by equation (2.5), where the binding factor compensates for the material morphology at different temperatures and binds it with the mechanical strain being applied  $\varepsilon_{me}$ . A positive or negative strain occurs depending on a heating or cooling rate, this is compensated by factor,  $k_m$ .

$$z = 1 - (1 + e^{|\ln(\mu_h/\mu_l)|^{-1}(T_g - 0.5\Delta T_{hl} - T)^{-1}}) \quad (2.4)$$

$$\varepsilon_{str} = z k_m \varepsilon_m \dot{\varepsilon}; \quad k_m = \begin{cases} +1, & \dot{T} < 0 \\ -1, & \dot{T} < 0 \\ 0, & \dot{T} = 0 \end{cases} \quad (2.5)$$

A recent attempt to describe the irrecoverable strain has also been tackled by Guo *et al.* [29]. The authors proposed that the irrecoverable strain in amorphous polymers happens as the summation of two contributions. The first arises from the programming stage due to a low cross-linking degree and can be accounted for by equation (2.6), where  $\sigma(t)$ ,  $\varepsilon$ ,  $\dot{\varepsilon}$ ,  $\mu_{2a}$  are the stress, strain, strain rate, and viscosity of their model's second dashpot. The second contribution is from the shape setting process, which is defined by equation (2.7), where  $T_h$  and  $\beta$  are the starting programming temperature and the cooling rate. The total irrecoverable strain  $\varepsilon_s$  can be described by equation (2.8).

$$\varepsilon_{irr,1}(t) = \int_0^{t_1} \frac{\sigma(t)}{\mu_{2a}} dt, \quad t = \frac{\varepsilon}{\dot{\varepsilon}} \quad (2.6)$$

$$\varepsilon_{irr,2}(t) = \int_0^{t_2} \frac{\sigma(t)}{\mu_{2a}} dt, \quad t = \frac{T_h - T}{\beta} \quad (2.7)$$

$$\varepsilon_s = \varepsilon_{irr,1} + \varepsilon_{irr,2} \quad (2.8)$$

Table 2.1 provides a summary of the mentioned models, the author has considered that these are some of the most important ones when describing the irrecoverable strain, which needs to be considered for future modelling approaches.

Table 2.1: Summary of irrecoverable strain functions

Reference	Equation	Variable Dependency
[89]	$\varepsilon_s = S\varepsilon_c$	
[93]	$\varepsilon_s = S(\varepsilon_c + \varepsilon_p)$	
[91, 92]	$\frac{\varepsilon_s}{\varepsilon_h} = S_p(1 - e^{-\frac{t_h - t_s}{c}})$	$t_h; t_s$
[3, 4]	$z = 1 - (1 + e^{ \ln(\mu_h/\mu_l) ^{-1}(T_g - 0.5\Delta T_{hl} - T)^{-1}})$	$\mu_h; \mu_l$
[29]	$\varepsilon_s(t) = \int_0^{t_2} \frac{\sigma(t)}{\mu_{2a}} dt$	$t = \frac{T_h - T}{\beta}; t = \frac{\varepsilon}{\dot{\varepsilon}}$

## Experimental Relationships that affect the SME

There are experimental relationships worth mentioning among the programming and shape memory variables that affect the overall behaviour of the shape memory effect and hence the shape recovery ratio. For instance, shape fixity has been found to be dependent on the relaxation modulus of the polymer [115] and therefore it will increase when shape holding time increases (step b in Figure 2.2), or when a higher temperature is used during shape programming. It has also been found that shape fixity decreases when a higher strain rate is used since it does not allow sufficient time for the polymer structure to set [98]. Works by Yu *et al.* [114] have found that a consistent high shape fixity usually leads to an increase in recovery rate. Chen *et al.* have also found that materials with high rubbery modulus and lower glassy modulus also recover their shape at a higher recovery rate [11].

Total recovery ratio has been found to be high when the relaxation modulus of the material is higher at the end of the shape programming cycle [107]. Factors that can decrease the recovery ratio are a high shape holding time and temperature because they create an irrecoverable strain due to creep, these effects were seen in both strain and load controlled shape programming methods [92, 78]. Guo *et al.* also found that a higher loading strain rate yields lower recovery ratios and recovery speeds [31].

Chen *et al.* found that constrained recovery, and therefore the study of the recovery force, is mostly affected by the Coefficient of Thermal Expansion (CTE) of the material, while both constrained and free recovery were highly affected by heating and cooling rates while setting of the temporary shape [11]. A low heating rate during shape training allows polymer chains to reorganize and increase their relaxation time, while a faster cooling rate when shape setting showed a decrease of the recovery rate. Following the same logic, a lower cooling rate again allows for chain relaxation to occur.

All these effects need to be accounted for to determine the irrecoverable strain and moreover the entire shape recovery effect. In the following sections the modelling approaches to capture the shape memory behaviour as a whole are described.

## 2.3 Modelling Approaches

Modelling the shape memory phenomena is complicated by nature. Mainly, researchers have approached this from two different angles. Shape recovery takes place at the transition region, if we characterize this driving phenomena from a force point of view, it can be said that structural relaxation will define the amount an SMP recovers and how it moves through time during the recovery

process [66]. From an energy point of view, when a polymer changes from the thermal stretched state to a cooled down state, entropy of the polymer system is frozen as motion of the chains is stopped. Therefore, the total energy in the system is in the form of internal stored energy [47].

It was mentioned in section 2.2.1 that the SME is based on the reaction of the application of thermo-mechanical loadings to the SMP. As a consequence, the material properties such as shape fixity, shape recovery rate and total shape recovery ratio are highly dependent on the material's structure and nature. Modelling has been approached from quantum mechanical calculations, molecular dynamics to the micro, meso and macro scale modelling [36]. The present review will focus on analytical thermo-mechanical modelling approaches at the macro and mesoscale due to the applicability of these models in direct simulation and reduced time of numerical implementation in contrast to molecular models [79].

The most common models belong to one of the two categories: a) those based on elastic and viscous elements (spring-dashpot models) and b) those based on a phase change concept. Although earlier modelling techniques using the spring-dashpot models rely heavily on experimentation, they have allowed the characterization of commercial SMPs that are useful for industrial applications [93, 89]. Attempts at modelling viscoelasticity using spring-dashpot models are more appropriate for amorphous polymers (Class I) [107, 66, 73, 105, 67, 106], while the phase change model are usually directed to modelling of semi-crystalline polymers (Class II, III, IV), and their implementation can be found in works by Scalet *et al.* [79] and Bouaziz *et al.* [8]. Thorough and excellent reviews have been conducted by Mather *et al.* [60, 36] and Zhao *et al.* [117] for these modelling approaches. It is for this reason that the present review will focus on summarizing the most relevant works in the area for completeness and reviewing the recent advances in the literature since their publications.

### 2.3.1 Models based on Elastic and Viscous Elements

This modelling technique describes the viscoelastic behaviour of a material by using constitutive equations of elastic solids and Newtonian fluids [58]. A material may therefore be described through combinations of springs and dash-pots placed in a series or parallel manner. Some of the most common models are the Generalized Maxwell, Kelvin Voigt and Zener Models. The elements in these models can describe the SME by incorporating time and temperature dependent parameters and nonlinearity within the constitutive elements. Intrinsically, the SME can be described as a function of viscosity with respect to temperature. In the permanent shape the spring-dashpot configuration is in a non-stressed condition. As the material heats up, the dashpots have lower viscosity and therefore an easiness to stretch. Once the temperature cools down, the viscosity increases drastically which stores and creates internal stresses within the polymeric structure (at the temporary shape). Upon heating the dash-pots in the system are softer and allow for the material

to return to its original configuration (permanent shape) [67]. The schematic of the described phenomena; when the polymer undergoes a thermo-mechanical training, can be seen in Figure 2.3. On the left, the general model is in nonstressed conditions and on the right, the configuration of the model is in the set temporary shape.

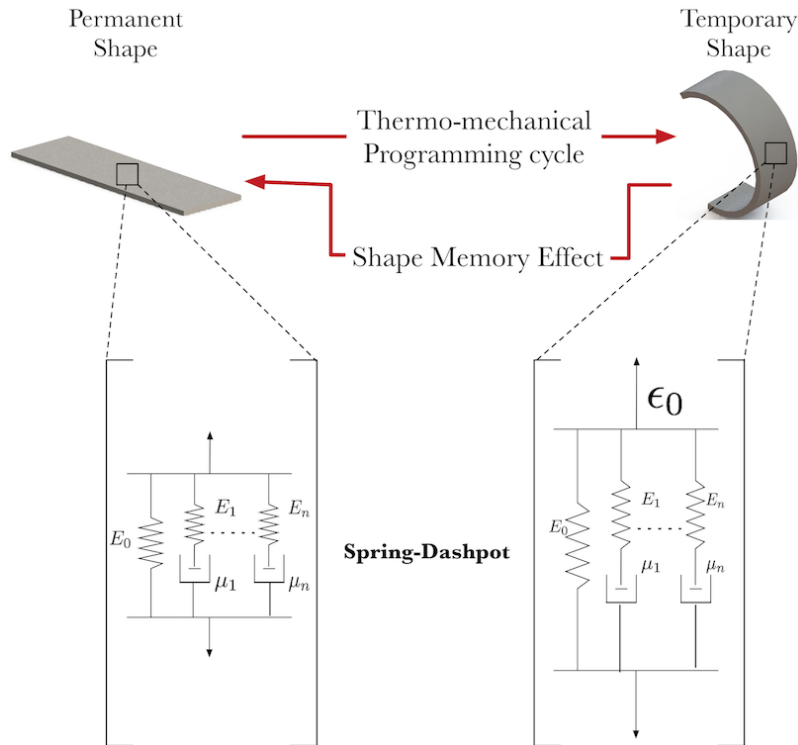


Figure 2.3: Spring-Dashpot model representation of an SMP configuration before shape programming and later recovery

In the literature, the SME was initially modelled using discrete and piecewise functions that describe the polymer during each thermo-mechanical process. Tobushi *et al.* [89] produced one of the earliest attempts to model the behaviour of an SMP for tension, where elastic and viscous elements were used to capture the SME and its irrecoverable strain. In their model the irrecoverable strain  $\varepsilon_s$ , portrayed in Figure 2.4(a), represents the slippage mechanism that accounts for the internal friction between polymer chains. This model is a derivation of the Standard Linear Viscoelastic model (SLV). Numerical values for this element were obtained experimentally by the authors from creep tests (for details on the irrecoverable strain see section 2.2.2 and refer to equations 2.1-2.3). Tobushi *et al.* [93] later improved their general viscoelastic model by increasing the order of the model ( $m$ ) to account for nonlinear behaviour when the material is subjected to larger strains.

Their model is still a function of the infinitesimal strain  $\varepsilon$ . It is important to mention that their work accounts for changes due to thermal expansion ( $\alpha$ ), which is independent of the mechanical behaviour. Constitutive equations for the linear [89] and nonlinear model [93] developed by the authors can be observed in equations 2.9 and 2.10, where material parameters  $\mu$ ,  $\lambda$ ,  $\sigma_y$  and  $\sigma_c$  represent the viscosity, the retardation time (delayed response to the applied stress), yield stress and creep limit, respectively.

$$\dot{\varepsilon} = \frac{\sigma}{E} + \frac{\sigma}{\mu} - \frac{\dot{\varepsilon} - \varepsilon_s}{\lambda} + \alpha \dot{T} \quad (2.9)$$

$$\dot{\varepsilon} = \frac{\dot{\sigma}}{E} + m \left( \frac{\sigma - \sigma_y}{k} \right)^{m-1} \frac{\dot{\sigma}}{k} + \frac{\sigma}{\mu} + \frac{1}{b} \left( \frac{\sigma}{\sigma_c - 1} \right)^n - \frac{\varepsilon - \varepsilon_s}{\lambda} + \alpha \dot{T} \quad (2.10)$$

Other discrete approaches besides the inclusion of a slippage mechanism seen in mentioned models have also been proposed to describe the SME, such as that by Lin *et al.* [53]. A representation of their model is portrayed in Figure 2.4 (b). The authors divided the effects of soft and hard segments of the polymer by implementing two Maxwell models connected in a parallel configuration. Attempts using simple models such as the Kelvin-Voigt to describe the SME have also shown to capture some of the shape memory behaviour for example the work by Morshedian *et al.* and Khonakdar *et al.* [63, 41]. Although this method successfully captures most of the behaviour of the SMP, it involves the implicit assumption of small strains and are limited to a 1D deformation. Another drawback of these modelling techniques is that these models cannot be generalized and are mostly based on curve fitting to experimental data from relaxation and creep experiments [77].

Further improvements have been done by adding different types of conditional strains to SLV, such as the works by Balogun *et al.* [4, 3]. The authors assume that mechanical strain storage is only dependent on heating rate, and therefore it is released when heated and stored when cooled. The authors assumed SMPs to be "thermo-rheologically simple" (assumption that a structure of a polymer is preserved and the stress-strain relation follows a singular trend despite their thermal histories [17]). The model used viscoelasticity and time-temperature superposition theories to produce a master curve of the relaxation modulus, which seems to capture the SM fixity and recovery in small deformations for amorphous and semi-crystalline SMP. Differences between these constitutive modelling techniques and obtained experimental data for semi-crystalline polymers were found [35] but high accuracy was shown for amorphous thermoplastics [15, 107].

Efforts have been directed towards continuous models as described by Mather *et al.* [60] and Hu *et al.* [36]. Although this allows the extension of models to finite strain, the modelling complexity increases substantially. Most of these models have decomposed the deformation gradient to account

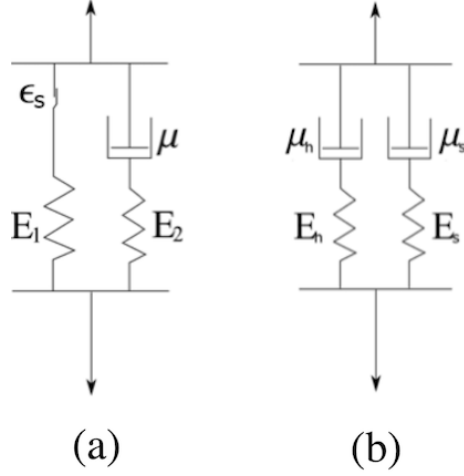


Figure 2.4: (a)SLV model with friction element to describe the SME [89], and (b) is the schematic of a model capturing hard and soft segment behaviour from [53]

for thermal-mechanical loadings and viscoelasticity with the use of the multiplicative decomposition from Lee *et al.* [44] and modern continuum mechanics [16]. The decomposition represented by equation 2.11 refers to the total obtained deformation gradient,  $\mathbf{F}$ , decomposed into  $\mathbf{F}^m$  and  $\mathbf{F}^{th}$  representing the mechanical and thermal parts. Where the mechanical deformation gradient is composed of an elastic  $\mathbf{F}^e$  and viscous part  $\mathbf{F}^v$ . Using the concept that within a transition temperature range the material is both elastic and viscous, Diani *et al.* [16] developed a model that followed two conditions. When the material is in the complete rubbery state, the contribution of changes in internal energy are negligible to the predicted stress, that is:  $\dot{\mathbf{F}}^v = \dot{\mathbf{F}}$ ;  $\mathbf{F}^e = \mathbf{1}$ . When the material is entirely glassy, the applied strain only creates internal energy (at the elastic region), hence  $\dot{\mathbf{F}}^v = \mathbf{1}$ . With the mentioned conditions and satisfying Clausius-Duhem law, a stress ( $\mathbf{S}$ ) equation can be obtained as portrayed in equation 2.12 and an evolution law of the changes of the viscous deformation gradient  $\mathbf{D}^v$  is the symmetric part of  $\mathbf{L} = \dot{\mathbf{F}}^v \mathbf{F}^{v-1}$  in equation 2.13. Where  $\mathbf{C} = \mathbf{F}^{eT} \cdot \mathbf{F}^e$  is the Cauchy-Green tensor of the elastic deformation and  $\mu$  is the viscosity. The present model did not consider any plastic strains or crazing effect, which produced deviations from the experimental results. However, following this technique and by obtaining different evolution laws, improved models may be obtained.

$$\mathbf{F} = \mathbf{F}^m \cdot \mathbf{F}^{th} \quad (2.11)$$

$$\mathbf{F} = \mathbf{F}^e \cdot \mathbf{F}^p$$

$$\mathbf{S} = 2 \frac{\partial T \mu}{\partial \mathbf{C}} + 2 \mathbf{F}^v \frac{\partial U}{\partial \mathbf{F}^{v-T}} \quad (2.12)$$

$$\mathbf{D}^v = \frac{1}{\mu} (\mathbf{C}^e \cdot \frac{\partial U}{\partial \mathbf{C}^e}) \quad (2.13)$$

Models that capture non-linearities have looked at mesoscale approaches that consider molecular mobility. One of the most commonly known models for amorphous SMPs is the work by Nguyen *et al.* [66, 67]. The authors based their work on the concept that the response of an SMP is dependent of time, temperature and structural mobility. A derivation from the Helmholtz free energy was used to obtain the stress relationships. Notice that the equation of the Helmholtz free energy is  $\psi = U - T\zeta$ , where  $U$  is the internal energy and  $\zeta$  is the entropy of the system. Nguyen *et al.* [66] used the Adam-Gibbs model to describe the mechanical properties between and above  $T_g$  and used the Williams-Landel-Ferry (WLF) model and the Arrhenius model below  $T_g$ . In their review, Nguyen *et al.* [67] describe in detail their proposed model. A 1D model representation can be seen in Figure 2.5. Their model has divided the total strain  $\varepsilon$  into a thermal and mechanical strain decomposition,  $\varepsilon_{th}$  and  $\varepsilon_{me}$  respectively. At the same time, the mechanical strain was decomposed into elastic ( $\varepsilon_{me}^e$ ) and viscous strains ( $\varepsilon_{me}^v$ ). Thermal strains were segmented into three parts, an instantaneous response paired with structural relaxation and thermal strains that drive the system to equilibrium, these were developed using a fictive temperature internal state variable.

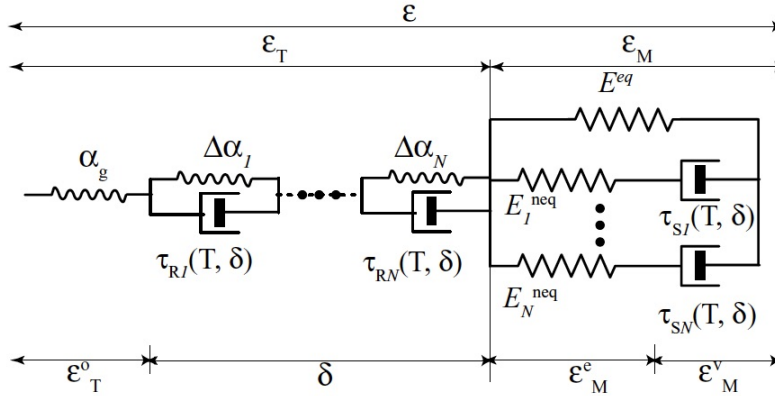


Figure 2.5: Representation of a 1D version of Nguyen *et al.*'s [67] model. Where descriptions for equilibrium and non-equilibrium are represented by *eq* and *neq*. The figure shows, Kelvin and Maxwell elements coupled until the Nth element. Reprinted with permission of [67]

Srivastava *et al.* [84] also used internal state variables to macroscopically represent the resistance to plastic flow of the polymer via micromechanisms ( $\gamma = 1, 2, 3$ ). By looking at the intermolecular (rotations of main-chain segments of the polymer) and molecular network resistance (rotations of the side groups), the model can capture the physics of the material in contrast to other modelling approaches (i.e. the phase change approach). When looking at temperatures below  $T_g$ , their model considers two micromechanisms, while three micromechanisms are used above  $T_g$  [84]. Each micromechanism can be associated with a spring-dashpot configuration.

For the first proposed micromechanism ( $\gamma = 1$ ), a nonlinear spring represents the elastic resistance to intermolecular and intramolecular bond stretching, while the dashpot represents resistance to plastic flow attributed to chain-segment rotations and slippage of polymer chains. An additional spring in parallel with the dashpot is placed for energy storage and captures local elastic incompatibilities produced by a viscoplastic flow mechanism. Micromechanisms two and three ( $\gamma = 2, 3$ ) as can be seen in Figure 2.6, are a combination of a nonlinear spring and a dashpot. The spring represents the elastic response of the stretching of the molecular chains between the mechanical cross-links. The dashpots represent thermally-activated plastic flow due to slippage of the mechanical cross-links, which are relatively strong below  $T_g$ . Unlike other models, this technique was able to capture the nonlinear hardening observed at large strains as well as the unloading response of the materials.

A common argument against the spring-dashpot modelling technique is the tedious experimentation that has to be implemented to obtain material parameters. Adding more elements to a spring-dashpot model can acquire a better material's behaviour description, however more experimentation needs to be done to acquire material parameters. The obtention of material parameters must be approached with care in order to avoid unstable material parameters. The use of fractional calculus-based constitutive models address this problem by reducing the number of material parameters needed to describe SMPs. In their work, Fang *et al.* [20] compared the fractional calculus approach to classical viscoelasticity to demonstrate the efficacy of the calculus based model. While classical viscoelasticity bases on the Kelvin and Maxwell viscoelastic models, fractional rheological models are based on the Koeller's 'spring-pot'. The constitutive law of this element can be seen in equation 2.14. Where,  $\sigma$ ,  $\varepsilon$ ,  $t$ ,  $E$  and  $\mu$  are the stress, strain, time, Young's modulus, viscosity, and therefore  $\tau$  is the relaxation time.  $D^\chi$  indicates fractional differentiation and  $\chi$  is the fractional derivative parameter between 0 and 1.

$$\sigma(t) = E^{1-\chi} \mu^\chi D^\chi \varepsilon(t) = E \tau^\chi D^\chi \varepsilon(t) \quad (2.14)$$

As such, many of the fractional models can be obtained correspondingly from the spring-pot configuration, such as the Poynting-Thomson model used in Fang *et al.*'s [20] work. With this technique,

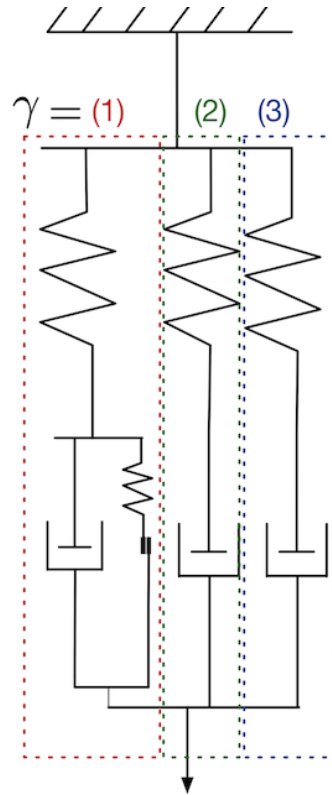


Figure 2.6: Representation of a 1D version of Srivastava *et al.*'s [84] model. The figure shows the micromechanisms implemented in a spring-dashpot representation

the authors required static and dynamic tests to obtain material parameters; such as the relaxation moduli and storage and loss factor data. The authors' model good fit to experimental data and simulated the isothermal recovery of an amorphous SMP.

### 2.3.2 Models based on Phase Change

Section 2.2.1 explained in detail the morphological structure of most SMPs. Although physically, amorphous polymers do not have a crystalline phase, researchers have argued that cross-links or even small fractions of polymer chains that possess a different morphology from the rest of the material can be regarded as a phase [59] and therefore a physical evidence of this morphology may not be necessarily present. This modelling technique has been applied to a range of materials. The concept of frozen and active phases has been explored in the area of SMA decades before applying them to SMP [102, 43, 2, 1, 64]. Unified modelling attempts of the SME in SMA and

SMP following this concept has been performed by Rogovoy *et al.* following the same phase change concept [75].

Models based on phase change have considered the physics of phase transition at the mesoscopic level. They typically propose that the SME consists of an anchoring mechanism within a movable polymeric phase also referred as frozen/glassy or active/rubbery phases respectively. The phase change concept includes the transformation of a frozen phase into an active phase and viceversa. Important thermodynamic characteristics to consider were described by Lendlein *et al.* [47]. At the beginning of the programming of the SME, below the transition temperature  $T_{trans}$ , the SMP and therefore its two phases (frozen and active) will act as an elastic solid, which may behave isotropically or an-isotropically as is the case for semi-crystalline polymers having oriented crystalline structures. Once the temperature reaches the  $T_{trans}$  range, commonly considered between ( $T_{trans} - 10^\circ C$  and  $T_{trans} + 50^\circ C$ ), the active phase produces the polymer to behave as an entropic rubber, making the polymer softer to deformation. After deformation of the programming step and following a cool down step,  $T < T_{trans}$ , both active and frozen phases return to their frozen state, which will cause them to lock entropy changes produced by a lack of chain movement. Consequently, this effect produces an energy storage within the internal energy. More specifically, for semi-crystalline polymers, the structure is made of a crystalline phase and an amorphous phase. Figure 2.7 represents a phase change before and after shape programming and recovery. Initially the material has an initial frozen crystalline phase represented as dark blue segments within an amorphous gray structure. After thermomechanical shape programming has occurred and as the polymer cools down, temporarily frozen segments coming from the amorphous region will form setting the shape, these are represented as light blue. When the temperature is raised above the transition region, these segments vanish, and yield the original configuration. The phase change produced during this procedure is considered to be a dissipative phenomena. It is to be noted that a phase change must be temperature and time dependent and therefore it should be represented as a continuous process.

The first approach to modelling SMP with this technique was done by Liu *et al.* [57]. The model was constrained for small deformations and was described with a 1D formulation, additionally it used on a glassy amorphous thermoset (Class I) polymer. It was assumed that the frozen and active phases within the structure add to the total composition. This concept is portrayed by equation 2.15, where  $\phi_f$  is the volume fraction of the frozen phase and  $\phi_a$  the volume fraction of the active phase. The frozen and active phases will vary to form the total state of the SMP [57].

$$\phi_f(T) = \frac{V_{frz}(T)}{V} \quad , \quad \phi_a = \frac{V_{act}}{V} \quad , \quad \phi_f + \phi_a = 1 \quad (2.15)$$

The mechanics of the material can be coupled between phases by assuming that the stress experi-

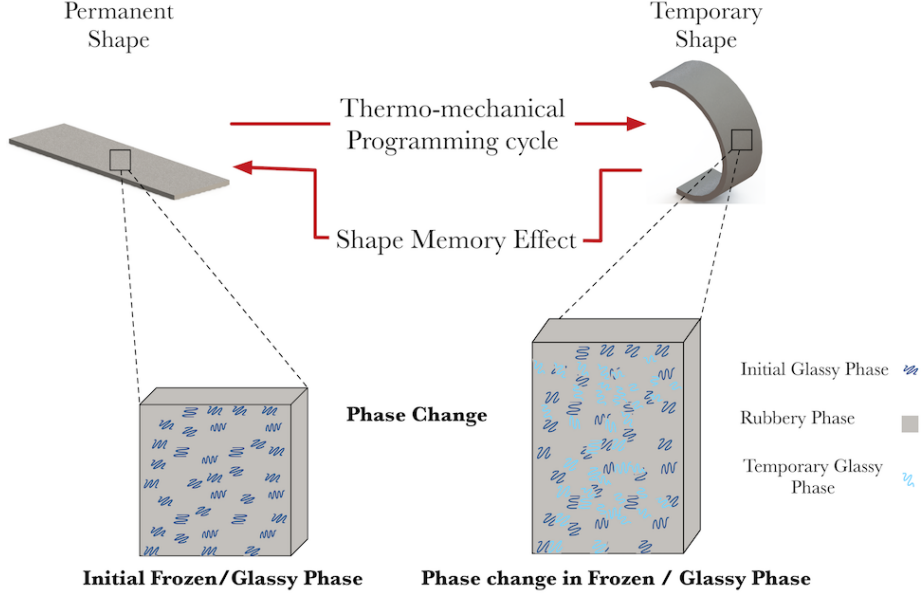


Figure 2.7: Representation of an SMP configuration before shape programming and later recovery

enced by the frozen phase  $\sigma_f$  is the same as that of the active phase  $\sigma_a$ , by  $\sigma_f = \sigma_a = \sigma$ , since both phases experience near perfect bondage. The strain  $\varepsilon$  can be described by  $\varepsilon = \phi_f \varepsilon_f + (1 - \phi_f) \varepsilon_a$ , where  $\varepsilon_f$  and  $\varepsilon_a$  are the strain of the frozen and active phase respectively. The mechanical evolution of the material can be described by determining a phase evolution law that transforms the material from frozen to active. The phase evolution law first proposed by Liu *et al.* [57] only depended on temperature, and as such, a fixed heating and cooling rate was defined (refer to Table 2.2 for evolution formula). Physically, however, the formation of phases is transient with time and at different points in time a newly formed phase will have different stress-free configurations [59]. The Helmholtz free energy function is then used to describe the energy storage after the thermo-mechanical training has occurred. Knowing that the mechanical strain  $\varepsilon_m = \varepsilon - \varepsilon_{str} - \varepsilon_{th}$ , the Helmholtz free energy can be defined by equation 2.16, where  $\psi_{mT}$  is compounded by the elastic mechanical, thermal energy and the initial energy with no storage. Therefore, the stress relationship for the thermomechanical process can be obtained by equation 2.17, and in the same manner the internal stress field that stores the entropic strain in the frozen phase ( $\sigma_{str}$ ) can be obtained.

$$\psi(\varepsilon, \varepsilon_{str}, T, \phi_f) = \psi_{mT}(\varepsilon_m, T, \phi_f) + \psi_{str}(\varepsilon_{str}, T) \quad (2.16)$$

$$\boldsymbol{\sigma} = \rho \frac{\partial \psi_{mT}}{\partial \varepsilon_m} \quad , \quad \boldsymbol{\sigma}_{str} = \frac{\partial \psi_{mT}}{\partial \varepsilon_m} \quad (2.17)$$

Similarly to the work proposed by Liu *et al.* [57] and Chen *et al.* [12], Chen *et al.*[13] developed a model based on the same micro-mechanical principle similar to that portrayed in equation (2.15). However, the authors proposed that Liu *et al.* [57] have only applied a storage of strain during cooling in their evolution law, therefore a strain recovery was derived by the authors to include the heating process. The authors later linearized the model for small deformations [13]. A detailed description of these models is presented in the work of Volk *et al.* [96].

The basic models mentioned before did not consider the phase evolution with respect to time. The authors of mentioned models justified this assumption by arguing that since shape programming occurs by holding the strain at a certain constant temperature, time effects are not relevant [59, 73]. However, plenty of experimental work has shown that shape holding time severely affects the SME (section 2.2.2). Since this modelling technique is based on the formation of a new phase with respect to temperature, a definition of a function  $\phi_f(T)$  is necessary. In their recent work, Yang *et al.* [111] provided a summary of the equations used to define the volume fraction of the phase evolution, which contains only works from a phase change approach, the summary is expanded to include a hybrid modelling approach and from recent advancements (section 2.3.2, 2.3.3, 2.4), shown in Table 2.2.

Table 2.2: Summary of frozen volume fraction function used, this has been adapted and completed from [111].

Reference	$\phi_f(T)$	Material Class	Dependency
[57]	$1 - \frac{1}{1+A(T_h-T)^n}$	I	$T$
[73]	$\frac{1}{1+e^{(-\frac{T-T_r}{A})}}$	I	$T$
[101]	$\alpha e^{-K(\frac{T}{T} \pm \tau)^m}$	I	$T$
[74]	$\frac{1}{1+e^{(2w(T-T_t))}}$	-	$T$
[97]	$C \frac{\tanh((T_h-A)/B) - \tanh((T-A)/B)}{\tanh((T_h-A)/B) - \tanh((T_l-A)/B)}$	III	$T$
[27]	$\left[ 1 - \left( \frac{T-T_l}{T_h-T_l} \right)^m \right]^n$	I	$T$
[30, 32]	$\int_T^{T_s} \frac{1}{S\sqrt{2\pi}} e^{-\frac{T-T_g}{2S^2}} dT$ , $S = \frac{T_h-T_g}{n}$	III	$T$
[111]	$1 - \int_{\infty}^{r_c(T)} p(r) dr \times \left\{ 1 - \left[ 1 - e^{\left( -\frac{\Delta H_a(T)}{k_B T} \right)} \right]^{\Delta t/\tau_0} \right\}$	I	$T, \dot{T}$

Each expression contains parameters i.e. A, B,  $T_r$ ,  $K$ ,  $n$  that need to be determined from a fit to experimental data.  $A$  and  $T_r$  are constants and can be determined by linear dielectric spectroscopy.  $T_h$  is the upper bound of the transition temperature usually at which deformation takes place, for example  $T_h = T_t + 20K$ , where  $T_t$  is the transition temperature and similarly for  $T_l$ . Other constants that have appeared during models are  $\lambda$  as the retardation time,  $\alpha$  the frozen final phase,  $w$  glass transition material parameter,  $K_b$  boltzman constant,  $\Delta H_a$  is defined as the energy barrier and  $\Delta/\tau_0$  as the heating rate term.

Other approaches to describe phase evolution have been more specific to certain materials. For instance Barot *et al.* [5] developed a constitutive model for crystallizable SMPs. The model used a predefined rate of crystallization and rate of melting to explain shape fixing and shape recovery. Again, the authors implemented the micro-mechanics equation in the total Helmholtz free energy (equation 2.16). This model was later improved and a thermodynamic framework was developed to further describe the crystallization process [6]. In their study, the authors proposed that in an entropy production process, the rate of entropy is maximized, and therefore the crystallization kinetics (the crystallized volume fraction) can be obtained. Time dependent modelling has also been proposed by Long *et al.* [59], where the authors proposed to obtain the mechanical response of the material by performing a convolution of deformation. Although the phase change model captures the crystallization process for semi-crystalline polymers. Discrepancies in models show that it is due to a viscoelastic behaviour that appears in the amorphous region of the polymer [79]. Therefore, a hybrid modelling approach would mitigate some of the discrepancies that older models have shown with respect to the observed experimental data.

### 2.3.3 Hybrid Models

Newer models have looked at a hybrid modelling approach, which integrates the spring-dashpot element modelling and some degree of phase change to capture the complete behaviour of the polymer. This method seems to describe more precisely semi-crystalline polymers, since each phase can be individually described by established models. Figure 2.8 shows an adapted version of a proposed methodology from the work of Li *et al.* and Yang *et al.* [50, 110]. The figure shows an individual description of each phase from which both models can be coupled to describe the SMP behaviour. Each phase can be coupled into a Representative Volume Element (RVE)

Different types of models describing each phase have been adopted. For semicrystalline polymers, specifically thermoplastic Polyurethane, Qi *et al.* [72] proposed a rate independent hyper-elastic rubbery spring that can capture softening of the material due to realignment of hard segments within the amorphous structure. This was coupled in parallel with a rate dependent viscoelastic-plastic component. Multiple shape memory cycles were studied and looked at, hence the authors argued that the behaviour of the material can be described by assuming that with time an evolution law of "effective" volume fraction between hard and soft domains differs between each cycle.

Other works such as that of Qi *et al.* [73] have segmented the shape memory behaviour with respect to the same ideology described by Liu *et al.* [57]. At the beginning of the process, the model proposes that the material will follow an initial glassy phase showing behaviours of viscoplasticity, followed by an isotropic hyperelastic material. Upon cooling the material is said to form a new frozen glassy phase. The glassy phase is best described by a 1D spring-dashpot system (Figure 2.9). In the same

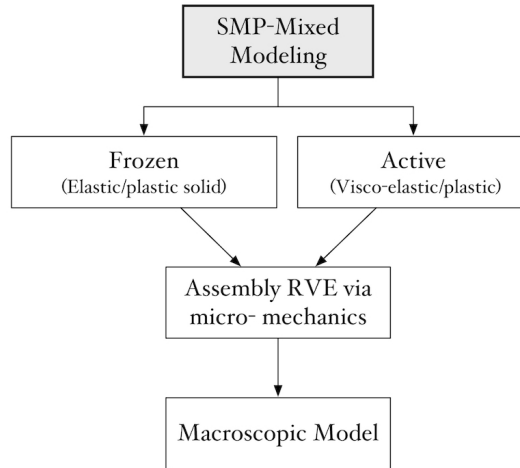


Figure 2.8: Model calculation flow chart. Figure adapted from [50].

manner, the isotropic behaviour can be modeled as a hyper-elastic spring based on the Langevin Arruda-Boyce eight chain model of the rubbery phase. As the deformation of the rubbery phase disappears, a new deformation is created for the frozen phase, which may not necessarily be the same to the common phase change model. As noted by Hu *et al.* [36] this model was not able to show the hysteresis in Stress-Temperature curves obtained in constrained recovery experiments but captured the general behaviour of the material appropriately.

Authors such as Kim *et al.* [42] have tried to model polyurethane based SMP (Class III) with segments corresponding to the hard segment (viscoelastic), soft frozen phase (hyperelastic) and the soft active phase (hyperelastic). The authors' model showed that the parallel arrangement of the elements behaved in a stiffer manner than the series mode and was more influenced by cooling rate. From the experiments of the constrained recovery, the parallel model seems to qualitatively capture better the SM performance.

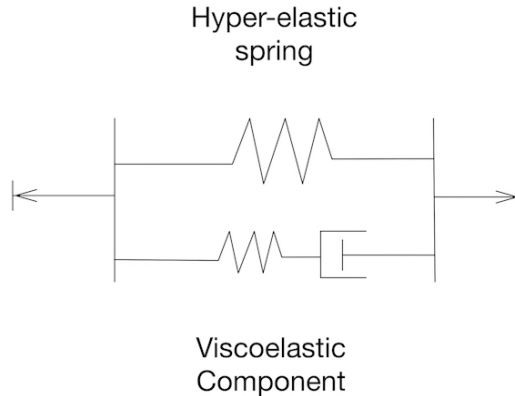


Figure 2.9: Spring-dashpot model representation of an SMP at the glassy initial phase. Figure adapted from [73]

## 2.4 Recent Modelling Techniques and Developments

The previous sections summarized the works that has been previously reviewed by many authors. In this section we have considered to include some of the more recently employed techniques.

Recent developments in the field have focused on improving and obtaining more thorough descriptions of the irrecoverable strain. Xiao *et al.* [107] established, in good agreement with experiments, a direct relationship between stress relaxation modulus at the end of the shape programming and the final recovery percentage by using a generalized Maxwell model and previous modelling techniques by Nguyen *et al.* [66, 67]. This relationship was applied for preliminary design studies in the work by Ge *et al.* [26].

Authors have also focused on modelling techniques that describe the glass transition phenomena of SMP, such as the use of internal state variables (variables representing the microstructure of the system), among those works are [107, 105, 106, 3, 4, 28]. When the material exhibits a history dependent behaviour, the material cannot be characterized by only current conditions. As such, a common approach has been to use a fictive temperature, as described by Tool *et al.* [95], which describes the temperature at which a glass will be in equilibrium after sudden cool down. It is mainly used to model structural relaxation processes. The fictive temperature is used as an internal variable that describes the structure in the transition range. Hence the final temperature of the material can be predicted by the temperature at which the structure is in equilibrium,  $T$ , and the final temperature,  $T_f$  as defined by (2.18), where the constant  $\tau_R$  is a factor inversely proportional to the viscosity of the material [66, 67]. Other internal state variables have also been implemented when modelling, Gu *et al.*[28] provide an excellent review of internal state variables

used when modelling amorphous SMP. A high fidelity between experimental and modelling data has been shown by using internal state variables [45]. The mentioned authors have also suggested that further work should be developed to take into account more internal state variables and represent properties at the glass transition range with higher precision.

$$\frac{dT_f}{dt} = -\frac{1}{\tau_R}(T_f - T) \quad (2.18)$$

Works have also focused on capturing non-linearities by defining the strain energy density of the material from statistical and continuum mechanics. Authors have used a meso-scale approach by using statistical mechanics with the use of the 8-chain Arruda-Boyce model [103, 84, 83, 85, 71, 28] to describe the material behaviour at high temperatures (the response at the rubbery phase) by capturing the molecular dynamics of the material such as the chain straightening and alignment. Models that use the viscoelastic response have modeled the hyperelastic response of SMPs is commonly by Neo-Hookean and Money-Rivlin models [10, 14, 8]. These material responses are usually coupled by using the decomposition of the deformation gradient  $\mathbf{F}$  into elastic and stored parts.

Different approaches have been investigated with respect to the decomposition of the deformation gradient. Chen *et al.* [10] proposed to separate the deformation gradient  $\mathbf{F}$  into a mechanical and thermal parts, where the mechanical part constitutes of the multiplicative decomposition of elastic and viscous elements  $\mathbf{F}^e \mathbf{F}^v$ , and the thermal part  $\mathbf{F}^{th}$  is responsible for thermal strains. Bouaziz *et al.* [8] propose to change the multiplicative decomposition into an elastic deformation gradient in the rubbery phase  $\mathbf{F}^e$  and a deformation gradient stored by the crystalline phase after the cooled down process  $\mathbf{F}^{str}$ . In the same manner they considered the crystalline volume fraction as part of their deformation gradient as seen in equation 2.19, where  $\mathbf{H}$  is the displacement gradient tensor and  $\mathbf{I}$  is the identity tensor.

$$\mathbf{F}_s = \mathbf{I} + \phi_f(T)\mathbf{H} \quad (2.19)$$

Advancements in the phase change modelling technique include the implementation of new phases to describe additional hard segments. Guo *et al.* [32] stated that an SMP consists of many molecule chains with different lengths and angles, and therefore the entropy of each chain will differ from others. Consequently, each group of molecules with the same phase transition temperatures can be regarded as one phase. Instead of using a simple active and frozen phases model, a generalization can be made as  $\phi_f + \sum \phi_i = 1$ . Therefore,  $\phi_f(T)$  is regarded as an integral form (refer to Table 2.2). Approaches on the phase change modelling technique are continuously becoming more attractive since they treat the SMP as a composite material with a frozen phase matrix and an

active phase filler. For instance, Yang *et al.* [111] used Mori-Tanaka composite model approach to predict effective mechanical properties of SMP. This technique can later be expanded to describe SMPCs.

Recent approaches have also tried to improve the time dependency of the phase evolution after Long *et al.* [59], to describe of the phase evolution with physically obtainable parameters. The work of Yang *et al.* [111] based their work on the spatial heterogeneous dynamics theory proposed by Ediger [19] to obtain a phase evolution expression. The theory demonstrates that the phase transition behaves similarly to an energy level transition and as such, work must be applied to overcome the energy barrier. From these concepts Long *et al.* proposed a phase evolution dependent on both temperature and heating rate.

Much like previous modifications of the generalized hybrid modelling concept, Park *et al.* [69] proposed a Ponynting-Thomson model for the rubbery phase and a modified version of the model for the glassy phase. The latter consists of a viscoplastic and a shape memory strain element in series with the Ponynting-Thomson model (viscoelastic). The authors defined this shape memory strain element as a storage strain that occurs during programming. The work showed a good accuracy when modelling a SMP sheet subjected to uniaxial deformations. Guo *et al.*[29] propose a definition of an active and a frozen phase as per previous models but each phase consists of three and four viscoelastic elements. Additionally two springs in parallel to describe the thermal expansion at high and low temperatures represented of the SMP.

Studies are also focusing on the multiple SME (explained in section 2.2) as developed by Xiao *et al.* [105] and Wang *et al.*[100]. Xiao *et al.*[105] implemented a simple finite deformation, nonlinear viscoelastic model to describe multiple shape memory effect of a Nafion membrane. Among other works, researchers have looked at cold-drawing of SMPs as a programming alternative. Li *et al.* [52] developed a viscoelastic visco-plastic model to capture the recovery of amorphous thermoset polymers under compression. They first adopted the modelling technique from Nguyen *et al.* [66] (equilibrium and nonequilibrium configuration) and later implemented a Narayanaswamy-Moynihan model to determine the structural relaxation. Li *et al.* [51] proposed new formulas to estimate the recovery ratio and argue that SME due to cold programming was mainly due to energetic force instead of entropic energy, which is the one attributed to when modelling the most common SM cycle.

## 2.5 Discussion Points

Modelling of SMP carry a high importance on potential designs for industrial applications. Simple modelling techniques (1D approximations) may offer engineers a preliminary idea before design

implementation in a computer software. Most of the applications of SMP have been used in bending mode, with big deflections but small strains, however there are only a few models that have looked at this type of loading. Although classic thermo-viscoelasticity can predict the shape memory behaviour around the transition temperature there are nonlinearities observed which appear at strains bigger than 3% [93]. Therefore a simple model that captures the behaviour of these materials will perform better with these nonlinearities needs to be considered. Models have tried to capture non-linearities by using rubber elasticity theories in the statistical and continuum mechanics field, care must be taken when obtaining parameter estimations [9].

Extensive and sophisticated modelling approaches have emerged in recent years with the aim to improve the prediction of the material behaviour. This is specially important for high precision applications such as those in micro-mechanical systems [83]. Much effort has been devoted to obtain high accuracy with different modelling techniques and although a common argument against these extense models is the tedious acquirement of material parameters by experimentation, a clear counter argument is that the material calibration may only have to be performed once for the use of the model on different applications. For instance the model may be implemented after in different loading conditions via a finite element software.

There has been much criticism on the frozen and active phases modelling techniques, since there is no physical evidence supporting that the polymer has frozen and active phases [83], although it could be argued that a phase distinction could be found in semi-crytalline polymers and a correction may be made to phases by grouping different morphologies within the polymer. However, on its own, this technique cannot capture the viscoelastic behaviour of a very popular class of SMP (semi-crystalline polymers). Obtainment of material parameters while using the phase change modelling approach has also been shown to be difficult since there is no physical way of determining the change of the volume fraction [107]. Even from Table 2.2 as stated by Yang *et al.*[111], the expressions relating volume fraction to temperature include many parameters that are physically unattainable. Recent works such as that by Yang *et al.* [111] have tried to implement relationships that are developed from a physical point of view, their obtained expression for the  $\phi_f$  can be seen in Table 2.2.

A hybrid modelling approach has been able to capture with high fidelity the SME of SMPs. This is particularly important since these approaches can be used for application where the multi-functionality of the material is further tailored by adding filler materials.

## 2.6 Conclusions

In this work, a general summary, explanation and review of the most recent modelling techniques for SMP has been presented. The work has classified the modelling techniques into three different kinds, those composed of Spring-Dashpot components (section 2.3.1), a Phase Change (section 2.3.2) and a hybrid modelling approach (section 2.3.3). The review provides with discussion points for current modelling techniques of SMP and a few discussion points to consider for those that would like to implement and start developing and applying a modelling methodology. Through this review, a gap in the literature was recognized. Although there have been many advances and complex models with high accuracy that have been proposed, there is still a lack of models that are easy to apply and comprehend. These models are particularly very important for engineers to start designing engineering applications with SMPs. Basic traits such as recovery time, speed, force and ratio are necessary to start designing. Particular little to no attention has been provided to one of the most important loading configurations, which is bending. Furthermore, most of the models assume isothermal conditions, although real engineering applications require of transient models to predict the recovery properties of SMPs.

## 2.7 References

- [1] F Auricchio, A Reali, and U Stefanelli. A three-dimensional model describing stress-induced solid phase transformation with permanent inelasticity. *International Journal of Plasticity*, 23(2):207–226, February 2007.
- [2] Ferdinando Auricchio and Lorenza Petrini. A three-dimensional model describing stress-temperature induced solid phase transformations: solution algorithm and boundary value problems. *International Journal for Numerical Methods in Engineering*, 61(6):807–836, October 2004.
- [3] Olaniyi A Balogun and Changki Mo. Shape memory polymers - Energy method superposition constitutive modeling. In *ASME 2014 Conference on Smart Materials, Adaptive Structures and Intelligent Systems, SMASIS 2014*. Washington State University Tri-Cities, Richland, United States, January 2014.
- [4] Olaniyi A Balogun and Changki Mo. Shape memory polymers - Viscoelastic thermomechanical constitutive modeling. In *ASME 2014 Conference on Smart Materials, Adaptive Structures and Intelligent Systems, SMASIS 2014*. Washington State University Tri-Cities, Richland, United States, January 2014.

- [5] G Barot and I J Rao. Constitutive modeling of the mechanics associated with crystallizable shape memory polymers. *Zeitschrift für angewandte Mathematik und Physik*, 57(4):652–681, March 2006.
- [6] G Barot, I J Rao, and K R Rajagopal. A thermodynamic framework for the modeling of crystallizable shape memory polymers. *International Journal of Engineering Science*, 46(4):325–351, April 2008.
- [7] Rahul Bhattacharyya, Claudio Di Leo, Christian Floerkemeier, Sanjay Sarma, and Lallit Anand. RFID tag antenna based temperature sensing using shape memory polymer actuation. In *Proceedings of IEEE Sensors*, pages 2363–2368. Massachusetts Institute of Technology, Cambridge, United States, IEEE, December 2010.
- [8] R Bouaziz, F Roger, and K Prashantha. Thermo-mechanical modeling of semi-crystalline thermoplastic shape memory polymer under large strain. *Smart Materials and Structures*, 26(5):055009, April 2017.
- [9] M C Boyce and E M Arruda. Constitutive models of rubber elasticity: A review. *Rubber Chemistry and Technology*, 73(3):504–523, January 2000.
- [10] Jianguo Chen, Liwu Liu, Yanju Liu, and Jinsong Leng. Thermoviscoelastic shape memory behavior for epoxy-shape memory polymer. *Smart Materials and Structures*, 23(5):055025, May 2014.
- [11] Xiang Chen and Thao D Nguyen. Influence of thermoviscoelastic properties and loading conditions on the recovery performance of shape memory polymers. *Mechanics of Materials*, 43(3):127–138, March 2011.
- [12] Yi-Chao Chen and Dimitris C Lagoudas. A constitutive theory for shape memory polymers. Part I. *Journal of the Mechanics and Physics of Solids*, 56(5):1752–1765, May 2008.
- [13] Yi-Chao Chen and Dimitris C Lagoudas. A constitutive theory for shape memory polymers. Part II. *Journal of the Mechanics and Physics of Solids*, 56(5):1766–1778, May 2008.
- [14] Fangda Cui, Swapnil Moon, and I Rao. Modeling the Viscoelastic Behavior of Amorphous Shape Memory Polymers at an Elevated Temperature. *Fluids*, 1(4):15, December 2016.
- [15] Julie Diani, Pierre Gilormini, Carole Frédy, and Ingrid Rousseau. Predicting thermal shape memory of crosslinked polymer networks from linear viscoelasticity. *International Journal of Solids and Structures*, 49(5):793–799, March 2012.
- [16] Julie Diani, Yiping Liu, and Ken Gall. Finite strain 3D thermoviscoelastic constitutive model for shape memory polymers. *Polymer Engineering & Science*, 46(4):486–492, 2006.

- [17] N J Distefano and K S Pister. On the identification problem for thermorheologically simple materials. *Acta Mechanica*, 13(3-4):179–190, September 1972.
- [18] Jiri George Drobny. *Handbook of Thermoplastic Elastomers*. PDL/Plastics Design Library. William Andrew, 2007.
- [19] M D Ediger. Spatially heterogeneous dynamics in supercooled liquids. *Annual review of physical chemistry*, 51:99–128, 2000.
- [20] C Q Fang, H Y Sun, and J P Gu. Application of Fractional Calculus Methods to Viscoelastic Response of Amorphous Shape Memory Polymers. *Journal of Mechanics*, 31(4):427–432, January 2015.
- [21] S Felton, M Tolley, E Demaine, D Rus, and R Wood. A method for building self-folding machines. *Science*, 345(6):644–646, August 2014.
- [22] S Felton, M Tolley, E Demaine, D Rus, and R Wood. Applied origami. A method for building self-folding machines. *Science*, 345(6197):644–646, August 2014.
- [23] S M Felton, K P Becker, D M Aukes, and R J Wood. Self-folding with shape memory composites at the millimeter scale. *Journal of Micromechanics and Microengineering*, 25(8):085004, August 2015.
- [24] I T Garces and C. Ayranci. A view into additive manufactured electro-active reinforced smart composite structures. *Manufacturing Letters*, 16:1–5, April 2018.
- [25] Qi Ge, Conner K Dunn, H Jerry Qi, and Martin L Dunn. Active origami by 4D printing. *Smart Materials and Structures*, 23(9):094007–16, August 2014.
- [26] Qi Ge, Kai Yu, Yifu Ding, and H Jerry Qi. Prediction of temperature-dependent free recovery behaviors of amorphous shape memory polymers. *Soft Matter*, 8:11098–, 2012.
- [27] Pierre Gilormini and Julie Diani. On modeling shape memory polymers as thermoelastic two-phase composite materials. *Comptes Rendus Mécanique*, 340(4-5):338–348, April 2012.
- [28] Jianping Gu, Jinsong Leng, and Huiyu Sun. A constitutive model for amorphous shape memory polymers based on thermodynamics with internal state variables. *Mechanics of Materials*, 111:1–14, August 2017.
- [29] Jianming Guo, Jingbiao Liu, Zhenqing Wang, Xiaofu He, Lifeng Hu, Liyong Tong, and Xiaojun Tang. A thermodynamics viscoelastic constitutive model for shape memory polymers. *Journal of Alloys and Compounds*, 705:146–155, May 2017.

- [30] Xiaogang Guo, Liwu Liu, Yanju Liu, Bo Zhou, and Jinsong Leng. Constitutive model for a stress- and thermal-induced phase transition in a shape memory polymer. *Smart Materials and Structures*, 23(10):105019, October 2014.
- [31] Xiaogang Guo, Liwu Liu, Bo Zhou, Yanju Liu, and Jinsong Leng. Influence of strain rates on the mechanical behaviors of shape memory polymer. *Smart Materials and Structures*, 24(9):095009, September 2015.
- [32] Xiaogang Guo, Liwu Liu, Bo Zhou, Yanju Liu, and Jinsong Leng. Constitutive model for shape memory polymer based on the viscoelasticity and phase transition theories. *Journal of Intelligent Material Systems and Structures*, 27(3):314–323, February 2016.
- [33] Martin D Hager, Stefan Bode, Christine Weber, and Ulrich S Schubert. Shape memory polymers: Past, present and future developments. *Progress in Polymer Science*, 49-50:3–33, October 2015.
- [34] Seok Jin Hong, Woong-Ryeol Yu, and Ji Ho Youk. Two-way shape memory behavior of shape memory polyurethanes with a bias load. *Smart Materials and Structures*, 19(3):035022, March 2010.
- [35] Seok Jin Hong, Woong-Ryeol Yu, Ji Ho Youk, and Yang Rae Cho. Polyurethane smart fiber with shape memory function: Experimental characterization and constitutive modelling. *Fibers and Polymers*, 8(4):377–385, 2007.
- [36] Jinlian Hu, Yong Zhu, Huahua Huang, and Jing Lu. Recent advances in shape-memory polymers: Structure, mechanism, functionality, modeling and applications. *Progress in Polymer Science*, 37(12):1720–1763, December 2012.
- [37] H M Jeong, J B Lee, S Y Lee, and B K Kim. Shape memory polyurethane containing mesogenic moiety. *Journal of Materials Science*, 35(2):279–283, 2000.
- [38] H U Jinlian. *Shape memory polymers and textiles*. Woodhead Publishing Limited, Hong Kong Polytechnic University, Kowloon, Hong Kong, January 2007.
- [39] Seno Jose, Jinu Jacob George, Suchart Siengchin, and Jyotishkumar Parameswaranpillai. Introduction to Shape-Memory Polymers, Polymer Blends and Composites: State of the Art, Opportunities, New Challenges and Future Outlook. In *Shape Memory Polymers, Blends and Composites*, pages 1–19. Springer, Singapore, Singapore, 2020.
- [40] Ayesha Kausar. Review on Technological Significance of Photoactive, Electroactive, pH-sensitive, Water-active, and Thermoresponsive Polyurethane Materials. *Polymer-Plastics Technology and Engineering*, 56(6):606–616, October 2016.

- [41] Hossein Ali Khonakdar, Seyed Hassan Jafari, Sorour Rasouli, Jalil Morshedian, and Hossein Abedini. Investigation and Modeling of Temperature Dependence Recovery Behavior of Shape-Memory Crosslinked Polyethylene. *Macromolecular Theory and Simulations*, 16(1):43–52, January 2007.
- [42] Ju Hyun Kim, Tae Jin Kang, and Woong-Ryeol Yu. Thermo-mechanical constitutive modeling of shape memory polyurethanes using a phenomenological approach. *International Journal of Plasticity*, 26(2):204–218, February 2010.
- [43] S Leclercq and C LExcellent. A general macroscopic description of the thermomechanical behavior of shape memory alloys. *Journal of the Mechanics and Physics of Solids*, 44(6):953–980, 1996.
- [44] E H Lee, American Society of Mechanical Engineers, and STANFORD UNIV CALIF DEPT OF APPLIED MECHANICS. *Elastic-plastic Deformation at Finite Strains*. 1968.
- [45] Ming Lei, Kai Yu, Haibao Lu, and H Jerry Qi. Influence of structural relaxation on thermomechanical and shape memory performances of amorphous polymers. *Additive Manufacturing*, 109:216–228, January 2017.
- [46] Andreas Lendlein, Marc Behl, Bernhard Hiebl, and Christian Wischke. Shape-memory polymers as a technology platform for biomedical applications. *Expert Review of Medical Devices*, 7(3):357–379, May 2010.
- [47] Andreas Lendlein and Steffen Kelch. *Shape-Memory Polymers*. John Wiley & Sons, Inc., Hoboken, NJ, USA, 2002.
- [48] Jinsong Leng, Xin Lan, Yanju Liu, and Shanyi Du. Shape-memory polymers and their composites: Stimulus methods and applications. *Progress in Materials Science*, 56(7):1077–1135, September 2011.
- [49] Christian LExcellent, Pauline Butaud, Emmanuel Folt te, and Morvan Ouisse. A Review of Shape Memory Polymers Thermomechanical Modelling: Analysis in the Frequency Domain. In *Advances in Shape Memory Materials*, pages 57–80. Springer International Publishing, Cham, March 2017.
- [50] Guoqiang Li. *Self-Healing Composites: Shape Memory Polymer Based Structures*. John Wiley & Sons Ltd, Chichester, United Kingdom, November 2014.
- [51] Guoqiang Li and Anqi Wang. Cold, warm, and hot programming of shape memory polymers. *Journal of Polymer Science Part B: Polymer Physics*, 54(14):1319–1339, March 2016.

- [52] Guoqiang Li and Wei Xu. Thermomechanical behavior of thermoset shape memory polymer programmed by cold-compression: Testing and constitutive modeling. *Journal of the Mechanics and Physics of Solids*, 59(6):1231–1250, June 2011.
- [53] J R Lin and L W Chen. Shape-memorized crosslinked ester-type polyurethane and its mechanical viscoelastic model. *Journal of Applied Polymer Science*, 73(7):1305–1319, 1999.
- [54] C Liu, H Qin, and P T Mather. Review of progress in shape-memory polymers. *Journal of Materials Chemistry*, 17(16):1543, 2007.
- [55] Changdeng Liu, Seung B Chun, Patrick T Mather, Lei Zheng, Elisabeth H Haley, and E Bryan Coughlin. Chemically cross-linked polycyclooctene: Synthesis, characterization, and shape memory behavior. *Macromolecules*, 35(27):9868–9874, December 2002.
- [56] Yanju Liu, Haiyang Du, Liwu Liu, and Jinsong Leng. Shape memory polymers and their composites in aerospace applications: a review. *Smart Materials and Structures*, 23(2):023001, February 2014.
- [57] Yiping Liu, Ken Gall, Martin L Dunn, Alan R Greenberg, and Julie Diani. Thermomechanics of shape memory polymers: Uniaxial experiments and constitutive modeling. *International Journal of Plasticity*, 22(2):279–313, February 2006.
- [58] F J Lockett. *Nonlinear viscoelastic solids*. London, New York, Academic Press, 1972.
- [59] Kevin N Long, Martin L Dunn, and H Jerry Qi. Mechanics of soft active materials with phase evolution. *International Journal of Plasticity*, 26(4):603–616, April 2010.
- [60] Patrick T Mather, Xiaofan Luo, and Ingrid A Rousseau. Shape Memory Polymer Research. *Annual Review of Materials Research*, 39:445–471, August 2009.
- [61] Amber J W McClung, Gyaneshwar P Tandon, and Jeffery W Baur. Deformation rate-, hold time-, and cycle-dependent shape-memory performance of Veriflex-E resin. *Mechanics of Time-Dependent Materials*, 17(1):39–52, February 2013.
- [62] Milad Momtaz, Mohammad Razavi-Nouri, and Mehdi Barikani. Effect of block ratio and strain amplitude on thermal, structural, and shape memory properties of segmented polycaprolactone-based polyurethanes. *Journal of Materials Science*, 49:7575–7584, November 2014.
- [63] Jalil Morshedian, Hossein A Khonakdar, and Sorour Rasouli. Modeling of Shape Memory Induction and Recovery in Heat-Shrinkable Polymers. *Macromolecular Theory and Simulations*, 14(7):428–434, August 2005.

- [64] Ziad Moumni, Wael Zaki, and Quoc Son Nguyen. Theoretical and numerical modeling of solid-solid phase change: Application to the description of the thermomechanical behavior of shape memory alloys. *International Journal of Plasticity*, 24(4):614–645, April 2008.
- [65] Robin M Neville, Jianguo Chen, Xiaogang Guo, Fenghua Zhang, Wenxin Wang, Yousef Dobah, Fabrizio Scarpa, Jinsong Leng, and Hua-Xin Peng. A Kirigami shape memory polymer honeycomb concept for deployment. *Smart Materials and Structures*, 26(5):05LT03, April 2017.
- [66] Thao D Nguyen, H Jerry Qi, Francisco Castro, and Kevin N Long. A thermoviscoelastic model for amorphous shape memory polymers: Incorporating structural and stress relaxation. *Journal of the Mechanics and Physics of Solids*, 56(9):2792–2814, 2008.
- [67] Thao D Nguyen, Christopher M Yakacki, Parth D Brahmhatt, and Matthew L Chambers. Modeling the relaxation mechanisms of amorphous shape memory polymers. *Advanced materials (Deerfield Beach, Fla.)*, 22(31):3411–3423, August 2010.
- [68] Cem Ozan, Wouter Van Der Zee, Martin Brudy, and Justin Vinson. Mechanical Modeling of Shape Memory Polyurethane Foam for Application as a Sand Management Solution. In *SPE Annual Technical Conference and Exhibition*. Society of Petroleum Engineers, 2011.
- [69] Haedong Park, Philip Harrison, Zaoyang Guo, Myoung-Gue Lee, and Woong-Ryeol Yu. Three-dimensional constitutive model for shape memory polymers using multiplicative decomposition of the deformation gradient and shape memory strains. *Mechanics of Materials*, 93:43–62, October 2015.
- [70] Devendra Patil and Gangbing Song. A review of shape memory material’s applications in the offshore oil and gas industry. *Smart Materials and Structures*, 26(9):093002–18, August 2017.
- [71] E A Pieczyska, M Staszczak, M Maj, K Kowalczyk-Gajewska, K Golasiński, M Cristea, H Tobushi, and S Hayashi. Investigation of thermomechanical couplings, strain localization and shape memory properties in a shape memory polymer subjected to loading at various strain rates. *Smart Materials and Structures*, 25(8):085002, August 2016.
- [72] H J Qi and M C Boyce. Stress-strain behavior of thermoplastic polyurethanes. *Mechanics of Materials*, 37(8):817–839, August 2005.
- [73] H Jerry Qi, Thao D Nguyen, Francisco Castro, Christopher M Yakacki, and Robin Shandas. Finite deformation thermo-mechanical behavior of thermally induced shape memory polymers. *Journal of the Mechanics and Physics of Solids*, 56(5):1730–1751, May 2008.

- [74] S Reese, M Böl, and D Christ. Finite element-based multi-phase modelling of shape memory polymer stents. *Computer Methods in Applied Mechanics and Engineering*, 199(21-22):1276–1286, April 2010.
- [75] A A Rogovoy and O S Stolbova. Modeling the behaviour of shape memory materials under large deformations. *IOP Conference Series: Materials Science and Engineering*, 208(1):012036–, June 2017.
- [76] Ingrid A Rousseau and Tao Xie. Shape memory epoxy: Composition, structure, properties and shape memory performances. *Journal of Materials Chemistry*, 20(17):3431–3441, June 2010.
- [77] Takenobu Sakai, Takayuki Tao, and Satoshi Somiya. Estimation of creep and recovery behavior of a shape memory polymer. *Mechanics of Time-Dependent Materials*, 19(4):569–579, November 2015.
- [78] David Santiago, Francesc Ferrando, and Silvia De la Flor. Influence of holding time on shape recovery in a polyurethane shape-memory polymer. In *Journal of Materials Engineering and Performance*, pages 2567–2573. Universitat Rovira i Virgili, Tarragona, Spain, January 2014.
- [79] G Scalet, F Auricchio, E Bonetti, L Castellani, D Ferri, M Pachera, and F Scavello. An experimental, theoretical and numerical investigation of shape memory polymers. *International Journal of Plasticity*, 67:127–147, April 2015.
- [80] Ward Small, Patrick R Buckley, Thomas S Wilson, William J Benett, Jonathan Hartman, David Saloner, and Duncan J Maitland. Shape memory polymer stent with expandable foam: a new concept for endovascular embolization of fusiform aneurysms. *IEEE Transactions on Biomedical Engineering*, 54(6 Pt 2):1157–1160, June 2007.
- [81] Ward Small IV, Pooja Singhal, Thomas S Wilson, and Duncan J Maitland. Biomedical applications of thermally activated shape memory polymers. *Journal of Materials Chemistry*, 20(17):3356–11, 2010.
- [82] Witold Sokolowski, Annick Metcalfe, Shunichi Hayashi, L’Hocine Yahia, and Jean Raymond. Medical applications of shape memory polymers. In *Biomedical Materials*, pages S23–S27. Jet Propulsion Laboratory, California Institute of Technology, Pasadena, United States, March 2007.
- [83] V Srivastava. *large-deformation thermo-mechanically coupled elastic-viscoplastic theory for amorphous polymers: modeling of micro-scale forming and the shape memory phenomenon*. PhD thesis, Massachusetts Institute of Technology, 2010.

- [84] Vikas Srivastava, Shawn A Chester, Nicoli M Ames, and Lallit Anand. A thermo-mechanically-coupled large-deformation theory for amorphous polymers in a temperature range which spans their glass transition. *International Journal of Plasticity*, 26(8):1138–1182, August 2010.
- [85] Vikas Srivastava, Shawn A Chester, and Lallit Anand. Thermally actuated shape-memory polymers: Experiments, theory, and numerical simulations. *Journal of the Mechanics and Physics of Solids*, 58(8):1100–1124, August 2010.
- [86] Andrew Stevenson. Effect of crystallization on the mechanical properties of elastomers under large deformations. In *American Society of Mechanical Engineers, Applied Mechanics Division, AMD*, volume 203, pages 1–8, Materials Engineering Research Lab, Ltd, 1995.
- [87] Yu-Chen Sun, Yimei Wan, Ryan Nam, Marco Chu, and Hani E Naguib. 4D-printed hybrids with localized shape memory behaviour: Implementation in a functionally graded structure. *Scientific Reports*, 9(1):18754, December 2019.
- [88] C Thill, J Etches, I Bond, K Potter, and P Weaver. Morphing skins. *Aeronautical Journal*, 112(1129):117–139, January 2008.
- [89] H Tobushi, T Hashimoto, S Hayashi, and E Yamada. Thermomechanical constitutive modeling in shape memory polymer of polyurethane series. *Journal of Intelligent Material Systems and Structures*, 8(8):711–718, August 1997.
- [90] H Tobushi, T Hashimoto, N Ito, S Hayashi, and E Yamada. Shape Fixity and Shape Recovery in a Film of Shape Memory Polymer of Polyurethane Series. *Journal of Intelligent Material Systems and Structures*, 9(2):127–136, 1998.
- [91] H Tobushi, S Hayashi, K Hoshio, and N Miwa. Influence of strain-holding conditions on shape recovery and secondary-shape forming in polyurethane-shape memory polymer. *Smart Materials and Structures*, 15(4):1033–1038, August 2006.
- [92] Hisaaki Tobushi, Syunichi Hayashi, Kazumasa Hoshio, and Yoshihiro Ejiri. Shape recovery and irrecoverable strain control in polyurethane shape-memory polymer. *Science and Technology of Advanced Materials*, 9(1):015009, January 2008.
- [93] Hisaaki Tobushi, Kayo Okumura, Shunichi Hayashi, and Norimitsu Ito. Thermomechanical constitutive model of shape memory polymer. *Mechanics of Materials*, 33(10):545–554, October 2001.
- [94] Michael T Tolley, Samuel M Felton, Shuhei Miyashita, Lily Xu, ByungHyun Shin, Monica Zhou, Daniela Rus, and Robert J Wood. Self-folding shape memory laminates for automated

- fabrication. In *IEEE International Conference on Intelligent Robots and Systems*, pages 4931–4936. Harvard University, Cambridge, United States, IEEE, December 2013.
- [95] A Q Tool. Viscosity and the Extraordinary Heat Effects in Glass. *Journal of Research of the National Bureau of Standards*, 37(2):73–90, 1946.
- [96] Brent L Volk, Dimitris C Lagoudas, and Yi-Chao Chen. Analysis of the finite deformation response of shape memory polymers: II. 1D calibration and numerical implementation of a finite deformation, thermoelastic model. *Smart Materials and Structures*, 19(7):075006–12, May 2010.
- [97] Brent L Volk, Dimitris C Lagoudas, and Duncan J Maitland. Characterizing and modeling the free recovery and constrained recovery behavior of a polyurethane shape memory polymer. *Smart Materials and Structures*, 20(9):094004, 2011.
- [98] Anqi Wang, Guoqiang Li, and Harper Meng. Strain rate effect on the thermomechanical behavior of a thermoset shape memory polymer. *Smart Materials and Structures*, 22(8):085033, August 2013.
- [99] Kaojin Wang, Satu Strandman, and X X Zhu. A mini review: Shape memory polymers for biomedical applications. *Frontiers of Chemical Science and Engineering*, 11(2):143–153, April 2017.
- [100] Xiaodong Wang, Haibao Lu, Xiaojuan Shi, Kai Yu, and Yong Qing Fu. A thermomechanical model of multi-shape memory effect for amorphous polymer with tunable segment compositions. *Composites Part B: Engineering*, 160:298–305, March 2019.
- [101] Z D Wang, D F Li, Z Y Xiong, and R N Chang. Modeling thermomechanical behaviors of shape memory polymer. *Journal of Applied Polymer Science*, 113(1):651–656, July 2009.
- [102] P Wollants, J R Roos, and L Delaey. Thermally- and stress-induced thermoelastic martensitic transformations in the reference frame of equilibrium thermodynamics. *Progress in Materials Science*, 37(3):227–288, January 1993.
- [103] Y S Wong, Z H Stachurski, and S S Venkatraman. Modeling shape memory effect in uncrosslinked amorphous biodegradable polymer. *Polymer*, 52(3):874–880, February 2011.
- [104] Jiangtao Wu, Chao Yuan, Zhen Ding, Michael Isakov, Yiqi Mao, Tiejun Wang, Martin L Dunn, and H Jerry Qi. Multi-shape active composites by 3D printing of digital shape memory polymers. *Nature Publishing Group*, 6(1):773, April 2016.
- [105] Rui Xiao, Jingkai Guo, and Thao D Nguyen. Modeling the multiple shape memory effect and temperature memory effect in amorphous polymers. *RSC Advances*, 5(1):416–423, 2015.

- [106] Rui Xiao and Thao D Nguyen. Thermo-mechanics of Amorphous Shape-memory Polymers. *Procedia IUTAM*, 12:154–161, 2015.
- [107] Rui Xiao, Christopher M Yakacki, Jingkai Guo, Carl P Frick, and Thao D Nguyen. A predictive parameter for the shape memory behavior of thermoplastic polymers. *Journal of Polymer Science Part B: Polymer Physics*, 54(14):1405–1414, January 2016.
- [108] B. Yang, W. M. Huang, C. Li, and L Li. Effects of moisture on the thermomechanical properties of a polyurethane shape memory polymer. *Polymer*, 47(4):1348–1356, January 2006.
- [109] Pengfei Yang, Guangming Zhu, Xuelin Shen, Xiaogang Yan, and Jing Nie. Poly( $\epsilon$ -caprolactone)-based shape memory polymers crosslinked by polyhedral oligomeric silsesquioxane. *RSC Advances*, 6(93):90212–90219, January 2016.
- [110] Qianxi Yang and Guoqiang Li. Investigation into stress recovery behavior of shape memory polyurethane fiber. *Journal of Polymer Science Part B: Polymer Physics*, 52(21):1429–1440, November 2014.
- [111] Qianxi Yang and Guoqiang Li. Temperature and rate dependent thermomechanical modeling of shape memory polymers with physics based phase evolution law. *International Journal of Plasticity*, 80:168–186, May 2016.
- [112] Wen Guang Yang, Haibao Lu, Wei Min Huang, Hang Jerry Qi, Xue Lian Wu, and Ke Yuan Sun. Advanced shape memory technology to reshape product design, manufacturing and recycling. *Polymers*, 6(8):2287–2308, January 2014.
- [113] Brahim Yarali, Ali Taheri, and Mostafa Baghani. A comprehensive review on thermomechanical constitutive models for shape memory polymers. *Journal of Intelligent Material Systems . . .*, pages 1–41, May 2020.
- [114] Kai Yu, Qi Ge, and H Jerry Qi. Effects of stretch induced softening to the free recovery behavior of shape memory polymer composites. *Polymer (United Kingdom)*, 55(23):5938–5947, November 2014.
- [115] Kai Yu, Qi Ge, and H Jerry Qi. Reduced time as a unified parameter determining fixity and free recovery of shape memory polymers. *Nature Communications*, 5:3066, 2014.
- [116] Kai Yu, Amber J W McClung, Gyaneshwar P Tandon, Jeffrey W Baur, and H Jerry Qi. A thermomechanical constitutive model for an epoxy based shape memory polymer and its parameter identifications. *Mechanics of Time-Dependent Materials*, 18(2):453–474, May 2014.

- [117] Qian Zhao, H Jerry Qi, and Tao Xie. Recent progress in shape memory polymer: New behavior, enabling materials, and mechanistic understanding. *Progress in Polymer Science*, 49-50:79–120, October 2015.
- [118] Yong Zhu, Jinlian Hu, Kwok-wing Yeung, Ka-fai Choi, Yequi Liu, and Haiming Liem. Effect of cationic group content on shape memory effect in segmented polyurethane cationomer. *Journal of Applied Polymer Science*, 103(1):545–556, January 2007.

## Chapter 3

# A Literature review on Advances in Additive Manufacturing of Shape Memory Polymer Composites

### Abstract

A version of this paper has been submitted for publication. This chapter is a review on additive manufacturing of Shape Memory Polymer Composites (SMPCs). In this chapter we highlight the progress made up to date, conduct a critical review and show the limitations and possible improvements in the different research areas within the different additive manufacturing techniques. The main purpose of this review is to identify academic and industrial opportunities. We introduce the reader to 3D and 4D printing of shape memory polymers (SMPs). Specifically, this review centers on manufacturing technologies based on material extrusion, photopolymerization, powder-based and lamination manufacturing processes. Additive manufacturing of shape memory polymer composites was classified according to the nature of the filler material: particle dispersed, i.e. carbon, metallic and ceramic, and long fibre reinforced materials, i.e. carbon fibres. We make a distinction for multi-material printing with SMPs since multifunctionality and exciting applications can be proposed through this method. Manufacturing strategies and technologies for SMPC are addressed in this review and opportunities in the research are highlighted.

We denote the existing limitations in the current additive manufacturing technologies and propose several directions that will contribute to better use and improvements in the production of additive manufactured shape memory polymer composites. With advances in additive manufacturing technologies, gradient changes in material properties can open diverse applications

of shape memory polymer composites. Thanks to multi-material printing, co-manufacturing sensors to 3D printed smart structures can bring this technology a step closer to obtain full control of the shape memory effect and its characteristics. We discuss the novel developments in device and functional part design using shape memory polymer composites, which should be aided with simple first stage design models followed by complex simulations for iterative and optimized design. A change in paradigm for designing complex structures is still to be made from engineers to exploit the full potential of additive manufactured SMPC structures.

Advances in additive manufacturing have opened the gateway to potential design and fabrication of functional parts with shape memory polymers and their composites. There have been many publications and reviews conducted in this area; yet, many focus mainly on shape memory polymers and reserve a small section to shape memory polymer composites. We present a comprehensive review directed solely on the additive manufacturing of shape memory polymer composites while highlighting the research opportunities.

## 3.1 Introduction

Additive Manufacturing (AM) is revolutionizing the way engineers and scientists are approaching design. Commonly referred to as 3 dimensional (3D) printing, AM, utilizes computer-assisted design (CAD) to generate tool-path patterns. These patterns are transferred to the AM machine and the material is deposited in a layer-by-layer fashion to construct a 3D object [86, 26, 163, 6, 144, 14]. Although 3D printing began as a rapid prototyping technology, it is evolving into an end-product manufacturing technique due to the use of specialized materials, improvements in printing resolution and manufacturing speeds, as well as the cost reduction for complex shape manufacturing [118, 22]. In the present day, desktop polymer 3D printers are readily available at low prices and are easily accessible. An extensive active online community of tinkers share knowledge and provide valuable feedback to manufacturers. There is widespread AM knowledge and know-how that provides support to materialize ideas rapidly. This leads to fast improvements of the AM technologies. At the present stage, AM is entering markets in many diverse industrial fields, including lightweight engineering, energy, medicine and food production [86]. Plastic AM is commercially being used for medical implants [177], prosthesis and tissue printing [85, 168], optical products [69], custom machine parts [176], sports equipment [106], wearables [28] and robotics [182] to name a few.

Smart materials such as Shape Memory Alloys (SMAs) and Shape Memory Polymers (SMPs) are materials that can store a temporary shape and return to their original/ permanent shape upon the application of a stimulus [79]. The ability to store a temporary shape and recover the permanent shape is often called Shape Memory Effect (SME). SMPs have the advantage of higher extensional deformation in comparison to that of metals, which is an advantage for many applications requiring high deformations [88, 79]. SMPs have been studied since the 1960's [45], but it is in recent years that the number of publications and potential applications have increased due to the use of 3D printing [139]. According to market research, areas of applications for 3D printing of materials showing a SME include aerospace [93], defense, robotics, automotive [129], clothing, utilities [54] and medicine for self-deployable stents, sutures and others [177, 143].

The ability for a material to store a temporary shape, coupled with the ability to be manufactured into complex shapes, opens the possibility to see materials as machines [105]. Since shape memory materials can reduce the number of machinery parts and eliminate bulky actuators to achieve dynamic movement, a wide range of complex shape transformations can be obtained through AM of SMPs, for instance: folding, bending, rolling, expansion, contraction, twisting and a combination of movements [116]. There are two main traits of SMP necessary to consider when implementing these in any engineering design, the Shape Recovery Force (SRF) and the Shape Recovery Ratio (SRR) [79]. The SRF is the force exerted by the material, while the SRR is the amount of deformation

recovered from the programmed temporary shape [79, 104]. High recovery forces are often desired for higher load-bearing applications, while high recovery ratios are desired for wide ranges of motion [165].

Despite their advantages, non-reinforced SMPs lack some properties, such as high load bearing mechanical properties. Enhancement of the material properties of SMP is possible by creating Shape Memory Polymer Composites (SMPCs). Addition of particles, short or long reinforcements or other polymer-based filler materials can enhance the recovery, stiffness and strength, thermal and electrical conductivity, as well as magnetic shielding and barrier properties. Improvements on these properties by particle doping have been covered in many reviews with respect to conventional manufacturing techniques [108, 63, 138, 107, 166].

AM allows the manufacturing of intricate multi-material structures. As a result, it is only in the last few years that the use of the SME has been investigated and its applicability sought. Multiple applications and possible industrialization of the SME has become possible due to the potential to combine complex manufacturing and multi-material 3D printing with SMPs [71].

Polymeric materials that show the SME are often classified in the literature into hydrogels, Liquid Crystal Elastomers (LCE) and thermoplastic and thermoset SMPs [12]. The SME mechanism of hydrogels is mainly based on material swelling. Hence, a hydrogel can be 3D printed next to a non-swelling polymer to create reversible bending actuators. Hydrogels are often very soft and have weak mechanical properties, which limits their capabilities and use in potential high load bearing applications [12]; however, many applications are promising in the biomedical sector such as for applications in tissue and organ regeneration [110]. LCEs are a mixture of liquid crystals with elastomeric components; hence, they have the properties of liquid crystals and entropic elasticity [52]. Shape change in LCEs is a consequence of the phase transition from anisotropic to isotropic when heated above a transition temperature  $T_t$  [71]. The advantage of LCE material is its ability to obtain hands-free reversible actuation from a two-step programming method [174]. Limitations of LCEs are still prevalent due to the difficulty of achieving macroscopic orientation [122, 71]. An excellent review of the activation methods and composites of LCE has been performed and is recommended for further details [72].

The present review primarily focuses on the advancements made in the area of use of additive manufacturing for SMPCs. There have been many reviews conducted in the area of additive manufacturing of SMP and their composites. However, an up-to-date critical comprehensive review based solely on SMPCs is still missing from the literature. In this work, firstly, we introduce the basics of 3D printing of SMP and 4D printing. We provide a quick overview of SMPC and the importance of multifunctionality. We then focus on the works that have used dispersed short reinforcements in SMP matrices and the corresponding manufacturing technologies used. We highlight the contri-

butions up to date to the field and discuss the drawbacks that each AM technology presents when applied to the manufacturing of SMPCs. We then move on to the addition of long reinforcements to SMP matrices and discuss the corresponding manufacturing technologies used. We denote the limitations of these technologies and highlight the advantages of continuous fibre placement on the material properties and the difficulties faced in manufacturing.

Although multi-material printing with SMPs has been thoroughly covered in the past [71], here we highlighted the advantages of multi-material printing and how, with SMPC, multiple functionalities may be accomplished, such as reversible shapes, actuation, and sensing. Finally, we discuss and highlight the potential opportunities for AM produced SMPCs for academy and industry.

### 3.1.1 3D printing of Shape Memory Polymers vs. 4D printing

The SME or shape-changing can occur by two different methods. First, it can be caused by the intrinsic properties of the material. Many polymers possess an intrinsic SME but only a few possess a functional SME (one with high exerting recovery forces or fast and high recovery ratios). Secondly, shape change can be produced by the creation of mismatched strains, either due to a mismatch in the coefficients of thermal expansion or hygroscopic coefficients, which produce residual stresses. Due to the versatility of 3D printing, this effect has been exploited for obtaining a shape change in structures. Although this shape change is not based on the intrinsic properties of the SMP, it shows the potential applications when applied to SMPCs for multiple shape storage and the possibility of hands-free shape training.

SMPs show a material intrinsic SME, which requires two main steps: a "shape training step" and an "activation step." The shape training step is the process in which the material stores its temporary shape by i) increasing the temperature of the material above its transition temperature  $T_t$ , ii) applying a constant strain to the material and iii) cooling the material below  $T_t$ . Activation of the SME will occur by increasing the temperature above  $T_t$  [79]. The training and activation process can be observed in Figure 3.1.

3D printing of SMPs is often designated as "4D printing" in the literature. The use of this terminology is widely popular and used for different circumstances. To accurately understand the differences between the terminology used, one must make a distinction between these terms.

In this review, 3D printing of SMPs is defined as the AM using SMPs, which after manufacturing will need a training and activation process to show the SME. The need to use AM with SMPs rises from the necessity to manufacture complex shapes for applications and to improve the recovery properties of the printed structures. For instance, it has been shown that the printing of cellular structures can increase the recovery force exerted by an SMPs compared to a solid material [92, 180, 20, 91]. 3D

printing of SMPs can also allow the manufacturing of structural components that have undergone topology optimization for reduced weight and to modify or take advantage of the anisotropy of the structure [184].

On the other hand, four-dimensional (4D) printing is defined as the 3D printing of SMPs but with an added time dimension [15, 49]. By tuning the 3D printing parameters, a 3D printed SMP structure can have a programmed shape by the end of the printing process. Hence, the material has had the training step during the manufacturing stage. From now on, we will denominate this printing strategy as 4D printing. Often, in the literature, it is referred to as "direct" 4D printing [71, 30]. In 2013 Tibbitts introduced 4D printing to the smart materials community [152]. In his work, he demonstrated the actuation of a structure by a moisture stimulus. The 3D printed part showed an SME when removed from the printing bed to a water immersion step. The applications for this technology were proposed for morphing structures with limitless shapes [130]. Ding et al. were also able to accomplish direct 4D printing using an ink-jet technology for thermoresponsive polymers [30]. In the present work, we will call 4D printing only to the process of 3D printing while storing a temporary shape during printing. A schematic of the difference between 3D and 4D printing can be observed in Figure 3.1.

4D printing has been achieved using several AM technologies. For an extrusion based AM, 4D printing can occur by producing internal stresses in the 3D printed structure as a product of the rapid heating and cooling rates during manufacturing. To restore the shape, an increase in temperature above the glass transition temperature  $T_g$  releases the internal stresses of the material [179]. The main benefit of 4D printing is the removal of the manual shape programming step, which can produce faster industrial procedures [77]. Although many of the 4D prints are mostly one way reversible (can only store a single shape), researchers have suggested that there is the possibility to create a two-way reversible 4D printing. For instance, two way activation has been done by using a bilayer laminate in which a pre-elongated SMP film can be attached to an un-elongated elastic PU film [18], this could eventually be applied to multi-material printing. Other works has shown reversibility using hydrogels in which a hydrogel is printed next to a polymer to achieve movement when hydrating and reversibility when dehydrating. A combination of activation methods (moisture and thermal) can be used on bilayer materials compounded of hydrogels and SMPs to produce a dual [77].

### 3.1.2 Additive Manufacturing techniques used for SMP

In this section, the most relevant techniques used for polymer 3D printing fabrication is discussed, focusing specifically on techniques used for shape memory 3D and 4D printing. Many reviews have summarized in detail the general AM techniques [112, 57, 113]. Hence, we will describe the AM

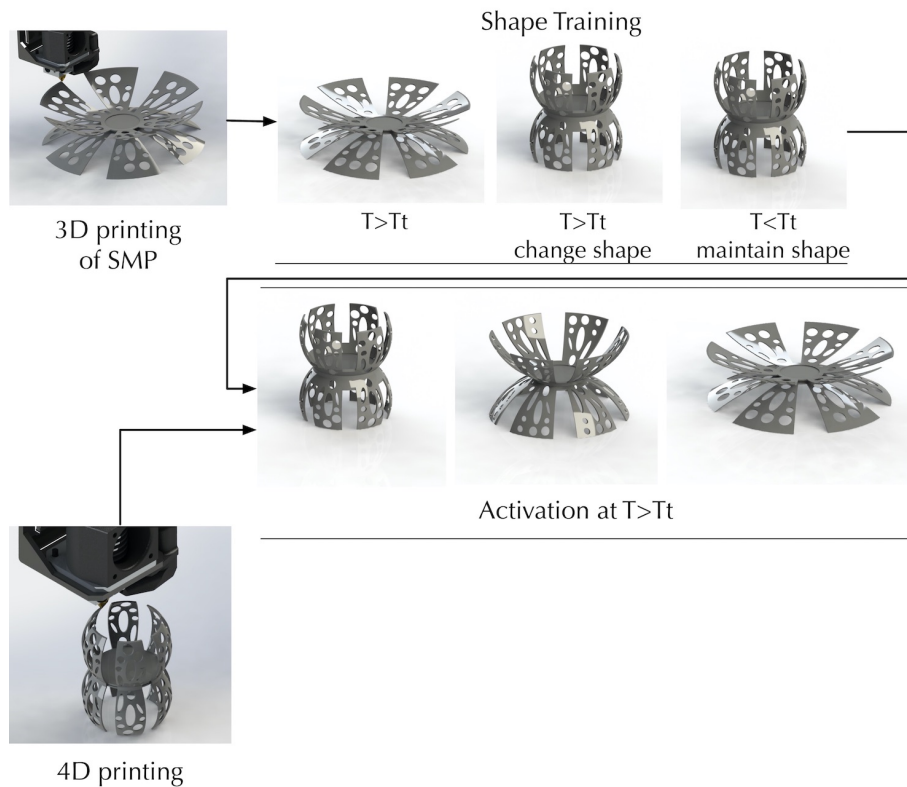


Figure 3.1: Schematic of a 3D printed structure. The difference in 3D vs 4D printing is shown.

techniques specifically for 3D printing with SMPs and 4D printing. We will elaborate in the next section specifically on SMPs.

1. **Material extrusion:** often referred to as Fused Deposition Modelling (FDM), Fused Filament Fabrication (FFF) or Extrusion Based Additive Manufacturing (EBAM), is a technique in which molten polymer is deposited when extruded and pushed through a small heated nozzle [97]. Multiple materials can be placed in one structure using a sequential deposition order. Part quality produced by FDM printers are usually subpar to their photo or laser curing counter parts. FDM printers can achieve a surface roughness of  $\sim 57 \mu m$  on desktop 3D printers while a photocuring desktop printer can achieve  $\sim 20 \mu m$  [96]. Despite this, FDM has been widely studied and used. The extensive use of this manufacturing technique offers a wide variety of material accessibility, low cost machines, and available trouble shooting information for a variety of materials and printers.

In recent years, many works have focused on understanding the effects of the printing parameters of FDM on the SME, such as printing speed and layer thickness [49, 128, 156, 56]. For

instance, Abishera et al. reported that a higher printing speed usually yields higher shape recovery forces due to the increase in internal stresses due to thermal gradients during the printing process [128]. In general, the materials that are most common for this type of manufacturing are TPU and PLA. Some other types of materials that researchers have investigated for their recovery properties are Nylon, PE, ABS, HIPS and PVDF [139].

Multi-material printing by FDM can provide mechanical reinforcement, provide materials as a base support for complex manufacturing, and add multifunctionality such as electro-responsiveness or self-sensing capabilities as was shown on an SMPC printed structured by Garces et al. [37]. Multiple material deposition by FDM has been applied to a variety of shape memory exhibiting materials, including hydrogels [141]. Printing of SMPCs can be done by feeding a particle reinforced filament or by placing long fibers as reinforcement. This is explained in detailed in the sections to follow.

2. ***Direct Writing Assembly (DWA)***: is a technique similar to the concept of writing on paper with a pen. As such, a viscous liquid is deposited on a substrate in a controlled manner. The deposited liquid is then set or cured by evaporating solvents when using thermoplastic solutions or using heat or UV curing to convert the viscous liquid into a solidified assembly. Materials that have been used to manufacture with this technique are polymer solutions, colloidal suspensions, UV-curable polymers, and polyelectrolytes [162, 76, 126, 42, 162, 1, 97]. Other names for this technique include Direct Writing (DIW), Robocasting (RC) or Micro robotic Deposition ( $\mu RD$ ) [81]. Since this technique uses a liquid polymer to manufacture parts, high precision prints may be achieved. 3D printing of SMP with DWA has been shown successfully in the past years [70, 17]. Applications for this technology are many, among those the manufacturing of cell scaffolds and vascular stents [83]. This technology has shown to be particularly helpful when distributing particles in a liquid resin, offering many opportunities for material functionalization. However, the equipment required is quite specialized and not as cheap or commercially available as FDM. One of the most prominent technologies shown in the past years was that by Kim et al. In their work, the authors showed the alignment of magnetic particles using DIW for smart material control [66]. Although this work is not SME based, it has been included in this review due to its potential use with SMPC. For instance, a hands free programming step of the SMPC could be implemented via a magnetic actuation, and can cause a reversible SME.

In recent years, large scale 3D printing using thermosets has been approached with this manufacturing principle [135]. Exothermic thermosetting resins are usually used for this type of manufacturing. The chemistry of these resins are a property of companies that have pursue this such as Magnum Venus Products. Although this method has not been used for SMPCs, it shows the potential of scalability.

3. ***Vat photopolymerization:*** In this technique, a liquid photopolymer undergoes photopolymerization in a controlled manner. This is done by irradiating an energy source layer by layer as material is deposited. The most common type of printing with this technique is stereolithography (SLA), which cures via a laser, and Digital Light Processing (DLP), which uses a light projector [71]. A form of DLP is the technology Continuous Liquid Interface Production (CLIP), which has become affordable in a desktop bench size configuration [97]. The resolution of this technology surpasses that of FDM since there is no restriction from the nozzle diameter. A high resolution in the nano-range can be achieved via projection micro-stereolithography, which has been proposed with DLP [71]. Photopolymers are a mixture of liquid monomers, oligomers and photo-initiators [181]. Therefore this technology is mainly focused on thermoset resins; hence they cannot be reprocessed. Applications of this technology are constrained to a small size scale due to the use of the liquid resin. However, due to the high resolution that this technology possesses, high detail applications are possible such as in tissue engineering [117], energy storage, acoustics, photonics, thermal management [148] and high detail mechanics such as microfluidic devices [11]. Thermoset SMPU and most commonly PCL has been used to manufacture with this technology [181, 71]. Addition of particles to a liquid resin is a possible manufacturing technique to produce SMPCs.
4. ***Material jetting:*** This technique uses printing heads, much like the ones for inkjet. The heads deposit droplets of photocuring material and solidifies them by UV curing in a consecutive manner. A clear advantage of this technique is high precision and multi-material depositing capability [97] with optimal interphase bonding in comparison to other technologies. Ge et al. [41] was able to accomplish 3D printing of SMPs using this technology. In their work, the authors synthesized a photopolymer that possessed high stretchability, required for the existence of the SME. In recent years, several advances have been made to 4D printing by using material jetting and multi-material printing as described in the in-depth review by Kuang et al. [71]. Printing of SMPCs is possible due to the excellent fusion between materials that this technique possess. Particle reinforced SMPCs is still an issue with this technology as is later explained in detail.
5. ***Sheet lamination:*** Sheets of material are placed on top of each other progressively to create a part, hence no support material is required for manufacturing complex parts [124]. This technology, often referred to as Lamination Object Manufacturing (LOM), offers high dimensional accuracy, but due to the nature of the manufacturing, a lot of material waste is created during the manufacturing process [133]. Advances in robotics have made this AM technique very attractive for multiple polymer sheets and composite material ply deposition [13]. Composite materials that show a shape change have been manufactured via this method

and will be described in the following sections.

6. ***Powder bed fusion:*** This technique relies on manufacturing by bonding layers of powdered material. The main advantage of this technique is that the materials do not need supporting structures since the support is the compacted surrounding material powder. The most common type of 3D printing of polymers with this technique is Selective Laser Sintering (SLS) [97]. This technique offers an excellent layer adhesion with no visible layers, unlike FDM. However, porosity and brittleness is a common issue for parts manufactured with this AM technique. Yuan et al. [175] 3D printed TPU SMP using SLS successfully. A reference to a solid injected part would be helpful to understand the decay in mechanical properties due to porosity.

Although there are many other AM techniques besides the ones highlighted in this section, we have focused on the ones used with SMPs. A summary of the AM techniques used for the manufacturing of SMPs is shown in Figure 3.2. Schematics modified from [97] are shown for each type of manufacturing. In the schematic, the AM techniques are divided into manufacturing processes such as material extrusion, photopolymerization, powder-based, and lamination. DWA and FDM were classified within material extrusion since the material is forced out of a nozzle or needle. SLA, CLIP and DWA are part of the photopolymerization manufacturing. SLS is part of powder based AM. For lamination, the most common techniques are LOM and we focus on an automated composite layup used to create an SME using fibre reinforced composite plies.

### 3.1.3 Overview of SMPC

Composite materials are a way to obtain materials with tailored properties in comparison to the individual properties of its constituents. In general, properties that can be modified are plenty, such as mechanical, thermal, electrical, magnetic, barrier, to name a few. As previously mentioned, SMPs have limitations and still require improvement in their activation, low strength mechanical properties and shape recovery properties. The enhancement of these properties can be done by using filler materials in an SMP matrix. Filler dispersed materials have been used to improve shape recovery characteristics, such as increasing the recovery rate and recovery force exerted by the material. In the same way, the effects of continuous fibres within an SMP matrix have been investigated to obtain high load-bearing SMPCs [108, 63, 138, 107, 166].

One of the essential uses of filler material in an SMP matrix is the activation of the SME by methods that allow for a field activation. Joule, induction and infrared heating have been conducted through the addition of filler material [159]. In addition to this, multi-material printing has allowed multifunctionality in materials such as sensing for health monitoring, temperature, motion and

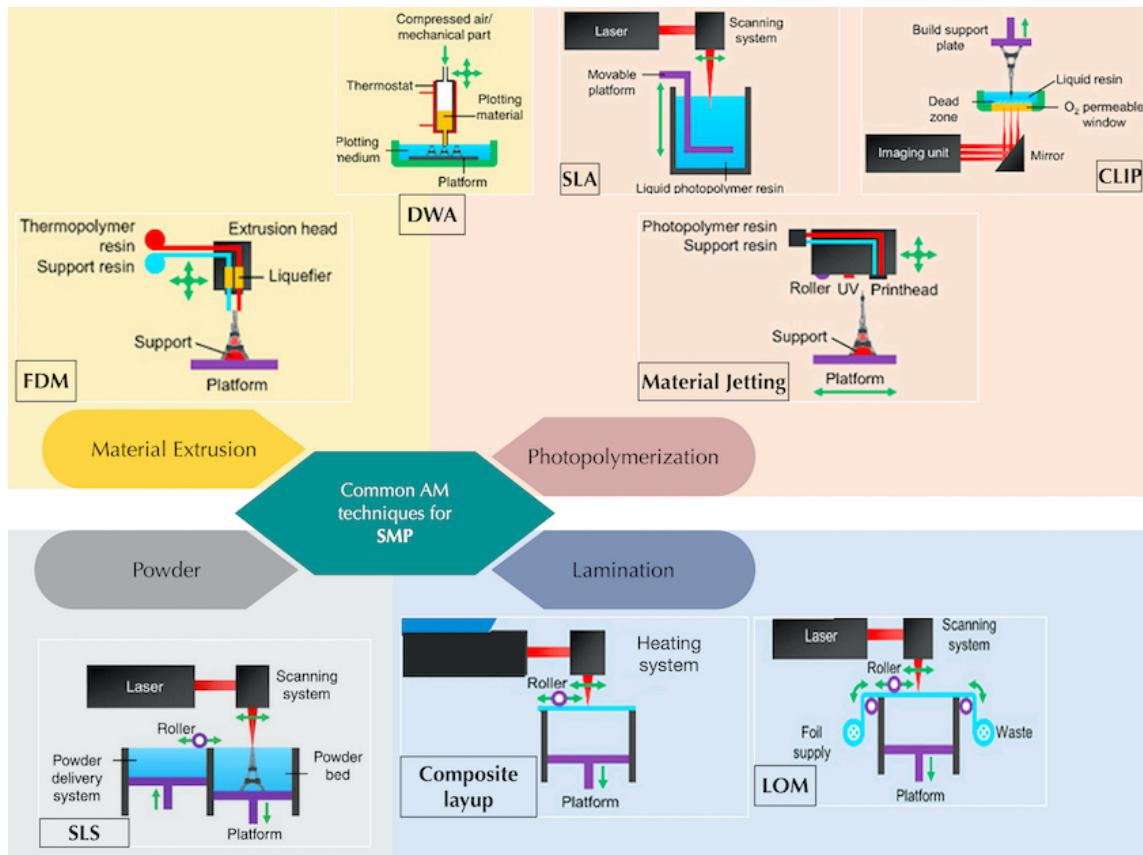


Figure 3.2: AM techniques for SMPs. Figure modified and adapted from [97] for the relevance of this chapter. (Open-source figure)

others. Materials that are commonly added to SMP are polymeric, carbon, metallic or ceramic-based [78]. Typical filler materials are listed in Table 3.1.

There are still considerations and issues to keep in mind when obtaining SMPCs, as explained by Lei et al. [78]. Works are still devoted to enhancing the properties of these materials. One of the main issues with SMPCs is getting a strong interphase between fillers and matrix material. A suitable interphase is crucial in SMPCs since they often undergo large deformations and cyclic activation. A consideration that needs always to be addressed when designing SMPCs is that filler material reduces the mobility of the polymer, which can affect the SME characteristics of the raw material [78].

In the present review, we focus primarily on AM of filler reinforced SMPCs, since a thorough review on this topic is missing in the open literature. There have been many works that have focused on

Table 3.1: Common fillers used for manufacturing SMPCs

<b>Nature</b>	<b>Examples</b>	<b>Refs.</b>
Natural	Chitosan CNC	[109] [35, 94]
Synthetic	Short glass fibres Woven glass fibers	[170] [33]
Carbon	CB CNT MWCNT long CF long CF	[80] [127] [119] [31] [82, 73]
Metallic	SMP-SMA	[132]
Hybrid	Cu-decorated CNT Grafted CNC with Silver nano-wiskers	[3] [153]
Ceramic	SiC Hexagonal-BN Modified BN	[87] [84] [7]
Multi-material	CB-SMPU/TPU layered (Reversible) Bilayer SMPC Bilayer SMPC with a silver nanowire layer	[19] [150] [99]

multi-layer and multi-material printing with SMPs to produce activation, multiple shape storage and reversible shape memory storage [78]. In the literature, these material combinations are also referred to as SMPCs. For this reason multimaterial printing has been added to this review. We will exclude polymer blends from this chapter since we do not consider them to be within the SMPCs' scope. This review will focus specifically on natural and synthetic particles and fibres, metallic, and ceramic fillers.

Effects of the AM printing parameters and obtained structure of parts when using composites is an area that is often overlooked. For instance, for the most simple AM technique, FDM, printing of filler dispersed polymers can be complicated due to nozzle clogging. Gradual nozzle clogging produces less material to be deposited during manufacturing, which can compromise the homogeneous fibre weight percentage in the composite and change the anisotropy of the material. Filler material will additionally cause effects on layer bonding, changes in viscosity of the material, filler alignment, changes in thermal properties that will impede the material to cool at the same rate as the non-doped material [46]. All these factors have an impact on the properties of the AM SMPCs, including the recovery properties, as is documented in the rest of this review paper.

### 3.1.4 Conductive Carbon based SMPC

A distinction is made in this section for conductive SMPCs, specifically carbon-based materials due to their ability to provide SMPCs with multifunctionality. Carbon based materials offer the advantage of high thermal and electrical conductivity, electromagnetic shielding capabilities, as well as the ability to increase stiffness of polymer based matrices [98, 171]. The ability to increase the mechanical properties of an SMP while obtaining the multifunctionality of activation by Joule heating [131, 37], and a self-sensing capability [37], can offer opportunities in soft-robotics [67, 43, 146], grippers [27], self-assembly structures [136], biomedical devices [143, 142], self-healing applications [60, 51], textiles [54], aerospace[93] and applications in electronics such as changing the dielectric properties of an structure [5], and limitless possibilities in sensors and actuators [25, 64, 145].

In a recent review, Panahi-Sarmad et al. [121] discussed the advancements in carbon-based filler materials in SMP matrices. The authors concluded that there are still some challenges, such as the proper dispersion of particles in the nano- and macro scale. Reduction in shape fixity and recovery ratio are usually the main affected parameters with particle addition [121]. Perhaps the primary and still occurring challenge that researchers encounter when using fillers in the nano-scale range is to obtain the perfect balance between weight percentage and electrical conductivity to achieve both mechanical reinforcement and electrical conductivity. An alternate solution to this issue could be the use of hybrid particles [61]. The authors would like to highlight some of the most common carbon based filler materials in the nano-scale range:

- Carbon Black (CB) particles ([8, 167])
- Carbon Nanotubes (CNT), MultiWalled Carbon Nanotubes (MWCNT) and Carbon Nanofibres ([119, 31, 25, 98, 44])
- Graphene Nanoplatelets ([74, 34])
- Graphene Oxide ([27, 149, 151])

Commonly used fillers in the macro range include short and continuous carbon fibers [140, 155]. The advantages of added particles and or fibres to SMPs are evident from the presented review. However, many of these composites require tedious manual manufacturing techniques. Product manufacturing, through conventional methods is usually expensive for complex parts and even more for specialized materials. A simple manufacturing technique that reduces cost and amplifies material design opportunities by using multi-material layering is AM.

## 3.2 Additive Manufacturing of SMPC

In this section, we review key aspects of AM of SMPCs; such as, manufacturing limitations, enhancement of SMPs' properties by use of fillers and use of filler materials for activation of the SME. We have divided this section according to filler type, i.e. particle dispersed and long fibres. A summary of the common AM techniques used for different types of SMPCs, is shown in Figure 3.3. These techniques will be discussed in further detail in the sections.

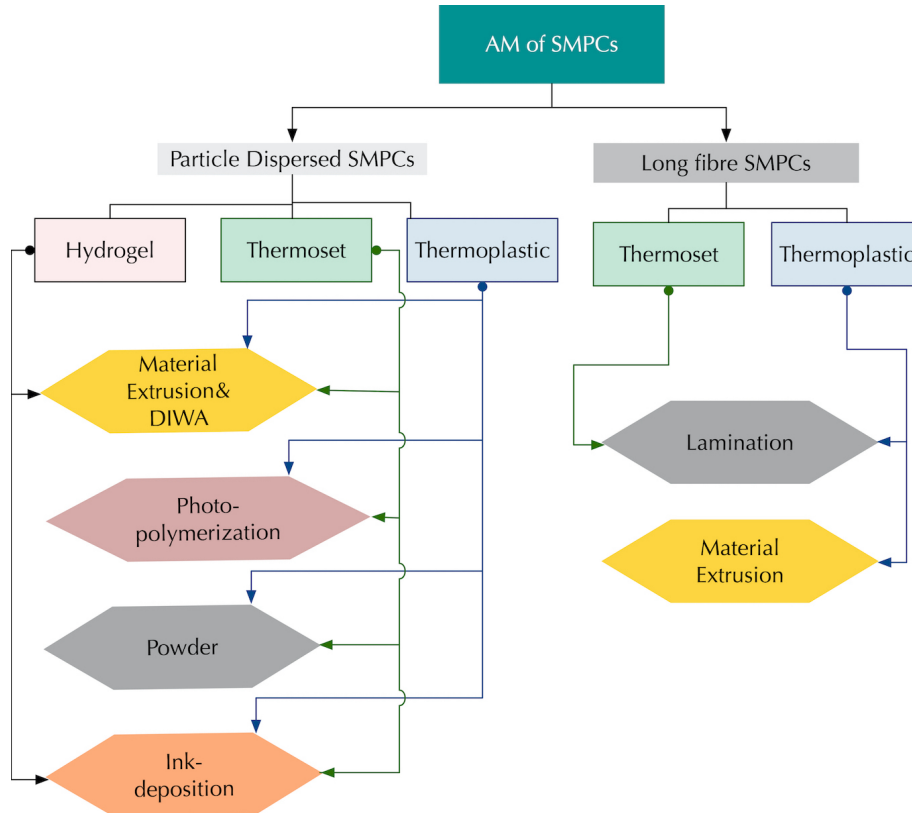


Figure 3.3: Common AM techniques for different types of reinforcements

### 3.2.1 Particle dispersed SMPC

Thermoplastics, thermosets and hydrogels are the the most commonly used matrices for AM of particle dispersed SMPCs. Due to the nature of these matrices only certain types of AM techniques are possible. We have summarized the techniques used in the literature as shown in the schematic on the left hand side of Figure 3.3. Although, some of these AM techniques have not yet been

achieved using SMPCs, we have included them here since we believe to be feasible in the future. For instance, although 3D printing of an SMP via powder-based AM has been achieved, 3D printing of SMPCs has not been reported yet, but it is undoubtedly possible since nanocomposite powder could be heated to create a fused manufactured part. In the same manner, successful SMP material jetting has been achieved, yet to the authors' knowledge implementation of this AM technique for SMPCs has not been yet conducted. Implementation of nanoparticles to inkjet could be deposited on the SMP resin. There have been a few works that have explored the activation of the SME by depositing inks on an SMP surface. These inks can be heated via joule heating or through radiation. These works will be discussed later on.

### **Material Extrusion**

FDM printing of SMPCs is based on the use of a filament compounded of an SMP thermoplastic matrix filled with particles [46, 138]. Many materials with a PLA matrix and CNT or graphite oxide particles are commercially available. Although it's well known that PLA shows an SME and much work has been done and focused on 3D printed PLA nanocomposites, these works have overlooked the SME or the effect of these particles on the SME [16]. Only a few studies have been conducted to understand and describe the shape memory behaviour of these additive manufactured parts. One of the earliest attempts to 3D print an SMPC was that of Yang et al. In their work, the authors designed a light-activated SMPC using PU as a matrix and CB filler particles. The authors showed a successful photothermal conversion, which was mainly achieved by the filler particles. The authors 3D printed multiple structures to show the application of their technology [169], an image of their results is shown in Figure 3.4. Other works have also incorporated MWCNT into PLA to produce photo-activated composites and actuators [50], primarily focusing on the impregnation of this composite on paper for the design of actuators due to their low cost. This technology was shown in very thin composites, the light can only reach a thin layer at the surface to activate the SME. As such, the authors did not show the recovery force that the proposed actuators exert. This limits the applicability of the technology.

A few preliminary works have been done to show the potential of 3D printed SMPCs activated via joule heating. In their work, Ly et al. mixed 3 wt.% CNT with SMP polyurethane based thermoplastic matrix (SMPU) [100]. The authors activated the SME via resistive heating. In their work, the authors stated that a high printing temperature produces a better bond between layers, which increases the conductivity of the samples. A low feed rate and high infill ratio also increase the conductivity of the sample printed. In general poor conductivity between layers was obtained but a decrease in resistance was observed after the printing process. The authors stated that there was much difficulty to 3D print SMPC due to nozzle clogging.

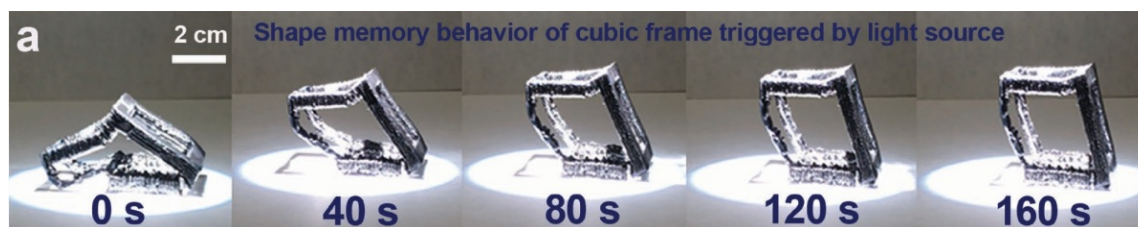


Figure 3.4: Figure reprinted with the permission from [169] (a section of this figure has been used for the relevance of this chapter). The recovery of a 3D printed photo-responsive structure can be observed in the image.

Following this work, Garcia et al. added CB spheres to SMPU via solvent casting, consequently, extruded, and then samples were manufactured via FDM. The highest conductivity was obtained by adding 7%wt. of particles. A series of mechanical and sensing testing were performed on the composite, however, a more in-depth analysis or results on the recovery behaviour of the composite is needed in the future [38]. Contemporary to this, Garces and Ayranci [36] proposed that PLA/-Graphene could be used for activation of SMP by using 3D printed PLA/Graphene oxide for resistive heating, the authors showed the temperature and SME characterization of the composite.

An exciting work by Liu et al. [89] added the semiconductor SiC and graphite to PLA. The authors observed a clear increase in thermal conductivity with the addition of SiC, which produced a faster shape recovery. Although this study shows potential in electrical properties and perhaps reinforcement, the authors reported difficulty in collecting reliable data. The shape programming of the samples was only 3% in strain, and low recovery forces were observed throughout the study, although a definite increase in recovery force by SiC was noticed. This work is promising and pioneering in using highly heterogeneous materials for FDM, which could be used in different applications in the future.

Following this work, in 2019, Liu et al. [90] prepared a PLA/CNT filament and characterized it for resistive heating. By using different angle-ply configurations for printing, the authors found that different configurations can produce different heating patterns. This is exceptionally interesting since anisotropy produced by printing can be used to modify and alter heating and activation of the SME. Furthermore, electrical properties will be affected by printing parameters such as speed, layer thickness and, of course, raster angle. The authors found that a slower printing speed, a larger thickness and  $0^\circ$  degree raster angle contributed to a faster resistive heating activation of the shape memory recovery. Following this, Liu et al. [92] manufactured a PLA/CNT filaments, and 3D printed braided-like structures and angle-ply laminated samples, these are shown in Figure 3.5. PLA/CNT specimens presented advantages over raw PLA printed samples, such as an earlier start in recovery, slower shape recovery rate, but a smaller final recovery ratio as expected in most

particle dispersed composites. However, this issue was ingeniously compensated by infusing silicon to the matrix. The authors found that the angle-ply lamina PLA/CNT printed structure displayed a higher recovery force than pure printed PLA, which is necessary for engineering applications with SMPs.

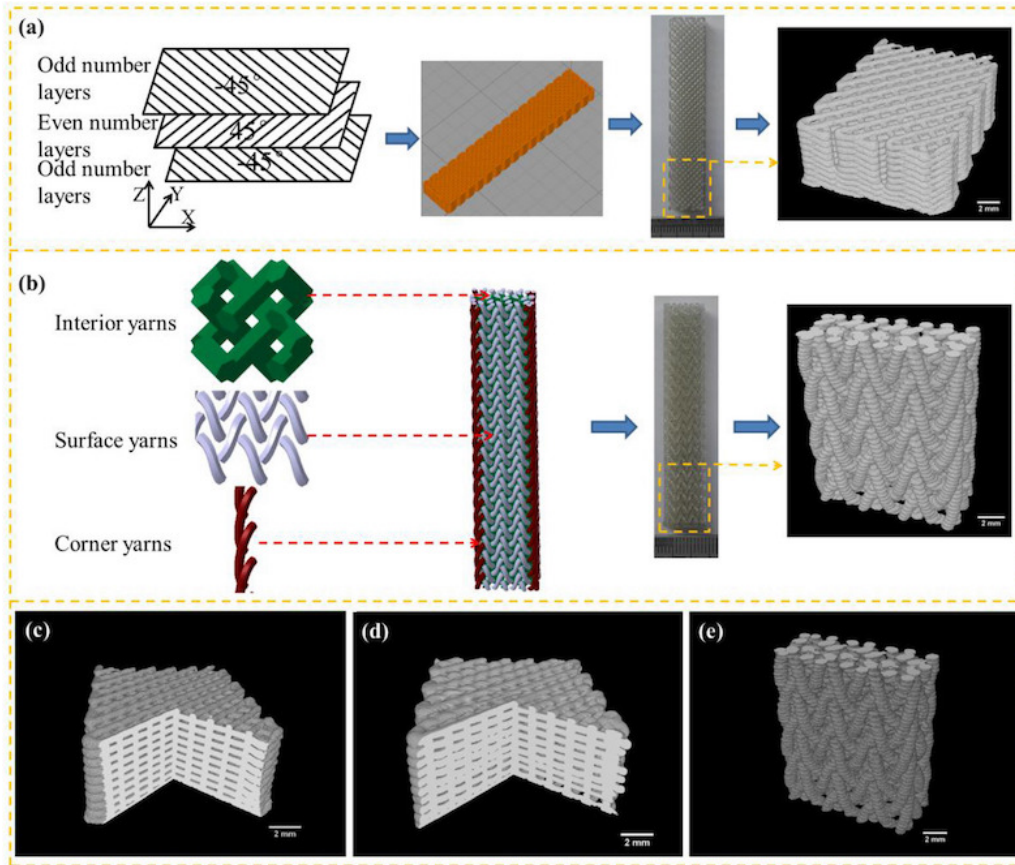


Figure 3.5: 3D printed structures printed with PLA/CNT filament in (a) a ply-angle oriented configuration and in a (b) braided configuration. This image was obtained and published with the permission of [92]

Due to the increasing environmental concerns, natural, environmentally friendly materials are the next logical step in the polymer industry. Specifically, natural fillers will be beneficial for applications in the biomedical sector due to their biocompatibility and their biological active nature, which promotes cellular adhesion [48]. In the past, 3D printed medical devices with SMPs have been proposed, such as the 3D printed stent by Zhang et al. [67]. Recently Yu et al. also proposed a 3D printed SMPU cardiovascular stent reinforced with CNC to obtain higher recovery forces than commercially available stents and less relaxation in recovery forces [21]. Reinforcement of plain

SMP matrices for 3D printing with natural fibres is still an area that has not been widely exploited and is expected to grow in the upcoming years with the increasing environmental impact of plastics. Fillers such as wood on PLA and PHA composites have been studied by Le Digou et al. [75]. In their work, wood chip fibres were seen to align during the material extrusion while printing. The actuation of the SME on the composite was induced by moisture swelling.

To the best of the authors' knowledge, limited work has been done in the area of 3D printing by FDM of filler dispersed SMPCs. There is plenty of evidence that the particle aspect ratio will affect the SMPC's material properties; however, the way the properties change is not entirely understood. For instance, effects of particle alignment for embedded rod-like and fibre like particles during material extrusion, is an area that has not been studied. Much work is still needed to understand the effects of particle alignment during printing on the shape recovery properties of the SMPCs. A thorough study on the printing parameters, such as printing speed and material feeding rate, on the recovery properties of the 3D and 4D printed SMPCs is also required to completely understand the effects of particle dispersion on additive manufactured SMPCs. For conductive SMPCs, effects of printing parameters on the conductivity and layer fusion and mechanical properties of the 3D printed part is still an area that needs further development.

### Direct Writing Assembly

One of the first attempts to 3D print SMP with DWA was by Rodrigez et al. [134]. In their work, the authors manufactured a bio-based thermoset printable SMP reinforced with 3%wt. CNF for enhanced mechanical (storage modulus increased by a factor of 100), electrical resistive heating and shape memory properties. Storage modulus was observed to increase significantly with the use of CNF concentration. Figure 3.6 shows the programmed and recovered shape of a 3D printed conductive stent with their technology. Although the work is promising, further characterization of the shape recovery is still needed, such as recovery speed and ratio.

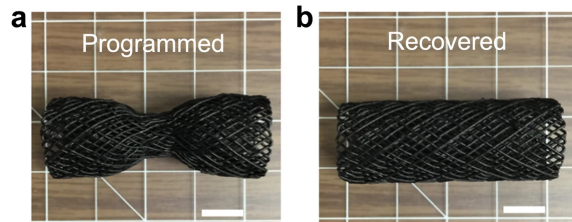


Figure 3.6: a) is a photo of the programmed and b) the recovered 3D printed thermoset SMPC stent. (Open source article and images) [134]

Thermoplastic matrices have also been shown to be 3D printable via DWA. For instance, ferromag-

netic PLA structures have been manufactured with high accuracy. A solution of PLA dissolved in dichloromethane, with Benzene and  $Fe_3O_4$  particles, was prepared for the printing process. The authors activated the SMPC by thermal induction and remote magnetic activation. The process of material deposition while being cured by UV while solvent evaporation occurs, followed by an example of the printed structure, as well as the magnetic actuation of the SME and the application for a stent can be observed in Figure 3.7.

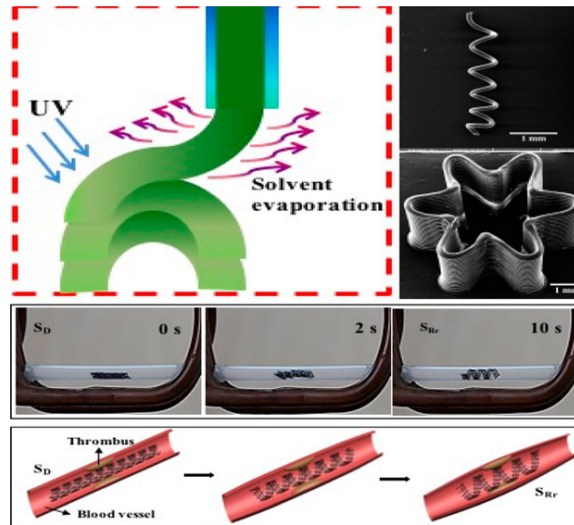


Figure 3.7: DWA manufacturing used for PLA-ferromagnetic SMPC and stents printed. Image reprinted with the permission of [162].

Dispersion in the liquid state of nanoparticles is more facile to achieve using a liquid matrix. DWA allowed Wei et al. to 3D print highly conductive material for use in electrical, magnetic insulation, joule heating and 3D printable shape-memory circuits [161]. The authors used a PLA matrix and hybrid particles made of CNF coated with silver. The proposed material and 3D printing technique showed great potential in conductivity and recovery properties. However, this study lacks an in-depth mechanical analysis, which is needed for further development into applications. Recently, Wang et al. [157] was able to obtain a prototype of 3D printed sensors for liquid detection. The material used was poly(D,L-lactide-co-trimethylene carbonate) (PLMC) and 10%wt. CNT to produce a conductive composite, able to trigger its SME by joule heating. The immersion of these structures in different liquids increased the resistivity of the material due to material swelling. The application to liquid sensing converts the prototyped structures into multifunctional sensors by triggering thermal activation of the SME and solvent sensing. Although the authors did not check the resistance with respect to temperature, it is something to be explored for further development. This work is potentially useful for feedback control of moisture sensing and even moisture swelling

activation of the SME. This technology could potentially be extended to other electronic applications such as small actuators, electromagnetic shielding and energy harvesting.

DWA is a technology that can be used with SMPCs and is an area that can obtain good particle dispersion. Development in industrial thermo, electro and moisture responsive SMPCs is possible using this technology. Due to the use of solvents and specialized materials, some of the mentioned manufacturing techniques might be limited when looking into large scale manufacturing. However, prototyped applications with SMPCs using DWA are promising in a variety of industries.

### **Vat Photopolymerization**

Using particle-dispersed composites with SLA or DLP is still challenging, firstly as with most particle dispersed composites, particle dispersion is an issue that needs to be studied meticulously. The main concern when printing via vat photopolymerization is the high viscosity of the composite resin, as well as the scattering produced by the filler particles. For instance, CNTs are strong UV absorbers; this presents problems when curing the photopolymer resin [32, 23]. Hengky et al. [32] suggested that using conductive nanoparticles such as CNT in SLA could provide enhanced mechanical properties, electrical and thermal conductivity. Particle alignment accomplished while printing is still something that is not fully understood. In general, printing speed by DLP photopolymerization is currently a slow process (approximately 30 mm/hr), hence scaling up this technology can be problematic [23]. Choon et al. [23] proposed the use of nano-silica particles ( $SiO_2$ ) as nucleation sites to improve photopolymerization, and as a consequence, this increases the curing speed of SMPs during AM. Besides improving curing time, the authors improved the elongation range of the matrix material, which is usually small in photopolymerized polymers. The elongation was  $\sim 85\%$ ; the reinforcement also kept the recovery range in about 87 – 90%, which is acceptable for many applications [23]. Although this is a slow process high detail and resolution for parts can be obtained, as can be observed in figure 3.8.

Due to the nature of this technology, scaling this technology is nearly impossible, since the resin vat is exposed in its liquid form to the air. However, for small size applications, resolutions is far superior to that of FDM, which and improve product quality of SMPCs. Increase in mechanical properties and curing time could be improved by the use of particles when printing with SMPCs.

### **Ink-deposition for SME trigger**

The deposition of conductive materials on top of an SMP matrix to produce activation of the SME via joule or infrared heating is a clever and perhaps the simplest way to achieve remote activation. Although this technique posses the advantage of simplicity, it cannot provide reinforcement

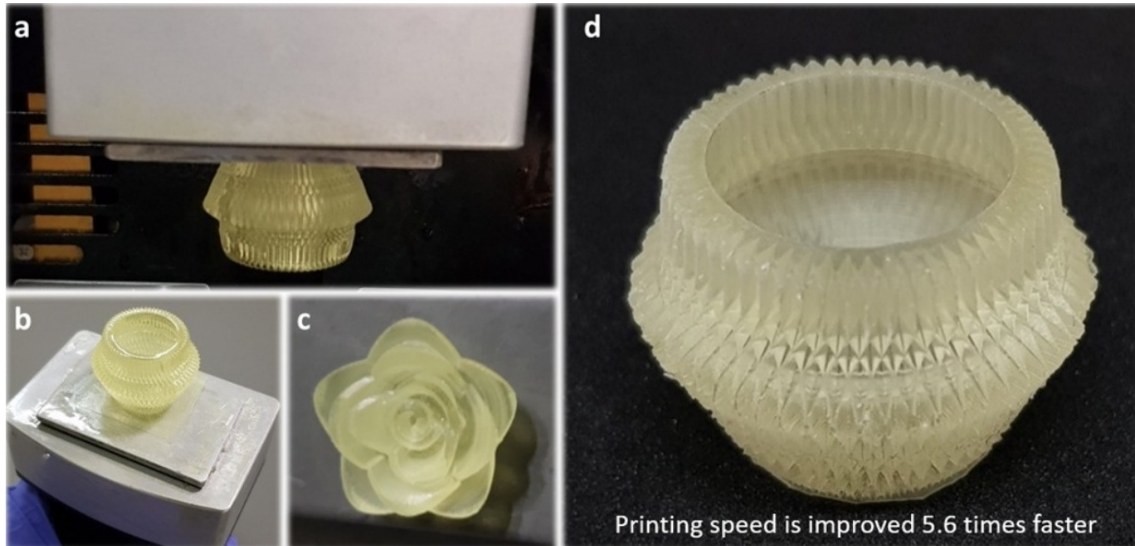


Figure 3.8: DLP manufacturing of a SMPC reinforced with nanosilica particles. Images reprinted with permission of [23]

and optimization of the SMP material's properties. Nevertheless, this technique could be used in combination with other AM techniques to achieve multifunctionality of SMPCs.

Using ink-deposition, Wang et al. [160] achieved the activation of the SME by proposing the application of a CNT ink suspension on top of an SMP matrix to produce the activation of the SME through joule heating. By spraying into an automated system, the authors were able to obtain differently shaped heating patterns. This technology poses some limitations, such as fine dimensional detailing due to ink spraying. A figure of their automated spraying system is observed in Figure 3.9.

The same concept has been applied by Liu et al. [95]. In their work, the authors used heat shrink sheets (PE sheets) and deposited black ink to activate via infrared light and bend the material to obtain self-assembly of structures. A similar idea of depositing carbon ink in different patterns was suggested by Zolfaghatian et al. [183]. In their work, a chitosan and CB ink was deposited on top of the heat shrink sheets to produce a similar activation. However, because of the use of their manufacturing technique, they were not able to deposit ink in different patterns. Hence the ink was deposited only as strips in bending joints for a self-folding structure.

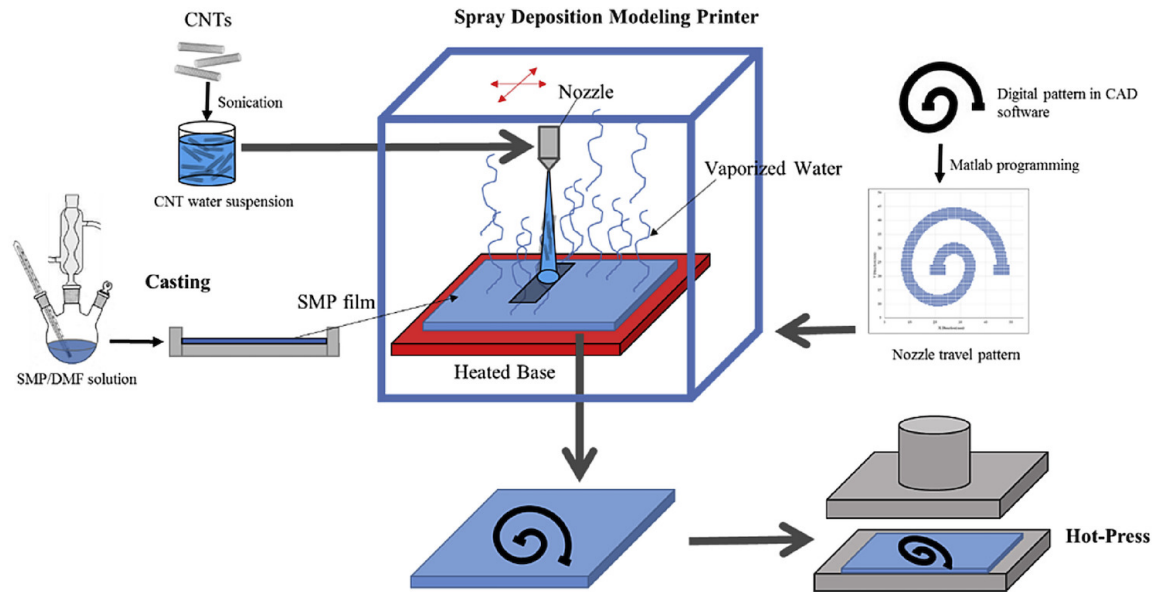


Figure 3.9: Ink deposition of CNT. Image reprinted with the permission of [160]

### 3.2.2 Long fibre reinforced SMPC

Although the multifunctionality of particle dispersed SMPCs has shown to be successful, achieving homogeneous dispersion is a constant issue for mass production. Continuous fibres have the advantage of reinforcing the material matrix far more than embedding particles, which can lead to high load-bearing applications. Although continuous fibre SMPCs exists mainly for thermosets, fibre-reinforced thermoplastics with automated fibre placement is a field that has been studied for decades in common thermoplastics [9]. 3D printing of this technology is challenging due to slow placement speeds to achieve consolidation between plies. This technology has become popular with the aid of affordable robotic systems. Works have shown that by manipulating fibre placement, the mechanical performance of composites can be altered due to their anisotropy [65]. There are mainly two methods that have been used to show an SME when using continuous fibre placement. The first, by material extrusion, used primarily with thermoplastic matrices, and the second by automated laminated ply fibre placement, a summary of the manufacturing techniques used for thermoplastic and thermoset long reinforced SMPCs is seen in the right hand side of Figure 3.3.

## Material Extrusion

A notable 3D printing brand Markforged<sup>TM</sup> was the first company to sell continuous fibre placement for FDM 3D printers. FDM printers commonly allow the placement of continuous synthetic fibres such as aramid based Kevlar<sup>TM</sup>, carbon and glass fibres continuously along the printing tool path. For instance, Wang et al. [158] used PA66 as the matrix and embedded continuous carbon fibres. Figure 3.10a and b show a 3D printing FDM extrusion head in which a carbon fibre thread is fed through an upper orifice. The fibre is coated with resin and extruded through the nozzle. Fibre content can be controlled by increasing the amount of resin extruded through the nozzle. This work did not take advantage of the intrinsic SME but showed shape shifting based on localized eigen strains produced by CTE mismatch. The shape-changing procedure can be observed in Figure 3.10c. Examples of the deployment of the technology can be observed in Figure 3.10 d and e. The authors also suggested that the SME could also be activated by Joule heating through the carbon-fibre plies. Although this technology is not based on the SME of SMPs, this 3D printed composite is a clear pathway for the future of smart thermoplastic composites in the AM world and can provide different functionalities such as multiple or reverse shape storage to SMPCs.

Following this work, and based on the same FDM principle, Shen et al. [140] introduced 3D printing of SMP thermoplastic matrix reinforced with continuous carbon fibre for reinforcement. The effects on the tensile mechanical properties of the SMPCs were studied, such as printing speed, temperature and ply angle. An SME was observed, but no quantitative results were presented in this work. Although the results shown in this work are preliminary, they show great potential in the reinforcement of thermoplastic SMPCs. Following this work, Zeng et al. [178] modified and used a commercially available desktop printer to manufacture an SMPC with a PLA matrix and continuous carbon fibres. The authors activated the SME of a bent sample via joule heating of the conductive fibres. The 3D printing parameters influence good fibre impregnation and, therefore, the mechanical and SMPC characteristics of the printed material. Thus this technology is constrained by low printing speeds at the moment, which is an issue for mass manufacturing and large scale product production. An opportunity to optimize printing and obtain adequate shape memory properties is currently available in this area.

Although not completely manufactured by additive manufacturing, there are a few works that are worth mentioning since they demonstrate the versatility of placing long filler material in an additive manufactured SMP matrix. A few works have added SMA wires to SMP in the past, but recently Kang et al. added it to an extrusion-based 3D printed structure by leaving gaps within the material for SMA wire placement. Material impregnation is a concern in this work [59]. The use of SMA in SMP matrices can be used for a two way reversible activation of the SME and potential use in crawling robots [154].

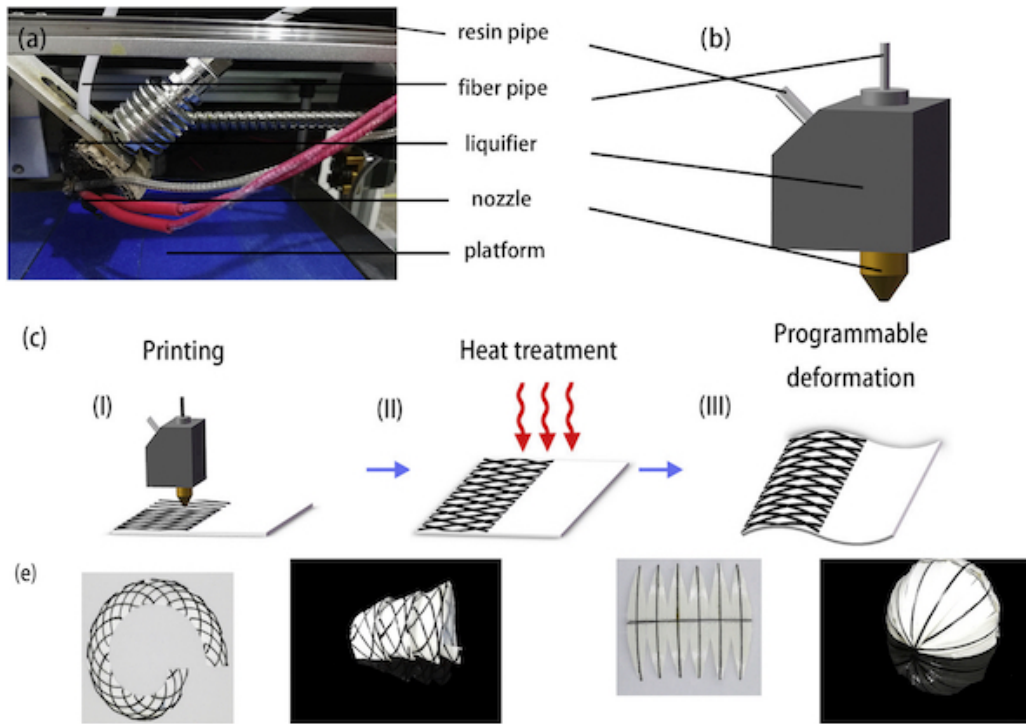


Figure 3.10: a) FDM Continuous fibre placement and (b) nozzle. (c) The 3D printing and shape memory storage of the process. (d) and (e) are examples of accomplished shape-shifting with the technology. All images were reprinted and with the permission of [158]. A section of two images from the publication have been joined in this figure for the relevance and purpose of this chapter.

### Lamination

The concept of 4D printing has been extended to different material composites. Hoa et al. [155, 47] proposed that by using an automated layup system, prepreg laminated epoxy carbon fiber plies can be placed in different angled orientations to exploit the warping created due to the anisotropy of the material, after this is heated. The novelty of this work is relevant to SMPs in the sense that a temporary shape can be stored due to the CTE mismatch between plies which causes a controlled warping. This technology removes the need for molds when using curved shapes. Figure 3.11 a is an image of a 4D printed laminate after it has been activated, while Figure 3.11b is a laminated showing a tubular structure after it has been activated. This technology can be useful for high load bearing applications that require a one time shape shifting.

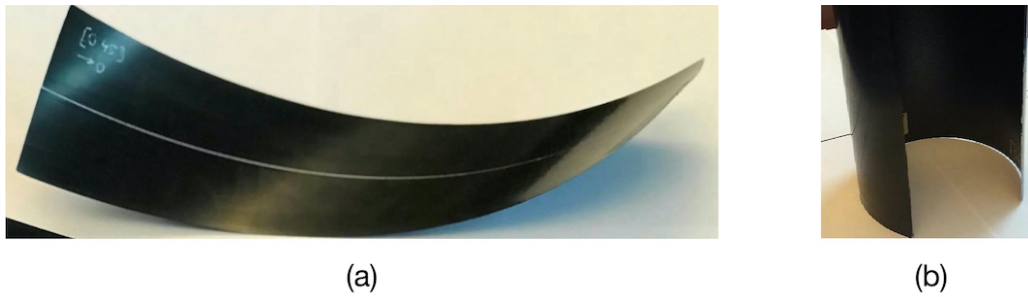


Figure 3.11: Figure (a) is a photograph of a laminate with a high curvature after activation and b) is a laminate with small curvature. Images reprinted with the permission of [47]

### 3.3 Multi-Material SMPC

Multi-material printing is a relative new approach in AM that will become popular in the coming years due to the ability to deposit materials next to each other with a good interphase bonding. This technique offers a wide range of advantages and has been exhaustively looked at in recent years. Pinho et al. has conducted an excellent review on the multiple actuation methods for 4D printing, and has made a special distinction to multimaterial bilayer printing [125]. We will provide here a summary and an introduction to understand and show the potential this technology has on the use of AM particle and fibre/particle reinforced SMPCs.

Design considerations and ideas include localized hinges that activate the SME in an SMPC for localized activation to use in an origami self-folding configuration. The use of LCE [174] next to SMP may enable multiple shapes and self-programming abilities for the SMPC [71, 39]. Perhaps one of the most crucial gaps at the moment, and the most interesting in multi-material printing, is the potential creation of functionally graded materials, where different reinforcing components or materials mix in a gradient manner to simulate materials found in nature such as cells, tissues, wood or teeth [120]. Gradient changes in stiffness, electrical and thermal conductivity could yield a sequential activation of the SME, obtain multi-functionality for SMPCs and avoid stress concentration and weak interphase bonding between materials.

Thermally actuated multi-material prints have enabled the use of particle filled composites to create a heating medium through resistive, inductive or infrared heating. One of the most exciting combinations of multi-material printing is the creation of Thermorph [4] by An et al. In their work, the authors 3D printed, using FDM, a PLA and TPU sequence to create a 4D printed structure. Complex geometries were created with this very accessible technology. The use of two materials, one active and one constraining, in this case, PLA and TPU respectively, created the programmable strains through rapid cooling. Printing speed and cooling in this process are crucial

to obtain the stored shape. In their work, the authors showed the 3D printing of a complex flower with this technology, and proposed different printing configurations to achieve a variety of kinetics. The possibility of Thermoform opens a few future avenues for the SMPC world, such as remote activation of the 3D printed shape. Following this work, Kacergis et al. investigated the printing parameters for 4D printing based on bilayer PLA/TPU composites but suggested that surrounding heat activation might not be the best choice to achieve field applications of 4D printing [58]. Garces et al. [37, 36] proposed the 3D printing of SMPU with a Graphene oxide/PLA bilayer composite. Although the authors did not look at the direct 4D print phenomena, they proposed the actuation of their bilayer composite. A smart design must always be considered since not all the structural material needs to be designed with a shape morphing material, rather sectional heating of the SME can be performed to obtain the required SME activation [111].

Previously, we mentioned that one of the advantages of polyjet printing is a great interphase bonding between various materials due to their liquid state before curing. Oxman et al. have previously discussed the possibility of gradient-like mixtures between a variety of materials using this 3D printing technology. [120]. By taking advantage of this capability, Ge et al. 3D printed what they identified as Printed Active Composites (PACs) [40]. PACs are composed of glassy polymer fibres as SMPs (with  $T_g$  of  $60^\circ C$ ) embedded in a rubbery matrix. The materials used for this structure are off the shelf with commercial names, Tango Black and Verowhite, respectively, from Stratasys. A study on the mechanical properties of these materials has been reported [55]. Using the same materials, Wu et al. showed that by mixing these two materials in different ratios, different glass transition temperatures  $T_g$  may be achieved and create what the authors called Digital Materials [164]. This material tailorability was used for sequential folding and activation of the SME [173]. Figure 3.12c shows the manufacturing process and (a) and (b) show the application of a self-folding box. Other works have demonstrated that this technique can also allow for material self-locking [103] such as for a self-locking box. Using this technology, authors also proposed the design of hinges and the activation of these by using resistive heating wires [2]. Additionally, DIW silver wires were deposited on an SMP 3D matrix by inkjet for sensing capabilities [114]. The pioneer research group in this technology has conducted a review on 4D printing and is recommended for the reader [71]. The activation process, the application of a self-folding box and the printing technology can be seen in Figure 3.12.

Multi-material printing with DIW is also possible by using different printing heads. The use of multiple materials is not new and has been used to print materials other than SMPs [68]. Kokkinis et al. demonstrated the multi-material printing of a 3D structure activated at two different temperatures. The authors used two different stimuli: direct heating and light irradiation. The authors used PCLMA as the SMP resin and modified it to create multiple activation temperatures. A CNT ink was deposited on top of the print to enhance heating by irradiation [137].

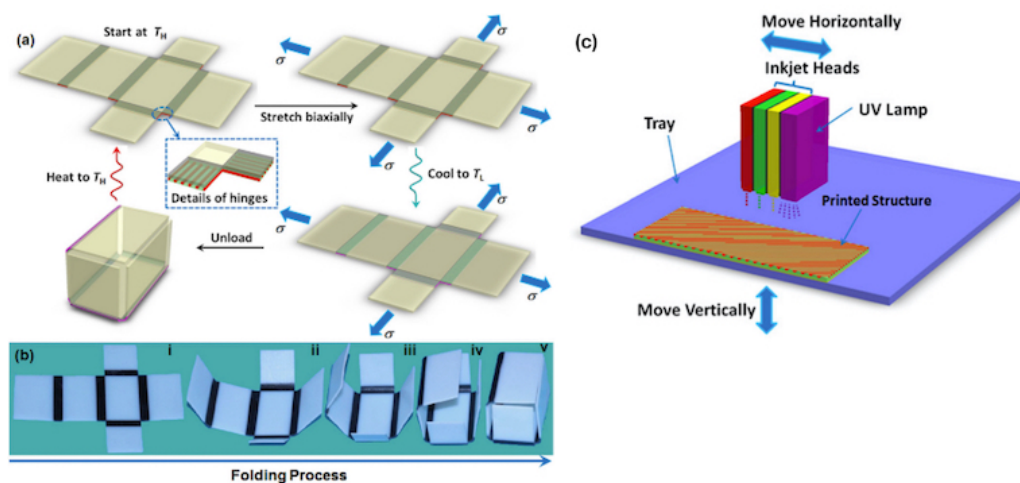


Figure 3.12: (a) shows the activation process of PACs, (b) a self-folding application and the (c) manufacturing of PACs. This image is reprinted with the permission from [40]. (In this image sections of two figures have been used for the purpose and relevance of this chapter)

Moisture actuation of multi-material printing lies heavily within the hydrogel material spectrum. Bilayer hydrogel-based bilayer composites have been investigated extensively. The shape change lies in a simple concept. Hydrophilic polymers absorb water molecules in their polymer network, which produces swelling. 3D printing a hydrophilic polymer next to a rubbery material can produce a bending actuation [125, 130]. Dehydration of the material will produce a reverse actuation of the composite. Material extrusion FDM has been used to manufacture multi-material structures based on this concept [10]. Baker et al. used thermoplastic PU hydrogel filaments to create a trilayer composite based on a hydrophilic polyurethane core (Tecophilic) and hydrophobic polyurethane skins (Ninjaflex) to promote actuation. Upon dehydration, the actuator return to its original configuration. Figure 3.13 shows the fabrication process (a) and the reversible actuation method by hydration.

Material jetting has also been used to create moisture activated multi-material active prints. The materials used are the Verowhite and Tangoblack by Stratasys. Verowhite is a hydrophilic polymer, while the second if a hydrophilic material. Thorough reviews on the use of these materials can be found in [125, 71, 130].

Finally, particle orientation to achieve shape change as demonstrated by Kokkinis is referred to as "5D" printing [68]. This is a technology that revolutionizes AM. In their work, the authors use multiple printing heads and inks to create a multifunctional material. The fifth dimension is defined as the ability to rotate the distributed particles in a resin. This was done by using an electromagnet to orientate particle deposition. At the moment, particle orientation has only been

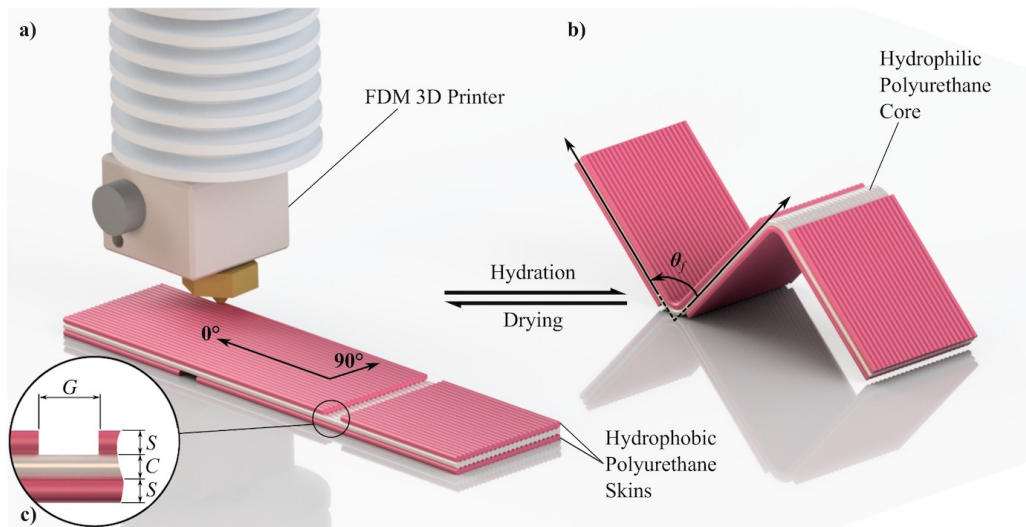


Figure 3.13: CAD model demonstrating the AM process in (a), followed by the activation of the shape change. (Open source article and image)[10]

achieved by using DIW, and there is still the opportunity to change particle dispersion for different manufacturing technologies and applications for SMPs [68].

### 3.4 Opportunities Ahead

Novel and exciting engineering applications of SMPCs are starting to become possible thanks to the advancements in AM. We believe there is still significant progress to be done in the areas of AM, SMP, and SMPC before furthering AM based SMP and SMPCs. Improvements are still needed in the areas of SMPs and SMPCs' material performance, optimization of AM methods for SMPs and SMPCs, models for design and optimization of additive manufactured material performance, as well as controlled activation methods of the SME.

At the core of this research area also lies a high cost and a lack of readily available materials to test their performance. Increasing accessibility to SMPs can increase the available data to researchers that can contribute to the optimization and design of better raw SMP resins. SMPs with higher recovery rates and higher recovery forces are desired for a variety of applications.

A more extensive data set could also mean better optimization algorithms and models for obtaining adequate printing parameters for different types of SMPs. Models and algorithms for re-calibration of these printing parameters based on the particles or fibre filler material can improve additive

manufactured material performance, and ease for device designing at an industrial scale.

Perhaps one of the main limitations of the AM technologies presented in this paper is the slow manufacturing speeds caused by the layer-by-layer manufacturing procedure. Most of the technologies present slow printing speeds, which is a definite obstacle in advancing industrial and mass-scale applications. Volumetric printing technologies like that presented by Kelly et al. [62] are a gateway to new fast printing techniques. This technique has not yet been applied to 3D printing of SMPs or 4D printing.

Common issues concerning 3D printing of particle doped SMPs are still vast. For material extrusion technologies, there is the issue of clogging due to high viscosities produced by filler material content. Researchers are forced to compromise printing resolution by increasing the nozzle diameter in the attempts to avoid clogging. Attempts at modifying the rheology of the composite have been done for DIW [24], and FDM [102] technologies to produce shear-thinning. However, research on shear-thinning produced by particle addition in different AM processes is still new and challenging since different aspect ratios of particles, and fibre lengths would affect the rheological characteristics [1]. Perhaps special additives used to tailor the polymer melt properties in well established extrusion technologies can be of help in tackling this issue in the near future. Effects of particle alignment produced by material extrusion based AM in SMPCs has not been investigated. Alignment of particles in SMPCs may also be achieved by using magnetic fields and 5D printing. For photopolymers, printing with conductive particles is still complicated since particles absorb UV light, which can affect the curing process and produce printing resolution drawbacks.

Besides the evident need for optimization of printing parameters for SMPs to minimize porosity, imperfections and crack growth on the printed parts, a study on the effects of the printing parameters on the 4D printed SME, i.e. cooling rate, in SMPs and SMPCs is an area that is still left untouched. To fully exploit AM of SMPCs, a study on 3D printing with various techniques at different scales is necessary to fully understand the applicability and limitations of specific manufacturing techniques and materials.

3D printing of SMPCs with continuous reinforcement is still challenging. Fibre dispersion and homogeneous impregnation is still problematic as it is severely affected by printing speed. Effects of fibre placement on the SME need also to be further investigated. Potential applications with different fibre orientations and effects on the SME is still an area that could be investigated in more depth.

Although much work has been done in the modelling area of SMPs and SMPCs [166], at the moment, there is still a lack of user-friendly models at the design stage to predict and understand the shape memory properties of SMPs and SMPCs with any filler material. Thermomechanical models that account for a 3D printed structure for SMP and their fillers are an area that is still

to be developed. A few works like that by Abishera et al.[128] have shown progress in predicting the recovery stress with respect to different printing speeds on 4D printed structures. This work is particularly interesting since most publications use generic thermoviscoelastic models that assume a solid part and ignore the AM process. Generalized coupled models that are relevant to activation methods of the SME i.e. via joule heating, infrared heating or induction for thermal-active SMPCs, are still in the early stages of development. Only a few have been conducted in this area for specific thermal activation of the SME [101, 123, 172].

Concerning the activation of SMPCs, there still exists an inaccurate activation of the SME in terms of the amount of recovery obtained in time. Still, there has been no evidence to show that one can stop and resume activation when desired. Activation of the SME is still done without fundamental understanding of control systems, and there is no feedback for the intermediary steps while activation has occurred. A few feedback close loops controls have been proposed for thermally activated SMPCs via resistive heating [37], but this is just the beginning in an area that is still in need of research. To the authors' knowledge, there has been no attempt to obtain feedback control from moisture activated materials, although there are some new moisture sensors incorporated in SMPC devices [157]. More advanced techniques, such as data-driven machine learning could be desired to predict and understand the activation of these SMPCs. The inclusion of 3D printed sensors within the SMPC structure, simulations, and FEM models are needed for data training models and general feedback control of the structures [184]. The addition of multi-functional particles could also be applied in energy harvesting. There have been works in which cathode and anode inks have been deposited to 3D print lithium-ion micro-batteries, the same could be implemented in an SMPC structure [147]. AM with complementary or multi-filler materials is still an area that can potentially accomplish a variety of applications for SMPCs.

More tailorable material properties of SMPCs will open endless opportunities. AM has opened the doors to obtain controlled gradient variability of material properties [129]. Gradient changes in mechanical, electrical and thermal properties applied to SMPCs can offer the possibility of sequential activation of parts and a blended fusion between different material parameters. For instance, Oxman et al. proposed [120] the concept of a 3D printed chair, where elastic materials for ergonomic back support could be 3D printed perfectly blended into the structural components. The same concept can be applied to foldable furniture for storage optimization and furniture transportation.

Finally, all these advances and possible areas of study contribute to opportunities in design using SMPCs in various applications. Simple designs concepts like origami-like actuation and use of self-reconfigurable structures like miteins can serve as an inspiration to redefine the design concepts. A framework for design with SMPCs has been put forward by Jian et al. [53]. The use of functional materials for end AM is proposed in their framework and is shown in the schematic in Figure 3.14. There exist a few key concepts that every engineer must account for in the design process when

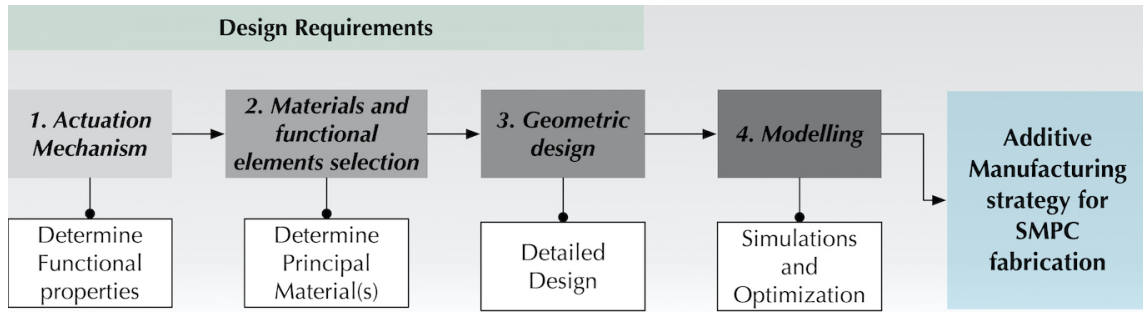


Figure 3.14: 4D SMPC design framework. Image modified from [53]

using SMPCs: the stimuli needed, the structural requirements and layout, material selection and geometrical requirements. The design process is to be aided by modelling and simulations. A summary, troubleshooting and potential design considerations to have for future SMP device design based on the literature has been proposed and is recommended for designers ready to implement AM with SMPCs [29]. Although SMPCs offer a wide variety of possible kinetics, the true advantages lie in the benefit of shape-shifting with complex curves, and surface topography [115]. With the use of AM, topology optimization can create lightweight 4D printed actuators for multiple applications. Ingenious application designs are the next opportunities in this area. However, a change in traditional design needs to be made to exploit the benefits of SMPC fully. Initial design stage models need to be supplied to engineers and designers, followed by complex simulations for design optimization implemented in CAD and CAM software.

### 3.5 Conclusions

AM of SMPC is the beginning of a new area for the multifunctional materials. Advances in 3D printing in different technologies, i.e. AM with material extrusion, photopolymerization, lamination and powder-based technologies, have enabled the potential for engineering design with complex shape-shifting materials. The multifunctionality of materials by the addition of short fibers, nanoparticles and continuous fibre placement to enhance material properties of 3D printed structures is the first step towards exploiting the shape memory capabilities of SMPCs. Perhaps the most crucial contribution and game-changing ability of AM is the opportunity to create multi-material structures with ease. Layered composites that enable self-sensing, programming, activating and correcting are the future and the next step to see materials as machines. With the ability to embed electronics into a polymeric structure, complete control of the shape-changing capabilities of SMPC becomes possible. This review paper looks at the advancements made by researchers in the areas of

AM of SMPC with respect to filler material addition and manufacturing strategy. An overview of research opportunities has been put forward to contribute to future SMPC advancements. Finally, design considerations have also been discussed as a reminder for researchers that design towards real-life applications is the ultimate goal for these materials using AM.

### 3.6 References

- [1] Shweta Agarwala, Guo Liang Goh, Guo Dong Goh, Vishwesh Dikshit, and Wai Yee Yeong. *Chapter 10 - 3D and 4D printing of polymer/CNTs-based conductive composites*. Elsevier Inc., 2020.
- [2] Saeed Akbari, Amir Hosein Sakhaei, Kavin Kowsari, Bill Yang, Ahmad Serjouei, Zhang Yuanfang, and Qi Ge. Enhanced multimaterial 4D printing with active hinges. *Smart Materials and Structures*, 27(6):065027–16, May 2018.
- [3] Javed Alam, Aslam Khan, Manawwer Alam, and Raja Mohan. Electroactive Shape Memory Property of a Cu-decorated CNT Dispersed PLA/ESO Nanocomposite. *Materials*, 8(9):6391–6400, September 2015.
- [4] Byoungkwon An, Hsiang-Yun Wu, Teng Zhang, Lining Yao, Ye Tao, Jianzhe Gu, Tingyu Cheng, Xiang 'Anthony Chen, Xiaoxiao Zhang, Wei Zhao, Youngwook Do, and Shigeo Takahashi. Thermorph : Democratizing 4D Printing of Self-Folding Materials and Interfaces. In *the 2018 CHI Conference*, pages 1–12, New York, New York, USA, 2018. ACM Press.
- [5] Soo Chan An, Eunsongyi Lee, Chang Hyun Lee, Hoon Yeub Jeong, Taek Sun Kwon, Jeong Hae Lee, and Young Chul Jun. Sharp Fano Resonance and Spectral Collapse in Stimuli-Responsive Photonic Structures. *Advanced Optical Materials*, 7(5):1801206–8, December 2018.
- [6] Jean-Claude André. *From Additive Manufacturing to 3D/4D Printing 2*. Current Techniques, Improvements and their Limitations. John Wiley & Sons, November 2017.
- [7] Xinling Ao, Deyan Kong, Ziyang Zhang, and Xinli Xiao. Enhancing recovery speed and anti-wear capability of high-temperature shape memory polymer with modified boron nitride nanoparticles. *Journal of Materials Science*, 55(10):4292–4302, December 2019.
- [8] D I Arun, P Chakravarthy, B S Girish, K S Santhosh Kumar, and B Santhosh. Experimental and Monte Carlo simulation studies on percolation behaviour of a shape memory polyurethane carbon black nanocomposite. *Smart Materials and Structures*, 28(5):055010, April 2019.

- [9] Z August, G Ostrander, and J Michasiow J. Recent developments in automated fiber placement of thermoplastic composites. In *SAMPE 2013*, Long Beach, 2013. SAMPE 2013, Education Green Sky.
- [10] Anna B Baker, Simon R G Bates, Thomas M Llewellyn-Jones, Laurie P B Valori, Michael P M Dicker, and Richard S Trask. 4D printing with robust thermoplastic polyurethane hydrogel-elastomer trilayers. *Materials and Design*, 163(C):107544, February 2019.
- [11] Sajad Razavi Bazaz, Omid Rouhi, Mohammad Amin Raoufi, Fatemeh Ejeian, Mohsen Asadnia, Dayong Jin, and Majid Ebrahimi Warkiani. 3D Printing of Inertial Microfluidic Devices. *Nature Publishing Group*, pages 1–14, March 2020.
- [12] Murat Bengisu and Marinella Ferrara. *Materials that Move*. Smart Materials, Intelligent Design. Springer, April 2018.
- [13] Prahar M Bhatt, Max Peralta, Hugh A Bruck, and Satyandra K Gupta. Robot Assisted Additive Manufacturing of Thin Multifunctional Structures. In *ASME 2018 13th International Manufacturing Science and Engineering Conference*, pages 1–10. American Society of Mechanical Engineers, September 2018.
- [14] H Bikas, P Stavropoulos, and G Chryssolouris. Additive manufacturing methods and modelling approaches: a critical review. *The International Journal of Advanced Manufacturing Technology*, 83(1-4):389–405, July 2015.
- [15] M Bodaghi and W H Liao. 4D printed tunable mechanical metamaterials with shape memory operations. *Smart Materials and Structures*, 28(4):045019–16, March 2019.
- [16] John Carrell, Garrett Gruss, and Elizabeth Gomez. Four-dimensional printing using fused-deposition modeling: a review. *Rapid Prototyping Journal*, ahead-of-print(ahead-of-print):155–15, January 2020.
- [17] Kaijuan Chen, Xiao Kuang, Vincent Li, Guozheng Kang, and H Jerry Qi. Fabrication of tough epoxy with shape memory effects by UV-assisted direct-ink write printing. *Soft Matter*, 14(10):1879–1886, 2018.
- [18] Shaojun Chen, Jinlian Hu, and Haitao Zhuo. Properties and mechanism of two-way shape memory polyurethane composites. *Composites Science and Technology*, 70(10):1437–1443, September 2010.
- [19] Shaojun Chen, Shixin Yang, Ziyu Li, Shiwei Xu, Hongming Yuan, Shiguo Chen, and Zhaochuan Ge. Electroactive two-way shape memory polymer laminates. *Polymer Composites*, 36(3):439–444, January 2015.

- [20] Tian Chen and Kristina Shea. An Autonomous Programmable Actuator and Shape Reconfigurable Structures Using Bistability and Shape Memory Polymers. *3D Printing and Additive Manufacturing*, 5(2):91–101, June 2018.
- [21] Yu Chen, Irina Tatiana Garces, Tian Tang, and C. Ayranci. Cellulose nanocrystals reinforced shape memory polymer cardiovascular stent. *Rapid Prototyping Journal*, ahead-of-print(ahead-of-print):19, December 2020.
- [22] Li Chong, Seeram Ramakrishna, and Sunpreet Singh. A review of digital manufacturing-based hybrid additive manufacturing processes. *International Journal Advanced Manufacturing Technology*, pages 1–20, February 2018.
- [23] Yu Ying Clarrisa Choong, Saeed Maleksaeedi, Hengky Eng, Suzhu Yu, Jun Wei, and Pei-Chen Su. High speed 4D printing of shape memory polymers with nanosilica. *Applied Materials Today*, 18:100515, March 2020.
- [24] Brett G Compton and Jennifer A Lewis. 3D-Printing of Lightweight Cellular Composites. *Advanced Materials*, 26(34):5930–5935, June 2014.
- [25] Xihua Cui, Jianwen Chen, Yutian Zhu, and Wei Jiang. Natural sunlight-actuated shape memory materials with reversible shape change and self-healing abilities based on carbon nanotubes filled conductive polymer composites. *Chemical Engineering Journal*, 382:122823, February 2020.
- [26] S C Daminabo, S Goel, S A Grammatikos, H Y Nezhad, and V K Thakur. Fused deposition modeling-based additive manufacturing (3D printing): techniques for polymer material systems. *Materials Today Chemistry*, 16:100248, June 2020.
- [27] Eleonora D’Elia, Hanaë Said Ahmed, Ezra Feilden, and Eduardo Saiz. Electrically-responsive graphene-based shape-memory composites. *Applied Materials Today*, 15:185–191, June 2019.
- [28] Massimo Di Nicolantonio, Emilio Rossi, and Paride Stella. Generative Design for Printable Mass Customization Jewelry Products. In *Advances in Additive Manufacturing, Modeling Systems and 3D Prototyping*, pages 143–152. Springer, Cham, Cham, July 2019.
- [29] Andrés Díaz Lantada. Systematic Development Strategy for Smart Devices Based on Shape-Memory Polymers. *Polymers*, 9(12):496–19, December 2017.
- [30] Zhen Ding, Chao Yuan, Xirui Peng, Tiejun Wang, H Jerry Qi, and Martin L Dunn. Direct 4D printing via active composite materials. *Science Advances*, 3(4):e1602890–8, April 2017.
- [31] Fei-Peng Du, En-Zhou Ye, Wen Yang, Tian-Han Shen, Chak-Yin Tang, Xiao-Lin Xie, Xing-Ping Zhou, and Wing-Cheung Law. Electroactive shape memory polymer based on optimized

- multi-walled carbon nanotubes/polyvinyl alcohol nanocomposites. *COMPOSITES PART B*, 68(C):170–175, January 2015.
- [32] Hengky Eng, Saeed Maleksaeedi, Suzhu Yu, Yu Ying Clarrisa Choong, Florencia Edith Wiria, Ruihua Eugene Kheng, Jun Wei, Pei-Chen Su, and Huijun Phoebe Tham. Development of CNTs-filled photopolymer for projection stereolithography. *Rapid Prototyping Journal*, 23(1):129–136, January 2017.
- [33] M Fejos and G Romhány. Shape memory characteristics of woven glass fibre fabric reinforced epoxy composite in flexure. *Journal of Reinforced . . .*, 2012.
- [34] Márta Fejős, Kolos Molnár, and József Karger-Kocsis. Epoxy/Polycaprolactone Systems with Triple-Shape Memory Effect: Electrospun Nanoweb with and without Graphene Versus Co-Continuous Morphology. *Materials*, 6(10):4489–4504, October 2013.
- [35] I T Garces, S Aslanzadeh, and Ayranci C. Boluk, Y. Cellulose nanocrystals (CNC) reinforced shape memory polyurethane ribbons for future biomedical applications and design. *Journal of Thermoplastic Composites*, 4(74003):089270571880633, October 2018.
- [36] I T Garces and C. Ayranci. A view into additive manufactured electro-active reinforced smart composite structures. *Manufacturing Letters*, 16:1–5, April 2018.
- [37] I T Garces and C. Ayranci. Active control of 4D prints: Towards 4D printed reliable actuators and sensors. *Sensors and Actuators, A: Physical*, 301:111717, January 2020.
- [38] Carlos A Garcia Rosales, Mario F Garcia Duarte, Hoejin Kim, Luis Chavez, Deidra Hodges, Paras Mandal, Yirong Lin, and Tzu-Liang Bill Tseng. 3D printing of shape memory polymer (SMP)/carbon black (CB) nanocomposites with electro-responsive toughness enhancement. *Materials Research Express*, 5(6):065704–10, June 2018.
- [39] Qi Ge, Conner K Dunn, H Jerry Qi, and Martin L Dunn. Active origami by 4D printing. *Smart Materials and Structures*, 23(9):094007–16, August 2014.
- [40] Qi Ge, H Jerry Qi, and Martin L Dunn. Active materials by four-dimension printing. *Applied Physics Letters*, 103(1):131901, September 2013.
- [41] Qi Ge, Amir Hosein Sakhaei, Howon Lee, Conner K Dunn, Nicholas X Fang, and Martin L Dunn. Multimaterial 4D Printing with Tailorable Shape Memory Polymers. *Nature Publishing Group*, 6:31110, August 2016.
- [42] Guo Liang Goh, Shweta Agarwala, and Wai Yee Yeong. Directed and On-Demand Alignment of Carbon Nanotube: A Review toward 3D Printing of Electronics. *Advanced Materials Interfaces*, 6(4):1801318–29, January 2019.

- [43] Jahan Zeb Gul, Memoon Sajid, Muhammad Muqet Rehman, Ghayas Uddin Siddiqui, Imran Shah, Kyung-Hwan Kim, Jae-Wook Lee, and Kyung Hyun Choi. 3D printing for soft robotics – a review. *Science and Technology of Advanced Materials*, 19(1):0–0, March 2018.
- [44] I Sedat Gunes, Guillermo A Jimenez, and Sadhan C Jana. Carbonaceous fillers for shape memory actuation of polyurethane composites by resistive heating. *Carbon*, 47(4):981–997, April 2009.
- [45] Martin D Hager, Stefan Bode, Christine Weber, and Ulrich S Schubert. Shape memory polymers: Past, present and future developments. *Progress in Polymer Science*, 49-50:3–33, October 2015.
- [46] Christopher J Hansen. 3D and 4D printing of nanomaterials: Processing considerations for reliable printed nanocomposites. In *3D and 4D Printing of Polymer Nanocomposite Materials*, pages 25–44. Elsevier, 2020.
- [47] Suong V Hoa and Xiao Cai. Twisted composite structures made by 4D printing method. *Composite Structures*, 238:111883, April 2020.
- [48] Alina-Maria Holban and Alexandru Grumezescu. *Materials for Biomedical Engineering: Nanobiomaterials in Tissue Engineering*. Elsevier, March 2019.
- [49] G F Hu, A R Damanpack, M Bodaghi, and W H Liao. Increasing dimension of structures by 4D printing shape memory polymers via fused deposition modeling. *Smart Materials and Structures*, 26(1):125023, December 2017.
- [50] Dechuan Hua, Xiaoqin Zhang, Zhongying Ji, Changyou Yan, Bo Yu, Yuandong Li, Xiaolong Wang, and Feng Zhou. 3D printing of shape changing composites for constructing flexible paper-based photothermal bilayer actuators. *J. Mater. Chem. C*, 6(8):2123–2131, 2018.
- [51] Marta Invernizzi, Stefano Turri, Marinella Levi, and Raffaella Suriano. 4D printed thermally activated self-healing and shape memory polycaprolactone-based polymers. *European Polymer Journal*, 101:169–176, April 2018.
- [52] Danish Iqbal and Muhammad Samiullah. Photo-Responsive Shape-Memory and Shape-Changing Liquid-Crystal Polymer Networks. *Materials*, 6(1):116–142, January 2013.
- [53] Bingcong Jian, Frédéric Demoly, Yicha Zhang, and Samuel Gomes. Towards a Design Framework for Multifunctional Shape Memory Polymer Based Product in the Era of 4D Printing. In *ASME 2018 Conference on Smart Materials, Adaptive Structures and Intelligent Systems*, pages 1–13. American Society of Mechanical Engineers, November 2018.
- [54] H U Jinlian. *Shape memory polymers and textiles*. Woodhead Publishing Limited, Hong Kong Polytechnic University, Kowloon, Hong Kong, January 2007.

- [55] Joanne Teoh, Jia An, Xiaofan Feng, Yue Zhao, Chee Chua, and Yong Liu. Design and 4D Printing of Cross-Folded Origami Structures: A Preliminary Investigation. *Materials*, 11(3):376–27, March 2018.
- [56] Cagri Ayrançi Jorge Villacres, David Nobes. Additive manufacturing of shape memory polymers: Effect of print orientation and infill percentage on shape memory recovery properties. *Rapid Prototyping Journal*, June 2020.
- [57] Siddharth Joshi, Krishna Rawat, Karunakaran C, Vasudevan Rajamohan, Arun Tom Mathew, Krzysztof Koziol, Vijay Kumar Thakur, and Balan A S S. 4D printing of materials for the future: Opportunities and challenges. *Applied Materials Today*, 18:100490–22, March 2020.
- [58] Lukas Kačergis, Rytis Mitkus, and Michael Sinapius. Influence of fused deposition modeling process parameters on the transformation of 4D printed morphing structures. *Smart Materials and Structures*, 28(10):105042–10, September 2019.
- [59] Minkyu Kang, Youngjun Pyo, Joon young Jang, Yunchan Park, Yeon-Ho Son, MyungChan Choi, Joo wan Ha, Young-Wook Chang, and Caroline Sunyong Lee. Design of a shape memory composite(SMC) using 4D printing technology. *Sensors and Actuators, A: Physical*, 283:187–195, November 2018.
- [60] Nand Jee Kanu, Eva Gupta, Umesh Kumar Vates, and Gyanendra Kumar Singh. Self-healing composites:A state of the art review. *Composites Part A*, 121:474–486, June 2019.
- [61] Kamal K Kar. *Composite materials: processing, applications, characterizations*. Landolt-Börnstein. SpringerMaterials fundamentals. Springer, Berlin, 2017.
- [62] Brett E Kelly, Indrasen Bhattacharya, Hossein Heidari, Maxim Shusteff, Christopher M Spadaccini, and Hayden K Taylor. Volumetric additive manufacturing via tomographic reconstruction. *Science*, 363(6431):1075–1079, March 2019.
- [63] Zhong Xun Khoo, Joanne Ee Mei Teoh, Yong Liu, Chee Kai Chua, Shoufeng Yang, Jia An, Kah Fai Leong, and Wai Yee Yeong. 3D printing of smart materials: A review on recent progresses in 4D printing. *Virtual and Physical Prototyping*, 10(3):103–122, September 2015.
- [64] Mohammad Reza Khosravani and Tamara Reinicke. 3D-printed sensors: Current progress and future challenges. *Sensors and Actuators, A: Physical*, 305:111916, April 2020.
- [65] Byung Chul Kim, Paul M Weaver, and Kevin Potter. Manufacturing characteristics of the continuous tow shearing method for manufacturing of variable angle tow composites. *Composites Part A*, 61(C):141–151, June 2014.

- [66] Yoonho Kim, Hyunwoo Yuk, Ruike Zhao, Shawn A Chester, and Xuanhe Zhao. Printing ferromagnetic domains for untethered fast-transforming soft materials. *Nature*, 558(7709):274–279, June 2018.
- [67] Hyunhyub Ko and Ali Javey. Smart Actuators and Adhesives for Reconfigurable Matter. *Accounts of Chemical Research*, 50(4):691–702, March 2017.
- [68] Dimitri Kokkinis, Manuel Schaffner, and Andr eacute R Studart. Multimaterial magnetically assisted 3D printing of composite materials. *Nature Communications*, pages 1–10, April 2019.
- [69] Fabian Kranert, Jana Budde, Philipp Neef, Robert Bernhard, Marius Lammers, Katharina Rettschlag, Tobias Grabe, Andreas Wienke, Jörg Neumann, Henning Wiche, Volker Wesling, Henning Ahlers, Roland Lachmayer, and Dietmar Kracht. 3D-printed, low-cost, lightweight optomechanics for a compact, low-power solid-state amplifier system. In Alexei L Glebov and Paul O Leisher, editors, *Components and Packaging for Laser Systems VI*, pages 4–13. SPIE, March 2020.
- [70] Xiao Kuang, Kaijuan Chen, Conner K Dunn, Jiangtao Wu, Vincent C F Li, and H Jerry Qi. 3D Printing of Highly Stretchable, Shape-Memory, and Self-Healing Elastomer toward Novel 4D Printing. *ACS Applied Materials & Interfaces*, 10(8):7381–7388, February 2018.
- [71] Xiao Kuang, Devin J Roach, Jiangtao Wu, Craig M Hamel, Zhen Ding, Tiejun Wang, Martin L Dunn, and Hang Jerry Qi. Advances in 4D Printing: Materials and Applications. *Advanced Functional Materials*, 29(2), January 2019.
- [72] Ruvini S Kularatne, Hyun Kim, Jennifer M Boothby, and Taylor H Ware. Liquid crystal elastomer actuators: Synthesis, alignment, and applications. *Journal of Polymer Science Part B: Polymer Physics*, 55(5):395–411, January 2017.
- [73] Xin Lan, Yanju Liu, Jinsong Leng, and Shanyi Du. Thermomechanical behavior of fiber reinforced shape memory polymer composite. In *International Conference on Smart Materials and Nanotechnology in Engineering*, pages 64235R–8. SPIE, December 2007.
- [74] S Lashgari, M Karrabi, I Ghasemi, H Azizi, M Messori, and K Paderni. Shape memory nanocomposite of poly(L-lactic acid)/graphene nanoplatelets triggered by infrared light and thermal heating. *Express Polymer Letters*, 10(4):349–359, 2016.
- [75] A Le Duigou, M Castro, R Bevan, and N Martin. 3D printing of wood fibre biocomposites: From mechanical to actuation functionality. *Materials and Design*, 96(C):106–114, April 2016.
- [76] Louis Laberge Lebel, Brahim Aissa, My Ali El Khakani, and Daniel Therriault. Ultraviolet-Assisted Direct-Write Fabrication of Carbon Nanotube/Polymer Nanocomposite Microcoils. *Advanced Materials*, 22(5):592–596, February 2010.

- [77] Amelia Yilin Lee, Jia An, and Chee Kai Chua. Two-Way 4D Printing: A Review on the Reversibility of 3D-Printed Shape Memory Materials. *Engineering*, 3(5):663–674, October 2017.
- [78] Ming Lei, Zhen Chen, Haibao Lu, and Kai Yu. Recent progress in shape memory polymer composites: methods, properties, applications and prospects. *Nanotechnology Reviews*, 8(1):327–351, November 2019.
- [79] Andreas Lendlein and Steffen Kelch. Shape-Memory Polymers. John Wiley & Sons, Inc., Hoboken, NJ, USA, 2002.
- [80] Jinsong Leng, Xin Lan, Yanju Liu, and Shanyi Du. Electroactive thermoset shape memory polymer nanocomposite filled with nanocarbon powders. *Smart Materials and Structures*, 18(7):074003–8, June 2009.
- [81] Jennifer A Lewis, James E Smay, John Stuecker, and Joseph Cesarano. Direct Ink Writing of Three-Dimensional Ceramic Structures. *Journal of the American Ceramic Society*, 89(12):3599–3609, December 2006.
- [82] Xiaofeng Li, Liancai Wang, Ziyang Zhang, Deyan Kong, Xinling Ao, and Xinli Xiao. Electroactive High-Temperature Shape Memory Polymers with High Recovery Stress Induced by Ground Carbon Fibers. *Macromolecular Chemistry and Physics*, 220(17):1900164–8, September 2019.
- [83] YueJia Li, Fenghua Zhang, Yanju Liu, and Jinsong Leng. 4D printed shape memory polymers and their structures for biomedical applications. *Science China Technological Sciences*, 63(4):545–560, February 2020.
- [84] Zhenghong Li, Haibao Lu, Yongtao Yao, and Long Lin. Thermomechanical performance and shape recovery behaviour of shape memory polymer nanocomposite incorporated with hexagonal boron nitride. *Pigment & Resin Technology*, 46(1):79–83, January 2017.
- [85] Chya-Yan Liaw and Murat Guvendiren. Current and emerging applications of 3D printing in medicine. *Biofabrication*, 9(2):024102–, June 2017.
- [86] Samuel Clark Ligon, Robert Liska, Jürgen Stampfl, Matthias Gurr, and Rolf Mühlhaupt. Polymers for 3D Printing and Customized Additive Manufacturing. *Chemical Reviews*, 117(15):10212–10290, July 2017.
- [87] Chutiwat Likitaporn, Phattarin Mora, Sunan Tiptipakorn, and Sarawut Rimdusit. Recovery stress enhancement in shape memory composites from silicon carbide whisker-filled benzoxazine-epoxy polymer alloy. *Journal of Intelligent Material Systems and Structures*, 29(3):388–396, May 2017.

- [88] C Liu, H Qin, and P T Mather. Review of progress in shape-memory polymers. *Journal of Materials Chemistry*, 17(16):1543, 2007.
- [89] Wenbo Liu, Nan Wu, and Kishore Pochiraju. Shape recovery characteristics of SiC/C/PLA composite filaments and 3D printed parts. *Composites Part A*, 108:1–11, May 2018.
- [90] Yang Liu, Fenghua Zhang, Jinsong Leng, Kun Fu, X Lucas Lu, Liyun Wang, Chase Cotton, Baozhong Sun, Bohong Gu, and Tsu-Wei Chou. Remotely and Sequentially Controlled Actuation of Electroactivated Carbon Nanotube/Shape Memory Polymer Composites. *Advanced Materials Technologies*, 4(12):1900600–8, November 2019.
- [91] Yang Liu, Wei Zhang, Fenghua Zhang, Xin Lan, Jinsong Leng, Shuang Liu, Xinqiao Jia, Chase Cotton, Baozhong Sun, Bohong Gu, and Tsu-Wei Chou. Shape memory behavior and recovery force of 4D printed laminated Miura-origami structures subjected to compressive loading. *COMPOSITES PART B*, 153:233–242, November 2018.
- [92] Yang Liu, Wei Zhang, Fenghua Zhang, Jinsong Leng, Shaopeng Pei, Liyun Wang, Xinqiao Jia, Chase Cotton, Baozhong Sun, and Tsu-Wei Chou. Microstructural design for enhanced shape memory behavior of 4D printed composites based on carbon nanotube/polylactic acid filament. *Composites Science and Technology*, 181:107692, September 2019.
- [93] Yanju Liu, Haiyang Du, Liwu Liu, and Jinsong Leng. Shape memory polymers and their composites in aerospace applications: a review. *Smart Materials and Structures*, 23(2):023001, February 2014.
- [94] Ye Liu, Ying Li, Guang Yang, Xiaotong Zheng, and Shaobing Zhou. Multi-Stimulus-Responsive Shape-Memory Polymer Nanocomposite Network Cross-Linked by Cellulose Nanocrystals. *ACS Applied Materials & Interfaces*, 7(7):4118–4126, February 2015.
- [95] Ying Liu, Julie K Boyles, Jan Genzer, and Michael D Dickey. Self-folding of polymer sheets using local light absorption. *Soft Matter*, 8(6):1764–1769, 2012.
- [96] Amit J Lopes, Mireya A Perez, David Espalin, and Ryan B Wicker. Comparison of ranking models to evaluate desktop 3D printers in a growing market. *Additive Manufacturing*, 35:101291, May 2020.
- [97] Ze-Xian Low, Yen Thien Chua, Brian Michael Ray, Davide Mattia, Ian Saxley Metcalfe, and Darrell Alec Patterson. Perspective on 3D printing of separation membranes and comparison to related unconventional fabrication techniques. *Journal of Membrane Science*, 523(C):596–613, February 2017.

- [98] Haibao Lu, Yongtao Yao, and Long Lin. Carbon-based reinforcement in shape-memory polymer composite for electrical actuation. *Pigment & Resin Technology*, 43(1):26–34, December 2013.
- [99] Hongsheng Luo, Zhiwei Li, Guobin Yi, Xihong Zu, Huan Wang, Yunjia Wang, Hailiang Huang, Jiwen Hu, Zhenfei Liang, and Benbin Zhong. Electro-responsive silver nanowire-shape memory polymer composites. *Materials Letters*, 134(C):172–175, November 2014.
- [100] Son Thai Ly and Joo Yong Kim. 4D printing – fused deposition modeling printing with thermal-responsive shape memory polymers. *International Journal of Precision Engineering and Manufacturing-Green Technology*, 4(3):267–272, July 2017.
- [101] Russell W Mailen, Michael D Dickey, Jan Genzer, and Mohammed A Zikry. A fully coupled thermo-viscoelastic finite element model for self-folding shape memory polymer sheets. *Journal of Polymer Science Part B: Polymer Physics*, 55(16):1207–1219, May 2017.
- [102] Sirisala Mamatha, Papiya Biswas, Pandu Ramavath, Dibakar Das, and Roy Johnson. 3D printing of complex shaped alumina parts. *Ceramics International*, 44(16):19278–19281, November 2018.
- [103] Yiqi Mao, Kai Yu, Michael S Isakov, Jiangtao Wu, Martin L Dunn, and H Jerry Qi. Sequential Self-Folding Structures by 3D Printed Digital Shape Memory Polymers. *Nature Publishing Group*, 5(1):13616–12, September 2015.
- [104] Patrick T Mather, Xiaofan Luo, and Ingrid A Rousseau. Shape Memory Polymer Research. *Annual Review of Materials Research*, 39:445–471, August 2009.
- [105] Joselle M McCracken, Brian R Donovan, and Timothy J White. Materials as Machines. *Advanced Materials*, 1060202:1906564–48, March 2020.
- [106] Marlon Meier, Kim Hua Tan, Ming K Lim, and Leanne Chung. Unlocking innovation in the sport industry through additive manufacturing. *Business Process Management Journal*, 25(3):456–475, June 2019.
- [107] Stephen Kirwa Melly, Liwu Liu, Yanju Liu, and Jinsong Leng. Active composites based on shape memory polymers: overview, fabrication methods, applications, and future prospects. *Journal of Materials Science*, pages 1–77, May 2020.
- [108] Harper Meng and Guoqiang Li. A review of stimuli-responsive shape memory polymer composites. *Polymer (United Kingdom)*, 54(9):2199–2221, April 2013.
- [109] Qinghao Meng, Jinlian Hu, KaiChiu Ho, Fenglong Ji, and Shaojun Chen. The Shape Memory Properties of Biodegradable Chitosan/Poly(l-lactide) Composites. *Journal of Polymers and the Environment*, 17(3):212–224, October 2009.

- [110] Shida Miao, Nathan Castro, Margaret Nowicki, Lang Xia, Haitao Cui, Xuan Zhou, Wei Zhu, Se-jun Lee, Kausik Sarkar, Giovanni Vozzi, Yasuhiko Tabata, John Fisher, and Lijie Grace Zhang. 4D printing of polymeric materials for tissue and organ regeneration. *Materials Today*, 20(10):577–591, December 2017.
- [111] Simone Micalizzi, Andrés Díaz Lantada, and Carmelo De Maria. Shape-memory actuators manufactured by dual extrusion multimaterial 3d printing of conductive and non-conductive filaments. *Smart Materials and Structures*, 28(10):105025–13, September 2019.
- [112] A Mitchell, U Lafont, M Holyńska, and C Semprimoschnig. Additive manufacturing — A review of 4D printing and future applications. *Additive Manufacturing*, 24:606–626, December 2018.
- [113] Farhang Momeni, Seyed M Mehdi Hassani N, Xun Liu, and Jun Ni. A review of 4D printing. *Materials and Design*, 122(C):42–79, May 2017.
- [114] Quanyi Mu, Conner K Dunn, Lei Wang, Martin L Dunn, H Jerry Qi, and Tiejun Wang. Thermal cure effects on electromechanical properties of conductive wires by direct ink write for 4D printing and soft machines. *Smart Materials and Structures*, 26(4):045008–14, February 2017.
- [115] Tong Mu, Liwu Liu, Xin Lan, Yanju Liu, and Jinsong Leng. Shape memory polymers for composites. *Composites Science and Technology*, 160:169–198, May 2018.
- [116] Seokwoo Nam and Eujin Pei. A taxonomy of shape-changing behavior for 4D printed parts using shape-memory polymers. *Progress in Additive Manufacturing*, 4(2):167–184, March 2019.
- [117] Wei Long Ng, Jia Min Lee, Miaomiao Zhou, Yi-Wen Chen, Kai-Xing Alvin Lee, Wai Yee Yeong, and Yu-Fang Shen. Vat polymerization-based bioprinting—process, materials, applications and regulatory challenges. *Biofabrication*, 12(2):022001–23, April 2020.
- [118] T D Ngo, A Kashani, G Imbalzano, KTQ Nguyen Composites Part B, and 2018. Additive manufacturing (3D printing): A review of materials, methods, applications and challenges. *Sensors and Actuators A:Physical*, 143:172–196, June 2018.
- [119] Qing-Qing Ni, Chun-sheng Zhang, Yaqin Fu, Guangze Dai, and Teruo Kimura. Shape memory effect and mechanical properties of carbon nanotube/shape memory polymer nanocomposites. *Composite Structures*, 81(2):176–184, November 2007.
- [120] Neri Oxman. Variable property rapid prototyping. *Virtual and Physical Prototyping*, 6(1):3–31, March 2011.

- [121] Mahyar Panahi-Sarmad, Mahbod Abrisham, Mina Noroozi, Arian Amirkiai, Parham Dehghan, Vahabodin Goodarzi, and Benjamin Zahiri. Deep focusing on the role of microstructures in shape memory properties of polymer composites: A critical review. *European Polymer Journal*, 117:280–303, August 2019.
- [122] Zhiqiang Pei, Yang Yang, Qiaomei Chen, Eugene M Terentjev, Yen Wei, and Yan Ji. Mouldable liquid-crystalline elastomer actuators with exchangeable covalent bonds. *Nature Materials*, pages 1–6, January 2013.
- [123] D M Phillips and J W Baur. A microvascular method for thermal activation and deactivation of shape memory polymers. *Journal of Intelligent Material Systems and Structures*, 24(10):1233–1244, 2013.
- [124] A Pilipovic, P Raos, M Sercer Tehnicki Vjesnik, and 2011. Experimental Testing of Quality of Polymer Parts Produced by Laminated Object Manufacturing- LOM. *Technical Gazette*, 18, 2011.
- [125] A C Pinho, C S Buga, and A P Piedade. The chemistry behind 4D printing. *Applied Materials Today*, 19:100611, March 2020.
- [126] Giovanni Postiglione, Gabriele Natale, Gianmarco Griffini, Marinella Levi, and Stefano Turri. Conductive 3D microstructures by direct 3D printing of polymer/carbon nanotube nanocomposites via liquid deposition modeling. *Composites Part A*, 76(C):110–114, September 2015.
- [127] Xiaodong Qi, Hao Xiu, Yuan Wei, Yan Zhou, Yilan Guo, Rui Huang, Hongwei Bai, and Qiang Fu. Enhanced shape memory property of polylactide/thermoplastic poly(ether)urethane composites via carbon black self-networking induced co-continuous structure. *Composites Science and Technology*, 139:8–16, February 2017.
- [128] Abishera Ravichandra Rajkumar and Kumar Shanmugam. Additive manufacturing-enabled shape transformations via FFF 4D printing. *Journal of Materials Research*, 33(24):4362–4376, December 2018.
- [129] Prasansha Rastogi and Balasubramanian Kandasubramanian. Breakthrough in the printing tactics for stimuli-responsive materials: 4D printing. *Chemical Engineering Journal*, 366:264–304, June 2019.
- [130] Dan Raviv, Wei Zhao, Carrie McKnelly, Athina Papadopoulou, Achuta Kadambi, Boxin Shi, Shai Hirsch, Daniel Dikovsky, Michael Zyracki, Carlos Olguin, Ramesh Raskar, and Skylar Tibbits. Active Printed Materials for Complex Self-Evolving Deformations. *Nature Publishing Group*, 4(1):153–8, December 2014.

- [131] Du Ren, Yujie Chen, Senlin Yang, Hua Li, Hafeez Ur Rehman, and Hezhou Liu. Fast and Efficient Electric-Triggered Self-Healing Shape Memory of CNTs@rGO Enhanced PCLPLA Copolymer. *Macromolecular Chemistry and Physics*, 220(21):1900281–8, September 2019.
- [132] Kailiang Ren, Robert S Bortolin, and Q M Zhang. An investigation of a thermally steerable electroactive polymer/shape memory polymer hybrid actuator. *Applied Physics Letters*, 108(6):062901–6, February 2016.
- [133] D A Roberson, D Espalin, and R B Wicker. 3D printer selection: A decision-making evaluation and ranking model. *Virtual and Physical Prototyping*, 8(3):201–212, October 2013.
- [134] Jennifer N Rodriguez, Cheng Zhu, Eric B Duoss, Thomas S Wilson, Christopher M Spadacini, and James P Lewicki. Shape-morphing composites with designed micro-architectures. *Nature Publishing Group*, pages 1–10, June 2016.
- [135] Stian Romberg, Christopher Hershey, John Lindahl, William Carter, Brett Compton, and Vlastimil Kunc. Large-scale Additive Manufacturing of Highly Exothermic Reactive Polymer Systems. In *SAMPE 2013 - Education & Green Sky*. SAMPE, April 2019.
- [136] Jonathan Rossiter and Sina Sareh. Kirigami design and fabrication for biomimetic robotics. In Akhlesh Lakhtakia, editor, *SPIE Smart Structures and Materials + Nondestructive Evaluation and Health Monitoring*, pages 90550G–9. SPIE, March 2014.
- [137] Ela Sachyani Keneth, Rama Lieberman, Matthew Rednor, Giulia Scalet, Ferdinando Auricchio, and Shlomo Magdassi. Multi-Material 3D Printed Shape Memory Polymer with Tunable Melting and Glass Transition Temperature Activated by Heat or Light. *Polymers*, 12(3):710–12, March 2020.
- [138] Kishor Kumar Sadasivuni, Kalim Deshmukh, and Mariam AlAli AlMaadeed. *3D and 4D Printing of Polymer Nanocomposite Materials*. Processes, Applications, and Challenges. Elsevier, October 2019.
- [139] A I Salimon, F S Senatov, V A Kalyaev, and A M Korsunsky. *Chapter 6 - Shape memory polymer blends and composites for 3D and 4D printing applications*. Elsevier Inc., 2020.
- [140] Xinxin Shen, Baoxian Jia, Hanxing Zhao, Xing Yang, and Zhengxian Liu. Study on 3D printing process of continuous carbon fiber reinforced shape memory polymer composites. *IOP Conference Series: Materials Science and Engineering*, 563:022029–8, July 2019.
- [141] MD Nahin Islam Shiblee, Kumkum Ahmed, Masaru Kawakami, and Hidemitsu Furukawa. 4D Printing of Shape-Memory Hydrogels for Soft-Robotic Functions. *Advanced Materials Technologies*, 4(8):1900071–10, June 2019.

- [142] Ming-You Shie, Yu-Fang Shen, Suryani Dyah Astuti, Alvin Kai-Xing Lee, Shu-Hsien Lin, Ni Luh Bella Dwijaksara, and Yi-Wen Chen. Review of Polymeric Materials in 4D Printing Biomedical Applications. *Polymers*, 11(11):1864–17, November 2019.
- [143] Ward Small IV, Pooja Singhal, Thomas S Wilson, and Duncan J Maitland. Biomedical applications of thermally activated shape memory polymers. *Journal of Materials Chemistry*, 20(17):3356–11, 2010.
- [144] Panagiotis Stavropoulos and Panagis Foteinopoulos. Modelling of additive manufacturing processes: a review and classification. *Manufacturing Review*, 5:2–26, March 2018.
- [145] Jian Sun, Qinghua Guan, Yanju Liu, and Jinsong Leng. Morphing aircraft based on smart materials and structures: A state-of-the-art review. *Journal of Intelligent Material Systems and Structures*, 27(17):2289–2312, July 2016.
- [146] Jiefeng Sun and Jianguo Zhao. An Adaptive Walking Robot With Reconfigurable Mechanisms Using Shape Morphing Joints. *IEEE Robotics and Automation Letters*, 4(2):724–731, April 2019.
- [147] Ke Sun, Teng-Sing Wei, Bok Yeop Ahn, Jung Yoon Seo, Shen J Dillon, and Jennifer A Lewis. 3D Printing of Interdigitated Li-Ion Microbattery Architectures. *Advanced Materials*, 25(33):4539–4543, June 2013.
- [148] James Utama Surjadi, Libo Gao, Huifeng Du, Xiang Li, Xiang Xiong, Nicholas Xuanlai Fang, and Yang Lu. Mechanical Metamaterials and Their Engineering Applications. *Advanced Engineering Materials*, 21(3):1800864, December 2018.
- [149] Lin Tan, Lu Gan, Jinlian Hu, Yong Zhu, and Jianping Han. Functional shape memory composite nanofibers with graphene oxide filler. *Composites Part A*, 76(C):115–123, September 2015.
- [150] Junkun Tang, Yan Zhou, Liqiang Wan, and Farong Huang. Automatically Programmable Shape-Memory Polymers Based on Asymmetric Swelling of Bilayer Structures. *Macromolecular Rapid Communications*, 39(9):1800039–7, March 2018.
- [151] Suman Thakur and Niranjan Karak. Bio-based tough hyperbranched polyurethane–graphene oxide nanocomposites as advanced shape memory materials. *RSC Advances*, 3(24):9476–7, 2013.
- [152] S Tibbits. The emergence of “4D printing”. TED, TED, 2013.
- [153] Antoniya Toncheva, Farid Khelifa, Yoann Paint, Michel Voué, Pierre Lambert, Philippe Dubois, and Jean-Marie Raquez. Fast IR-Actuated Shape-Memory Polymers Using in Situ

- Silver Nanoparticle-Grafted Cellulose Nanocrystals. *ACS Applied Materials & Interfaces*, 10(35):29933–29942, September 2018.
- [154] Takuya Umedachi, Vishesh Vikas, and Barry A Trimmer. Highly deformable 3-D printed soft robot generating inching and crawling locomotions with variable friction legs. *2013 IEEE/RSJ International Conference on Intelligent Robots and Systems*, pages 4590–4595, November 2013.
- [155] Suong Van Hoa. Development of composite springs using 4D printing method. *Composite Structures*, 210:869–876, February 2019.
- [156] Jorge Villacres, David Nobes, and C. Ayranci. Additive Manufacturing of Shape Memory Polymers: Effects of print orientation and infill percentage on mechanical properties. *Rapid Prototyping Journal*, 24(4):744–751, 2018.
- [157] Xue Wan, Fenghua Zhang, Yanju Liu, and Jinsong Leng. CNT-based electro-responsive shape memory functionalized 3D printed nanocomposites for liquid sensors. *Carbon*, 155:77–87, December 2019.
- [158] Qingrui Wang, Xiaoyong Tian, Lan Huang, Dichen Li, Andrei V Malakhov, and Alexander N Polilov. Programmable morphing composites with embedded continuous fibers by 4D printing. *Materials and Design*, 155(C):404–413, October 2018.
- [159] Wenxin Wang, Yanju Liu, and Jinsong Leng. Recent developments in shape memory polymer nanocomposites: Actuation methods and mechanisms. *Coordination Chemistry Reviews*, 320-321:38–52, August 2016.
- [160] Xin Wang, John Sparkman, and Jihua Gou. Electrical actuation and shape memory behavior of polyurethane composites incorporated with printed carbon nanotube layers. *Composites Science and Technology*, 141:8–15, March 2017.
- [161] Hongqiu Wei, Xavier Cauchy, Ivonne Otero Navas, Yahya Abderrafai, Kambiz Chizari, Utandaraman Sundararaj, Yanju Liu, Jinsong Leng, and Daniel Therriault. Direct 3D Printing of Hybrid Nanofiber-Based Nanocomposites for Highly Conductive and Shape Memory Applications. *ACS Applied Materials & Interfaces*, 11(27):24523–24532, July 2019.
- [162] Hongqiu Wei, Qiwei Zhang, Yongtao Yao, Liwu Liu, Yanju Liu, and Jinsong Leng. Direct-Write Fabrication of 4D Active Shape-Changing Structures Based on a Shape Memory Polymer and Its Nanocomposite. *ACS Applied Materials & Interfaces*, 9(1):876–883, January 2017.
- [163] David Ian Wimpenny, Pulak M Pandey, and L Jyothish Kumar. *Advances in 3D Printing & Additive Manufacturing Technologies*. Springer, Singapore, August 2016.

- [164] Jiangtao Wu, Chao Yuan, Zhen Ding, Michael Isakov, Yiqi Mao, Tiejun Wang, Martin L Dunn, and H Jerry Qi. Multi-shape active composites by 3D printing of digital shape memory polymers. *Nature Publishing Group*, 6(1):773, April 2016.
- [165] Rui Xiao, Cheng Zhang, and Wei Min Huang. *Chapter Four. Programming of Shape-Memory Polymers: The Temperature Memory Effect and Triple/Multiple-Shape-Memory Effect in Polymers*. Elsevier Inc., 2017.
- [166] Xiaozhou Xin, Liwu Liu, Yanju Liu, and Jinsong Leng. Mechanical Models, Structures, and Applications of Shape-Memory Polymers and Their Composites. *Acta Mechanica Solida Sinica*, 32(5):535–565, June 2019.
- [167] B. Yang, W. M. Huang, C. Li, L Li, and J H Chor. Qualitative separation of the effects of carbon nano-powder and moisture on the glass transition temperature of polyurethane shape memory polymer. *Scripta Materialia*, 53(1):105–107, July 2005.
- [168] Gi Hoon Yang, Miji Yeo, Young Won Koo, and Geun Hyung Kim. 4D Bioprinting: Technological Advances in Biofabrication. *Macromolecular Bioscience*, 19(5):1800441–10, March 2019.
- [169] Hui Yang, Wan Ru Leow, Ting Wang, Juan Wang, Jiancan Yu, Ke He, Dianpeng Qi, Changjin Wan, and Xiaodong Chen. 3D Printed Photoresponsive Devices Based on Shape Memory Composites. *Advanced Materials*, 29(33):1701627–7, June 2017.
- [170] Wang Yongkun, Zhu Guangming, Tang Yusheng, Liu Tingting, Xie Jianqiang, and Ren Fang. Short glass fiber reinforced radiation crosslinked shape memory SBS/LLDPE blends. *Journal of Applied Polymer Science*, 131(17):n/a–n/a, April 2014.
- [171] Kai Yu, Yanjiu Liu, and Jinsong Leng. Conductive Shape Memory Polymer Composite Incorporated with Hybrid Fillers: Electrical, Mechanical, and Shape Memory Properties. *Journal of Intelligent Material Systems and Structures*, 22(4):369–379, May 2011.
- [172] Kai Yu, David M Phillips, Jeffery W Baur, and H Jerry Qi. Analysis of shape-memory polymer composites with embedded microvascular system for fast thermal response. In *Journal of Composite Materials*, pages 1881–1893. The George W. Woodruff School of Mechanical Engineering, Atlanta, United States, January 2015.
- [173] Kai Yu, Alexander Ritchie, Yiqi Mao, Martin L Dunn, and H Jerry Qi. Controlled Sequential Shape Changing Components by 3D Printing of Shape Memory Polymer Multimaterials. *Procedia IUTAM*, 12:193–203, 2015.

- [174] Chao Yuan, Devin J Roach, Conner K Dunn, Quanyi Mu, Xiao Kuang, Christopher M Yakacki, T J Wang, Kai Yu, and H Jerry Qi. 3D printed reversible shape changing soft actuators assisted by liquid crystal elastomers. *Soft Matter*, 13(33):5558–5568, 2017.
- [175] Shangqin Yuan, Jiaming Bai, Chee Kai Chua, Kun Zhou, and Jun Wei. Characterization of Creeping and Shape Memory Effect in Laser Sintered Thermoplastic Polyurethane. *Journal of Computing and Information Science in Engineering*, 16(4):489–5, November 2016.
- [176] Shangqin Yuan, Fei Shen, Chee Kai Chua, and Kun Zhou. Polymeric composites for powder-based additive manufacturing: Materials and applications. *Progress in Polymer Science*, 91:141–168, April 2019.
- [177] Matt Zarek, Nicola Mansour, Shir Shapira, and Daniel Cohn. 4D Printing of Shape Memory-Based Personalized Endoluminal Medical Devices. *Macromolecular Rapid Communications*, 38(2):1600628–6, December 2016.
- [178] Chengjun Zeng, Liwu Liu, Wenfeng Bian, Yanju Liu, and Jinsong Leng. 4D printed electro-induced continuous carbon fiber reinforced shape memory polymer composites with excellent bending resistance. *COMPOSITES PART B*, 194:108034, August 2020.
- [179] Quan Zhang, Dong Yan, Kai Zhang, and Gengkai Hu. Pattern Transformation of Heat-Shrinkable Polymer by Three-Dimensional (3D) Printing Technique. *Nature Publishing Group*, 5:8936, March 2015.
- [180] Wei Zhang, Fenghua Zhang, Xin Lan, Jinsong Leng, Amanda S Wu, Taylor M Bryson, Chase Cotton, Bohong Gu, Baozhong Sun, and Tsu-Wei Chou. Shape memory behavior and recovery force of 4D printed textile functional composites. *Composites Science and Technology*, 160:224–230, May 2018.
- [181] Tingting Zhao, Ran Yu, Xinpan Li, Bing Cheng, Ying Zhang, Xin Yang, Xiaojuan Zhao, Yulei Zhao, and Wei Huang. 4D printing of shape memory polyurethane via stereolithography. *European Polymer Journal*, 101:120–126, April 2018.
- [182] Mingzhu Zhu, Mengying Xie, Xuanming Lu, Shima Okada, and Sadao Kawamura. A soft robotic finger with self-powered triboelectric curvature sensor based on multi-material 3D printing. *Nano Energy*, 73:104772, July 2020.
- [183] Ali Zolfagharian, Akif Kaynak, and SY Khoo A. Pattern-driven 4D printing. *Sensors and Actuators A:Physical*, March 2018.
- [184] Ali Zolfagharian, Akif Kaynak, and Abbas Kouzani. Closed-loop 4D-printed soft robots. *Materials and Design*, December 2019.

## Chapter 4

# Effect of Moisture on Shape Memory Polyurethane Polymers for Extrusion-Based Additive Manufacturing

### Abstract

Extrusion-based additive manufacturing (EBAM) or 3D printing is used to produce customized prototyped parts. The majority of the polymers used with EBAM show moisture sensitivity. However, moisture effects become more pronounced in polymers used for critical applications, such as biomedical stents, sensors, and actuators. The effects of moisture on the manufacturing process and the long-term performance of Shape Memory Polyurethane (SMPU) have not been fully investigated in the literature. This study focuses primarily on block-copolymer SMPUs that have two different hard/soft (h/s) segment ratios. It investigates the effect of moisture on the various properties via studying: (i) the effect of moisture trapping within these polymers and the consequences when manufacturing; (ii) and the effect on end product performance of plasticization by moisture. Results indicate that higher h/s SMPU shows higher microphase separation, which leads to an increase of moisture trapping within the polymer. Understanding moisture trapping is critical for EBAM parts due to an increase in void content and a decrease in printing quality. The results also indicate a stronger plasticizing effect on polymers with lower h/s ratio but with a more forgiving printing behavior compared to the higher h/s ratio.

## 4.1 Introduction

Over the last decade, extrusion-based additive manufacturing (EBAM), commonly referred to as thermoplastic 3D printing, has gained much attention due to the major advantages it offers for producing customized prototyped parts. To convert EBAM from a prototyping technique to end-use manufacturing that can be utilized for novel and critical applications, it is necessary to learn about some of the difficulties the technology faces. For the majority of the polymers used with EBAM, including polylactic acid (PLA), acrylonitrile butadiene styrene (ABS) and various grades of polyamide (Nylon®), moisture is an obstacle during the manufacturing process and later during the part's life cycle. However, this effect is a more pronounced problem when the printed parts are intended for critical applications, such as in the case of polyurethane-based shape memory polymers (SMPU). It is important to understand the effects of moisture in these materials for EBAM in order to obtain void-less consistent printing quality and predict engineering part performance. Some of the most promising applications of EBAM-based SMPU are biomedical applications such as customized airflow and 3D-printed cardiovascular stents (Figure 4.1a), casts and splints [24, 12, 27]. Other critical and promising applications include grippers, actuators for soft robotics [23], origami-based self-assembly structures for smart manufacturing [26, 8] and potential printing of smart self-deployable sports equipment such as a shape memory polymer (SMP) 3D-printed kayak [11]. The prototype of a small-scale kayak that may be folded to a temporary shape for storage/transportation and later deployed onsite is seen in Figure 4.1b.

In general, SMPs are classified into two main categories, those that show a shape memory effect (SME) by means of chemical bonds (commonly in thermosets) and those by means of physical bonds or hydrogen bonding (commonly in thermoplastics) [29]. SMPUs are a type of thermoplastic SMP and many studies have focused in this particular polymer since their commercialization in 1997 [15, 38].

SMPU thermoplastics consist of hard-crystallized and soft-amorphous segments [29]. Hard segments commonly have higher transition temperatures—the temperature at which polymeric chains acquire mobility—than do soft segments. This thermodynamic incompatibility causes immiscibility between segments, provoking these two blocks to segregate and produce a microphase separation that leads to an SME [43, 22, 9]. Within the SME, crystallized segments function as links to the amorphous soft segments [22, 37]. Polymeric chains can be set temporarily above the transition temperature and frozen upon cooling. When the polymer is reheated to  $T > T_{transition}$ , the chains return to their original configuration [25].

Different ratios of hard to soft segments (h/s ratio) affect the molecular mobility and determine the properties of a SMPU. This ratio alters the intrinsic properties of the polymer such as its glass transition temperature ( $T_g$ ), melting temperature ( $T_m$ ), mechanical properties, shape memory

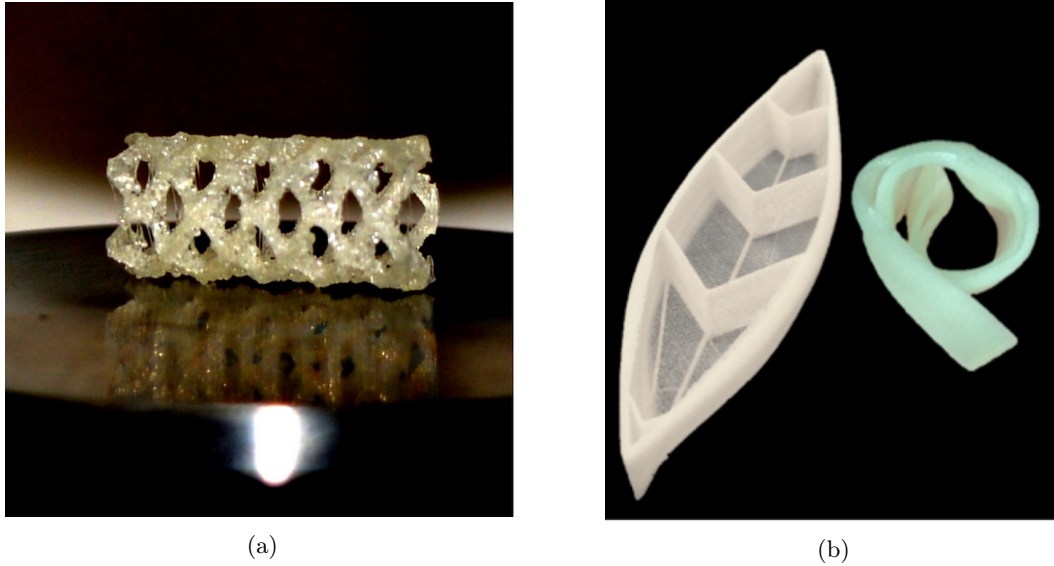


Figure 4.1: Examples of 3D-printed applications of Shape Memory Polyurethane (SMPU) by EBAM. (a) A photograph of an in-house 3D-printed generic stent and (b) 3D-printed kayak prototype based on reference [11].

characteristics and effects of moisture on the polymer by plasticization or moisture trapping [22, 37]. The individual characteristics of hard and soft segments affect the resulting SMPU. Soft-segments are generally amorphous structures characterized by a low  $T_g$ ; they are flexible by nature and contribute to the elastic properties of the resulting SMPU [22]. The crystalline structures of hard segments do not change over the range of temperatures used to program the SMPU and act as embedded fillers within the amorphous polymeric structure. In SMPU, urethane segments act as hard segments and polyether or polyester glycols act as soft segments [40, 31, 4, 21, 35]. Hydrogen bonding within these hard crystalline structures can potentially serve to set the initial permanent shape [22]. Studies on the chemical, mechanical and shape recovery properties of SMPU have been reported to obtain a better understanding of their properties and functioning [26, 30, 36, 42].

The effects of moisture on SMPUs have been previously studied by investigating the effects of immersion of a thermoplastic SMPU in water. It has been reported that hydrogen bonding, also known as plasticization, alters the  $T_g$  and elastic modulus of the SMPU [50, 32, 16, 46, 33, 44, 7]. Plasticization by water lowers the glass transition temperature, mechanical properties and melt-viscosity of the SMPU [45, 18, 19, 47, 48, 5, 13, 34, 10, 39]. An alteration of the glass transition temperature may produce an uncontrolled activation of the SME and undefined mechanical characteristics of the moisture-affected polymer.

Although moisture effects on thermoplastic SMPUs have been studied, investigations have not related moisture effects according to the h/s ratio of different SMPUs and have not linked this to manufacturing technologies such as EBAM. The present study focuses first on the common moisture problem when manufacturing and second on the effect of plasticization by moisture on the chemical, mechanical and shape memory properties of SMPUs and the effects on the 3D-printed part. Understanding the effects of these parameters will significantly increase the use of SMPUs in aforementioned applications. The study outlines an in-depth analysis of moisture effects on two different types of SMPU, one with a low and the other with a higher h/s segment ratio. The study demonstrates the material behavior after a part has been manufactured and the effects of moisture on EBAM manufacturing.

## 4.2 Raw Materials

The SMP materials used in this study were purchased from SMP Technologies (Tokyo, Japan). Two different types of ether block copolymer polyurethane thermoplastic SMPs, MM4520 and MM7520, were used. According to the technical sheet provided by the manufacturer, the SMP materials are prepared from diphenylmethane-4,4'-diisocyanate, adipic acid, ethylene glycol, ethylene oxide, polypropylene oxide, 1,4-butanediol and bisphenol A. MM4520 and MM7520 were received in pellet form and have prescribed glass transition temperatures of  $45^{\circ}C$  and  $75^{\circ}C$ , respectively. These materials are semicrystalline by nature, their amorphous parts are made of polyester polyols and their crystalline hard part are made of urethane segments, the chemical composition is presented in Figure 4.2.

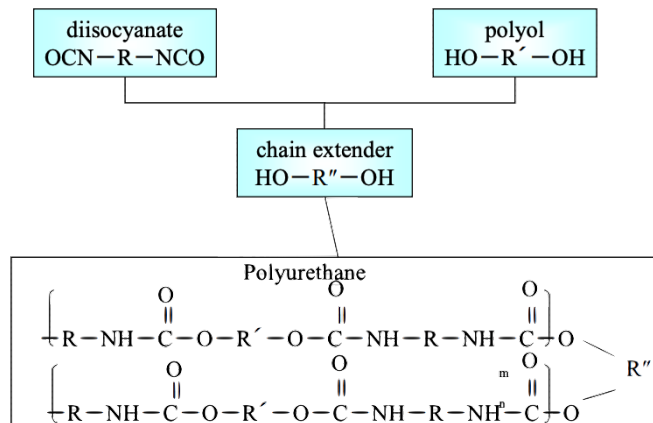


Figure 4.2: Schematic of the chemical formula of SMP MM series, provided by the manufacturer ([www2.smptechno.com](http://www2.smptechno.com))

### 4.3 Methodology

The methodology is divided into two sections: (i) the effect of moisture trapping in the SMPUs on 3D-printed parts and (ii) a study of the plasticization effect of moisture on two different SMPUs. The latter is relevant to EBAM SMPU parts' performance under moisture-affected conditions. For both sections, to avoid any embedded moisture gas bubbles, the SMP pellets were dried for 12 h at 80°C in a Lindberg/Blue M<sup>TM</sup> vacuum oven before the melt extrusion processes. Drying time was selected as recommended by the manufacturer and verified by TGA analyses.

The study of moisture trapping by the SMPU was done on melt-extruded filaments, which were later fed to a commercial EBAM printer to study the effects on printing quality. Studies of moisture absorption characteristics and effects of plasticization by moisture were conducted on melt-extruded SMPU ribbons since this represents the best scenario possible for a 3D-printed part.

#### 4.3.1 Ribbon Preparation, Compounding and Water Absorption

The samples were prepared by melt-extrusion using a HAAKE<sup>TM</sup> Haake MiniLab Rheomex CTW5 twin-screw extruder (Waltham, MA, USA). Each screw has a length of 109.5 mm and conical diameters of 5 and 14 mm respectively. The material was poured into a pneumatic feeder and the torque level was adjusted to keep it at a constant 70 N·cm. The extrusion parameters were set to 195°C and 50 rpm. Ribbons were manufactured using a die with cross sectional dimensions of 4 mm by 0.5 mm. The extruded ribbons were pulled using an LME take up roll system (Dynisco, Franklin,

Table 4.1: Printing parameters used when 3D printing with each respective material (MM4520 and MM7520).

Material	Nozzle Temperature ( $^{\circ}C$ )	Printing Speed (mm/s)	Build Plate Temperature ( $^{\circ}C$ )	Fan Speed (%)
MM4520	210	10	50	10
MM7520	230	10	80	10

MA, USA) (the diameter of rolls used for the pulling was 1 inch, below the rpm of the roll reported). The pulling speed of the take-up system was kept constant at 9.74 rpm and was measured using an encoder (4096 counts per revolution quadrature encoder, US Digital, Washington, USA).

### 4.3.2 Filament Preparation for EBAM

To prepare the samples, filaments for the EBAM were melt-extruded using a 3-mm circular cross section die using a Brabender<sup>TM</sup> single screw extruder attached to an ATR Plasti-Corder drive system (Brabender, Duisburg, Germany). Extrusion parameters for SMPU MM4520 were adapted from Villacres et al.[39], with heating zones of  $170^{\circ}C$ ,  $180^{\circ}C$ ,  $190^{\circ}C$  and  $195^{\circ}C$ , and extrusion rates and pulling speed of 20 rpm. For MM7520, temperatures were set as  $175^{\circ}C$ ,  $185^{\circ}C$ ,  $195^{\circ}C$  and  $205^{\circ}C$ , for the four different heating zones of the extruder. Extrusion rates and pulling speeds were set at 15 rpm.

### 4.3.3 EBAM Manufactured Samples

Printed (EBAM manufactured) samples were prepared using an Ultimaker<sup>TM</sup> 2 desktop 3D printer (Ultimaker, Geldermalsen, Netherlands) with a nozzle diameter of 0.4 mm. Printing parameters for MM4520 and MM7520 are portrayed in Table 1. Geometrical parameters such as infill density (100%), infill pattern ( $\pm 45^{\circ}$ ) and layer height (0.2 mm) were kept the same for both polymers. Square samples of  $30 \times 30$  mm were printed with an inner central circle of 10 mm and thickness of 3 mm.

## 4.4 Experimental Methodology

### 4.4.1 Moisture Manufacturing Effects: Moisture Trapping

After the extrusion process, filaments were thermally conditioned in an oven and dried at  $80^{\circ}C$  for 24 h. Filaments were then immersed in distilled water for different periods. The filaments

were immediately fed to the 3D printer and square samples were manufactured. Moisture content after printing was visually and microscopically inspected and compared between both types of SMPU.

#### 4.4.2 Moisture on Manufactured Parts: Effect of Moisture by Plasticization

After the extrusion process, samples were thermally conditioned and oven dried at  $T_g + 5^\circ C$  for each respective polymer prior to performing water immersion tests. The drying temperatures were chosen to avoid crystallization temperatures of the polymers. To correlate moisture impact on SMPU post-processing to EBAM manufacturing, samples (ribbons) were subjected to 100% moisture content by immersing them in distilled water. Water absorption by the samples was therefore related to the immersion time in distilled water at room temperature. Samples were tested immediately after they were withdrawn from the water.

##### Thermogravimetry (TGA) Analysis

TGA samples, weighing 10–15 mg, were cut from the manufactured ribbons and immersed in water for periods of 0, 48, 72, and 112 h at room temperature. TGA analyses were performed to measure the water content of each sample. The analyses were conducted on TA Instruments Q50 Thermogravimetry analyzer (TA Instruments, New Castle, USA). Samples were heated from  $25^\circ C$  to a maximum temperature of  $400^\circ C$  at a heating rate  $10^\circ C/min$ .

##### Differential Scanning Calorimetry (DSC) Analysis

DSC tests were conducted using DSC Q1000 (TA Instruments, New Castle, USA). The tests were carried out to examine the potential effect of immersion time (humidity) on  $T_g$ . Specimens of 2 – 5 mg were cut from the manufactured ribbons and were tested using a heating rate of  $20^\circ C/min$ . The heating rate was chosen to allow comparison with previous studies [46]. The analyses were carried out from  $-40^\circ C$  to  $240^\circ C$ . Glass transition temperatures were obtained from DSC experimental data. Sample DSC curves of dried polymers are shown in the supplementary information in Appendix B.3. The average of three measurements of the glass transition temperatures of the dried polymers were  $\approx 44.5^\circ C$  and  $74.5^\circ C$  for MM4520 and MM7520, which is similar to those reported by the manufacturer.

## Infrared Spectra Analysis (FT-IR)

Attenuated total reflectance (ATR) was used to collect Fourier transform-infrared spectroscopy (FT-IR) with the aim of recognizing the interaction of water with the polymers. Infrared band analyses were performed using a DIGILAB FTS 7000 Fourier Transform Infrared Spectrometer with UMA 600 microscope (Hopkinton, MA, USA). FT-IR spectra were obtained by averaging 75 scans for each spectrum at a resolution of  $2\text{cm}^{-1}$  in reflection mode. The characterization technique was done on a thin film produced by depositing a layer of 0.4mm of polymer on a heated glass bed using an extrusion-based additive manufacturing desktop printer (Ultimaker <sup>TM</sup>2+).

## Tensile Testing

Ribbons were cut to 25 mm length samples for testing. A length of 10 mm was left at each side as gripping aids. A final gauge length of 5 mm was left for testing. Tensile tests were conducted using Electroforce® 3200 Series by TA instruments<sup>TM</sup> (New Castle, DE, USA). Tensile grips were tightened using 17.6 lb-in at each side. The specimens were stretched to 100% in strain using a rate of 0.02 mm/s. Elastic modulus was calculated according to ISO 527-1 for plastics [28]. Due to a high sample elongation and stroke limitation of the tensile device, only elastic moduli were determined for this study.

## Shape Recovery Tests

For MM4520, seven samples at 0, 12 and 24 h each were tested. For MM7520, seven samples at 0 and 24 h each were tested. Samples were cut to 45 mm lengths. Gripping lengths of 10 mm were used, leaving a final gauge length of 25 mm for testing. The gauge length was chosen due to the limitation of the machine's stroke. The shape programming was done using Electroforce® 3200 Series by TA instruments<sup>TM</sup> equipped with a heated forced-air convection chamber.

Figure 4.3 shows the schematic representation of the programming cycle done on SMP specimens. The surrounding temperature was raised from room temperature to  $50^\circ\text{C}$  ( $T_g + 5^\circ\text{C}$ ) for MM4520 samples and to  $80^\circ\text{C}$  ( $T_g + 5^\circ\text{C}$ ) for MM7520 at a heating rate of  $0.50^\circ\text{C}/\text{sec}$  during 3 minutes. To obtain an optimal recovery and allow for the polymer to store energy, a programming temperature of  $50^\circ\text{C}$  was chosen for MM4520, similar temperatures have been considered in previous studies for materials having a glass transition temperature close to that mentioned previously [46, 44, 2]. Therefore, a temperature of  $80^\circ\text{C}$  was chosen for MM7520. Figure 4.3a shows a sample fixed at both ends. From Figure 4.3a to 4.3b, the sample was stretched to 100% strain, from the original length ( $L_0$ ) to the prescribed length ( $L_p$ ), at a rate of 0.2mm/s. Immediately after, the sample was

cooled down to  $T_g$  using forced air to prevent any further recovery. The samples were then placed in a cooler until activation. The activation, or recovery, process was conducted in a Lindberg/Blue M<sup>TM</sup> vacuum oven (Waltham, MA USA) set to  $70^\circ\text{C}$  ( $T_g + 25^\circ\text{C}$ ) for MM4520 samples and to  $100^\circ\text{C}$  ( $T_g + 25^\circ\text{C}$ ) for MM7520 samples. During activation, a small constant load, corresponding to  $\sim 0.2\text{N}$ , was applied at the free end of the sample to prevent curling during recovery. Samples recovered their shape from Figure 4.3c to 4.3d. For analysis, pictures were taken at 4 Hz for 5 min during activation and change in length was measured according to [1].

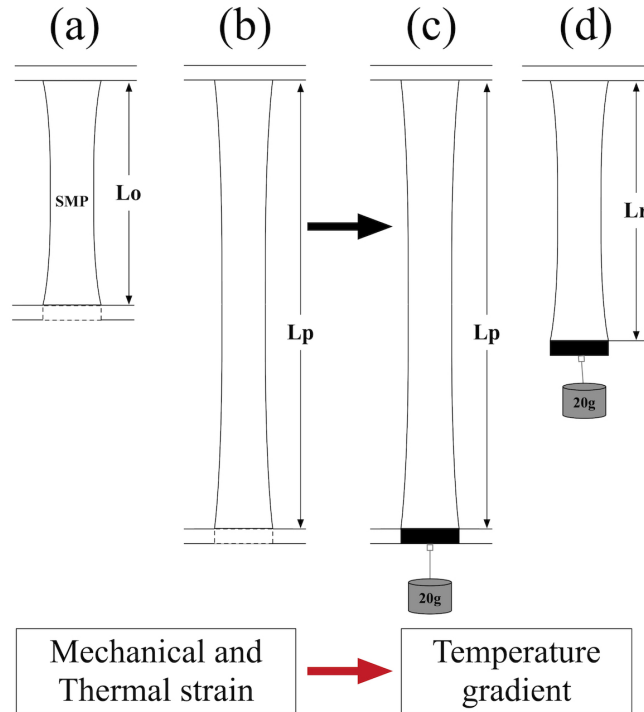


Figure 4.3: Schematic showing the programming and shape recovery procedure of a Shape Memory Polymer ribbon, where (a) shows the original sample (b) and (c) the sample while and after shape programming, respectively and (d) the recovered sample.

## 4.5 Results and Discussion

### 4.5.1 Moisture Manufacturing Effects: Moisture Trapping

Moisture trapping within SMPUs is significant for any melt-extrusion manufacturing process. Figure 4.4 shows photographs of the outcome of 3D-printed SMPU parts when the material is affected

by moisture prior to the EBAM process. Figures 4.4(a1), 4.4(b1), 4.4(c1) and 4.4(d1) are images of MM4520 printed parts manufactured with filaments immersed in water for controlled moisture exposure (0 min, 10 min, 5 h, and 24 h). From afar, printed part quality is not affected by moisture absorption of the filaments. Figures 4.4(a2), 4.4(b2), 4.4(c2) and 4.4(d2) show zoomed-in views of the printed surfaces. These images show an increase of imperfections of the surface (circle like patterns), which indicates moisture trapping before reaching water saturation. These imperfections are clear voids within the 3D-printed structure. There is a gradual increase in the number of voids in the specimen from the dried specimen to the moisture-saturated specimen.

Figures 4.4(e1), 4.4(f1) and 4.4(g1) are images of MM7520 printed parts manufactured with filaments immersed in water for 0, 10 min and 24 h. The printed part quality decreases significantly with respect to moisture affected filaments. The effects can be seen by a color and surface change from uniform transparent to white rough surfaces. This whiter surface has a high percentage of voids, as can be closely seen in Figure 4.4(e2, f2, g2). The images show that moisture trapping increases dramatically after only 10 min of water absorption.

## 4.5.2 Moisture on Manufactured Parts: Effect of Moisture by Plasticization

### Moisture Absorption Content

The TGA plots of moisture-saturated materials, MM4520 and MM7520, are presented in Figures 4.5a and b, respectively. The tests were done with samples that were first immersed in water for 0, 48, 72, and 112 h. Both the polymer matrices absorbed water and reached a saturation point after 72 h. Figure 4.5a,b also show the degradation temperature ( $T_d$ ). Both of the polymer samples started to decompose at  $\sim 300^\circ C$ . Therefore, thermal degradation of the polymers was independent of the absorbed water content. The most water evaporation (removal) occurs before 48 h, as seen by the greatest weight loss percentage in the TGA. After 72 h, weight loss gradually decreased and eventually stabilized.

Figures 4.5c and d show the derivative thermogravimetric analysis (DTGA) for MM4520 and MM7520, respectively. These were obtained by taking the derivatives of the data presented in Figures 4.5a and b with respect to temperature (i.e., zoomed in between 45 and  $200^\circ C$ ). The peak represents the point of maximum moisture removal (in Figure 4.5c for MM4520). The peak values for the various immersion times of samples are shown in Figure 4.5c for MM4520. As the immersion time of the polymer in water increased, the maximum point of the rate of desorption shifted to a lower temperature by a few degrees. On the other hand, no visible desorption trend found in MM7520 with various water immersion times (Figure 4.5d). This data suggests that a greater

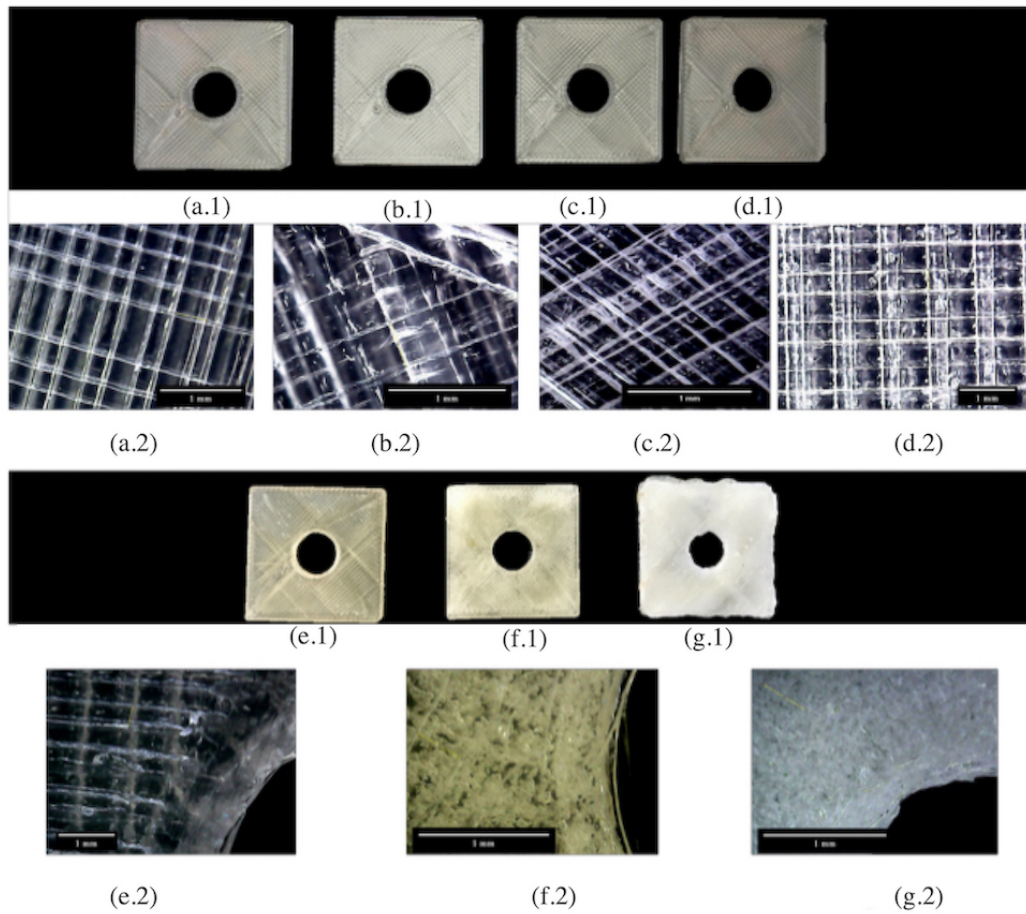


Figure 4.4: Photographs showing the effects of moisture in filaments on EBAM manufactured parts. Figure (a1), (b1), (c1) and (d1) are images of MM4520 printed parts manufactured with filaments immersed in water for 0, 10 min, 5 h and 24 h. Figures (a1), (b2), (c2) and (d2) show zoomed-in views of the printed surfaces. Similarly (e1), (f1) and (g1) are images of MM7520 printed parts manufactured with filaments immersed in water for 0, 10 min and 24 h, the close-up versions are shown in (e2), (f2) and (g2).

amount of water was absorbed and free water moved more readily from MM4520 than MM7520. This is especially interesting for drying purposes since a drying procedure will have to be performed on 3D printing filaments. Yang et al. also suggested that free water has a negligible effect on  $T_g$  and can be fully removed below  $100^\circ\text{C}$ , whereas bound water directly affects  $T_g$ . Bound water can be removed by heating above  $120^\circ\text{C}$  [46]. Because of the nature of the EBAM process, thermal history will be wiped after melting the material, therefore drying conditions for EBAM filaments can include bounded water removal temperature ranges.

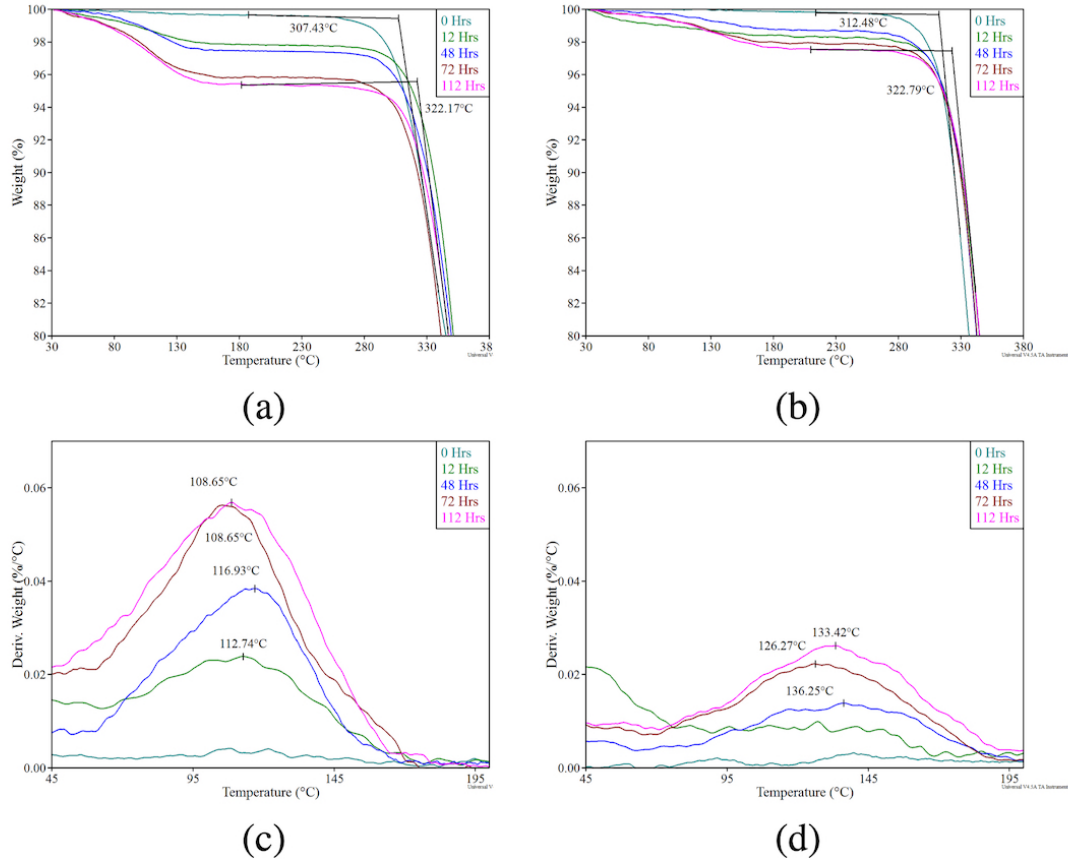


Figure 4.5: TGA and DTGA curves of (a) and (c) MM4520; and (b) and (d) MM7520 after different immersion times in water

Figure 4.6a shows the water content (weight %) of MM4520 and MM7520 samples as a function of their immersion time in water. Plots were generated by calculating the water content values from Figure 4.5a,b data at around 240°C, assuming that all weight loss was due to the evaporation of water and that the polymer became completely free of moisture. The plots indicate that MM4520 contained 4.22% moisture intake compared to 2.28% for MM7520 at saturation. The differences between SMP samples are due to the different amounts of soft segment content of each polymer.

Figure 4.6b shows the plot of water saturation values vs. glass transition temperatures of the SMPU samples. In addition to our measurements of MM4520 and MM7520, the data for MM3520 was compiled from the literature [46]. Glass transition temperature has been reported to increase linearly with respect to hard segment content [31]. A linear relationship of total moisture saturation can

Table 4.2: Bonding frequencies for dry materials.

Material	FTIR-Wavenumbers [ $cm^{-1}$ ]				
	Bonded C=O	Free C=O	Bonded N-H	Free N-H	Bonded C-O
MM4520	1703	1724	3306	3400	1059
MM7520	1701	1730	3304	3383	1057

be related to the ratio soft/hard segments, or the glass transition temperatures of SMPU samples; thus, the soft segments of the SMPU can be directly associated to plasticization in the polymer matrix.

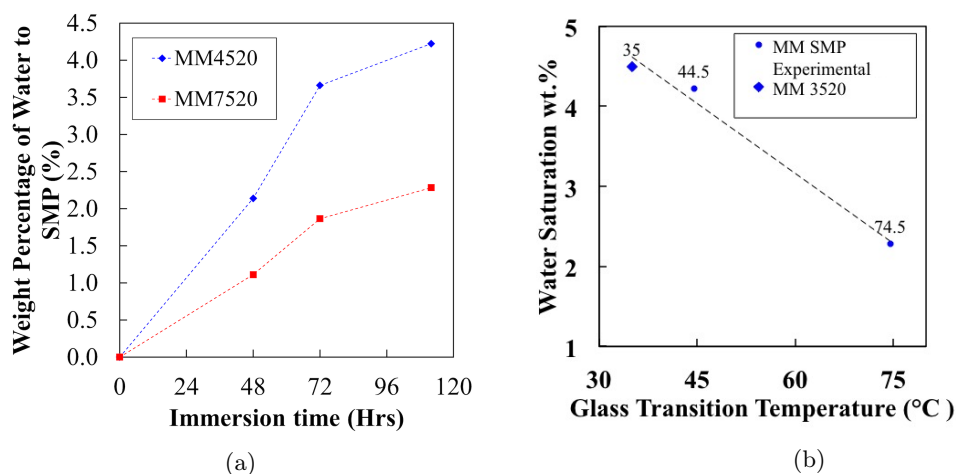


Figure 4.6: (a) Ratio of water content to MM4520 and MM7520 after different immersion times in water (b) water Saturation with respect to Shape Memory Polyurethane  $T_g$  series.

### Moisture and Its Effect of Hydrogen Bonding (Plasticization)

The literature covers extensively the matter of hydrogen bonding in SMPUs due to moisture absorption [50, 16, 46, 44, 49, 6, 41]. This phenomenon can be characterized by observing a wave number shift of C=O and N-H stretching to lower values from the original non-interacted peaks [49, 6, 41]. The Infrared Spectroscopy for (a) MM4520 and (b) MM7520 can be found in the supplementary information in Appendix B.3. Comparative values of the peaks of dried and water-immersed samples are summarized in Table 4.2.

The intrinsic properties of shape memory polymers, such as shape recovery and mechanical properties, are closely related to their degree of phase separation ( $D_{ps}$ ). The intermolecular hydrogen

bonding between the carbonyl group (peak at  $\sim 1700\text{cm}^{-1}$ ) and the NH group, from the urethane hard segment, can be used to determine the degree of phase separation. Merline et al.[31] suggested that the degree of phase separation can be calculated through (Equation 4.1). The comparison is thus considered between the bonded absorption bands ( $A_b$ ) and free absorption bands ( $A_f$ ) of the carboxyl groups.

$$D_{ps} = \frac{(A_b/A_f)}{(1 + A_b/A_f)} \quad (4.1)$$

From the obtained calculation, Figure 4.7a shows a plot of the calculated degree of phase separation for three different commercially available polymers, MM3520, MM4520 and MM7520. Data for MM3520 was obtained from [46]. The figure shows a linear increasing trend between the calculated degrees of phase separation as glass transition temperature of SMPU increases. Because the glass transition temperature is closely related to the amount of hard segment content within the polymer, it can be directly inferred that an increase of hydrogen bonding between hard segments occurs [46]. Wen et al.[41] also showed that there exists a proportional relation between hard to hard hydrogen bonding and phase separation between soft and hard segments for thermoplastic polyether-based polyurethane (N-H $\cdots$ O=C bond). Thus, the degree of phase separation plays a significant role in determining the shape memory characteristics of the material.

Studies have revealed that water has a direct effect on hydrogen bonding within the SMPU's structure. It has been suggested that water molecules act as bridges between hydrogen-bonded N-H and C=O groups [44]. The degree of phase separation has also been determined with respect to absorbed moisture by the polymers (i.e., immersion time in water). Figure 6b shows the variation of degree of phase separation with respect to immersion time in water for MM4520 and MM7420. There is a clear decrease in phase separation for MM4520 but no visible effect for MM7520. Although water molecules function as bridges, theoretically increasing the phase separation and the free volume, through this calculation method it can be seen that phase separation decreases for MM4520 perhaps due to intramolecular hydrogen bonding.

From the FT-IR results, bond stretching (a) N-H (b) C-O and (c) C=O for MM4520 and MM7520 were studied after different immersion times in water. An increase in wavenumber was observed from (N-H $\cdots$ H) and (C-O $\cdots$ H) groups for MM4520 in contrast to MM7520 (Figure 4.8a,4.8b). These results show a weakening of hydrogen bonding for MM4520 as water absorption occurs [44, 20]. The loosely bound water weakens the hydrogen bond and decreases  $T_g$ . A weakening of hydrogen bonding is also related to a phase separation between soft and hard segment, as suggested by Wen et al.[41].

Hydrogen bonded C=O shows a slight increase for MM7520 and a slight decrease in MM4520

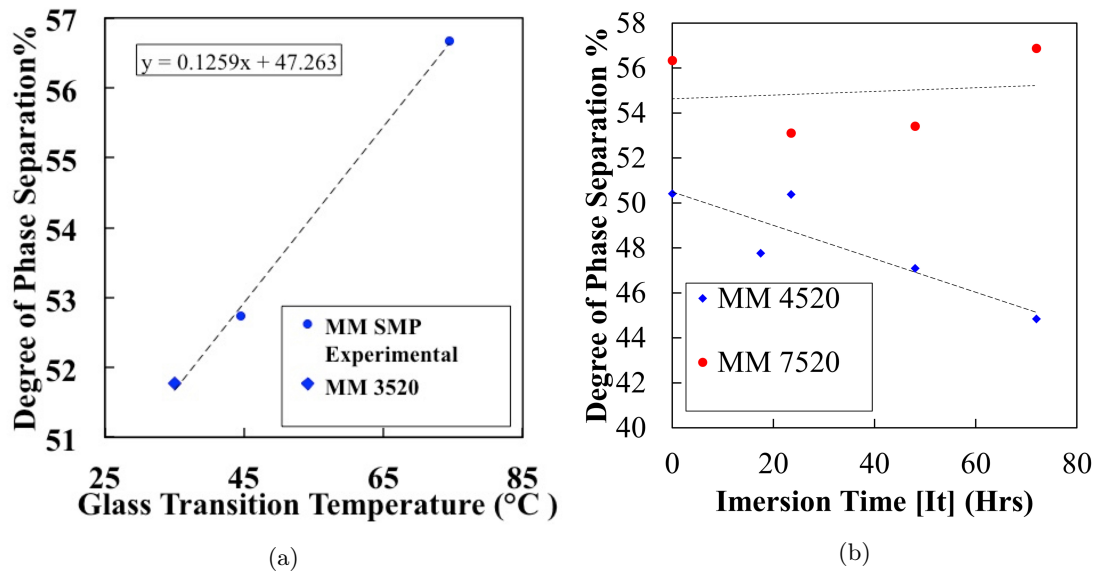


Figure 4.7: (a) Degree of phase separation with respect to different SMPU series (MM3520, MM4520 and MM7520) and (b) change in the degree of phase separation with respect to moisture absorption for MM4520 and MM7520.

(Figure 4.8c), this result is in agreement with Yang's [44] study of MM3520. Yang showed that within the chemical structure of SMPU MM3520 hydrogen bonding is present at two points of the C=O group. The two hydrogen bonds provoke a counter reaction, forcing the infrared band peak to decrease [44]. Because of the close glass transition temperatures between MM3520 and MM4520, the same phenomena can be inferred for MM4520. Contrary to MM3520 and MM4520, the infrared band on the C=O group for MM7520 increases, suggesting that there is only one place at which bonded water occurs. Studies have shown that bounded water affects the shape fixity and shape recovery of SMPUs and directly affects their glass transition temperature. Free water, on the other hand, has a negligible effect [50, 16, 46]. In contrast to MM7520, MM4520 shows more bound water and presents a visible decrease in phase separation; moisture will have a more severe effect on MM4520 than on MM7520.

### Moisture Absorption and Glass Transition Temperature

Figure 4.9 shows the change and decrease in glass transition temperature ( $T_g$ ) for MM4520 and MM7520 as the immersion time in water increases. Previous studies have shown that moisture has a plasticization effect on thermoplastic polyurethanes causing a decrease on the glass transition temperature [50, 16, 46, 48]. Yang et al [46] showed that bound water reduces the glass transition

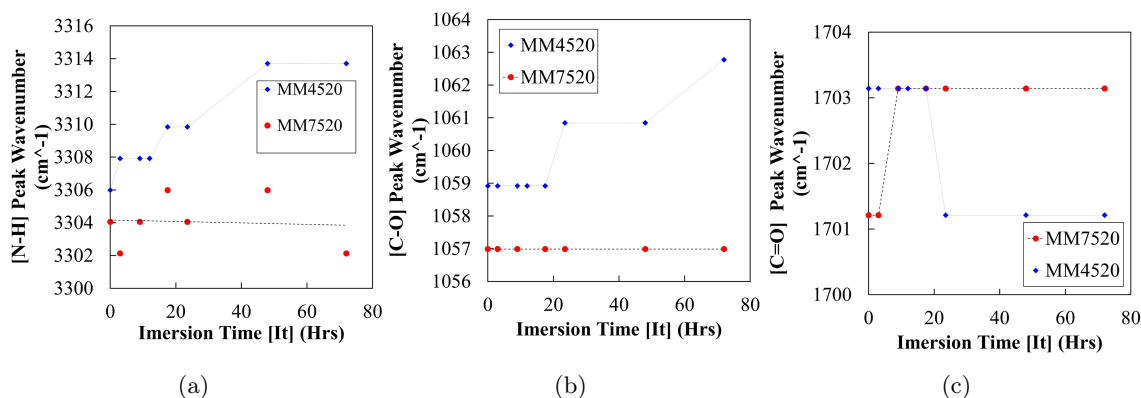


Figure 4.8: Values of bond stretching for (a) N–H bond, (b) C=O and (c) C–O bonds.

temperature in a linear manner. On the other hand, free water has been shown to have a negligible effect on the glass transition temperature and mechanical behavior, as expected from the degree of phase separation in Figure 4.7b. Figure 4.9 shows a rapid change in  $T_g$  for MM4520, while the decrease of  $T_g$  for MM7520 is much slower, with a faster saturation. The  $T_g$  decrease of MM4520 is similar to the decrease of MM3520 found by Yang et al. [46]. It can be observed that plasticization by water occurs in both polymers but is more prominent for MM4520 than for MM7520. This is possibly due to a higher bound-to-free water ratio in MM4520 than in MM7520, when in contact with water.

### Moisture Absorption and Mechanical Properties

Of all the materials tested, the effect of moisture on mechanical properties is the most significant for MM4520. Figure 4.10a shows the evolution of mechanical behavior for MM4520 and MM7520. MM4520 changes from a tough material with a defined yield point to a material without a clear yield point when immersed in water (see plots corresponding to legends MM4520 0/5/10/24HRS). Nevertheless, almost no significant effect on MM7520 was observed (see plots corresponding to legends MM7520 0/120HRS). This is caused by the lubrication of chains and a decrease of phase separation due to plasticization, which improves the elasticity of the material.

Figure 4.10b shows the elastic modulus ( $E_y$ ), and one standard deviation at each side, obtained from tensile tests conducted for MM4520 and MM7520 with respect to immersion times in water. The elastic modulus of dried MM4520 (717 MPa) and MM7520 (803 MPa) did not differ significantly. Additionally, a rapid decrease of the elastic modulus for MM4520 was observed as immersion time in water increased. There was no significant effect for MM7520. The obtained difference between both polymers is given by a higher plasticization of the polymer with a lower hard-to-soft segment

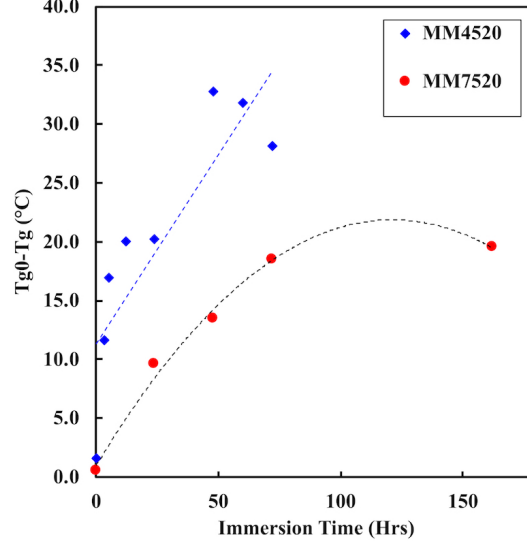


Figure 4.9: Graph showing a change in  $T_g$  with respect to immersion time in water for MM4520 and MM7520.

ratio (MM4520) compared to MM7520, just as it was seen by Yang et al. on a polymer with lower hard-to-soft segment ratio [46, 44].

### Model Description of MM4520 Elastic Modulus and $T_g$ Relationship

The plasticization effect is often convenient for many engineering and biomedical applications, such as body temperature-activated devices, including stents; an understanding of the material's behavior is also necessary to predict product performance. In the present study a model is proposed to predict the mechanical properties, with respect to moisture content, of a material with a lower  $T_g$ . Reimschuessel et al.'s logarithmic model [34] is used to obtain, via a regression analysis, an approximate solution of MM4520's uniaxial elastic modulus with respect to immersion time in water. Reimschuessel et al. described a decreasing logarithmic model that shows the relationship between the elastic modulus and water content percentage for the plasticization effect in polymers [34]. Equations were adapted from Reimschuessel et al.[34] model.

The experimental data shows that the modulus ( $E_y$ ) of MM4520 decays with respect to immersion time in water, reaching a saturated Elastic Modulus ( $E_S$ ). The initial elastic modulus for water content at 0 h is described by ( $E_o$ ), where immersion time in water is  $W(0) = 0$ . Therefore, the boundary condition is as follows ( $E_y(0) = E_o$ ).

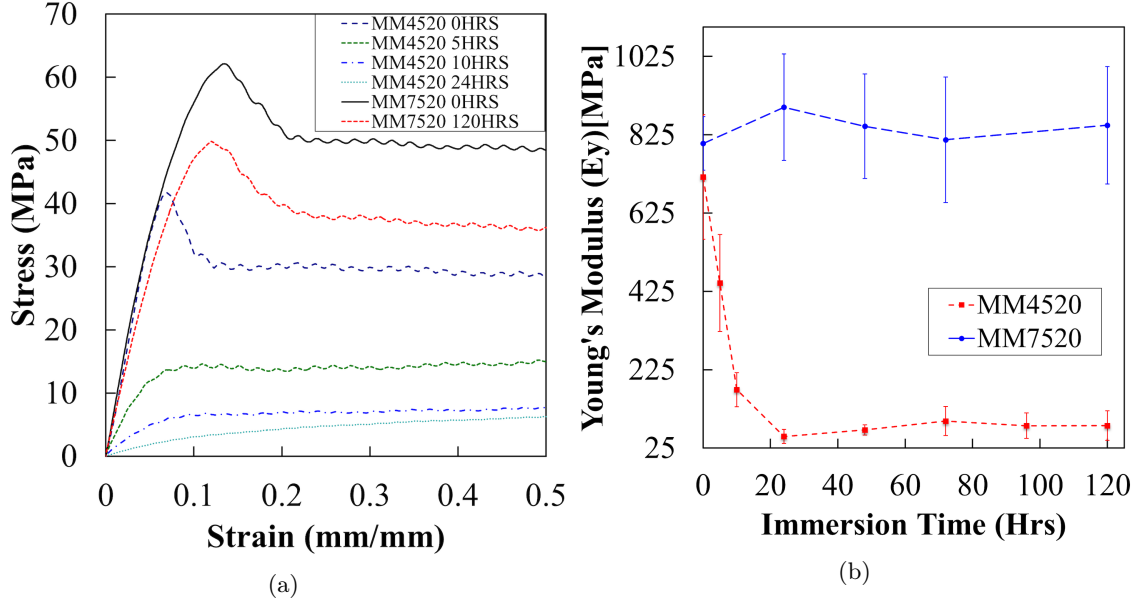


Figure 4.10: Graphs showing the mechanical behavior of both materials. (a) Describes the evolution in mechanical behavior while (b) shows the drop in elastic modulus with respect to immersion time in water.

$$\frac{dE_y}{dW} = -k_{(E_o, E_s, W_s)} \cdot (E_y - E_s) \quad (4.2)$$

$$E_y = (E_o - E_s)e^{-kW} + E_s \quad (4.3)$$

$$k_{(E_o, E_s, W_s)} = \frac{\ln\left[\frac{E_o - E_s}{E_{s+1} - E_s}\right]}{W_{s-1}} = \frac{E_o - E_s}{W_s - \delta_w} = \ln[E_o - E_s]\eta/W_s \quad (4.4)$$

$$E_y = (E_o - E_s)e^{-\ln[E_o - E_s]\eta/W_s W} + E_s \quad (4.5)$$

In this model, the elastic modulus decreases to a finite value  $E_s$  after an amount of water, indicated as  $W_s$ , has saturated the polymer. This is identified as  $E_y(W_s) = E_s$  and therefore  $(dE_y)/dW = 0$ ,  $W_s \rightarrow \infty$ . The speed at which the modulus decreases, described mathematically by  $k$ , is a function of  $E_o$ ,  $E_s$  and  $W_s$  (Equation 4.2). The solution to the ordinary differential equation and its constant for the initial boundary condition results in Equation 4.3). To write this in terms of a saturation time or water saturation content,  $W$ , a value of 1 is defined as an artifice, where  $E_{s+1} - E_s = 1$ . Consequently,  $W_{s-1} - W_s = \delta_w$ , and, using  $\eta = W_s/(W_s - \delta_w)$ , an expression for constant  $k$  is obtained.

Using a nonlinear least squares fit in MATLAB<sup>TM</sup>, the experimental data was weighted with respect to the number of experiments conducted and fitted to find the coefficients of the following model  $f(x) = a_1 e^{-\frac{x}{b_1}} + c_1$  which is in the same form as equation (Equation 4.5). Coefficients were obtained with 95% confidence intervals and their values are portrayed in Table 4.3. Figure 4.11a shows the obtained Young's modulus from the experimental data, model curve fit and statistical lower and upper bounds. Regression residuals for MM4520 are presented in Figure 4.11b. The curve fit results in an adjusted coefficient of determination of  $R^2 = 0.9895$ , showing that Reimschuessel et al.'s model correlates with our experimental data. For the predicted model, water saturation is considered at 99% of water saturation value, with a resolution of 0.01 h. of immersion time in water. The final generic model shown in Table 4.3 was calculated from the obtained curve fit model coefficients. Without any more experiments, the elastic modulus can be predicted with respect to immersion time in water for SMP MM4520. Similarly, the same procedure can be applied to determine the glass transition temperature of both materials. However, a statistical model will be more significant with a higher sample size that the one obtained in this study.

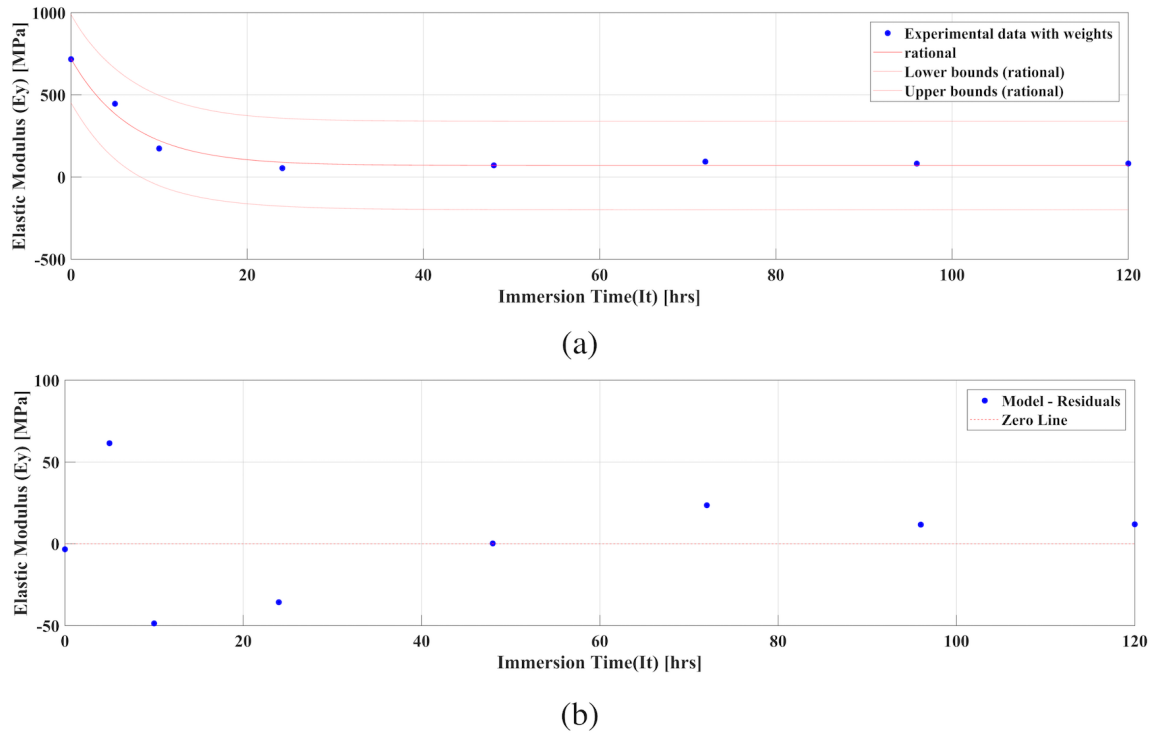


Figure 4.11: Graph of elastic modulus ( $E_y$ ) for MM4520 for (a) fitted model and (b) residuals.

Table 4.3: Estimated coefficients for MM4520 elastic modulus with respect to immersion time in water.

<b>Estimation curve:</b>		$f(x) = a_1 e^{-x/b_1} + c_1$		
<b>Estimated Coefficients:</b>	$a_1$ (95%CI)	$b_1$ (95%CI)	$c_1$ (95%CI)	
	650	6.888	70.4	
<b>Final generic model:</b>		$E_y = (e_o - E_s)e^{-(\ln[E_o - E_s]\eta/W_s)W} + E_s$		
<b>Estimated Constants:</b>	$E_o$ (MPa) (95%CI)	$E_s$ (MPa) (95%CI)	$W_s$ (h) (95%CI)	$\eta$ (1 MPa) (95%CI)
	720.4	70.4	31.17	-0.698

### Moisture Absorption and Shape Recovery Properties

To observe the possible effects of moisture in the strain recovery process, a one free end recovery with an application of 0.2 N in force was applied. The strain recovery percentage, portrayed in Equation 4.6, was obtained from the ratio of the difference between the prescribed strain ( $\varepsilon_p = 100\%$ ) and the recovered strain  $\varepsilon_r$  to the original prescribed strain [4]. Figures 4.12a and 4.12b, respectively, show the recovery for samples of MM4520 at 0, 12 and 24 h and 0 and 24 h for MM7520. The longer the samples were in water, the less able they were to recover, as can be seen in the figures. Recovery percentage was measured at 90% of the maximum recovery's plateau. See Figure 4.12a.

$$R_r = (\varepsilon_p - \varepsilon_r)/\varepsilon_p \quad (4.6)$$

The tests showed that both materials recovered the same amount after being activated (Figure 4.13a). As moisture percentage increased, 90% of the maximum recovery decreased significantly for both materials, as portrayed in Figure 4.13b. The ANOVA returned a P-value =  $1.992 \times 10^{-10} < 0.05$  for MM4520 and a P-value =  $0.027 < 0.05$  for MM7520. The amount of recovery found is less than what has been reported [3]. This may be caused by the applied strain and the additional force (0.2 N) placed at the free end of the samples. However, the procedure was kept constant allowing a comparison of the relative values for water-immersed samples and dried. The effect on glass transition temperature may have an effect on the programming temperature and the ability of the material to recover to a maximum strain. The programming temperature does not change. Therefore when these polymers reach a temperature where plastic deformation occurs, the polymer loses the ability to store elastic stress [17].

The required time to reach 90% of the maximum recovery's plateau was also recorded. Recovery

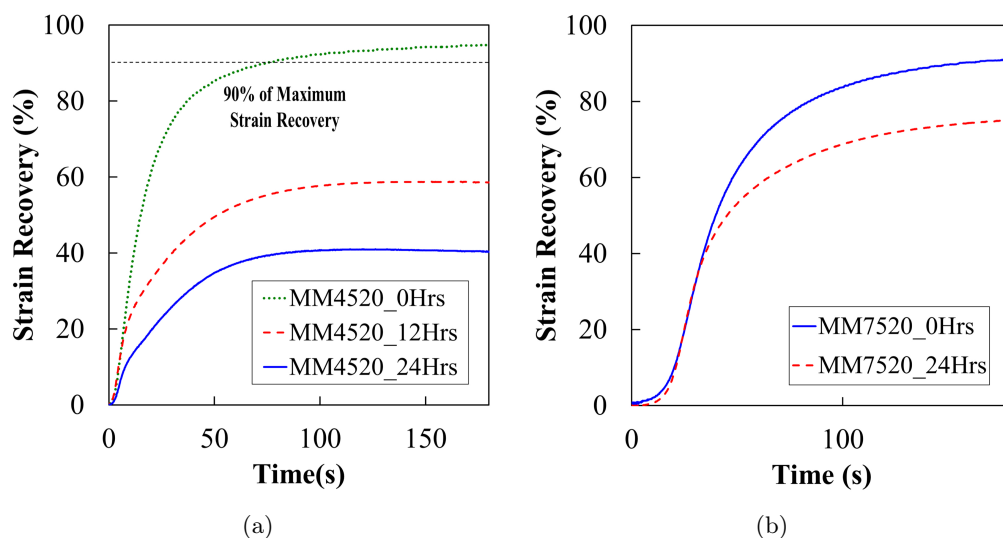


Figure 4.12: Representation curves for strain recovery of (a) MM4520 at activation temperature  $T = 50^{\circ}\text{C}$  and (b) MM7520 after different immersion times in water at activation temperature  $T = 80^{\circ}\text{C}$ .

rate for both materials was obtained from the slope of the strain recovery percentage with respect to time. Figure 4.14a shows the recovery rate with respect to time for MM4520 and MM7520. P-values obtained for MM4520 and MM7520 were  $8.47 \times 10^{-8}$  and 0.0070, respectively, showing a significant difference in recovery rate for both materials. Because both materials lose their elastic capacity when being programmed, their ability to recover at a fast rate is also affected, just like a spring would be when being deformed. Consequently, a trend of increasing required time with an increase in moisture content is observed in Figure 4.14b. P-values of 0.0123 and 0.9231 for MM4520 and MM7520 were obtained, respectively, showing a significant effect of moisture on recovery time for MM4520 while no significant effect was found for MM7520.

Effects of moisture on recovery rate and time may be caused by the evaporation of bounded and free water molecules within the samples. It is noted that free water is easier to evaporate than bounded water [16, 14]. Because of its higher hard-segment to soft-segment ratio, the recovery of MM7520 is not as affected by moisture as MM4520. Therefore, it is able to evaporate moisture content quicker because it is harder to produce hydrogen bonds within its structure.

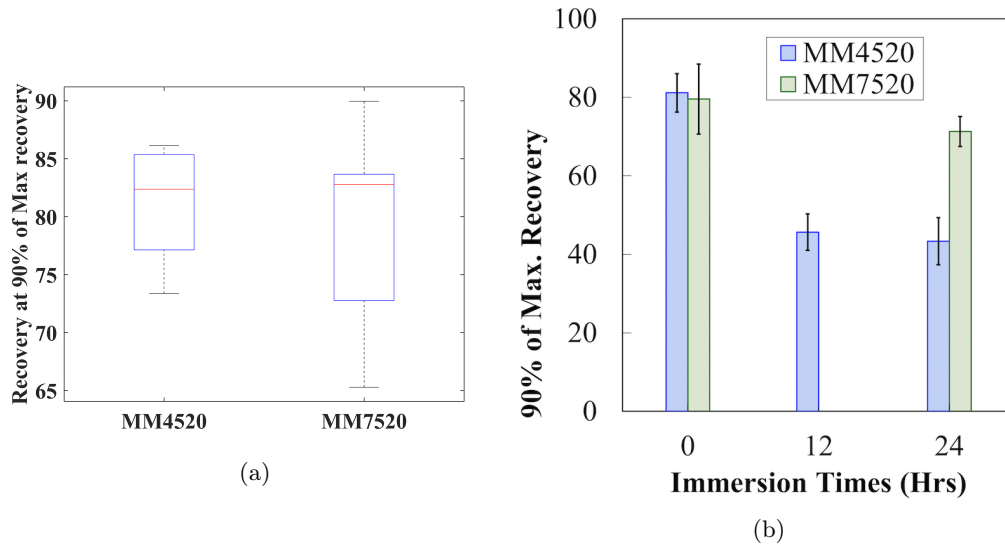


Figure 4.13: (a) Box plot showing recovery of MM4520 and MM7520 dried materials and (b) maximum recovery of MM4520 and MM7520 after water immersion.

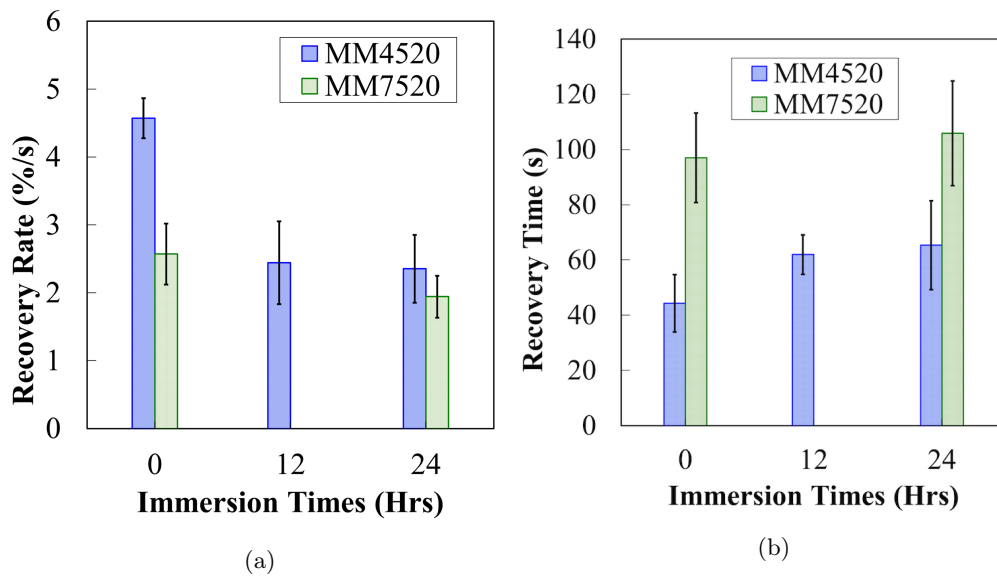


Figure 4.14: (a) Recovery rate for MM4520 and MM7520 with respect to immersion times in water (b) Recovery time for MM4520 and MM7520 with respect to immersion times in water.

## 4.6 Conclusions

The influence of moisture on the preprocessing stage of manufacturing and in the post manufacturing stage of two SMPUs containing hard to soft segment ratios was investigated. For the preprocessing stage, filaments of SMPU were manufactured and immersed for different periods in distilled water and immediately fed into a commercial 3D printer. The results showed that the polymer with higher  $T_g$  (higher h/s ratio) trapped more moisture, affecting dramatically the printing quality only 10 min after moisture exposure. This phenomenon is inferred to have occurred due to water molecules trapped within the phase separation that produce voids when evaporated.

The degree of phase separation increases as the transition temperature ( $T_g$  or h/s ratio) of the SMPUs increases. As the degree of phase separation increases, there exists a wider space for water molecules to be stored and create voids when the polymer is being heated and extruded during EBAM. This is clearly seen in the printed qualities of the two SMPUs. Although moisture content is related to water immersion, effects of moisture were also seen in filaments exposed to ambient conditions for less than 48 h (with uncontrolled moisture exposure).

SMPUs with higher h/s segments (higher  $T_g$ ), such as MM 7520, are more susceptible to moisture trapping. The final quality of a melt-extruded part is severely affected by moisture in polymers with a higher  $T_g$ . Although a higher h/s segment ratio is more affected by moisture trapping, because of its resistance to hydrogen bonding and therefore plasticizing, these SMPUs are more beneficial for manufacturing. To obtain void-less printed parts and therefore a better printing quality when using an SMPU with a higher  $T_g$  for 3D printing, rigorous precautions must be taken to maintain the dry conditions of the printing filaments.

Although the polymer with higher  $T_g$  was more affected in the preprocessing stage, in the post-manufacturing stage the material was less affected by plasticization effects. The polymer with the lower  $T_g$  was more affected by the formation of hydrogen bonding into (N-H) and (C-O) groups when immersed in water. This is caused by a lower hard-to-soft segment ratio in the polymer with a lower  $T_g$ . This study also showed that, due to plasticization, moisture absorption has a more severe effect on the mechanical properties of the material with a lower  $T_g$ . The elastic modulus slowly reached a saturated modulus for the polymer with lower  $T_g$ , while there was no visible effect on the polymer with the higher  $T_g$ . From these observations, a generic model for predicting the elastic modulus with respect to immersion time was obtained for an SMP with a  $45^\circ\text{C}$   $T_g$ . A similar decreasing exponential effect was observed for the mechanical properties on the polymer with nominal  $45^\circ\text{C}$   $T_g$ . A linear decreasing trend was observed on the other polymer.

Moisture also had a significant effect on the shape recovery properties of the material. The ability to reach 90% of the maximum recovery and the recovery rate for both materials decreased when the

material was immersed in water. This may be caused by the plastic deformation that the polymeric chains suffer from the decrease of  $T_g$  and the applied strain. Moisture did not have a significant effect on the time required to reach 90% of the maximum recovery on the polymer with a higher  $T_g$ , but had a significant effect on the polymer with a 45°C  $T_g$ . This may be caused by the evaporation time for free water in contrast to bound water. Since the polymer with the higher  $T_g$  has a higher hard-segment ratio, it can be inferred that it will have less bounded water than the polymer with lower  $T_g$ .

An SMPU with a higher  $T_g$ , which has a higher h/s segment ratio, resists hydrogen bonding and therefore plasticization. This makes it more desirable for ambient moisture exposure applications. However, due to a higher degree of phase separation, moisture trapping has a significant effect when subjected to melt extruded manufacturing techniques. This effect becomes critical in EBAM-3D printing manufacturing. The present study contributes information for engineers and designers regarding the material selection for shape memory polyurethane designs for emerging manufacturing technologies such as 3D printing.

## 4.7 References

- [1] Daniel R Aldrich, C. Ayranci, and D. S Nobes. OSM-Classic : An optical imaging technique for accurately determining strain. *SoftwareX*, 6:225–230, August 2017.
- [2] C Azra, C J G Plummer, and J A E Månson. Tailoring the time-dependent recovery of shape memory polymers. In Nakhiah C Goulbourne and Zoubeida Ounaies, editors, *SPIE Smart Structures and Materials + Nondestructive Evaluation and Health Monitoring*, pages 834212–9. SPIE, March 2012.
- [3] G Baer, T S Wilson, D L Matthews, and D J Maitland. Shape-memory behavior of thermally stimulated polyurethane for medical applications. *Journal of Applied Polymer Science*, 103(6):3882–3892, 2006.
- [4] Marc Behl and Andreas Lendlein. Shape-memory polymers. *Materials Today*, April 2007.
- [5] Paolo Blasi, Susan S D’Souza, Francesca Selmin, and Patrick P DeLuca. Plasticizing effect of water on poly(lactide-co-glycolide). *Journal of Controlled Release*, 108(1):1–9, November 2005.
- [6] C M Brunette, S L Hsu, and W J MackKnight. Hydrogen-Bonding Properties of Hard-Segment Model Compounds in Polyurethane Block Copolymers. *Macromolecules*, 15(1):71–77, 1982.

- [7] Shaojun Chen, Jinlian Hu, Chun-wah Yuen, and Laikuen Chan. Novel moisture-sensitive shape memory polyurethanes containing pyridine moieties. *Additive Manufacturing*, 50(19):4424–4428, September 2009.
- [8] Samuel M Felton, Michael T Tolley, ByungHyun Shin, Cagdas D Onal, Erik D Demaine, Daniela Rus, and Robert J Wood. Self-folding with shape memory composites. *Soft Matter*, 9(32):7688–8, 2013.
- [9] Bradley Finnigan, Darren Martin, Peter Halley, Rowan Truss, and Kayleen Campbell. Morphology and properties of thermoplastic polyurethane nanocomposites incorporating hydrophilic layered silicates. *Additive Manufacturing*, 45(7):2249–2260, March 2004.
- [10] Felix Franks. *Water Science Reviews 3: Volume 3*. Water Dynamics. Cambridge University Press, Cambridge, October 1988.
- [11] I T Garces and C. Ayranci. A view into additive manufactured electro-active reinforced smart composite structures. *Manufacturing Letters*, 16:1–5, April 2018.
- [12] Qi Ge, Amir Hosein Sakhaei, Howon Lee, Conner K Dunn, Nicholas X Fang, and Martin L Dunn. Multimaterial 4D Printing with Tailorable Shape Memory Polymers. *Nature Publishing Group*, 6:31110, August 2016.
- [13] B C Hancock and G Zografi. The Relationship Between the Glass-Transition Temperature and the Water-Content of Amorphous Pharmaceutical Solids. *Pharmaceutical Research*, 11(4):471–477, April 1994.
- [14] T Hatakeyama, K Nakamura, and H Hatakeyama. Determination of bound water content in polymers by DTA, DSC and TG. *Thermochimica Acta*, 123:153–161, 1988.
- [15] S Hayashi. Shape memory polyurethane elastomer molded article, September 1992.
- [16] A Herrera-Gómez, G Velázquez-Cruz, and M O Martín-Polo. Analysis of the water bound to a polymer matrix by infrared spectroscopy. *Journal of Applied Physics*, 89(10):5431–8, 2001.
- [17] Jin Lian Hu, Feng Long Ji, and Yuen Wah Wong. Dependency of the shape memory properties of a polyurethane upon thermomechanical cyclic conditions. *Polymer International*, 54(3):600–605, 2005.
- [18] W. M. Huang, B. Yang, L An, C. Li, and Y S Chan. Water-driven programmable polyurethane shape memory polymer: Demonstration and mechanism. *Applied Physics Letters*, 86(11):1–3, March 2005.

- [19] W. M. Huang, B. Yang, Y. Zhao, and Z. Ding. Thermo-moisture responsive polyurethane shape-memory polymer and composites: A review. *Journal of Materials Chemistry*, 20(17):3367–3381, June 2010.
- [20] Yong Huang, W Yang, and Bin Fu. Effects of Moisture on Electrically Conductive Polyurethane Shape Memory Polymers. In *Future of Polyurethane Shape Memory Polymers*, pages 93–116. CRC Press, December 2011.
- [21] F L Ji, J L Hu, and J P Han. Shape memory polyurethane-ureas based on isophorone diisocyanate. *High Performance Polymers*, 23(3):177–187, June 2011.
- [22] Hong-Yang Jiang and Annette M Schmidt. Shape-Memory Polymers and Multifunctional Composites. pages 1–43, May 2010.
- [23] Zhong Xun Khoo, Joanne Ee Mei Teoh, Yong Liu, Chee Kai Chua, Shoufeng Yang, Jia An, Kah Fai Leong, and Wai Yee Yeong. 3D printing of smart materials: A review on recent progresses in 4D printing. *Virtual and Physical Prototyping*, 10(3):103–122, September 2015.
- [24] Taeyoung Kim and Yong-Gu Lee. Shape transformable bifurcated stents. *Nature Publishing Group*, 8(1):13911, September 2018.
- [25] Jinsong Leng, Xin Lan, Yanju Liu, and Shanyi Du. Shape-memory polymers and their composites: Stimulus methods and applications. *Progress in Materials Science*, 56(7):1077–1135, September 2011.
- [26] Yanju Liu, Haiyang Du, Liwu Liu, and Jinsong Leng. Shape memory polymers and their composites in aerospace applications: a review. *Smart Materials and Structures*, 23(2):023001, February 2014.
- [27] Yiqi Mao, Zhen Ding, Chao Yuan, Shigang Ai, Michael Isakov, Jiangtao Wu, Tiejun Wang, Martin L Dunn, and H Jerry Qi. 3D Printed Reversible Shape Changing Components with Stimuli Responsive Materials. *Nature Publishing Group*, 6(1):24761, April 2016.
- [28] American Society for Testing and Materials. *ISO and IEC selected standards for the plastics industry*. Astm Intl, 1996.
- [29] Patrick T Mather, Xiaofan Luo, and Ingrid A Rousseau. Shape Memory Polymer Research. *Annual Review of Materials Research*, 39:445–471, August 2009.
- [30] Harper Meng and Guoqiang Li. A review of stimuli-responsive shape memory polymer composites. *Polymer (United Kingdom)*, 54(9):2199–2221, April 2013.

- [31] J Dyana Merline, C P Reghunadhan Nair, C Gouri, G G Bandyopadhyay, and K N Ninan. Polyether polyurethanes: Synthesis, characterization, and thermoresponsive shape memory properties. *Journal of Applied Polymer Science*, 107(6):4082–4092, 2007.
- [32] Elzbieta Alicja Pieczyska, Michal Maj, Katarzyna Kowalczyk-Gajewska, Maria Staszczak, Leszek Urbanski, Hisaaki Tobushi, Shunichi Hayashi, and Mariana Cristea. Mechanical and Infrared Thermography Analysis of Shape Memory Polyurethane. *Journal of Materials Engineering and Performance*, 23(7):2553–2560, April 2014.
- [33] Debdatta Ratna and J Karger-Kocsis. Recent advances in shape memory polymers and composites: a review. *Journal of Materials Science*, 43(1):254–269, 2008.
- [34] H K Reimschuessel. Relationships on the effect of water on glass transition temperature and young’s modulus of nylon 6. *Journal of Polymer Science: Polymer Chemistry Edition*, 16(6):1229–1236, June 1978.
- [35] Christian Schuh, Kerstin Schuh, Maria C Lechmann, Louis Garnier, and Arno Kraft. Shape-Memory Properties of Segmented Polymers Containing Aramid Hard Segments and Polycaprolactone Soft Segments. *Polymers*, 2(2):71–85, June 2010.
- [36] L Sun, W M Huang, Z Ding, Y Zhao, C C Wang, H Purnawali, and C Tang. Stimulus-responsive shape memory materials: A review. *Materials and Design*, 33(1):577–640, January 2012.
- [37] T Takahashi, N Hayashi, and S Hayashi. Structure and properties of shape-memory polyurethane block copolymers. *Journal of Applied Polymer Science*, 60(7):1061–1069, 1996.
- [38] SMP Technologies. SMP technologies.
- [39] Jorge Villacres, David Nobes, and C. Ayranci. Additive Manufacturing of Shape Memory Polymers: Effects of print orientation and infill percentage on mechanical properties. *Rapid Prototyping Journal*, 24(4):744–751, 2018.
- [40] Wenshou Wang, Peng Ping, Xuesi Chen, and Xiabin Jing. Biodegradable polyurethane based on random copolymer of L-lactide and  $\epsilon$ -caprolactone and its shape-memory property. *Journal of Applied Polymer Science*, 104(6):4182–4187, 2007.
- [41] Ten-Chin Wen, Ming-Sieng Wu, and Chien-Hsin Yang. Spectroscopic Investigations of Poly(oxypropylene)glycol-Based Waterborne Polyurethane Doped with Lithium Perchlorate. *Macromolecules*, 32(8):2712–2720, April 1999.
- [42] Xuelian Wu, Wei Huang, Yong Zhao, Zheng Ding, Cheng Tang, and Jiliang Zhang. Mechanisms of the Shape Memory Effect in Polymeric Materials. *Polymers*, 5(4):1169–1202, December 2013.

- [43] Wei Xu, Ruoyu Zhang, Wei Liu, Jin Zhu, Xia Dong, Hongxia Guo, and Guo-Hua Hu. A Multiscale Investigation on the Mechanism of Shape Recovery for IPDI to PPDI Hard Segment Substitution in Polyurethane. *Macromolecules*, 49(16):5931–5944, 2016.
- [44] B. Yang. Influence of moisture in polyurethane shape memory polymers and their electrically conductive composites. 2007.
- [45] B. Yang, W. M. Huang, C. Li, C M Lee, and L Li. On the effects of moisture in a polyurethane shape memory polymer. *Smart Materials and Structures*, 13(1):191–195, February 2004.
- [46] B. Yang, W. M. Huang, C. Li, and L Li. Effects of moisture on the thermomechanical properties of a polyurethane shape memory polymer. *Polymer*, 47(4):1348–1356, January 2006.
- [47] B. Yang, W. M. Huang, C. Li, L Li, and J H Chor. Qualitative separation of the effects of carbon nano-powder and moisture on the glass transition temperature of polyurethane shape memory polymer. *Scripta Materialia*, 53(1):105–107, July 2005.
- [48] Kenjiro Yazawa, Kana Ishida, Hiroyasu Masunaga, Takaaki Hikima, and Keiji Numata. Influence of Water Content on the  $\beta$ -Sheet Formation, Thermal Stability, Water Removal, and Mechanical Properties of Silk Materials. *Biomacromolecules*, 17(3):1057–1066, March 2016.
- [49] E Yilgor, I Yilgor, and E Yurtsever. Hydrogen bonding and polyurethane morphology. I. Quantum mechanical calculations of hydrogen bond energies and vibrational spectroscopy of model compounds. *Additive Manufacturing*, 43(24):6551–6559, November 2002.
- [50] C Zhang. Computational study of hydrogen-bonding interactions in shape memory polymers. 2014.

## Chapter 5

# A Viscoelastic Model for Shape Memory Polymers Under Bending

### Abstract

Shape Memory Polymers (SMPs) are materials that can be used for many engineering applications. Predicting and understanding the response of these materials is still an area that is vastly investigated. Many great efforts have been made in modelling SMPs; however, most developed models are designed for a uniaxial tension or compression loading mode and/or are often too complex to allow easy application and interpretation, which makes it difficult and overly complicated. SMPs have the most significant applicability in the bending loading mode for soft robotics and morphing structures.

The present work provides a phenomenological viscoelastic transient model for bending applications to address the aforementioned shortcomings. Among the most crucial data required for engineering design are the maximum shape recovery force, the shape recovery deflection and ratio with respect to time, which can be determined with the proposed model. This model is derived from Tobushi et al.'s model and by using the bending consideration for small strains of a beam, which refers to a linear relationship between strain and curvature at a given time. The bending moment of the beam can then be calculated from the stress distribution of each cross-section. Consequently, the deflection, shape recovery force and ratio can be determined with respect to time by using a discretization in x, y-direction, and time, and by changing the loading conditions for each step. Additionally, this work provides a method to extract the material parameters via Dynamic Mechanical Analysis, which reduces experimentation time and has not been shown in the past. This model has been experimentally validated in constrained recovery and free end recovery tests.

# Contents

## 5.1 Introduction

SMPs can maintain a temporary shape and then recover their original-permanent shape when triggered via an activation method, eg. UV light, pH, temperature, moisture, among others [22]. The phenomenon of storing and recovering a temporary shape is often referred to as Shape Memory Effect (SME). Thermally activated SMPs are the most common shape memory materials due to the ease of activation via a temperature change [16]. A shape training, followed by the SME activation, is obtained by following four different steps: i) Heating of the material above its activation temperature (often the glass transition temperature) ii) loading of the material at a constant temperature and iii) cool-down of the material with a constant applied load or constraint. These steps results in storing a temporary shape. The recovery of the original shape occurs by increasing the temperature to or above the activation temperature (often the glass transition temperature) [15].

SMPs are used in self-deployable [29, 17], self-folding and self-assembled structures [4, 10, 26], including actuators such as grippers [31] and crawling devices [30]. Many of the described applications require an understanding of the expected material's movement and behaviour after activation. The vast majority of studies that focused on the behaviour of SMPs are based on the experimental characterization [25, 13, 12, 14]. However, models are required to predict the behaviour of SMPs to start designing for real-life applications. Although significant advances have been made in this area, scientists need to provide designers with models that can predict essential features required for engineering design, such as recovery rate, ratio, and shape recovery force.

The vast majority of the proposed models have been for a tensile and or compressive loading form [11], these models were extensively reviewed in (Chapter 2). In this section, a summary of the different modelling approaches will be provided and a modelling review focused to the relevance of this chapter. In summary, models are based on two different modelling techniques: 1) a phase and 2) a spring-dashpot modelling technique. Developed by Liu et al. [19], the phase change modelling

technique has been widely used and has shown promising modelling results. This technique assumes a thermodynamically based evolution law to determine a phase change between frozen and active phases. This modelling technique has received criticism from authors that have stated that there is no physical evidence that supports the existence or change between these mentioned phases [27], but other have argued that the existence of these can appear in semicrystalline polymers [27]. Due to the phase change concept, this model often yields physically unattainable material parameters and furthermore, on its own, it is unable to predict the rubber-like behaviour of thermoplastic polymers.

On the other hand, a viscoelastic modelling approach focuses on the history of the thermo-mechanical loading of the material. One of the earliest modelling attempts was that by Tobushi et al. [28]. Their model is based on the Standard Linear Solid model (SLS) and added a slippage mechanism as illustrated in Figure 5.1. The slippage mechanism captures the irrecoverable strain occurred by the internal friction between polymer chains [28]. The strain undergone by the slippage mechanism is denominated as  $\epsilon_s$  in Figure 5.1, and it is placed in series to an elastic spring with elastic constant of  $E_2$ . These elements are in parallel to a Maxwell element with spring constant  $E_1$  and dashpot viscosity,  $\eta$ . In Tobushi's model, the described slippage element is assumed to be responsible for the remaining strain and is also responsible for the SME. This model, although simple, captures the irrecoverable strain occurred.

A viscoelastic modelling approach bases on using constitutive equations of elastic solids and Newtonian fluids, which can be represented by spring and dashpot components. The resulting behaviour of these elements is, therefore, time dependant, hence for a transient model the material properties will also be time dependant. In the permanent shape, the spring-dashpot configuration is in a non-stressed condition. As the material heats up, the dashpots have lower viscosity, and therefore a higher stretchability. The deformation at high temperature will be locked in the dashpot elements once the temperature cools down. The viscosity will increase drastically as temperature decreases and internal stresses will be produced. Once reheating, the viscosity decreases and allows the internal stresses to drive the material to recover the equilibrium position [23].

Only a few models have attempted to capture the bending behaviour of SMPs using a viscoelastic approach. Wang et al. [32] used a generalized Maxwell model coupled with the Williams-Landel-Ferry (WLF) equation to describe relaxation and changes in material properties [18]. This was implemented for a three-point bending load using commercial FEA software, hence no bending formulation was proposed. In their work, different heating rates were tested to obtain key characteristics of recovery rate and recovery force. However, this model lacks experimental validation and requires commercial software or extensive FEA coding to reproduce the results and or apply to different materials. Wu et al. [33] developed a bending model for the shape recovery behaviour of polyurethane-based laminates based on the SLS model. Although their model considers a viscoelas-

tic approach, it does not predict the possible irrecoverable strain that occurs in the process, and the recovery happened along the path of a circular arc with changing central angle, restraining the applicability of the model to the cantilever loading they have proposed. Another method of modelling is through the phase change modelling approach. There are only a few models that attempted this by using a phase change approach. For instance, Gosh et al. [9] developed a beam theory for SMPs and implemented it in a finite element framework. Based on their previous experience [1], Bahani et al. [2] used the phase change model and implemented it to Euler-Bernoulli beams for bending applications. Although, numerically the model is simple; this study did not show shape recovery ratio or force curves needed for quick engineering design.

This chapter presents the author’s main contribution to the viscoelastic formulation for flexural loading. This model can predict the transient bending behaviour of an SMP and its irrecoverability. Furthermore, this model provides with the necessary trend, and prediction of the programming and recovery behaviour of SMPs. This model was fully validated and verified with respect to experimental data. The author also proposes a way to obtain the material parameters by using DMA data and a model derived from Bhattacharyya *et al.* [3].

## 5.2 Model

### 5.2.1 Viscoelastic Model

The representation of the spring-dashpot configuration of Tobushi’s model [28] can be seen in Figure 5.1.

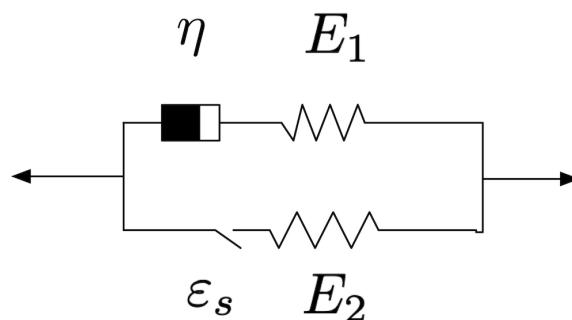


Figure 5.1: Graphic representation of the viscoelastic model used by Tobushi et al. [28]

The governing equation for this model is presented in equation 5.1. Where, the strain rate  $\dot{\epsilon}$  can be expressed in terms of the strain  $\epsilon$  and the stress  $\sigma$ . Additionally, the model considers thermal expansion, where  $\alpha$  is the coefficient of thermal expansion and  $\dot{T}$  is the temperature rate. The

contributions of the coefficient of thermal expansion is ignored in the following expression for the sake of simplicity. The material parameters,  $E$ ,  $\mu$ , and,  $\lambda$  represent the elastic, viscous responses of the system and the retardation time respectively. These parameters are related to the rheological model in Figure 5.1 by equations 5.2, 5.3 and 5.4, where  $E_1$ ,  $E_2$  and  $\eta$  are the temperature dependant rheological parameters.

$$\dot{\varepsilon} = \frac{\dot{\sigma}}{E} + \frac{\sigma}{\mu} - \frac{\varepsilon - \varepsilon_s}{\lambda} + \alpha \dot{T} \quad (5.1)$$

$$E(T) = E_1(T) + E_2(T) \quad (5.2)$$

$$\mu(T) = \frac{\eta(T)E(T)}{E_1(T)} \quad (5.3)$$

$$\lambda(T) = \frac{\mu(T)}{E_2(T)} \quad (5.4)$$

The friction element represented by  $\varepsilon_s$ , portrayed in Figure 5.1, was first suggested by looking at the relationship of experimental data by Tobushi et al. [28]. The authors performed a series of creep tests under different temperatures and noticed that the material always has a temperature dependent irrecoverable strain for a certain temperature [3]. The creep strain,  $\varepsilon_c$ , is defined as the total strain,  $\varepsilon$ , minus the elastic response as observed in equation 5.5. Hence,  $\varepsilon_s$  will only appear if the creep strain surpasses a thershold value  $\varepsilon_L$ . The threshold value,  $\varepsilon_L$ , is defined solely as a temperature dependent material parameter.

$$\varepsilon_c = \varepsilon(t) - \frac{\sigma(t)}{E(T)} \quad (5.5)$$

Given the loading conditions, three different regimes appear depending on the model conditions and the strain history at a time ( $\tau$ ). Regime I and II occur when the creep strain rate  $\dot{\varepsilon}_c > 0$  and regime III will occur when  $\dot{\varepsilon}_c < 0$ . Regime I appears when  $\varepsilon_c(\tau) < \varepsilon_L(T)$  while regime II appears when this condition is not met. If the process is isothermal, for the programming stage, the material will be subjected to regimes I and II since the material is being loaded. Recovery will therefore occur when the material is being unloaded, hence in regime III. The three regimes are ruled by the behaviour of  $\varepsilon_c$  at different conditions. The expressions for  $\varepsilon_s$  are shown in equation 5.6. Tobushi *et al.* [28] proposed a temperature dependant parameter  $C(T)$ , which is introduced to capture the ratio of the excess creep strain ( $\varepsilon_c - \varepsilon_L$ ) that is irrecoverable, hence this parameter is limited to  $0 \leq C(T) \leq 1$ .

$$\varepsilon_s(t, T) = \begin{cases} 0 & \varepsilon_c(t_1) < \varepsilon_L(T) \\ C(T)(\varepsilon_c(t) - \varepsilon_L(T)) & \varepsilon_c(t_1) \geq \varepsilon_L(T), \dot{\varepsilon}_c(t_1) > 0 \\ \varepsilon_s(\tau, T) & \dot{\varepsilon}_c(t_1) \leq 0 \end{cases} \quad (5.6)$$

Using equations 5.1-5.6, equation 5.7 is generated along with the definition of the effective parameters found in equations 5.8-5.10. Hence these effective parameters  $\mu_{EFF}$ ,  $\lambda_{EFF}$  and  $\varepsilon_{sEFF}$  can be rewritten according to the three different regimes.

$$\dot{\varepsilon}(\tau < t) = \frac{\dot{\sigma}(t)}{E(T)} + \frac{\sigma(t)}{\mu_{EFF}(T)} - \frac{\varepsilon(t)}{\lambda_{EFF}(T)} + \frac{\varepsilon_{s,EFF}(t, T)}{\lambda_{EFF}(T)} \quad (5.7)$$

$$\mu_{EFF}(t > \tau) = \begin{cases} \mu(T) & \varepsilon_c(\tau) < \varepsilon_L(T), \dot{\varepsilon}_c(\tau) > 0 \\ \left[ \frac{\mu(T)}{1 - \frac{\mu(T)C(T)}{E(T)\lambda(T)}} \right] & \varepsilon_c(\tau) \geq \varepsilon_L(T), \dot{\varepsilon}_c(\tau) > 0 \\ \mu(T) & \dot{\varepsilon}_c(\tau) \leq 0 \end{cases} \quad (5.8)$$

$$\lambda_{EFF}(t > \tau) = \begin{cases} \lambda(T) & \varepsilon_c(\tau) < \varepsilon_L(T), \dot{\varepsilon}_c(\tau) > 0 \\ \frac{\lambda(T)}{1 - C(T)} & \varepsilon_c(\tau) \geq \varepsilon_L(T), \dot{\varepsilon}_c(\tau) > 0 \\ \lambda(T) & \dot{\varepsilon}_c(\tau) \leq 0 \end{cases} \quad (5.9)$$

$$\varepsilon_{sEFF}(t > \tau) = \begin{cases} 0 & \varepsilon_c(\tau) < \varepsilon_L(T), \dot{\varepsilon}_c(\tau) > 0 \\ -\frac{C(T)\varepsilon_L(T)}{1 - C(T)} & \varepsilon_c(\tau) \geq \varepsilon_L(T), \dot{\varepsilon}_c(\tau) > 0 \\ C[\varepsilon_c(\tau) - \varepsilon_L(T)] & \dot{\varepsilon}_c(\tau) \leq 0 \end{cases} \quad (5.10)$$

It is necessary to relate these regimes to programming and recovery cycle of the SMP. At the beginning of the programming cycle ( $t = 0$ ), the temperature of the sample is at a low temperature below  $T_L$ , which is at least  $T_g - 25^\circ C$ . Programming begins in step i) where, heating of the material usually occurs in a set of predefined conditions to  $T_h > T_g$ . During step ii) programming of the sample is done by loading the sample. If the load has not provoked  $\varepsilon_c(\tau)$  to surpass  $\varepsilon_L(T_h)$  then the material will behave as regime I, else, the behaviour can be described by regime II. In step iii) the sample will be cooled to below  $T_g$ , therefore  $\varepsilon_L(T_h)$  will change to  $\varepsilon_L(T_L)$ , this will change the value of  $\varepsilon_s$  as expressed by equation 5.6. An increasing value of  $\varepsilon_s$  appears in regime II, which is only dependent on temperature and time. Let's make the time at the end of the programming step

to be  $\tau$ . Therefore at the beginning of the recovery stage, the creep strain will be equal to  $\varepsilon_c(\tau)$ . The recovery of the original shape will occur by an increase of temperature from  $T_L$  to  $T_h$ . In this step the recovery will start and since recovery starts in a stress free condition,  $\dot{\varepsilon}_c < 0$  will occur and this will cause regime III to take place.

This section explains only the governing equation of the viscoelastic model and can only be used in a uniaxial loading mode. In the following section a description of the bending formulation will be proposed.

### 5.2.2 Bending Model

In the present work a viscoelastic model (Tobushi's model) has been applied to bending. A formulation for bending has been proposed. The formulation has been implemented to a 3-point bending situation for the purpose of model verification. However, the formulation can be easily extended to other bending conditions. Loading conditions for a 3-point-bending test will be assumed in this section, where the load,  $P$  is applied to the middle of a simply supported beam as seen in Figure (5.2a). The beam is assumed to be thin and hence the deformation is small, therefore the strains along the  $y$  axis of the beam can be defined according to equation 5.11, where  $\kappa$  is the curvature of the beam and  $y$  is the distance from the neutral axis  $N$  to a point in the  $y$  direction. An assumption that the material behaves in the same manner in compression as in tension has been made, and hence its neutral axis,  $N$  will be placed in the middle of the thickness of the beam as shown in Figure 5.2b. Hence, because of the symmetry that the system has, it is sufficient to analyze half the beam.

The length, height and width of the beam are denominated as  $L$ ,  $H$  and  $b$  respectively. The moment,  $M(t, x)$  can be calculated according to equation 5.12, where  $dA = bdy$ . By substituting equation 5.4 onto 5.7, a generalized expression for the moment at every cross section of the beam can be obtained as following.

$$\varepsilon = \kappa y \tag{5.11}$$

$$M(t, x) = \int \sigma(t, x, y)y dA = 2 \int_0^{H/2} \sigma(t, x, y)by dy \tag{5.12}$$

At this point, we can recapitulate the proposed equations. Equation 5.11 is replaced in equation 5.7 to obtain an expression of the stress. The moment can be calculated by integrating the obtained stress by equation 5.12. The reader may notice that the stress will be dependant on  $x, y$ , and  $t$ . The simplest way to solve equation 5.12 is by discretizing these three variables. The stress can

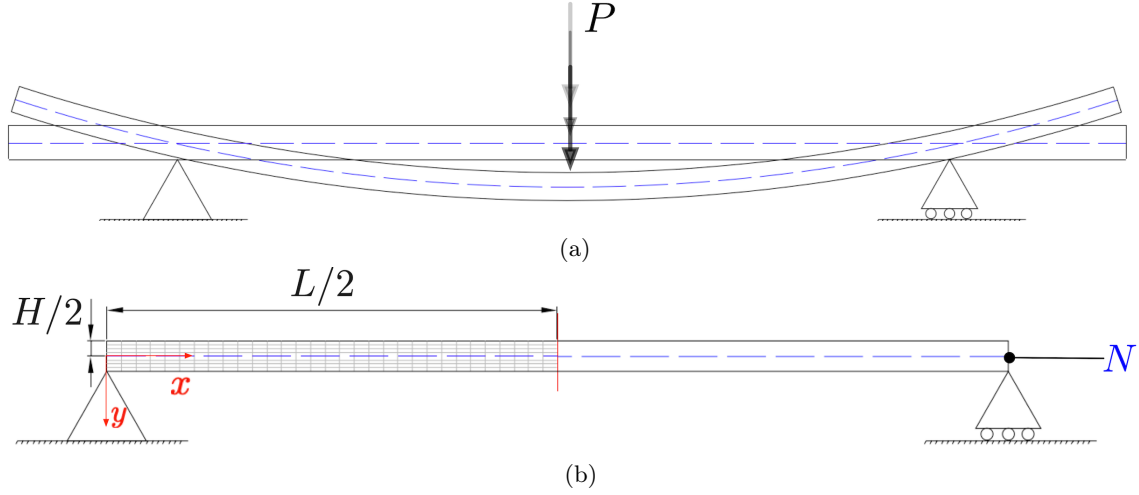


Figure 5.2: (a) Exaggerated schematic of a three point bending test, (b) Discretization of half the beam. The figure shows the neutral axis "N" in blue.

be discretized by using Euler's approximation,  $\dot{\varepsilon} = \frac{\varepsilon_{n+1} - \varepsilon_n}{\Delta t}$  and  $\dot{\sigma} = \frac{\sigma_{n+1} - \sigma_n}{\Delta t}$ . In the equation, time  $t_n$  denotes the present time,  $t_{n+1}$  denotes the time in the future after one step, and  $\Delta t$  is the time step. Hence by discretizing equation 5.7 and solving for the stress, an expression for the stress for  $\sigma(t_{n+1})$  as shown in equation 5.13 can be explained. The bending formulation, numerical integration and discretization has been previously addressed by Ma [20].

$$\begin{aligned} \sigma(x, t_{n+1}, y) = & E(t_n)\varepsilon(x, t_{n+1}, y) + \sigma(t_n, y) \left( 1 - \frac{E(t_n)\Delta t}{\mu_{EFF}(t_n)} \right) + \\ & \varepsilon(x, t_n, y) \left( \frac{E(t_n)\Delta t}{\lambda_{EFF}(t_n)} - E(t_n) \right) - \frac{\varepsilon_{sEFF}(x, t_n, y)\Delta t E(t_n)}{\lambda_{EFF}(t_n)} \end{aligned} \quad (5.13)$$

The moment at  $t_{n+1}$  can be found by using the definition of equation 5.12 as shown in equation 5.14. Substituting equation 5.13 into 5.14, the solution for the moment can be seen in equation 5.15.

$$M(t_{n+1}) = 2 \int_0^{H/2} \sigma(t_{n+1}, x, y) by \, dy \quad (5.14)$$

$$\begin{aligned} M(t_{n+1}) = & 2 \int_0^{H/2} E(T)\kappa(t_{n+1})by^2 \, dy + 2 \int_0^{H/2} \left(1 - \frac{E(T)\Delta t}{\mu_{EFF}}\right)\sigma(t_n, y)by \, dy \\ & + 2 \int_0^{H/2} \left(\frac{E(T)\Delta t}{\lambda_{EFF}} - E(T)\right)\kappa(t_n)by^2 \, dy - 2 \int_0^{H/2} \frac{\varepsilon_{sEFF}E(T)\Delta t}{\lambda_{EFF}}by \, dy \end{aligned} \quad (5.15)$$

Rearranging equation 5.15, an expression of the curvature of the beam as seen in equation 5.16a can be obtained, where  $I$ , is the inertia of the beam and  $M(t_n) = 2 \int_0^{H/2} \sigma(t_n, x, y)bydy$ . The expression has been simplified and the three integrals are named  $\Omega$ ,  $\Psi$ ,  $\Gamma$ .

$$\kappa(t_{n+1}) = \kappa(t_n) + \frac{1}{EI}[M(t_n + 1) - M(t_n)] + \frac{b\Delta t}{I}(\Omega - \Psi - \Gamma) \quad (5.16a)$$

$$\Omega = 2 \int_0^{H/2} \frac{\varepsilon_{sEFF}}{\lambda_{EFF}}y \, dy \quad (5.16b)$$

$$\Psi = 2 \int_0^{H/2} \frac{1}{\lambda_{EFF}}\kappa_n y^2 \, dy \quad (5.16c)$$

$$\Gamma = 2 \int_0^{H/2} \frac{1}{\mu_{EFF}}\sigma_n y \, dy \quad (5.16d)$$

### 5.2.3 Numerical Procedure

The logic of the model works according to the flow chart shown in Figure 5.3, where the material parameters are  $E(T)$ ,  $\mu(T)$ ,  $C(T)$ ,  $\varepsilon_L(T)$ , and  $\lambda(T)$ . In the flow chart the variable  $x$  is discretized from  $x = 0$  to  $x = L/2$  as  $x_0$  at  $t_n = 0, x_1, x_2, \dots, x_q, x_{q+1}$ , similarly variable  $y$  is discretized from  $y = 0$  to  $y = L/2$  as  $y_0$  at  $t_n = 0, y_2, \dots, y_m, y_{m+1}$ . Given the initial conditions and the loading history for a cross section along the beam (at a given  $x$ ), the values  $M(t_n)$ ,  $M(t_{n+1})$ ,  $\kappa(t_n)$ ,  $\kappa(t_{n+1})$ ,  $\varepsilon(t_n, y)$  and  $\sigma(t_n, y)$  can be calculated with equations provided in section 5.2.2. Depending on the initial conditions some of these will come from the initial conditions and some will be calculated.

Given the initial conditions, the model can be provided with either the curvature at  $t_n$ ,  $\kappa(t_n)$ , or the moment  $M(t_n)$ , or analogically the stress,  $\sigma(t_n, y)$ , or strain,  $\varepsilon(t_n, y)$ , at a given point along the  $x$  axis from Figure 5.2b. This logic sequence can be applied to any loading conditions, however to explain the logic sequence, let us follow the programming step when applying a load ( $P$ ) at a

constant loading rate. For a given  $x$  in the beam and at a given time, the material parameters ( $E(T)$ ,  $\mu(T)$ ,  $C(T)$ ,  $\epsilon_L(T)$ ,  $\lambda(T)$ ) are calculated by assuming that the temperature increases in a linear manner and that the temperature everywhere in the beam is the same, i.e. the beam is uniformly heated. This assumption is valid since we have assumed a thin material and due to experimental constraints somewhat low heating rates,  $Q$ . The temperature increases from a given low temperature,  $T_L$ . For the programming stage, the initial condition is a stress free material with a strain of zero. The stress is then calculated at a given position in  $x$ , time and  $y$ . The creep strain  $\epsilon_c$  is calculated. The rate of change of the creep strain,  $\dot{\epsilon}_c$ , is calculated at the given  $x$ , time and  $y$  using Euler's formula. If  $\dot{\epsilon}_c$  is greater than 0, the point in the beam at a given time will be in either regime I or II, else it will be in regime III. The properties are calculated accordingly. For the programming stage, the beam will be in regime I or II, at the beginning it will be at regime I and later with time it will be regime II at a given cross section. Since the moment can be obtained from the applied stress  $M = xP/2$ , the curvature of the beam at each cross section can be calculated, followed by the total deflection at the midspan.

To obtain the deflection of the curvature and be able to obtain the evolution of the deflection with respect to time, one can relate the curvature to the deflection of the beam by equation 5.17.

$$\frac{\partial^2 w(t, x)}{\partial x^2} = -\kappa(t, x) \quad (5.17)$$

The Boundary Conditions (BC) for a 3-point bending test are specified by equation 5.18 and 5.19.

$$w(x = 0) = 0 \quad (5.18)$$

$$\frac{\partial w}{\partial x}(x = L/2) = 0 \quad (5.19)$$

For different stages during the SME cycle, the initial conditions will change. To better explain the model, this section will be divided into the programming stage and the recovery stage. The recovery stage will have two subsections, the free end recovery and a constrained recovery test.

**Shape Setting cycle:** Although this has been briefly explained as an example, shape setting may be done in a variety of ways, in this work a constant loading rate was considered, hence the load,  $P = \text{LoadRate} * t$  at the midspan. Using basic statics the initial moment along the beam can be obtained. However, shape setting is usually performed under a constant temperature, for which the heating rate is  $Q = 0$ , and  $T_L$  will be the desired programming temperature, usually close to  $T_g$ . Since the initial condition is a defined moment, the curvature of the system  $\kappa$  can be calculated,

which can then allow to obtain the strain of the entire beam. To calculate the stress, the regime needs to be determined, since the cycle is under a loading condition,  $\dot{\epsilon}_c > 0$ . The stress can then be calculated according to equation 5.13.

**Free end and Constrained recovery:** After shape setting has occurred, usually two tests are performed to obtain valuable data; namely (a) the constrained recovery and (b) the free end recovery. From the constrained recovery, the shape recovery force (SRF) can be obtained, whereas for the free end recovery, the shape recovery ratio (SRR) and recovery rate can be obtained.

During the constrained recovery (after the programming stage, Figure 5.2a to 5.2b). The position of the two ends and the midspan were kept constant. Therefore, the strain is assumed to be the same and constant as that from the final step in the shape setting step. The curvature will be assumed to be constant throughout the constrained recovery. For the recovery, an increase in temperature is applied at a give rate  $Q$ . For a thin structure, and with relatively low heating rates, the temperature may be approximated in a liner fashion  $T = T_L + Q\Delta t$ . The logic of the step will follow Figure 5.3. After calculating the integrals  $\Omega$ ,  $\Psi$ ,  $\Gamma$ , the expression of the moment is calculated with respect to the curvature. With the applied moment, the recovery force  $P_r$  exerted at the midspan can be calculated as equation 5.20.

$$P_r = \frac{4 \times M(L/2, t, H/2)}{L} \quad (5.20)$$

During free end recovery, the material is in a free state condition. The beam has deformed from Figure 5.2a to 5.2b. Therefore the initial curvature of the beam is defined by the last curvature obtained during the programming step. A temperature increase is applied with a heating rate  $Q$ . The curvature,  $\kappa$ , is then determined at every point in time. Since the beam is free and in an unstressed condition, the moment ( $M(t_n)$  and  $M(t_{n+1})$ ) are zero at all times. Once the curvature is determined, the derivation of the deflection can be calculated by equation 5.17. As reference and ease for the reader, a summary of the initial conditions for each step is portrayed in Table 5.1.

Table 5.1: Steps and initial conditions, where  $\tau$  is the time at the end of the programming stage

History	Initial Conditions
Programmming	$\sigma_0 = 0, \varepsilon_0 = 0, M = Px$
Constrained Recovery	$\sigma_0 = 0, \kappa = \kappa(x, \tau, y) = cte, \varepsilon_0 = \varepsilon(x, \tau, y)$
Free Recovery	$\sigma_0 = 0, \kappa = \kappa(x, \tau, y), \varepsilon_0 = \varepsilon(x, \tau, y), M = 0$

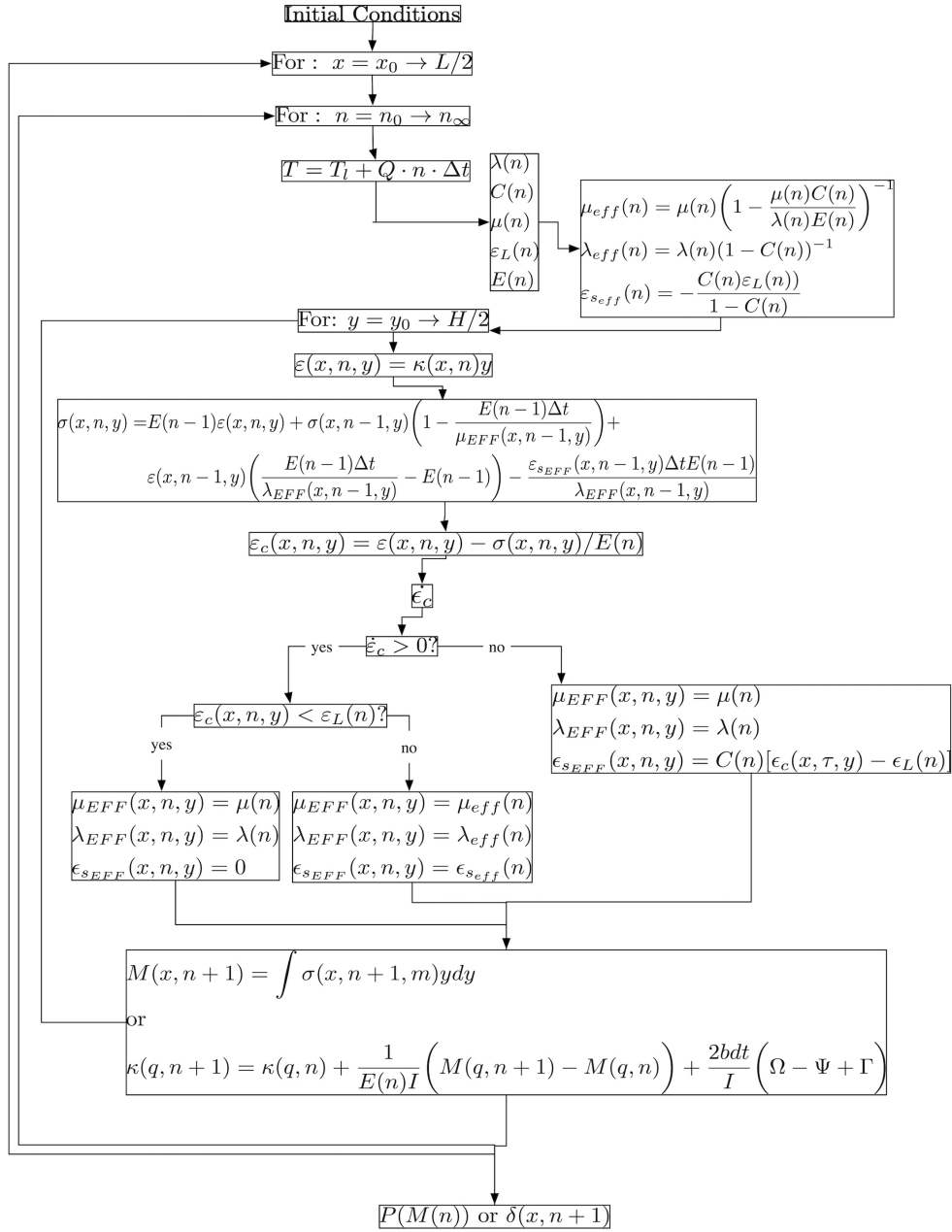


Figure 5.3: Flow Chart that describes the logic of the model

### 5.3 Material Parameters Estimation

One of the most tedious parts of viscoelastic modelling is the determination of the material parameters, for this model is the determination of  $E(T)$ ,  $\lambda(T)$ ,  $\mu(T)$ ,  $\epsilon_L$  and  $C(T)$ , which requires a vast number of testing and extraction from experimental data, specifically from tensile, creep and strain relaxation tests. These materials change with respect to temperature, and testing at different temperatures must be conducted which increases experimentation time significantly. In the past, many have approximated these material parameters with respect to temperature using the William-Landel-Ferry equation, or have segmented different material behaviour into below, in between or over  $T_g$  [28, 8, 18, 3].

By introducing Dynamic Mechanical Analysis (DMA) tests, the number of testing can be reduced since DMA can provide with the static and dynamic behavior of the material. In a DMA test, the storage modulus  $E_s$ , the loss modulus,  $E_l$ , and the phase angle between these two,  $\delta$  are obtained [21] (The conventional notation for the storage modulus  $E'$  and  $E''$  were not used to align this work to Bhattacharyya *et al.*'s [3] terminology). When the material is more elastic, the storage modulus increases as the phase angle decreases. These material properties are a good representation of the ability of the material to store or lose energy.

Bhattacharyya *et al.* [3] in their study for a uniaxial loading showed the analytical solution of an SMP model to obtain the storage modulus  $E_s$  and  $\tan\delta$  by applying a periodic strain. The applied strain was assumed to have an amplitude of  $\epsilon_0^{B1}$  at a frequency  $\omega$ , and an applied constant strain  $\epsilon_0^{A1}$ , in such a way that the total applied strain can be defined as equation 5.21.

$$\epsilon(t) = \epsilon_0^{A1} + \epsilon_0^{B1} \cos(\omega t) \quad (5.21)$$

The proposed strain will yield a stress of the form seen in equation 5.22.

$$\sigma(t) = \sigma_0^{A1} + \sigma_0^{B1} \cos(\omega t + \delta) \quad (5.22)$$

A relationship of the stress and strain can be obtained by substituting equation 5.21 and 5.22 into equation 5.7, to obtain equation 5.23.

$$-\epsilon_o^B \omega \sin(t\omega) = \frac{\dot{\sigma}(t)_o^A - \sigma_o^B \omega \sin(\delta + \omega t)}{E} + \frac{\sigma_o^A(t) + \sigma_o^B \cos(\omega t + \delta)}{\mu} - \frac{\epsilon_o^A + \epsilon_o^B \cos(\omega t)}{\lambda} + \frac{\epsilon_s}{\lambda} \quad (5.23)$$

From here, one can assume that the periodic strain yields the periodic stress. Hence, the nonperiodic

part seen in equation 5.24 can be solved as seen in equation 5.25. The relationship from regime II (equation 5.7) can be substituted to get the solution for  $\sigma_0^{A_1}$  (equation 5.25), where  $t_0$  is the initial time. It is sufficient to express this relationships with the effective material parameters, since these will change according to the regime of loading.

$$0 = \frac{\dot{\sigma}_o^A(t)}{E} + \frac{\sigma_o^A}{\mu_{eff}} - \frac{\epsilon_o^A - \epsilon_{s_{eff}}}{\lambda_{eff}} \quad (5.24)$$

$$\sigma_0^{A_1}(t) = \frac{\mu_{eff}}{\lambda_{eff}}(\epsilon_0^{A_1} - \epsilon_{s_{eff}}) + \left[ \sigma(t_0) - \frac{\mu_{eff}}{\lambda_{eff}}(\epsilon_0^{A_1} - \epsilon_{s_{eff}}) - \sigma_0^{B_1} \cos(\omega t_0 + \delta) \right] e^{-\frac{E}{\mu_{eff}}(t-t_0)} \quad (5.25)$$

The periodic relationship between stress and strain can be solved by using equations 5.23, 5.26 and 5.27. The solution for  $\sigma_0^{B_1}$  can be described and related to the DMA test as shown in equation 5.26. From these equations a solution for the storage modulus and the loss modulus can be obtained as seen in equations 5.28 and 5.29.

$$\sigma_0^{B_1} = \epsilon_0^{B_1} \sqrt{E_s^2 + E_l^2} \quad (5.26)$$

$$\delta = \tan^{-1} \frac{E_l}{E_s} \quad (5.27)$$

$$E_s = \frac{\frac{\omega^2}{E} + \frac{1}{\mu_{eff}\lambda_{eff}}}{\frac{\omega^2}{E^2} + \frac{1}{\mu_{eff}^2}} \quad (5.28)$$

$$E_l = \frac{\omega}{\mu_{eff}} \frac{1 - \frac{\mu_{eff}}{\lambda_{eff}E}}{\frac{\omega^2}{E^2} + \frac{1}{\mu_{eff}^2}} \quad (5.29)$$

The solution can be rewritten by setting  $A = \frac{E}{\lambda_{eff}\mu_{eff}}$  and  $B = \left(\frac{E}{\mu_{eff}}\right)^2$  which result in equations 5.30 and 5.31.

$$\frac{E_s}{E} = \frac{\omega^2 + A}{\omega^2 + B} \quad (5.30)$$

$$\ln\left(\frac{E_s}{E}\right) = \ln\left(\frac{x + A}{x + B}\right) \quad (5.31)$$

Let  $x = \omega^2$  and  $y = \ln(E_s)$

$$y = \ln\left(\frac{x + A}{x + B}\right) + \ln(E) \quad (5.32)$$

$$\text{At } x = 0, \quad y = \ln\left(\frac{A}{B}\right) + \ln(E) = y_0 \quad (5.33)$$

$$\text{At } x = \infty, \quad E = e^{(y_\infty)} \quad (5.34)$$

$$\mu_{eff} = \frac{E}{\sqrt{B}} \quad , \quad \lambda_{eff} = \frac{E}{A\mu_{eff}} \quad (5.35)$$

By looking at the initial conditions, that is when the frequency is 0,  $x = 0$  and hence the initial value for  $\ln(E_s)$  is equal to equation 5.33. In the same manner if we evaluate when  $x$  approaches infinity, we see that the elastic modulus can be obtained from equation 5.34. Hence, the three material parameters  $\lambda_{eff}$ ,  $\mu_{eff}$  and  $E$  can be extracted from  $E_s$ , defined in equation 5.28 by fitting the DMA experimental data to the expression in equation 5.32. The extraction of the material parameters  $\mu$ ,  $\lambda$  and  $C$  will be described in section 5.5.1.

It is worth mentioning that in this thesis, the material properties are assumed to be mainly driven by the changes in temperature. Note that the threshold value,  $\epsilon_L$  cannot be estimated through this method and will be fitted to the final model in bending.

## 5.4 Materials and Methods

A description of the materials and experimental methods are provided in this section. Experimentation was carried out for DMA testing, flexural testing and the programming and recovery methods necessary for model validation.

### 5.4.1 Materials

Shape Memory Polyurethane thermoplastic type (MM7520) was used for all experimental validation. The material was purchased in the form of pellets from DiAPleX, (Tokyo-Japan from [www.smp techno.com](http://www.smp techno.com)). This type of material has a prescribed glass transition temperature ( $T_g$ ) of  $75^\circ C$ . All samples were fabricated via injection molding on a Sumitomo SE-DUZ (Tokyo-Japan). The material was dried for 24 hrs at  $100^\circ C$  in a Lindberg/Blue M (Waltham-USA) prior to injection and according to previous works done [7]. Samples with dimensions of 52 mm x 12.7 mm x 3.2 mm were manufactured by injection molding and then sanded to obtain flat surfaces. The dimensions of the cross section of the samples were in average of  $2.86 \pm 0.07$  (mm)  $\times$   $12.62 \pm 0.04$  (mm).

The injection was performed with a fill peak pressure of 13157(*psi*) at a velocity of 17(*in/s*), with temperature heating zones of 176°C, 232°C, 243°C, and at the nozzle tip 247°C.

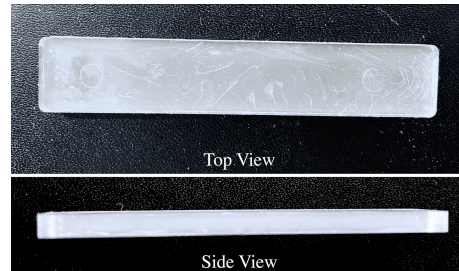


Figure 5.4: Pictures of an injected sample before sanding

#### 5.4.2 Dynamic Mechanical Analysis (DMA)

A series of cyclic frequency sweep DMA tests were conducted at different isothermal temperatures. The range of frequency for the tests was between 0-50 Hz and the isothermal temperatures were taken between the ranges of 55°C and 80°C with intervals of 5°C. The test were conducted at different amplitudes to ensure that the material entered strain regimes as explained in the model. Amplitudes of 15, 150, 200 and 350 $\mu\text{m}$  were used. The DMA set-up and double cantilever mode is shown in Figure 5.5.



Figure 5.5: Picture of a double cantilever mode DMA set-up

### 5.4.3 Flexural Testing and Shape Setting

Flexural (bending) tests were performed using an Electroforce BOSE 3200-TA Instruments (New Castle-USA) testing system, equipped with a heating chamber. The equipment was installed with a 10N load cell. The testing occurred by increasing the temperature of the chamber to  $75^{\circ}\text{C}$ , and then the temperature was equilibrated at said temperature for 5 minutes to obtain isothermal loading conditions. The specimens were then loaded at a constant rate of  $P = 1\text{N}/\text{s}$ , up to a maximum deflection of 5mm at the midspan. After reaching the maximum deflection and with the applied load, the temperature was decreased to  $\sim 30^{\circ}\text{C}$ . Measurements of deflection with respect to time were recorded at a frequency of 10 Hz. A picture of the test is provided in Figure 5.6. In the image, the loading actuator and the span length of 40 mm can be seen. The programming stage was kept constant for the constrained and free recovery tests, yielding approximately 35 sample repetitions.

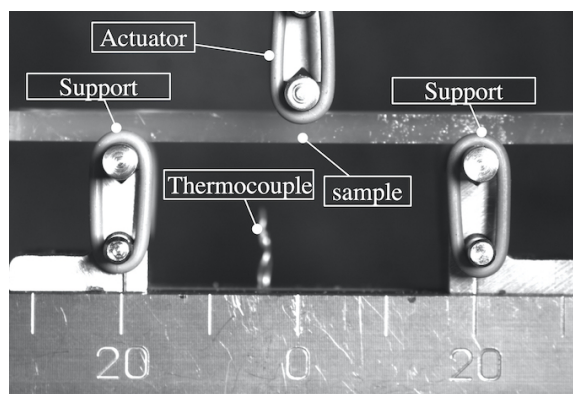


Figure 5.6: Picture of a three point bending test of an SMP sample.

### 5.4.4 Constrained Recovery

After shape setting occurred, the samples were heated using three different heating rates, i.e. 0.2, 0.4,  $0.8^{\circ}\text{C}/\text{s}$  from  $30^{\circ}\text{C}$  to  $90^{\circ}\text{C}$ . Five repetitions of each were performed. The loading actuator was kept fixed during the constrained recovery process, in such a way that the specimen exerted a force while trying to recover onto the loading actuator. The load cell is attached to the loading actuator and it captures the exerted force by the specimen at sampling rate of 10 Hz. The programming and constraining cycle is described in Figure 5.7. In both (a) and (b) of the figure, the lines in orange represent the temperature with respect to time while in blue is the displacement in Figure 5.7a. Notice that there is an increase in displacement at approximately 300(s) where the ma-

terial is strained, the displacement is then held constant throughout the cycle. The force response is shown on the blue left axis of Figure 5.7b. Notice that there is a peak of force at approximately 300(s) where the material is strained and then relaxation occurs. Once the temperature is dropped to approximately  $30^{\circ}C$  at 700(s), it is later raised to the activation temperature, as a response, the sample shows a recovery force at around 900(s).

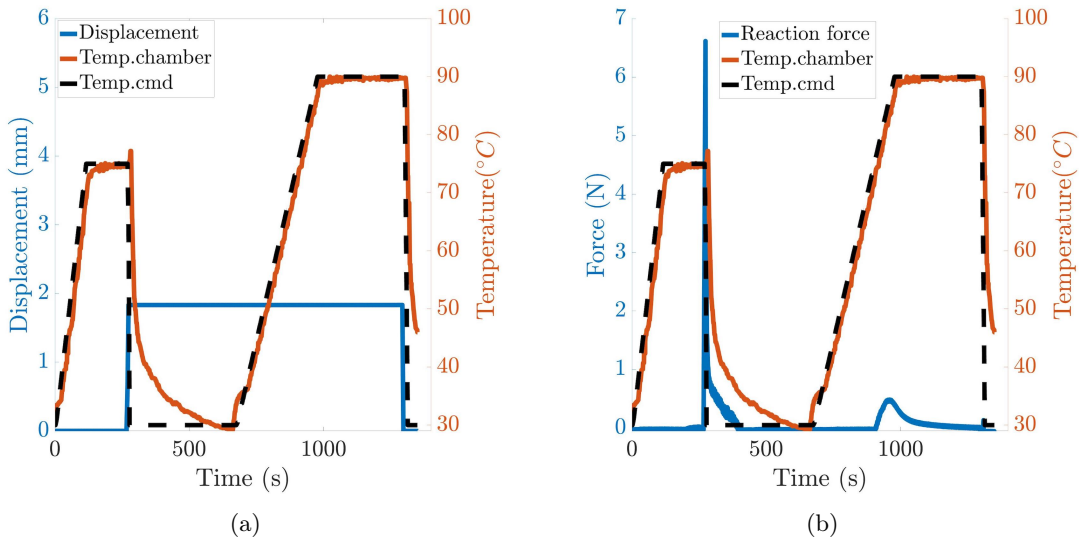


Figure 5.7: Programming and constrained recovery cycle, where (a) is the holding of the displacement and (b) is the response to temperature changes.

### 5.4.5 Free End Recovery

For the recovery process, the specimens were left and placed in the deflected shape in the three point bending test set-up. Recovered deflection with respect to time was measured via particle tracking of speckles impregnated on the sample as can be observed in Figure 5.8. Five repetitions with different heating rates, i.e.  $0.2, 0.4, 0.8^{\circ}C/s$  were applied to the specimens from  $30^{\circ}C$  to  $90^{\circ}C$ .

Each speckle was recognized and tracked via image processing in MATLAB using a modified code for particle tracking [24]. A sample of the initial stage, beginning of recovery and final recovered shape is shown in Figure 5.9a. The movement of each speckle in the  $y$  direction with respect to frame taken as well as any movement tracked in  $x$  and the trajectories with respect to frames were found via this method. A sample of the obtained is shown in Figure 5.9b. For model validation the speckle at the midspan was tracked.

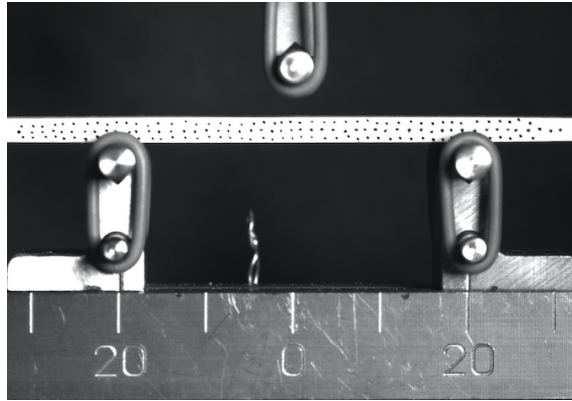


Figure 5.8: Picture of a free end recovery test.

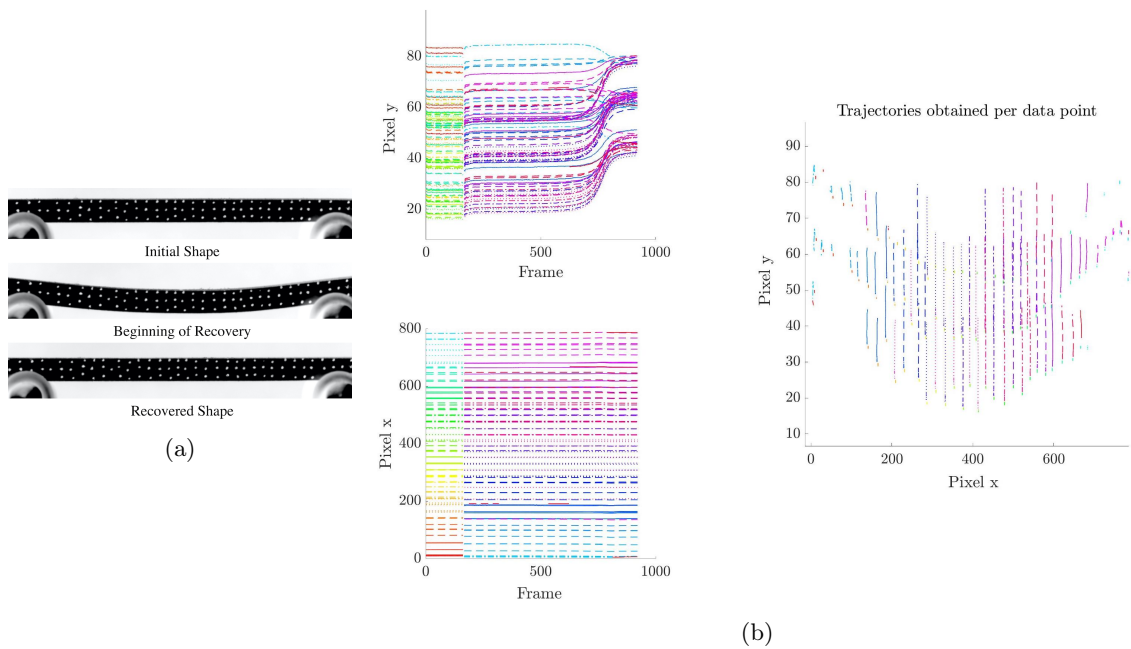


Figure 5.9: (a) photographs of the initial, beginning of recovery and recovered state of a the beam  
 (b) Trajectories detected at every single point in the beam

## 5.5 Experimental Validation Results

Experimental validation of the model is shown in 4 stages. Stage-1 is the obtention of the material parameters extracted from DMA tests. Stage-2 is the prediction of the isothermal programming or shape setting. Stage-3 is the constrained recovery followed in Stage-4 by the free end recovery.

### 5.5.1 Material Parameters Estimation

The DMA frequency sweep results are presented in Figure 5.10. The storage modulus  $E_S$  with respect to frequency  $\omega$  is shown in Figure 5.10a, while  $\text{Tan}(\delta)$  with respect to frequency  $\omega$  is shown in Figure 5.10b. As can be observed in these figures, there exists a consistent decreasing trend of the storage modulus and an increasing trend of the  $\text{Tan}(\delta)$  curves with an increase in temperature as expected per the material's viscoelastic behaviour. The experimental results of the storage modulus  $E_s$ , and the  $\text{tan}(\delta)$  curves are plotted in figure 5.10. The material parameters  $\lambda_{eff}$ ,  $\mu_{eff}$  and  $E$  can be obtained by fitting equation 5.30 to  $E_s$ . The fit was performed at every single temperature.

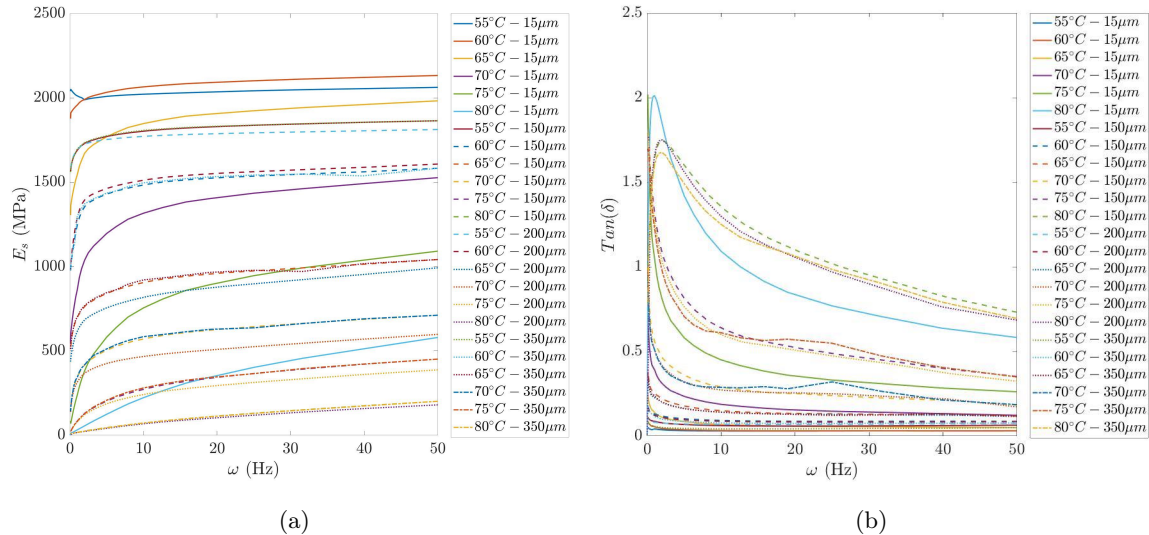


Figure 5.10: Results from DMA using various amplitudes

The DMA experiments were classified into two different regimes and verified by the fit feasibility. Regime I, where there is no creep strain and that at higher strains where creep strain appears. The experimental validation of the first regime was obtained at a small amplitude of 15  $\mu\text{m}$ . The material parameter  $E$  at each temperature is collected from the initial fits, the trend and fit can be

observed in Figure 5.11a. Although there can be multiple methods to solve for  $\mu$  and  $\lambda$ , this method has been constrained to obtain a material parameter  $0 < C < 1$  for the presented model.

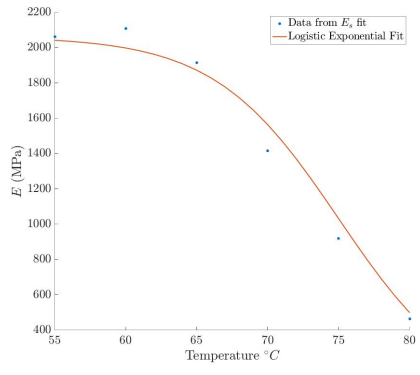
The material parameter  $C(T)$  determines the ratio at which the creep strain will be recovered. The trend proposed for this material parameter follows an exponential decaying trend as shown in Figure 5.11b.  $C$  was estimated using the extraction of  $\lambda_{eff}$  at a small amplitude and assuming those values are within regime I, for which  $\lambda_{eff} = \lambda$ . The trend and values obtained for  $\lambda_{eff}$  and  $\lambda$  can be observed in Figure 5.11c. Notice that the prediction of  $\lambda_{eff}$  deviates from the experimentally obtained values at low temperatures. Following the same logic as that for  $\lambda$ , the material parameter  $\mu$  was extracted and the trends can be observed in Figure 5.11d.

Notice that as the applied amplitude increases the values of  $\lambda$  increase at each point except after  $T_g$ , while for  $\mu$  only the initial values increase with  $T_g$ . Since the proposed model is transient, the expressions that are used to predict the change in material parameters are summarized in Table 1. The author understands that different models have been proposed to capture the glassy phase and the viscoelastic phase of the material, however a simplification of this is proposed that the author believes will capture the change in material behaviour. A concern needs to be noted for the users of this model when material parameters approach very small numbers close to zero, since singularities may be produced when solving the moment equations.

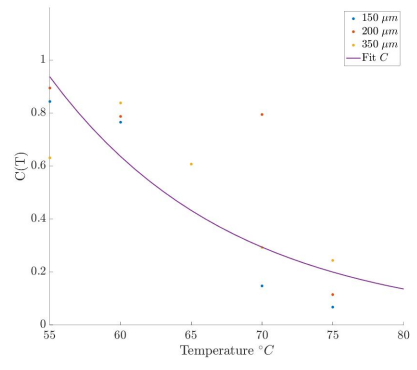
Table 5.2: Material Parameter fits

Material Parameter	Equation fit	Coefficients
$E(T)$	$\frac{E_\infty e^{-ae*T_g} + E_o * e^{-ae*T}}{e^{-ae*T_g} + e^{-ae*T}}$	$ae = 0.2286; E_\infty = 0.0003; E_o = 2063$
$\lambda(T)$	$al e^{-\left(\frac{T-bl}{cl}\right)^2} + dl$	$al = 0.3099; bl = 84.2400; cl = 13.8100; dl = 0.0130$
$\mu(T)$	$au e^{-\left(\frac{T-bu}{cu}\right)^2} + du$	$au = 104.9; bu = 66.04; cu = 8.635; du = 0$
$C(T)$	$ac e^{-bc T}$	$ac = 66.7900; bc = 0.0780$
$\varepsilon_L(T)$	$\frac{\varepsilon l_\infty e^{-ap*T_g} + \varepsilon l_o * e^{-ap*T}}{e^{-ap*T_g} + e^{-ap*T}}$	$ap = 0.4; \varepsilon l_o = 0.0001; \varepsilon l_\infty = 0.0020$

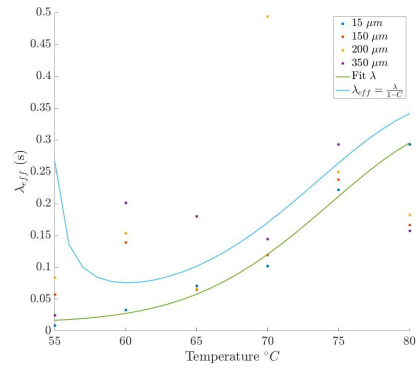
The author would like to point out that  $\varepsilon_L$  is included in Table 1, although it has not been extracted from the DMA and has been chosen to fit the flexural programming results of the model.



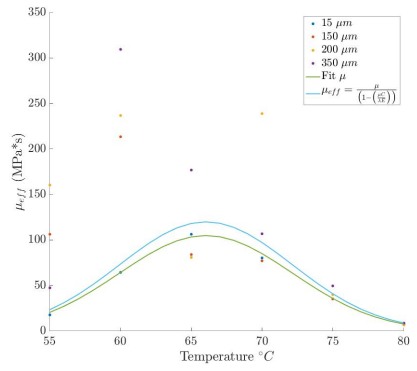
(a)



(b)



(c)



(d)

Figure 5.11: Material Parameters

## 5.5.2 Software Logic Validation and Convergence

An overview of the software validation and convergence is presented here for completeness. The software was tested to match the analytical solution provided by Bhattacharya *et al.*[3] for a strain relaxation test. The code was slightly modified by ignoring the relationship in equation 5.11 and it was subjected to a constant strain and unloading. This allowed to test different regimes throughout the code.

The strain applied in tensile mode for an isothermal strain relaxation test (performed at  $T_g$  for validation purposes) follows equation 5.36. The stress response follows equation 5.37.

$$\varepsilon = \begin{cases} \varepsilon_0, & 0 \leq t \leq t_b, \varepsilon_0 > 0 \\ 0, & t \geq t_b \end{cases} \quad (5.36)$$

$$\sigma = \begin{cases} \varepsilon_0 \frac{\mu_g}{\lambda_g} + \varepsilon_0 \left( E_g - \frac{\mu_g}{\lambda_g} \right) e^{-\frac{E_g t}{\mu_g}} & 0 \leq t \leq t_a, t_a \leq t_b \\ \frac{\mu_{eff}}{\lambda_{eff}} (\varepsilon_0 - \varepsilon_{seff}) + \left( \sigma(t_a) - \frac{\mu_{eff}}{\lambda_{eff}} (\varepsilon_0 - \varepsilon_{seff}) \right) e^{-\frac{E_g (t-t_a)}{\mu_{eff}}} & t_a \leq t \leq t_b \\ -\varepsilon_s(t_b) \frac{\mu_g}{\lambda_g} + (\sigma(t_b) - \varepsilon_0 E_g + \varepsilon_s(t_b) \frac{\mu_g}{\lambda_g}) e^{-\frac{E_g (t-t_b)}{\mu_g}} & t_b \leq t \end{cases} \quad (5.37)$$

To test the solution, the strain is constant up to 5 seconds and then is unloaded as seen in the Figure 5.12. The comparison between the analytical solution from Bhattacharyya *et al.* [3] and the software proposed is also observed in the figure. As can be appreciated, the numerical solution matches closely the analytical solution. In the figure, the stress response in regimes 1, 2 and 3 are shown in sequence, where as the analytical solution is graphed as a piece-wise function from equation 5.37.

Finally, convergence of the code was tested for different time steps for the shape setting stage (which is explained in the next section). The shape setting stage was chosen since it is isothermal and the material properties are therefore constant. The convergence to a maximum displacement at the midspan with respect to the time step can be observed in Figure 5.13. A tradeoff between precision and computational resources was made. A time step of  $\Delta t = 0.001(s)$  was chosen for the comparison of model to experimental results.

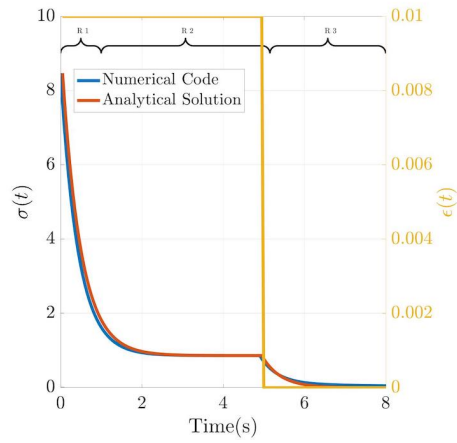


Figure 5.12: Comparisson between analytical solution for a strain relaxation test and the numerical model

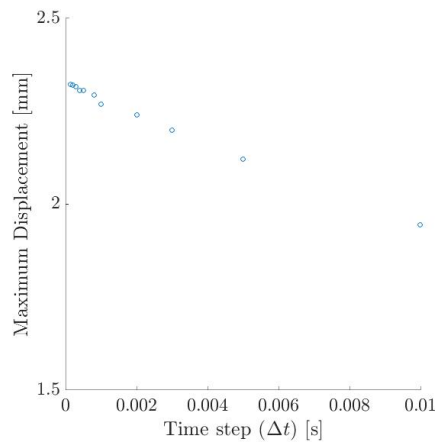


Figure 5.13: Convergence for shape setting

### 5.5.3 Shape Setting

Shape setting or shape programming of the material occurs isothermally. Values for the material parameters are obtained directly from the DMA fit at  $75^{\circ}C$ , i.e.  $E_g = 920.4$  (MPa),  $\mu_g = 39.815$  (MPa·s),  $\lambda_g = 0.2214$ (s) and  $C_g = 0.066$ . For the set of samples, the maximum applied force was 7N which yielded an average displacement of approximately 1.8 mm. A sample of the prediction and a representative experimental data is shown in Figure 5.14a. The ranges for  $R1$  and  $R2$  denote the regimes I and II respectively, under which the model is running.

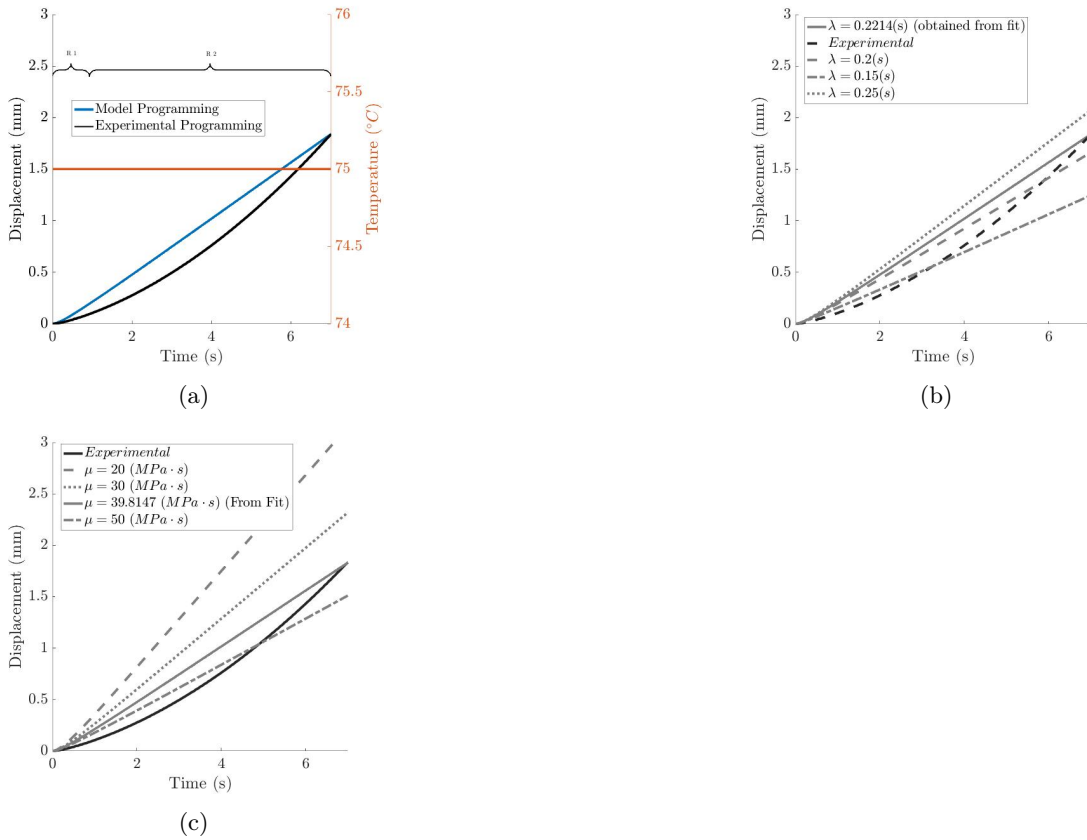


Figure 5.14: Results of the programming stage where (a) are the result of the model prediction and experimental validation of the displacement with respect to time. (b) Effect of changing  $\lambda(T_g)$ . (c) Effect of changing  $\mu(T_g)$

The model showed to capture the behavior of the beam although there exists discrepancies between the maximum obtained deflection with the model and experiments as can be observed in Table 2. The average difference in deflection with the predicted parameters is approximately  $0.190 \pm 0.140$  in which the model consistently overestimates the magnitude of the deflection that occurs during programming.

A summary of the comparison between experimental results and the model can be observed in Table 2. Due to the sample size variability, the maximum experimental deflection has a variation of 0.201 (mm). The discrepancy of the model to the experimental values could be caused by a few possible sources of error. Firstly, there could exist a slight temperature difference between oven and sample, which can cause a slight difference between material parameters of the real experimental temperature values. For instance, if the sample was only two degrees below  $75^\circ C$ ,  $\lambda$  would change

to half its value.

Table 5.3: Summary of the model validation with experiments for the shape setting stage

Maximum Model Deflection (mm)	Maximum Experimental Deflection (mm)	$\ Model - Experiment\ $ Deflection (mm)
$1.8 \pm 0.1$	$1.7 \pm 0.2$	$0.19 \pm 0.1$

The parameters that most influences magnitudes, values and behaviour of the model is  $\lambda(T)$  and  $\mu(T)$ . As reference and as comparisson, it can be shown that by solely adjusting  $\lambda$ , the prediction of the maximum deflection changes drastically as observed in Figure 5.14b. The same effect was observed by  $\mu$  as seen in Figure 5.14c.

The material parameter,  $\varepsilon_L(T)$  was determined from the programming stage. The value of  $\varepsilon_L(T_g)$  was obtained where the discrepancy in prediction was minimized, therefore yielding a value of approximately  $\varepsilon_L = 0.0015$ . An exponential logistic trend was assumend and forced to fit the value at  $75^\circ C$  obtained from the programming stage. The trend of the proposed formula can be observed in Figure 5.15.

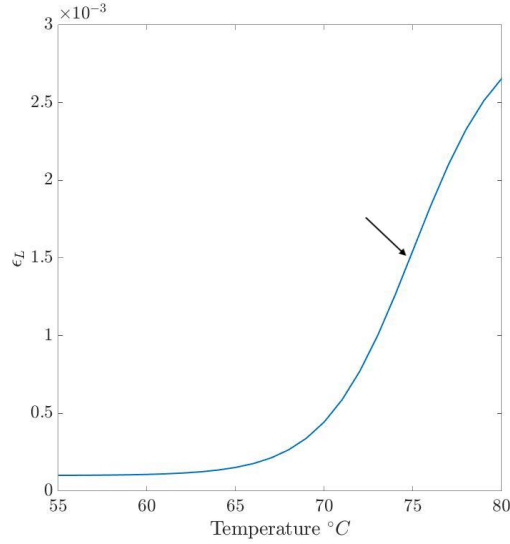


Figure 5.15: fit of  $\varepsilon_L(T)$

### 5.5.4 Constrained Recovery

In this section, the results of the constrained recovery tests and modelling results are described. The recovery force was obtained at three different heating rates after the programming stage. Results of the experimental and modelling runs are shown in Figure 5.16. The experimental results are shown in Figure 5.16a and modelling results in 5.16b. On both graphs the recovery force is plotted on the left axis, while the temperature increase is plotted on the right side of the axis (in orange). The results are shown with respect to time. As observed, there is an incremental time shift in the time it takes the force to appear between experimental runs with different heating rates, as shown in Figure 5.16a. The shape recovery force starts to increase when the oven has reached approximately  $70^{\circ}\text{C}$ . Notice that the time shift is more prominent from  $0.2^{\circ}\text{C}/\text{s}$  to  $0.4^{\circ}\text{C}/\text{s}$  but less so for  $0.4^{\circ}\text{C}/\text{s}$  to  $0.8^{\circ}\text{C}/\text{s}$ . The difference in this time shift decreases with higher heating rates (i.e.  $0.6, 0.8^{\circ}\text{C}/\text{s}$ ) since the material has changed from glassy to viscoelastic whenever the transition temperature is reached (Figure 5.16a). The model was able to capture this behaviour at different heating rates, as seen in Figure 5.16b.

Experimentally, the maximum SRF tends to decrease as the heating rate decreases, as can be observed in Figure 5.16a. The average maximum SRF for  $0.2, 0.4$  and  $0.8^{\circ}\text{C}/\text{s}$  are  $0.579 \pm 0.159$ ,  $0.631 \pm 0.040$ , and  $0.668 \pm 0.011$ , respectively. An explanation for this could be that the time the material is given to relax reduces, provoking a decrease in force. This particular trait could not be captured in the present model, where the maximum predicted SRF is assumed to be the same with changes in heating rate, as observed in Figure 5.16b.

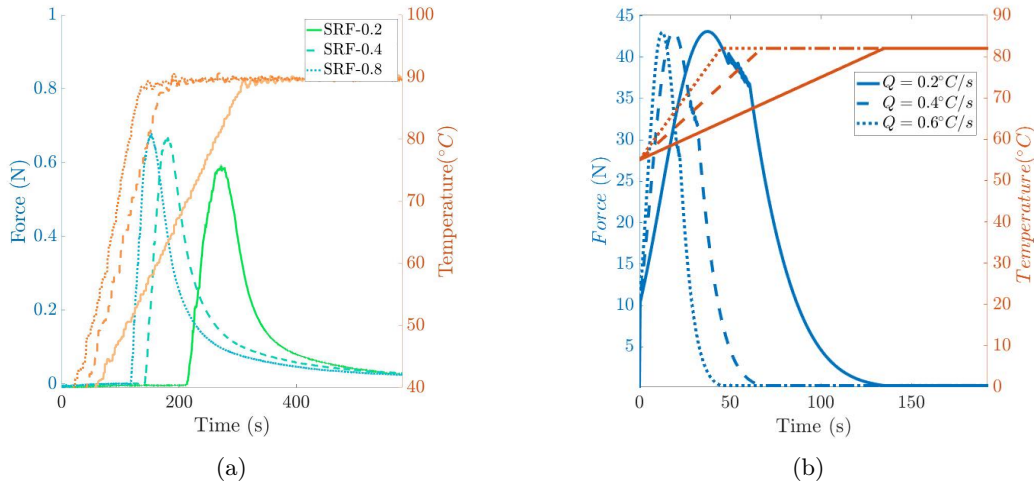


Figure 5.16: (a) Experimental results of sample curves of the shape recovery force at different heating rates and (b) are model runs at different heating rates

From Figure 5.16, the temperatures at which experimental recovery begins are not the same as those assumed by the model. This is caused by the discrepancy between the measured temperature of the oven and the assumption that the material heats instantaneously. There is room for improvement, and the inclusion of the heat transfer on the sample could be implemented according to the experimental setup. However, this model provides with a base that can be used to adapt models to activate the SME from within the structure, using techniques such as joule heating. For the model validation, the experimental curves were shifted to account for the difference in temperature and time of activation.

Since there is not a significant difference in heating rate above  $0.4^{\circ}\text{C}/\text{s}$ , the experimental data of  $0.2$  and  $0.4^{\circ}\text{C}/\text{s}$  was used to clearly show the capability of the model to capture the SRF. The model enters regime III, followed by regime II, and back to regime III as observed in Figure 5.17a. Although the model captures the overall trend and behaviour, the maximum values are quite different from the experimental values when using the material parameters extracted from the DMA. The comparison can be observed for different heating rates in Figure 5.17b, where the discrepancy in magnitude is highlighted in two different axes (at the left, in blue, the modelling result and at the right in black the experimental results). Moreover, the relaxation of the force is not well captured by the proposed model. However, the model estimates an excellent overall trend approximation and a reminder force. The model predicts a faster relaxation than the experimental value, which is a conservative approach.

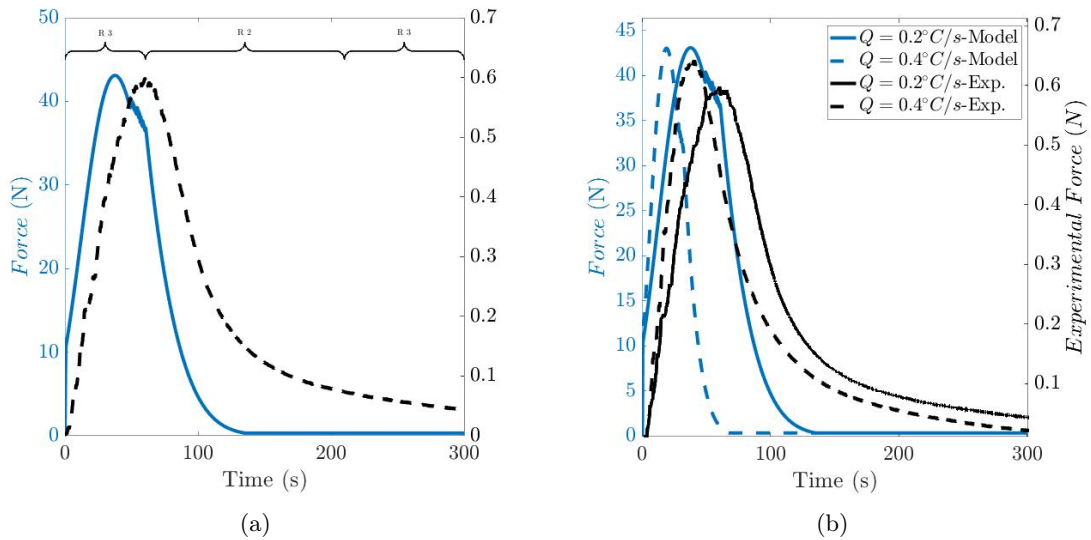


Figure 5.17: (a) Comparison between model and experimental data, the figure shows the regimes in which the model enters (b) Shape Recovery Force results and comparison to experimental data at different heating rates

The discrepancy between model and experimental values was looked at in-depth since it is much more during the constrained recovery than during the programming process. The recovery model is based on the programming stage; the error carrying at the programming stage was a possible source for the discrepancy between the experimental results and model. Runs were performed carrying and not carrying the error from the programming stage, the error was not very significant to cause the mentioned discrepancy. Furthermore, just as in the programming stage, changing the initial value of  $\lambda_0$  or  $dl$ , from the expression  $\lambda(T)$ , was observed to approximate the predicted values to the experimental ones. The major effect of changing  $\lambda_0$  onto the experiments was on the maximum value predicted of the SRF. The effect and a clear decrease in the maximum SRF with an increase in  $\lambda_0$  can be observed in Figure 5.18a. The observed discrepancy in magnitude is significant and there might be a few possibilities for this discrepancy.

There are still questions for the proposed trend of the material parameters. A change of the trend of the material parameters,  $\mu$  and  $\lambda$ , to the William-Landel-Ferry (WLF) equations was also considered as seen in Figure 5.18b. Using the WLF causes a few changes on the trend of the model. Firstly, the change in slope for different heating rates is not properly captured, implying an immediate recovery below the glass transition temperature. For this reason, it is suggested that the DMA fit of the parameters fits the model better although there are still exist a discrepancy in magnitude.

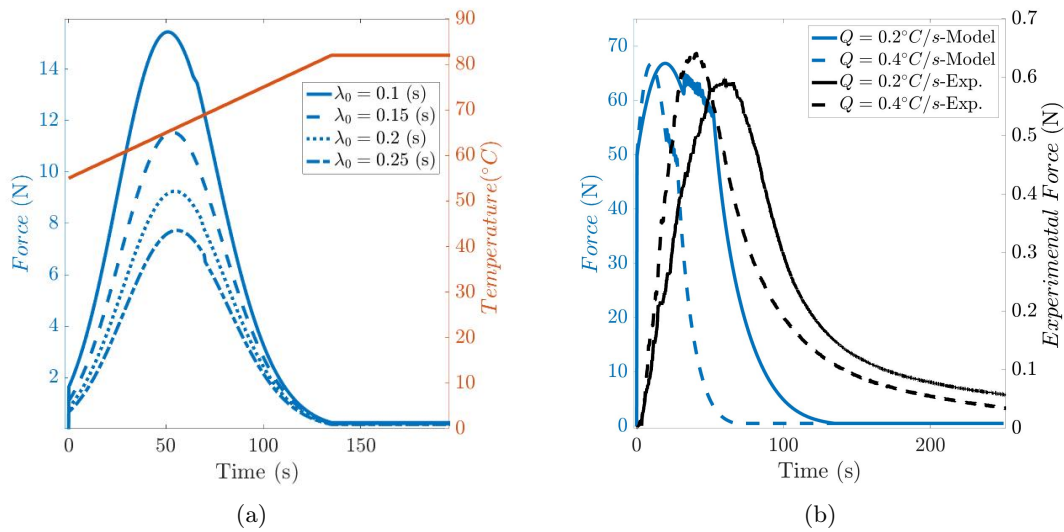


Figure 5.18: (a) Changes in the magnitude quantity by increasing the values of  $\lambda_0$  (c) Effect of material parameters using WLF equations

Other possibilities for the discrepancy may include some physical aspects such as a change in the material microstructure due to cooling, which causes the material parameters to change,  $\lambda$  being

the most affected. The second possibility is the relationship of the initial  $\lambda_0$  with the applied programming strain in the material since, during the recovery, the material begins with an applied strain in contrast to the programming stage. Thirdly, the author is aware that the assumption that the curvature remains constant during the recovery is a strong assumption, which could have influenced the discrepancy between the predicted SRF values and the experimental values. The author believes that this area could be looked at and pursued on future work and explored in detail in a future publication.

### 5.5.5 Free End Recovery

Different heating rates were tested to observe the change in the rate of recovery. The experimental displacement from the beginning of the recovery with respect to time can be observed in Figure 5.19a. Notice that this is the displacement tracked by a single speckle at the midspan of the beam. In the experimental data it can be seen that the displacement is much higher for 0.2, 0.3 and 0.4°C/s than for 0.8°C/s, this could be due to the fast relaxation that the sample undergoes since high temperature is reached in a small period. With respect to the heating rate, there is a big difference in activation time between 0.2°C/s and 0.3°C/s whereas there is little difference between 0.3 and 0.4°C/s. Notice that the slope at which the displacement increases is also very similar between 0.3 and 0.4°C/s, but much more different between 0.2 and 0.4°C/s. To obtain a better visualization, the experimental data from 0.2 and 0.4°C/s was selected to compare to the modelling results. Deflection at the midspan with respect to time from the modelling perspective and with the obtained model parameters can be observed in Figure 5.19b. The difference with heating rate follows the same trend as those observed in the experiments, showing a greater recovery time difference between 0.2°C/s and 0.4°C/s to 0.6°C/s.

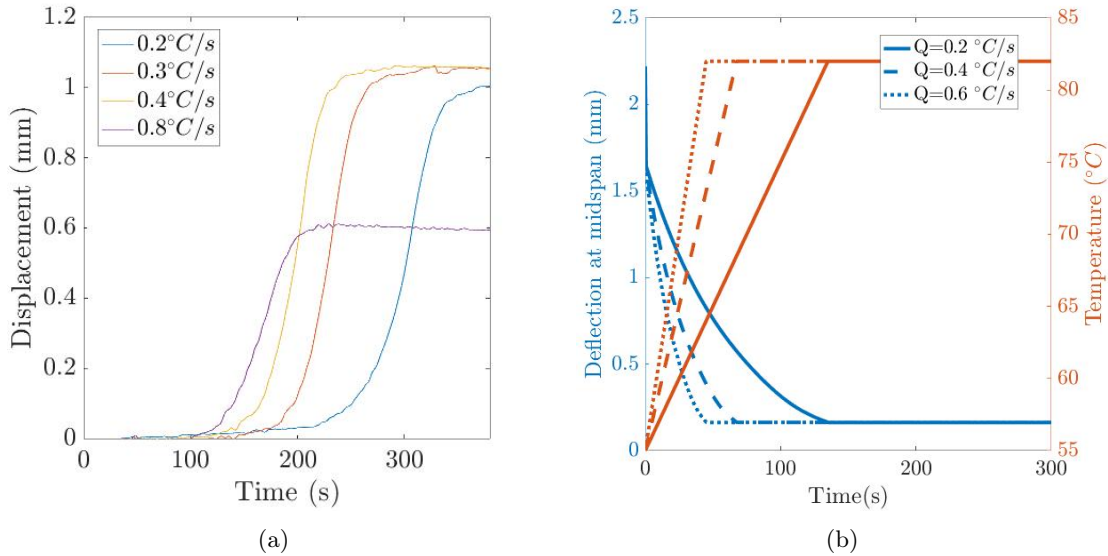


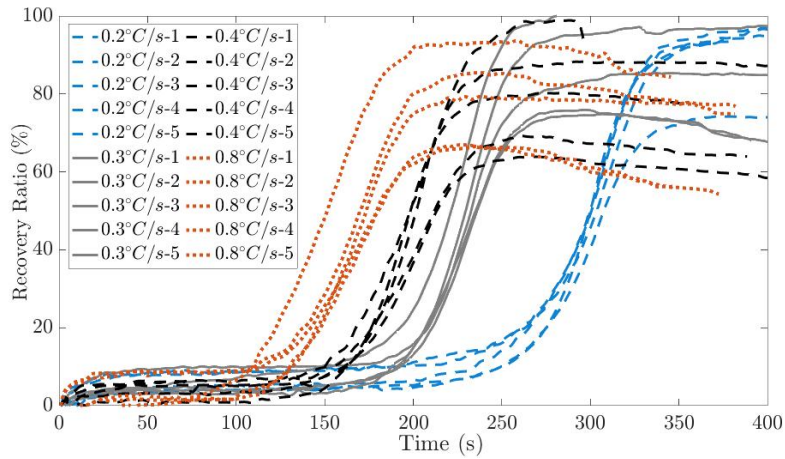
Figure 5.19: (a) Recovery of the deflection with different heating rates (b) Model recovery with different heating rates

The initial state of the sample must be considered and to be able to normalize the data, which is usually done by using the recovery ratio. The recovery ratio is defined in this case as  $R_r$  and the expression for it can be observed in equation 5.38, where  $S_i$  is the initial deflection at the midspan

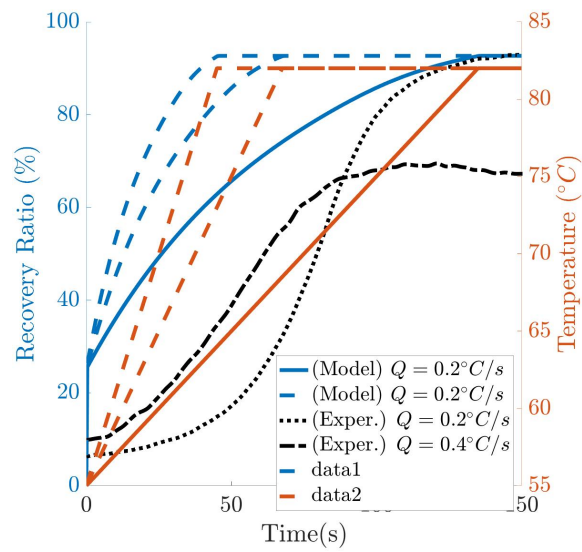
at the beginning of the recovery,  $S_0$  is the initial position at the midspan before the programming stage, and  $S_n(t)$  is the deflection at the midspan with respect to time. Hence, when  $S_n = S_i$  at the beginning of the process, the recovery is 0 and towards the end, assuming complete recovery,  $S_n = S_0$ . Using this definition, the experimental results can be observed in Figure 5.20a for all the heating rates. The author noticed a high deviation between samples, but the recovery rate followed the same trend. Furthermore, irrecoverability was difficult to predict due to the sample deviation. In general terms, the maximum recovery was more consistent and higher when the sample is heated at a rate of  $0.2^\circ C/s$  ( $77\% \pm 35$ ) and decreased as the heating rate increased for  $0.3, 0.4, 0.8^\circ C/s$ , showing average values of  $72 \pm 34\%$ ,  $66 \pm 32\%$ , and  $65 \pm 30\%$ , respectively. A general decrease in recovery with increased heating rate could be due to a faster relaxation of the sample.

$$R_r = \frac{S_i - S_n}{S_i - S_0} \times 100 \quad (5.38)$$

By using the material parameters extracted from the DMA, the recovery is much faster than the one predicted. The difference can be observed in Figure 5.20b. Notice that the model approximates the irrecovery ratio and it is directly dependent on the material property  $\varepsilon_L$ , however the irrecovery ratio changes significantly with heating rate. This relationship between the irrecovery ratio and the heating rate is an area still to look at in further detail. An improvement of the expression for the evolution of the irrecoverable strain is required to capture this trait. Just as with the constrained recovery, the authors have noticed that by solely changing the material parameter  $\lambda_0$ , the approximation of the recovery could be drastically adjusted. The effect of  $\lambda_0$  on the recovery rate can be observed in Figure 5.21a, where  $\lambda_0$  has been varied from 1 to  $35(s)$ . To validate the material properties, a comparison of the recovery with WLF material properties has also been proposed and shown in Figure 5.21b. The difference between WLF and the DMA extracted parameters on the recovery do not vary significantly. However, just as with the SRF, the material with WLF properties showed to be activated right away before the material reached the activation temperature.

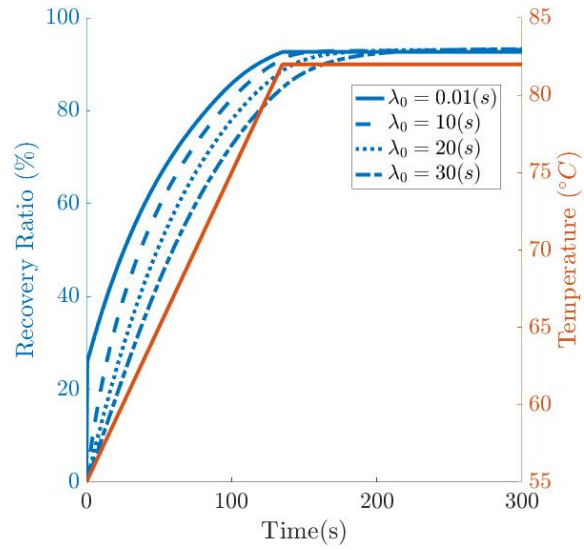


(a)

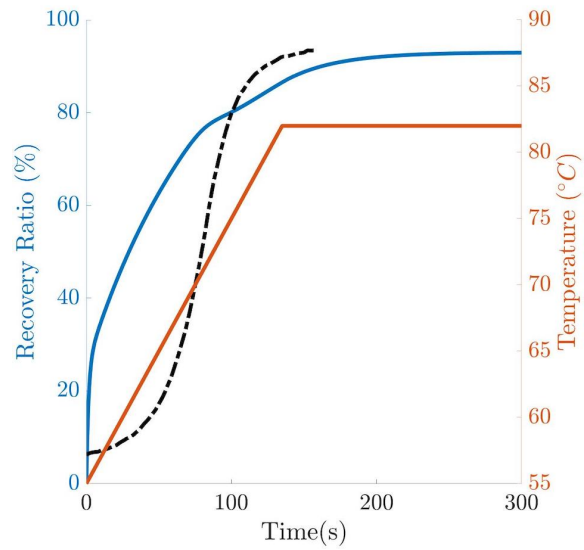


(b)

Figure 5.20: (a) Recovery ratio with different heating rates (b) Model comparison and experimental comparison with different heating rates



(a)



(b)

Figure 5.21: Changes in the recovery ratio with respect to  $\lambda_0$  and (b) Comparison of recovery ratio using WLF

## 5.6 Discussion and Recommendations

The present model seeks to capture the transient recovery behaviour of SMPs under flexural loading applications. This model is based on Tobushi *et al.*'s model and has been modified to account for the change in strain along the  $y$ -axis for a thin beam under small deformations. A linear relationship between strain and curvature was considered for this model. Furthermore, the model was formulated by calculating the bending moment at each cross section of the beam from the stress distribution. The solution can be obtained by discretizing in  $x$ ,  $y$ , and time,  $t$  and by changing the loading conditions at each time step. By applying a temperature function with respect to time, the material properties will change, therefore changing the behaviour of the material in a transient manner. With this methodology the deflection and movement of the material with respect to time can be identified.

A DMA procedure has been proposed to facilitate the extraction of the material parameters, which is tedious and commonly done through a series of time-consuming creep or stress relaxation tests. By using a model from Bhattacharya *et al.* The material properties were extracted. Results for the programming stage and recovery have been shown with the extracted parameters. A trait was observed that by solely changing the initial value of  $\lambda(T)$  but keeping the evolution of  $\lambda$  with respect to time, the results could be further approximated to the results. Simulations with the DMA parameters and WLF functions have been presented, however the DMA extracted properties capture the behaviour of the recovery closer to the solution than by just using a WLF function.

The proposed model although simple in formulation captures the overall behaviour of the programming, shape recovery force and shape recovery ratio. There still exist a few questions left for future improvement of the model and a few causes to investigate on the magnitude discrepancy between model and experimental results. During the programming stage the model assumes the material to be more viscous and overestimates the programmed deflection. On the other hand, during the recovery, the model estimates the material to be much more elastic than the real behaviour shown in the experimental data, hence the recovery force is overestimated.

Although a discrepancy between predicted and experimental values is shown, the model can capture an overall trend of the shape recovery force and shape recovery ratio. Furthermore, a detailed explanation of every step has been provided. In contrast, many other models do not show how the material parameters were extracted nor obtained, and many assumptions about the shape and change of the material properties are made. For the present model, besides the material parameter  $\varepsilon_L$ , we have not assumed the function or form of any material parameters. Fits were used to capture the change in material properties with respect to temperature from the DMA data.

A few of the points that need to be further investigated and causes for model and experimental

discrepancy need to be addressed. The first possible cause of the divergence could be caused by the assumption made during the recovery procedure that the curvature is constant throughout the constrained recovery. This assumption is strong and could produce a discrepancy in the model's values. The second possible cause for divergence is the energy loss due to friction between the specimen and supports, which could delay recovery. This friction was observed as a little bump at the beginning of the recovery ratio curves. This possible loss in energy has not been accounted for in the model during the recovery process. Thirdly, there is a possibility that  $\lambda_0$  could be the most affected parameter by the applied deformation, and hence  $\lambda(t)$  could potentially be a function of strain. This is indicated by the shifting of  $\lambda_0$  from Figure 5.11c with an increase of applied amplitude. This hypothesis has not been proven and further investigation is required to test this theory.

Another consideration to take is the cooling process of the material. Microstructural changes may occur during the cooling process, which can produce the material parameters to have changed during this step. A transformation of the material to a more viscous one could have occurred and caused a drastic increase in retardation time  $\lambda(T)$ . A modelling of the cooling process might be required to fully account for discrepancies in the model.

Furthermore, the material parameters on this model are crucial to obtain a good approximation. We have proposed an extraction of the parameter with DMA but a thorough validation of the DMA extraction will be investigated for an upcoming publication. Lastly, there exists a discrepancy between the  $\lambda_{eff}$  and  $\mu_{eff}$  proposed. The expression for these parameters could be improved to capture the behaviour more accurately. There is the central assumption that  $\mu_{eff} > \mu$ , which is accurate for temperatures below  $T_g$  and not correct for temperatures above  $T_g$ . Further investigation and capture of the material properties are required after a cooling process has occurred.

Future recommendations include testing the model at different applied strains. An in-depth look at the microstructure of the SMPs before and after cooling should be considered to understand if the material parameters have changed. Better expressions to estimate  $\mu_{eff}$  and  $\lambda_{eff}$  are necessary to obtain a better model approximation. Testing DMA at higher amplitudes to be performed as well as more recovery tests with different strain levels can improve the material parameter estimation.

A correction for material heating and delay of activation is a possible next step to take. The addition of material swelling due to thermal expansion's coefficient is to be considered in future investigations as well. Furthermore, this model can be used with technologies that include Joule heating or resistive heating since only a few modifications are needed to account for this technology.

## 5.7 Future Case Study

In recent studies, the authors have focused on the possibility of activating, and controlling 3D printed self-sensing and self-activated SMP structures [6, 5]. The potential for this technology is exciting, which may offer possible 3D printed actuators and sensors. Figure 5.22 shows a potential application for a robotic self-sensing leg for a crawling robot, where its legs are bended to store a temporary bent up shape. GPLA in the figure denotes a heating element that is embedded inside a surrounding SMP matrix. This may offer the possibility to change the dynamics and motion of the robot, while activating the permanent shape during field applications. The authors wanted to provide as first steps a general model without the heating element embedded so that engineers may start exploring design with SMPs. A more specific model to the technology can be developed in the future.

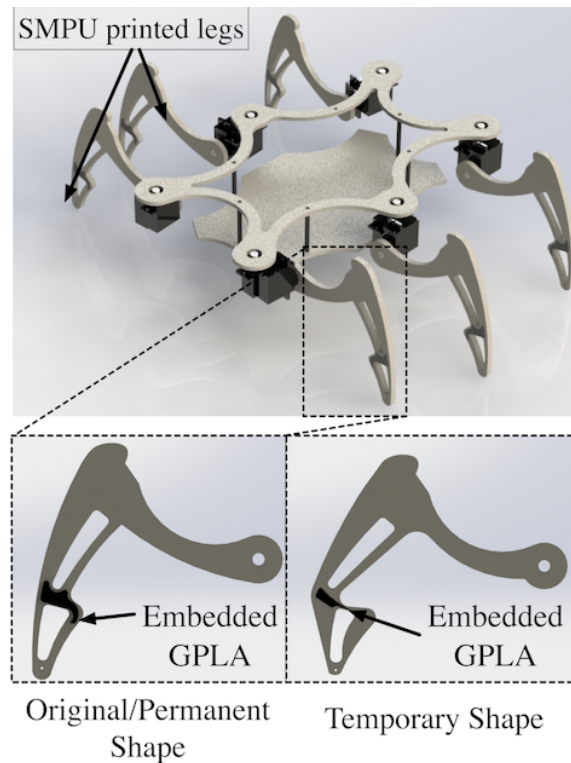


Figure 5.22: Render image of a robotic spider with reconfigurable SMPC legs

## 5.8 Conclusions

A transient model for flexural loadings of thin SMP beams is proposed in this work. Although simple in formulation, the model captures the transient behaviour of SMPs at different heating rates. A logic behind the model has been proposed which is easily adaptable to any coding language. A procedure for acquiring the DMA parameters has been proposed in order to decrease experimentation time. A thorough experimental procedure was carried out to validate and compare the model to experimental results. experimentation of the programming, constrained recovery and free end recovery was done at different heating rates to validate the model predictions. Further investigation is necessary on this model to capture in a more precise manner the relaxation procedure and magnitudes. However, this model provides with a stepping stone for models to be given to engineers for first stage design of devices with shape memory polymers.

## 5.9 References

- [1] M Baghani, R Naghdabadi Journal of Intelligent, and 2012. A constitutive model for shape memory polymers with application to torsion of prismatic bars. *journals.sagepub.com*, 23(2):107–116, February 2012.
- [2] M Baghani, H Mohammadi, and R Naghdabadi. An analytical solution for shape-memory-polymer Euler-Bernoulli beams under bending. *International Journal of Mechanical Sciences*, 84:84–90, January 2014.
- [3] A Bhattacharyya and H Tobushi. Analysis of the isothermal mechanical response of a shape memory polymer rheological model. *Polymer Engineering & Science*, 40(12):2498–2510, December 2000.
- [4] Pinar Boyraz, Gundula Runge, and Annika Raatz. An overview of novel actuators for soft robotics. *Actuators*, 7(3), September 2018.
- [5] I T Garces and C. Ayranci. A view into additive manufactured electro-active reinforced smart composite structures. *Manufacturing Letters*, 16:1–5, April 2018.
- [6] I T Garces and C. Ayranci. Active control of 4D prints: Towards 4D printed reliable actuators and sensors. *Sensors and Actuators, A: Physical*, 301:111717, January 2020.
- [7] Irina T Garces, Samira Aslanzadeh, Yaman Boluk, and C. Ayranci. Effect of Moisture on Shape Memory Polyurethane Polymers for Extrusion-Based Additive Manufacturing. *Materials*, 12(2):244, January 2019.

- [8] Qi Ge, Kai Yu, Yifu Ding, and H Jerry Qi. Prediction of temperature-dependent free recovery behaviors of amorphous shape memory polymers. *Soft Matter*, 8:11098–, 2012.
- [9] P Ghosh, J N Reddy, and A R Srinivasa. Development and implementation of a beam theory model for shape memory polymers. *International Journal of Solids and Structures*, 50(3-4):595–608, February 2013.
- [10] Jahan Zeb Gul, Memoon Sajid, Muhammad Muqet Rehman, Ghayas Uddin Siddiqui, Imran Shah, Kyung-Hwan Kim, Jae-Wook Lee, and Kyung Hyun Choi. 3D printing for soft robotics – a review. *Science and Technology of Advanced Materials*, 19(1):0–0, March 2018.
- [11] Jinlian Hu, Yong Zhu, Huahua Huang, and Jing Lu. Recent advances in shape-memory polymers: Structure, mechanism, functionality, modeling and applications. *Progress in Polymer Science*, 37(12):1720–1763, December 2012.
- [12] W. M. Huang, B. Yang, Y. Zhao, and Z. Ding. Thermo-moisture responsive polyurethane shape-memory polymer and composites: A review. *Journal of Materials Chemistry*, 20(17):3367–3381, June 2010.
- [13] Wei Min Fu Yong Qing Yang Bin Huang. Polyurethane Shape Memory Polymers. pages 1–374, October 2011.
- [14] H U Jinlian. *Shape memory polymers and textiles*. Woodhead Publishing Limited, Hong Kong Polytechnic University, Kowloon, Hong Kong, January 2007.
- [15] Andreas Lendlein, Marc Behl, Bernhard Hiebl, and Christian Wischke. Shape-memory polymers as a technology platform for biomedical applications. *Expert Review of Medical Devices*, 7(3):357–379, May 2010.
- [16] Jinsong Leng and Shanyi Du. *Shape-Memory Polymers and Multifunctional Composites*. CRC Press, May 2010.
- [17] Jinsong Leng, Kai Yu, Jian Sun, and Yanju Liu. Deployable morphing structure based on shape memory polymer. *Aircraft Engineering and Aerospace Technology*, 87(3):218–223, January 2015.
- [18] J R Lin and L W Chen. The mechanical-viscoelastic model and WLF relationship in shape memorized linear ether-type polyurethanes. *Journal of Polymer Research*, 6(1):35–40, January 1999.
- [19] Yiping Liu, Ken Gall, Martin L Dunn, Alan R Greenberg, and Julie Diani. Thermomechanics of shape memory polymers: Uniaxial experiments and constitutive modeling. *International Journal of Plasticity*, 22(2):279–313, February 2006.

- [20] Xiaoang Ma. Bending of a polyurethane based shape memory polymer: modeling and experiment . June 2018.
- [21] Kevin P Menard. *Dynamic Mechanical Analysis. A Practical Introduction*, Second Edition. CRC Press, May 2008.
- [22] Harper Meng and Guoqiang Li. A review of stimuli-responsive shape memory polymer composites. *Polymer (United Kingdom)*, 54(9):2199–2221, April 2013.
- [23] Thao D Nguyen, Christopher M Yakacki, Parth D Brahmabhatt, and Matthew L Chambers. Modeling the relaxation mechanisms of amorphous shape memory polymers. *Advanced materials (Deerfield Beach, Fla.)*, 22(31):3411–3423, August 2010.
- [24] Martin Pastor. Simple particle tracking, matlab central file exchange.
- [25] Debdatta Ratna and J Karger-Kocsis. Recent advances in shape memory polymers and composites: a review. *Journal of Materials Science*, 43(1):254–269, 2008.
- [26] Jonathan Rossiter and Sina Sareh. Kirigami design and fabrication for biomimetic robotics. In Akhlesh Lakhtakia, editor, *SPIE Smart Structures and Materials + Nondestructive Evaluation and Health Monitoring*, pages 90550G–9. SPIE, March 2014.
- [27] V Srivastava. *large-deformation thermo-mechanically coupled elastic-viscoplastic theory for amorphous polymers: modeling of micro-scale forming and the shape memory phenomenon*. PhD thesis, Massachusetts Institute of Technology, 2010.
- [28] H Tobushi, T Hashimoto, S Hayashi, and E Yamada. Thermomechanical constitutive modeling in shape memory polymer of polyurethane series. *Journal of Intelligent Material Systems and Structures*, 8(8):711–718, August 1997.
- [29] Michael T Tolley, Samuel M Felton, Shuhei Miyashita, Lily Xu, ByungHyun Shin, Monica Zhou, Daniela Rus, and Robert J Wood. Self-folding shape memory laminates for automated fabrication. In *IEEE International Conference on Intelligent Robots and Systems*, pages 4931–4936. Harvard University, Cambridge, United States, IEEE, December 2013.
- [30] Takuya Umedachi, Vishesh Vikas, and Barry A Trimmer. Highly deformable 3-D printed soft robot generating inching and crawling locomotions with variable friction legs. *2013 IEEE/RSJ International Conference on Intelligent Robots and Systems*, pages 4590–4595, November 2013.
- [31] Wei Wang, Hugo Rodrigue, Hyung-II Kim, Min-Woo Han, and Sung-Hoon Ahn. Soft composite hinge actuator and application to compliant robotic gripper. *Composites Part B: Engineering*, 98:397–405, August 2016.

- [32] Zhaojing Wang, Pan Li, and Yuxi Jia. Predicting shape memory characteristics of polyurethane in three-point bending deformation. *Polymers for Advanced Technologies*, 25(10):1130–1134, January 2014.
- [33] Shuiliang Wu, Wensen Xu, G Prasath Balamurugan, Michael R Thompson, Kent E Nielsen, and Frank A Brandys. Recovery behaviour of shape memory polyurethane based laminates after thermoforming. *Smart Materials and Structures*, 26(1):115002, November 2017.

## Chapter 6

# A view into additive manufactured thermally actived-reinforced smart composite structures: Manufacturing viability

### **Abstract**

Shape Memory Polymers (SMPs) and their composites (SMPCs) offer great properties, such as low cost and tailorability. Heat-activated SMPs and SMPCs are widely studied under controlled laboratory conditions, but their field applications did not receive thorough attention because manufacturing them with integrated heating elements for this use is very challenging. This work proposes and demonstrates an alternative novel solution to manufacture and activate a SMPC through resistive heating by using extrusion based additive manufacturing. Successful manufacturing of these materials can lead to broader use in strategically critical applications (biomedical stents, sports equipment, and unmanned air vehicles (UAVs)). This chapter focuses on the manufacturing viability and activation of a SMPC via additive manufacturing, while focusing solely on the activation and potential uses of this technology.

## 6.1 Introduction

Shape Memory Materials (SMMs) have been proposed as prime candidates to substitute common mechanical actuators in many engineering applications. In contrast to mechanical actuators, these materials have the potential to reduce weight, cost and energy losses due to friction. SMMs have the ability to store a temporary shape and recover their original permanent shape upon the application of a stimulus such as temperature, uv-light exposure, pH and moisture content [12]. The phenomenon of storing a temporary shape is often referred to as the Shape Memory Effect (SME).

A temperature activated SME can be achieved in two major steps: i) Setting of the temporary shape and ii) activation of the SME. The temporary shape is set by increasing the temperature of the material above its transition temperature, sequentially applying and holding a mechanical strain and decreasing the temperature below the transition temperature. Increasing the temperature above the transition temperature can later activate the SME, i.e. the temporary shape of the material can be recalled.

Some of the most commonly used SMMs are Shape Memory Ceramics (SMCs), Alloys (SMAs) and Polymers (SMPs). Among these, SMPs often have more desirable features such as biocompatibility, recyclability, ease of manufacturing for thermoplastic SMPs, and tailorability in comparison to metallic or ceramic SMMs. Applications of SMPs have focused on strategically important applications such as morphing origami-like structures [5], self-deployable antennae for space applications [17], crawling robots [5], self-actuated hinges [19], wings for gliders and micro aerial vehicles [8, 1, 15] and medical devices such as stents, surgical sutures, among others [16, 13]. Other applications in the fashion industry include jewelry and textiles [9, 21].

Majority of these materials are currently being used in applications that are demonstrated in well-controlled laboratory conditions, e.g. temperature chambers. However, many of the aforementioned SMP applications require activation of the SME in the field, i.e. field activation. Activation of the SME has been attempted by inductive heating [12, 3, 10, 4], embedding microvascular tubes [14, 2] and resistive heating [5, 16, 22, 7, 11, 20]. Inductive heating and the use of microvascular tubes defeat the lightweight advantage of SMPs since additional mechanisms (coils and pumping system respectively) are required to activate the SME. Changing the conductivity of the material and applying a voltage across the material to provoke an increase in temperature can implement resistive heating within the SMP (a.k.a Joule heating). Conductivity of the material can be changed by the addition of conductive filler material such carbon particles and or addition of a metallic conductor to the surface of the SMP. However, the design of these Shape Memory Polymer Composites (SMPCs) requires tedious and impractical manufacturing techniques such as proper particle dispersion in solvents and additional manufacturing steps. Insertion of heating elements within the

material is beneficial for field application and in addition can provide a homogenous heating of the structure.

The present work proposes an alternate manufacturing method of a SMPC that can be activated by means of resistive heating. A desktop Extrusion Based Additive Manufacturing (EBAM), commonly referred to as FDM printers, can be used to manufacture these SMPCs that can be tailored to electrically activate and increase their load bearing capabilities. A thermoplastic SMP and a conductive filler embedded polymer, e.g. a polymer matrix such as Poly-Lactic Acid (PLA) with Graphene Nano-platelet particles, can be fed into a EBAM machine to produce SMPC with simple or complex shapes. This manufacturing concept will significantly broaden the future use of SMPCs and multifunctional composites, and allow this technology to be used in many new applications.

## 6.2 Experimental Methods

A SMPC was manufactured with a SMP matrix and a conductive filler material embedded in a Polylactic Acid (PLA) polymer. Lines of the conductive material, that serve as heating elements, were placed close together within the SMP matrix by using a desktop-type EBAM 3D printer. The printer was equipped with a dual-extruder system (Ultimaker 3<sup>TM</sup>). The two filaments were a SMP and a conductive-particle polymer (Graphene-PLA) filament with 3 mm diameters.

The SMP filaments were produced in house using polyurethane based SMP pellets with a glass transition temperature ( $T_g$ ) prescribed as  $75^\circ C$  (MM7520, SMP Technologies (Japan) [6, 18]. Graphene-PLA was chosen as the conductive-particle polymer because of its lower  $T_g$  compared to the surrounding matrix  $T_g$  at  $65^\circ C$ ). The conductive filament was purchased from Black Magic 3D, Calverton, NY. Although PLA shows a SME in its own, filler loading impedes a complete recovery of its shape, reason why it is only used as an activation mechanism for a known high recovery percent polymer such as SMP-Polyurethane based.

Figure 6.1 shows a representative Gcode implemented to print the SMPC lamina (with dimensions of  $15\text{mm} \times 50\text{mm} \times 1.5\text{mm}$ ). In the figure, the conductive material (heating elements) that is deposited in the longitudinal direction of the specimen, the adjacent SMP matrix regions, and the connecting ends are indicated. A voltage can be applied at the connecting ends to produce a change in temperature. Using the Gcode files, different types of actual samples were printed. Some of these contained a complete layer of Graphene-PLA (Figure.2.a) and some contained lines (Figure 6.2.b and 6.2.c) to reduce the conductive area and increase the contact area between materials. The sample in Figure 6.2.a, with a complete layer of graphene-PLA, was approximately 0.5mm in thickness representing 33.3 *w.t%* of the entire composite. The sample in Figure 6.2.b shows the

upper surface of the deposited Graphene-PLA printed lines (printed half way) and Figure 6.2.c represents 20 *w.t%* of embedded graphene lines in a SMP matrix (SMP on top and between of Graphene-PLA lines).

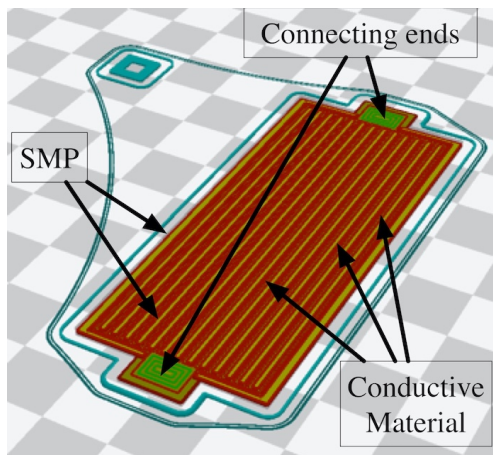


Figure 6.1: Representation of Gcode manufacturing of samples.



Figure 6.2: a) Sample with an entire layer in between representing 30 *wt.*% content of Graphene/PLA b) Sample showing the surface of printed Graphene/PLA layer with 20 *wt.*% embedded Graphene/PLA and c) Sample showing the embedded printed Graphene/PLA layer of 20 *wt.*% inside the SMP.

### 6.3 Results and Discussion

3D printed SMPC lamina, with a straight original/permanent shape, was deformed at  $80^{\circ}C$  (using an Electroforce TA Instruments thermal conditioned tensile tester) to have a bent shape (temporary shape). A total deflection of 5mm was applied at the middle of a 10 mm span of the beam. Later, the SME was activated (recovery of the original shape) by applying a voltage across the sample. Figure 6.3. shows a series of photographs of the activation of the SMPC lamina at different stages in time after applying a voltage of  $\sim 28V$  (14 V in series). The resistance obtained by the sample was  $\sim 400\Omega$  after manufactured. After the application of the voltage, the resulting current was 0.11A. The provided voltage provoked the temperature to reach to  $\sim 100^{\circ}C$  at steady state at the bottom surface of the sample. The figure also shows the activation steps of the sample. The sample took approximately 30mins to completely recover its shape.

The results demonstrate that a thermally active SMPC lamina can be produced in a one-step manufacturing process using EBAM. Possible improvements in resistive heating may be done by changing the percent loading of conductive material within the SMPC, that is by changing the ratio of SMP to conductive polymer. Alternatively, the conductivity of the conductive-filler material can be increased by addition of silver spheres or other nano-particles.

The tailorability and design of the multifunctional materials can dramatically change using this novel technique. For example, the presented manufacturing mechanism can be used to create

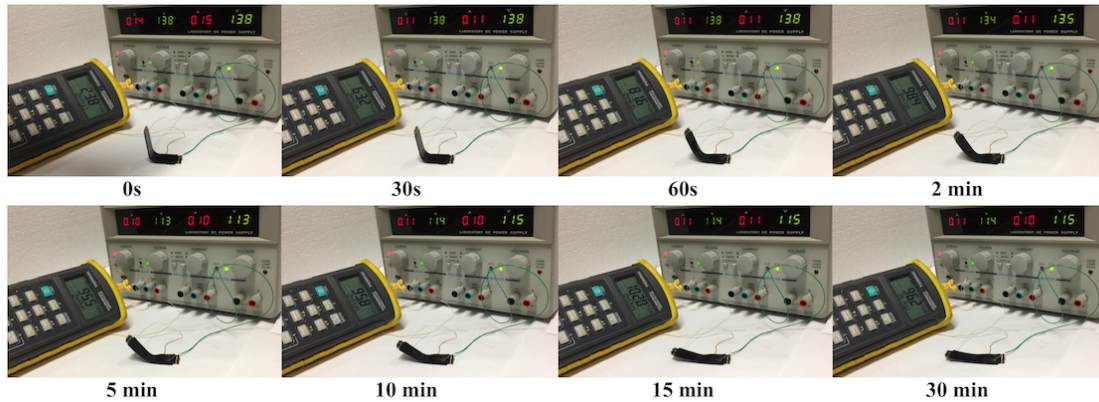


Figure 6.3: Recovering sequence of 3D printed SMPC laminate of size  $15 \times 50$  mm.

multifunctional SMPCs by using filler material that, in addition to providing electrical activation, reinforces the matrix material. Two tailoring mechanisms may be done to find an optimal SMPC structure. The first method is by changing volume fraction of the constituents. The ratio between filler material and the surrounding matrix portrayed by the dimensions (a) and (b) in Figure 6.4a can be changed to alter the volume fraction content in each lamina. The second method to tailor mechanical properties can be done by stacking laminae together at different angles (i.e. printing different laminae on top of each other to form a laminate) to further change and control the mechanical properties. Figure 6.4b shows a representation of a laminate compounded of stacked laminae at different angles. These angles can be changed to improve the material's load bearing capabilities or tailor the properties of the laminate from anisotropic to orthotropic or quasi isotropic.

The presented technology can be scaled up in size, from desktop printers to large-scale printers and larger production quantities. An example of the potentially novel applications is the production of a SMPC Kayak using SMP matrix and conductive and reinforcing fillers in a large scale EBAM machine, as illustrated in Figure 6.5b. As proof of concept a prototype of a 3D printed kayak of SMP has been manufactured and is portrayed in Figure 6.5a. The 3D printed Kayak can be folded and stored away using the SME of the SMPC by connecting it to a power source in site, such as a vehicle's power outlet. There are high end Kayak's available in the market manufactured of military grade polyurethane that can be assembled and disassembled using many parts and fasteners and are currently quite costly. The proposed idea can change the way such sports equipment is designed, manufactured, and utilized.

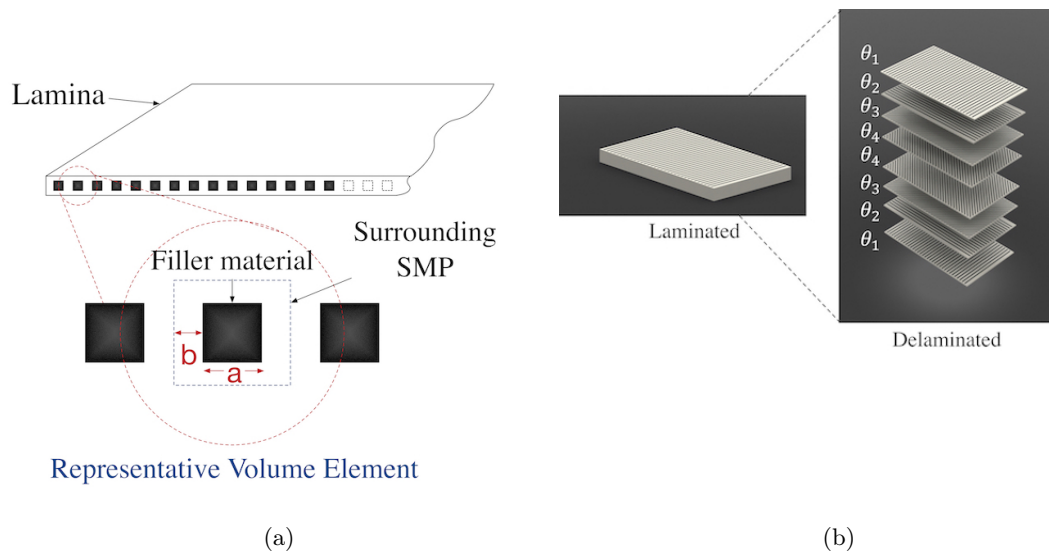


Figure 6.4: a) Lamina showing a detail of the embedded Graphene-PLA lines showing an alteration of volume fraction by changing ratio between distances a and b. b) Laminate showing exploded delaminated view compounded of different angle oriented laminae.

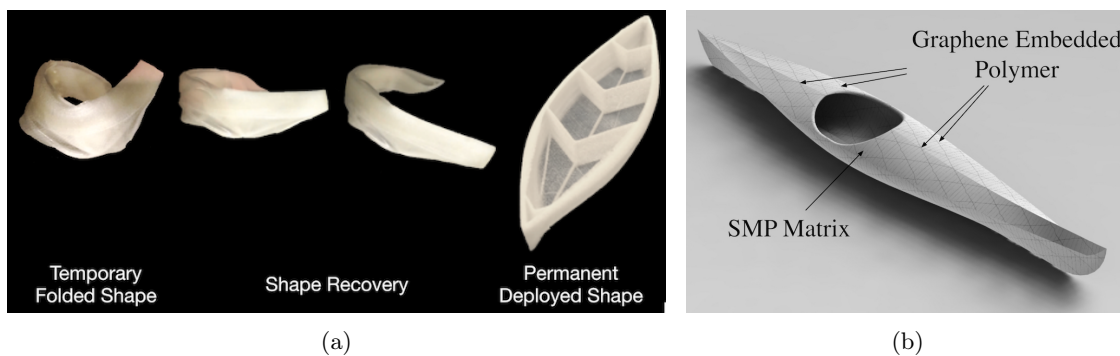


Figure 6.5: a) Printed prototype of a kayak made of SMP deploying, b) concept of a 3D printed Kayak with graphene embedded polymer on a SMP matrix. CAD adapted from [6].

## 6.4 Conclusions and Recommendations

The present study proposes an innovative, low cost methodology of manufacturing SMPCs by using Extrusion Based Additive Manufacturing. Resistive heating can be used to electrically activate SMPCs. A SMPC can be manufactured to improve the mechanical properties of raw SMPs. The proposed manufacturing mechanism obtains a SMPC that can be activated in the field and have high load bearing capabilities.

In this work a SMP-Polyurethane based was the base material used for this study. Additionally, Graphene-PLA polymer was investigated as possible conductive filler material. Both materials were 3D printed next to each other to form a lamina like structure. The mechanical properties of SMPC can be tailored by changing the volume fraction percent content of conductive/reinforce material and by printing laminae stacked together at different angles to form a laminate like structure, much like what is seen in the aviation industry with the use of fiber reinforced composites. The present work will propel SMPs and SMPCs into the consumer industry by contributing with an alternate, low cost manufacturing technique. The method includes an activation procedure of the SME and a reinforcing mechanism of the raw SMP material. The present technology may redefine the way sports equipment like a kayak is transported and utilized. This work is part of a much bigger investigation related to SMPCs and the manufacturing of a conductive shape memory polymer composite smart laminated structures.

This chapter focuses solely on the manufacturing of a thermally active SMPC activated via joule heating, while looking at the activation viability. The following chapter will focus on the sensing and activation capabilities of SMPCs with the manufacturing technique proposed.

## 6.5 References

- [1] Silvestro Barbarino, Onur Bilgen, Rafic M Ajaj, Michael I Friswell, and Daniel J Inman. A review of morphing aircraft. *Journal of Intelligent Material Systems and Structures*, 22(9):823–877, June 2011.
- [2] M Bodaghi, A R Damanpack, and W H Liao. Self-expanding/shrinking structures by 4D printing. *Smart Materials and Structures*, 25(10):105034–16, October 2016.
- [3] P R Buckley, G H McKinley, T S Wilson, W Small, W J Bennett, J P Bearinger, M W McElfresh, and D J Maitland. Inductively Heated Shape Memory Polymer for the Magnetic Actuation of Medical Devices. *IEEE Transactions on Biomedical Engineering*, 53(10):2075–2083, 2006.
- [4] Sergio Conti, Martin Lenz, and Martin Rumpf. Hysteresis in magnetic shape memory composites: Modeling and simulation. *Journal of the Mechanics and Physics of Solids*, 89(C):272–286, April 2016.
- [5] S Felton, M Tolley, E Demaine, D Rus, and R Wood. A method for building self-folding machines. *Science*, 345(6):644–646, August 2014.
- [6] Irina T Garces, Samira Aslanzadeh, Yaman Boluk, and C. Ayranci. Effect of Moisture on Shape Memory Polyurethane Polymers for Extrusion-Based Additive Manufacturing. *Materials*, 12(2):244, January 2019.

- [7] I Sedat Gunes, Guillermo A Jimenez, and Sadhan C Jana. Carbonaceous fillers for shape memory actuation of polyurethane composites by resistive heating. *Carbon*, 47(4):981–997, April 2009.
- [8] Lindsey Hines, Veaceslav Arabagi, and Metin Sitti. Shape Memory Polymer-Based Flexure Stiffness Control in a Miniature Flapping-Wing Robot. *IEEE Transactions on Robotics*, 28(4):987–990.
- [9] Steven K Leist, Dajing Gao, Richard Chiou, and Jack Zhou. Investigating the shape memory properties of 4D printed polylactic acid (PLA) and the concept of 4D printing onto nylon fabrics for the creation of smart textiles. *Virtual and Physical Prototyping*, 12(4):290–300, July 2017.
- [10] Jinsong Leng, Haibao Lu, and Shanyi Du. Multifunctional Shape-Memory Polymers and Actuation Methods. CRC Press, Boca Raton, 2010.
- [11] Fei Liang, Jihua Gou, He Shen, Yunjun Xu, and Bob Mabbott. Carbon fiber reinforced shape memory nanocomposites incorporated with highly conductive carbon nanopaper for electro actuation. In *ASME 2013 Conference on Smart Materials, Adaptive Structures and Intelligent Systems, SMASIS 2013*. University of Central Florida, Orlando, United States, January 2013.
- [12] Harper Meng and Guoqiang Li. A review of stimuli-responsive shape memory polymer composites. *Polymer (United Kingdom)*, 54(9):2199–2221, April 2013.
- [13] L De Nardo, S Bertoldi, M C Tanzi, H J Haugen, and S Far. Shape memory polymer cellular solid design for medical applications. *Smart Materials and Structures*, 20(3):035004–6, February 2011.
- [14] D M Phillips and J W Baur. A microvascular method for thermal activation and deactivation of shape memory polymers. *Journal of Intelligent Material Systems and Structures*, 24(10):1233–1244, 2013.
- [15] S G Rauscher. Testing and analysis of shape-memory polymers for morphing aircraft skin application. 2008.
- [16] Ward Small IV, Pooja Singhal, Thomas S Wilson, and Duncan J Maitland. Biomedical applications of thermally activated shape memory polymers. *Journal of Materials Chemistry*, 20(17):3356–11, 2010.
- [17] M Straubel, J Block, M Sinapius, and C Hüne. Deployable composite booms for various gossamer space structures. *arc.aiaa.org*, 468:107, June 2012.

- [18] Jorge Villacres, David Nobes, and C. Ayranci. Additive Manufacturing of Shape Memory Polymers: Effects of print orientation and infill percentage on mechanical properties. *Rapid Prototyping Journal*, 24(4):744–751, 2018.
- [19] Wei Wang, Hugo Rodrigue, Hyung-Il Kim, Min-Woo Han, and Sung-Hoon Ahn. Soft composite hinge actuator and application to compliant robotic gripper. *Composites Part B: Engineering*, 98:397–405, August 2016.
- [20] Xin Wang, John Sparkman, and Jihua Gou. Electrical actuation and shape memory behavior of polyurethane composites incorporated with printed carbon nanotube layers. *Composites Science and Technology*, 141:8–15, March 2017.
- [21] Matt Zarek, Michael Layani, Shira Eliazar, Nicola Mansour, Ido Cooperstein, Efrat Shukrun, Atara Szlar, Daniel Cohn, and Shlomo Magdassi. 4D printing shape memory polymers for dynamic jewellery and fashionwear. *Virtual and Physical Prototyping*, 11(4):263–270, November 2016.
- [22] L Zhu and R Pitchumani. Analysis of a process for curing composites by the use of embedded resistive heating elements. *Composites Science and Technology*, 60(14):2699–2712, November 2000.

## Chapter 7

# Active control of 4D prints: Towards 4D Printed reliable actuators and sensors

### Abstract

The viability of using Shape Memory Polymers (SMP), and their composites, as sensors and actuators has tremendously increased over the years as a result of the new emerging knowledge and techniques related to multifunctional composite materials science and additive manufacturing. The present study proposes the use of Extrusion Based Additive Manufacturing (EBAM, a.k.a. Fused Filament Fabrication (FFF)) to create a Shape Memory Polymer Composites (SMPC) that is electrically activated. The presented work investigates SMPC's motion trigger by a voltage application via studying a unit cell. This unit cell can be printed consecutively in the thickness or width direction to produce a large repetitive structure and satisfy dimensional requirements. A control unit was designed and manufactured specifically for this SMPC. The developed controller regulates power input to the composite in order to characterize the material's heating behaviour despite variations in resistance caused by changes in strain or temperature during the activation and use of the 4D printed SMPC. Different geometries of unit cells were analyzed to describe heat dissipation within the SMPC. The proposed technology enables exciting possibilities for 4D printed materials. As an example, the aforementioned resistance measurements of the proposed system can be used to correlate change in strain that has occurred in the SMPC during the recovery process, like a structural health monitoring system. The proposed technology has the potential to manufacture any intricate geometry of an actuator or sensor, such as the leg of a crawling robot; in which different leg designs may be

programmed to change the dynamics of the robot. This is just one of the many applications that this material could have, other uses include the development of sports equipment such as a deployable kayak, use on wings for glider micro aerial vehicles, among others.

## 7.1 Introduction

Shape memory materials have the ability to store a temporary shape and recover their original, i.e. permanent, shape with the application of an external stimulus i.e. heat, UV light, pH change, among others [18]. Their ability to recover the permanent shape is usually referred to as a Shape Memory Effect (SME) and it requires a two step process: a programming step and a recovery step [17, 15, 21]. Among this class of smart materials, some of the most commonly utilized ones are Shape Memory Alloys, Ceramics and Polymers. Shape Memory Polymers (SMP), specifically thermally activated SMP have been one of the main subjects of research in the past decade due to their lightweight, ease of forming and manufacturing, low costs associated with manufacturing, high deformations and high shape recovery ratios [13, 34]. Following this, these materials could be applied in various engineering applications, such as deployable structures, morphing aircrafts [22], casts, sutures [34], catheters and other medical devices [2] as well as actuators such as grippers [33], and origami robotics [14].

Thermo-responsive SMP have been extensively studied in recent years [13, 28, 25, 12], but most of the research is conducted in well controlled laboratory conditions, where activation has been done using ovens or controlled heat sources. Consequently, SMP's technological potential has still not been fully exploited due to the difficulty in supplying heat to activate the SME for out-of-laboratory conditions. As such, different heating methods have been proposed, such as joule and induction heating [22, 1]. The latter technique, generally requires surrounding coils to produce heat, whereas joule heating components can be embedded within the material. Therefore resistive heating activation of SMP has been the primary choice due to their potential for a controlled heat during activation.

SMPCs that can be activated via resistive heating can be produced via addition of conductive fillers to an SMP matrix such as carbon black, graphene, carbon nanotubes, conductive fibers, ferromagnetic particles, among others [19]. Commonly achieved conductivity values vary in range, some of the reported values have been  $\sim 2.5 \times 10^{-3} \rightarrow 10^{-1} Scm^{-1}$  [19]. Although successful, filler addition can be expensive and time consuming to manufacture for big quantities, this restricts the amount of material that can be obtained by this technique. Other attempts to manufacture conductive Shape Memory Polymer Composites (SMPC) have been done by embedding conductive materials, among the most successful attempts include activation with carbon fibers [16, 9], and shape memory alloys

[26, 23]. These techniques usually face the difficulty of (i) achieving a good interphase, reason why most of these studies focused on using SMP thermosets, which can wet the interface between materials, and (ii) interruptions in manufacturing processes to include these elements manually during production.

Extrusion Based Additive Manufacturing (EBAM; or a.k.a. fused deposition modeling (FDM) or Fused Filament Fabrication (FFF)) has become increasingly reliable and accessible in recent years due to the vast demand of the market and the corresponding research efforts on the process. As a consequence, thermoplastic filaments and filaments with functional filler materials, such as reinforced and conductive filaments, have become more readily available. Joule-heating these conductive thermoplastic materials is possible as long as the required temperatures do not reach polymer degradation temperatures [31, 3, 11]. Co-printing a conductive thermoplastic with SMP can enable heating which will trigger the SME while producing a sensing material with minimum manufacturing requirements.

Using Shape Memory Polymers (SMP) and composites (SMPC) as sensors and actuators has come within reach thanks to recent advances in knowledge of polymeric material science and manufacturing techniques such as 3D printing EBAM, commonly referred to as 3D printing. 4D printing defined as the 3D printing of smart shape changing materials [15], is a result of intense developments in SMP and EBAM. Our group has contributed in this research over the years [7, 5, 4, 30, 20]. This technology is expected to hit the market in approximately  $\sim 10$  years [15]. As such, efforts to create new and smarter materials have intensified during the past years, specifically those that can be used in out-of-laboratory applications [15]. A 4D printed material that is able activate electrically via Joule heating could be a potential breakthrough for the mentioned technology. Applications of the technology could vary in range from sports equipment, clothing or in soft robotics such as re-configurable legs on crawling robots [5, 8, 10, 27].

To this end, the present study proposes the manufacture of a thermo-responsive thermoplastic SMP, specifically Polyurethane (PU) based SMP (SMPU), via EBAM as studied by [7, 33, 30, 20], but with the inclusion of thin layers of conductive material (Graphene-Polylactic Acid thermoplastic material) to trigger the SME of the SMPU via resistive heating (Joule Heating). Previously, the authors [5, 6] proposed this technology as a proof of concept and showed preliminary results.

In this study, the authors expand their findings on this technology. A unit cell is proposed as the base of EBAM-SMPC. Different geometries of this unit cell were tested to describe and study the internal heat dissipation. These unit cells may be repeated in the thickness and in the width direction to reproduce bigger desired geometries. A control unit was designed and built to regulate power input to the system to compensate for possible resistance changes when an increase in strain and or temperature occurs. As such, by applying a constant power supply to the unit cell, changes in

temperature and resistance can be characterized with respect to time and temperature. If a control unit was not used, heating and resistance behaviour characterization during the recovery process would not be precise and invalid; furthermore it can cause degradation of the polymer by reaching excessive temperatures. Moreover, in the future, resistance readings can be used to determine amount of strain that the SMPC has sustained. The mentioned ability makes this material an active self-sensing multifunctional composite material.

## 7.2 Materials and Methods

### 7.2.1 Materials

SMP matrix, Shape Memory Polyurethane (SMPU) type MM7520, was purchased from DiAPleX, (Tokyo-Japan from [www.smptechno.com](http://www.smptechno.com)). The material has a manufacturer's prescribed glass transition temperature ( $T_g$ ) of  $75^\circ C$ . In house filaments were manufactured with procedure found in [7] and dried for 24 hrs at  $100^\circ C$  prior to 3D printed sample manufacturing.

Conductive filaments, Graphene PLA (GPLA) purchased from Black Magic 3D (Operated by Graphene 3D Labs, Ny-USA), were used in the printing of the heating material. The manufacturer reported an electrical conductivity of  $0.6 \text{ ohm-cm}$  ( $\sim 1.66 \text{ Scm}^{-1}$ ), which allows for resistive-heating to occur at a relatively low power supply.

#### Material Characterization

- **Thermogravimetric Analysis (TGA)**: was performed on GPLA to observe the thermal stability of the material and obtain an estimated particle weight percent content as this information was not provided by the supplier. The TGA tests were performed at a heating rate of  $10^\circ C/min$  to  $600^\circ C$ . TGA of MM7520 was reported in [7].
- **Modulated Differential Scanning Calorimetry (MDSC)**: was performed to determine the  $T_g$  of both materials. Temperature of the tests was stabilized for 10 minutes at  $105^\circ C$ , followed by lowering the temperature to  $10^\circ C$  and keeping it for 10 minutes. The test was then carried at a heating rate of  $2^\circ C/min$  with a modulated temperature of  $1^\circ C$  every 60 seconds to  $230^\circ C$ . MDSC was used due to its improved sensitivity and resolution in comparison to a traditional DSC.

## 7.2.2 Specimen Manufacturing

The proposed composite consists of a surrounding SMPU matrix with embedded GPLA cores, in a way that layers of this composite can be placed on top of each other to obtain bigger and larger structures as seen at the top of Figure 7.1a. The section view of Figure 7.1a shows the embedded GPLA cores with surrounding SMPU matrix. Therefore, the GPLA is being used as a carrier of the conductive material. Because PLA's Tg is lower than 75 deg C (this is verified in section 3.1.2) it will be soft when programming and activation occurs, therefore interfering little with the main driving force of the composite which in this case is the Shape Memory Polyurethane (SMPU). The authors are striving to use SMPU in future larger scale applications since SMPU has demonstrated great mechanical properties and higher ductility as studied by our group [7], [30].

The specimens were designed in a way that a unit cell, that is the smallest repeating unit that is representative of the overall structure, can be studied (modeled with red ink, Figure 7.1b). This unit cell is primarily defined in this study to understand the heat transfer from within the structure. The unit cell has a length of three-widths and it has four-widths at both ends to eliminate end effects. The 3D printed specimens were manufactured as the part dotted with blue ink in Figure 7.1b.

Samples were manufactured using a dual extrusion capable EBAM desktop 3D printer (Ultimaker <sup>TM</sup>3). Both SMPU and GPLA materials were fed to produce the thermally activated SMPC. Figure 7.1c shows a manufactured sample, where the surrounding SMPU matrix has a yellowish transparent color and the conductive GPLA core can be seen in black. Connection tabs were manufactured at the bottom. The software CURA(R) was used to generate the GCode to manufacture with printing parameters set to Table 7.1. Additionally, a printing tower (seen in Figure 7.1d) was used to help clean the nozzle after each printing pass.

Printing Parameters	Material	
	SMPU	GLPA
Nozzle diameter (mm)	0.8	0.8
Layer height (mm)	0.2	0.2
Line width (mm)	0.8	0.8
Line overlap (mm)	0.4	0.4
Speed (mm/s)	15	21
Printing temperature ( $^{\circ}C$ )	223	220
Build plate temperature ( $^{\circ}C$ )	75	75
Stand by temperature ( $^{\circ}C$ )	175	170

Table 7.1: Used Printing Parameters

Different unit cell configurations were manufactured (Configuration 1 and 2) as seen in Figure 7.2b.

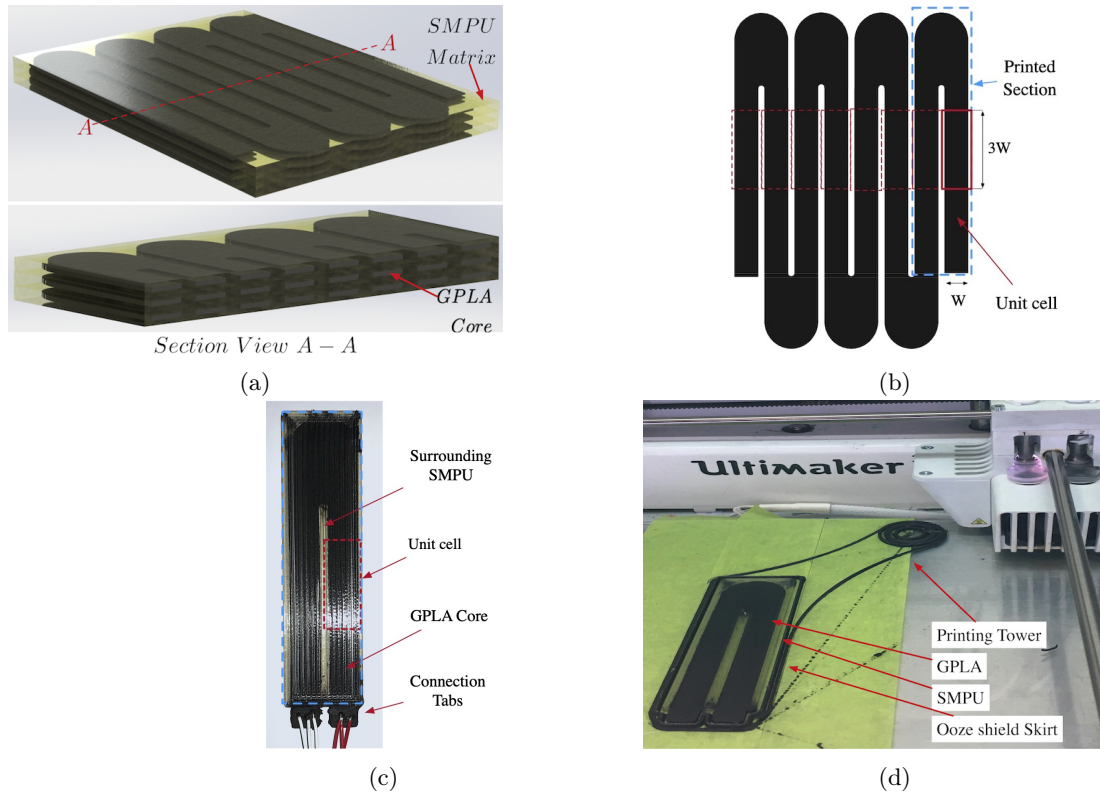


Figure 7.1: (a) 3D illustration of the proposed composite. The illustration shows a section view A-A at the bottom. (b) Schematic of the proposed unit cell to print.(c) Photograph of a manufactured sample (d) Picture of the 3D printing process of a sample[6]

Configuration 1 (C1) samples was used throughout the manuscript to describe heating aspects and shape recovery properties. Configuration 2 (C2) specimens were used as verification for the consistency of the manufacturing procedure, specifically dealing with resistance obtained after printing each sample. The specimens were manufactured with dimensions seen in Figure 7.2a and were set according to Table 7.2. Values  $a$ ,  $b$ , and  $w$  represent the thickness of the conductive material, the thickness of the surrounding SMPU and the width of the conductive material, respectively. Configuration 1 (C1) varies the surrounding thickness of SMPU represented by values (b). Configuration 2 (C2) samples have different width lengths of conductive material but kept the total resistance values. Three types of samples of each configuration were manufactured (T1, T2 and T3). Specimens were designed to have a resistance between the ranges of 65-250  $\Omega$  which is critical for the design of the control unit. All dimensions were determined as functions of the total conductive thickness (a) and surrounding SMPU (b). Notice that four widths were left at the top and bottom to avoid end effects during the thermal characterization (refer to Figure 7.2a).

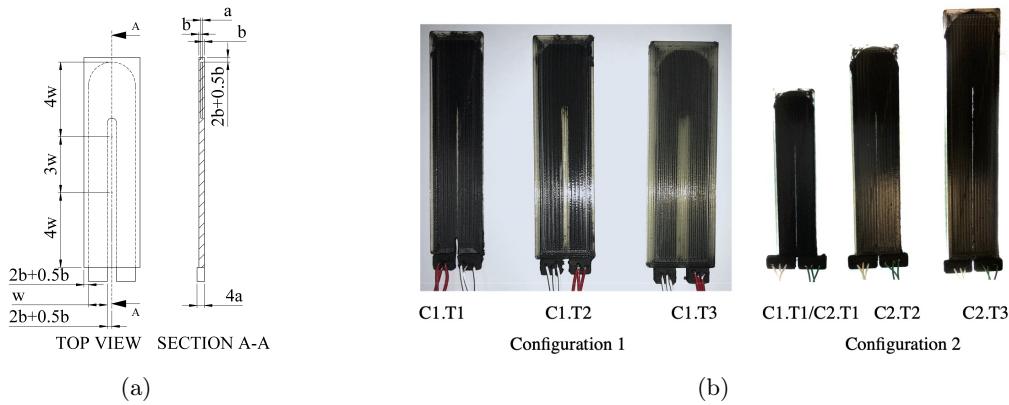


Figure 7.2: Schematics of (a) Sample design with base dimensions and (b) sample configurations

Dimensions (mm)	Sample Configuration and types					
	C1.T1	C1.T2	C1.T3	C2.T1	C2.T2	C2.T3
$a$	0.8	0.8	0.8	0.8	0.8	0.8
$b$	0.4	0.8	1.6	0.8	0.8	0.8
$w$	8	8	8	8	10	12

Table 7.2: Dimensions for different sample configurations. Dimensions are in mm.

### 7.2.3 Equipment

A control unit was designed and built to control the power input to the specimens during activation of the SMP. This was done to characterize the heating capabilities of the specimens. The schematic and photograph of the designed control unit is shown in Figure 7.3a. The supplied voltage is controlled via a Pulse Width Modulated (PWM) signal, which is regulated from a teensy 3.2 microcontroller board control (PJRC, Sheerwood-USA). The signal reaches a Wheatstone Bridge (WB) shown as point (B) in the schematic shown in Figure 7.3a. The bridge allows a high current to flow through the sample to obtain a temperature increase. The signal is amplified at point (C). At point (D), three thermocouples read the temperature of the samples within the unit cell. A picture of the components can be observed in Figure 7.3b.

At all times the control unit regulates voltage to supply a constant power input defined by the user. This power was set to 2 , 4 or 6 Watts in this study to characterize the heating distribution and activation of the SMPC. The flow-chart of the control logic can be seen in Figure 7.3c. The logic starts by making an initial resistance measurement read with 5% duty cycle. The supplied power by the initial reading is calculated and the PWM is regulated to obtain the required power input. The equipment has a resolution of  $\sim 1\%$  of the obtained readings. A thorough calibration

of the equipment was performed, and details can be found in ADC values that are transformed to resistance via the calibration curve as seen in the supplementary information for this chapter found in Appendix B.4.

## 7.2.4 Experimental Set-up and Methodology

### Specimen Resistance

Resistance from the samples was obtained by measuring through the connectors with a high precision Ohmmeter (Fluke 289 True-RMS, Washington-USA) and verified with the built DAQ system at room temperature.

- Configuration 1: Resistance measurements were collected from five samples of each sample types (C1.T1, C1.T2 and C1.T3).
- Configuration 2: These samples were used to check the manufacturing procedure of the conductive material. A change in resistance is prone to occur with an increase in length and thickness of the deposited conductive material. As such, different areas and lengths were manufactured for configuration 2 samples but resistance was kept constant. This allowed to verify the validity of the equation used for conventional conductor that is shown in equation 7.1.

$$R = \rho(A/L) \tag{7.1}$$

where  $\rho$ ,  $R$ ,  $L$  and  $A$  are the resistivity, total resistance of sample, length and cross sectional area of the conductor, respectively. Please note that configuration 2 samples were only used for this purpose throughout the study and to verify this, one sample of each configuration was manufactured.

### Sample Heating

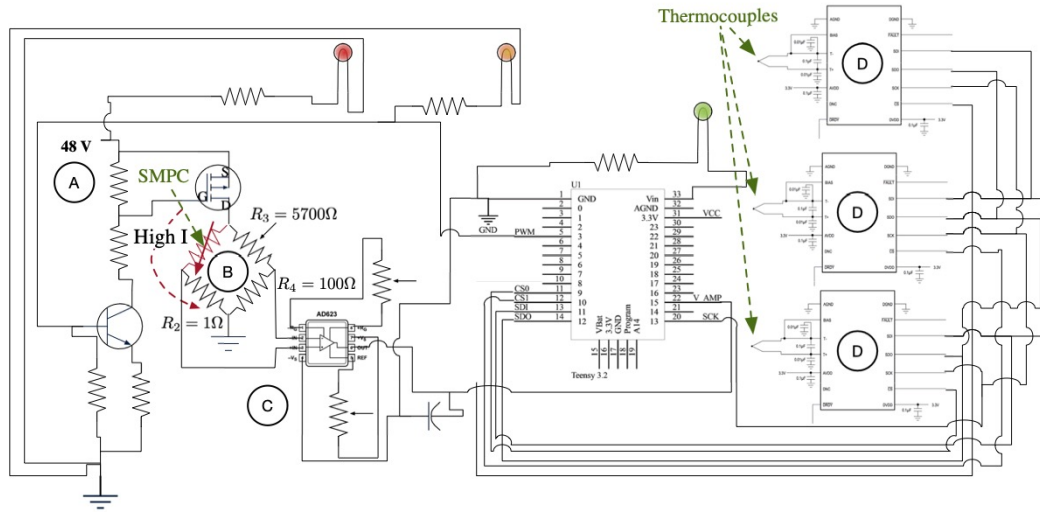
To lead into the description of the SME and the development of this thermally active conductive composite, three different aspects needed to be investigated using Configuration 1 type specimens (C1.T1, C1.T2, C1.T3). Firstly, the behaviour of the heating material with respect to different power inputs, that is, the steady temperature it can reach at a certain power input despite changes in resistance caused by thermal changes. Secondly, the speed at which the heat dissipates for different types of unit cells (thicker surrounding material), which is crucial for the rate and total shape recovery. Thirdly, the behaviour of the heating material after it is undergone several heating cycles since the SME could be used multiple times.

Power inputs 2 and 4 Watts were applied three consecutive times, while 6 watts was applied for 6 consecutive times to observe the state each sample reaches. The experiments were conducted on three samples of each type C1.T1, C1.T2, and C1.T3. Samples were heated and later cooled to room temperature in a cyclic manner for the three different power inputs. Figure 7.4 shows the top view of the experimental set-up used to characterize the heating and temperature distribution. The photograph shows an infrared camera (IR), a room temperature thermocouple reader and a sample connected to the data acquisition system. All data acquisition was set to 10 Hz. Temperatures at points, t1, t2 and t3 were collected by surface thermocouples and were placed according to the photograph shown in Figure 7.4. Laboratory conditions were kept constant by avoiding air disturbances.

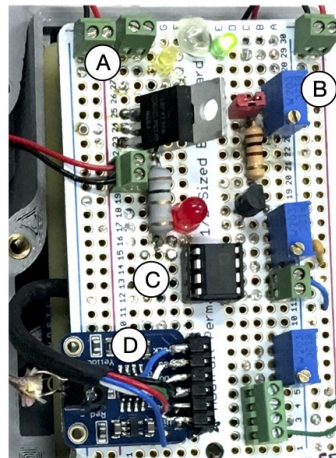
### Shape Memory Effect

Samples of configuration C1.T1 and C1.T2 were programmed in an enclosed chamber to form a repeatable base information. An electroforce BOSE 3200-TA Instruments (New castle-USA) system was used in bending mode to program all samples. The shape programming consists of four different steps as seen in Figure 7.5. The procedure starts by increasing the temperature above  $T_g$  to  $T_g + 20^\circ C \approx 95^\circ C$  for 3 minutes followed by an application of the desired strain (Step 2 in Figure 7.5). In this step, samples were bent to obtain a 90 degree angle with respect to the horizontal. The applied strain of the sample was kept and samples were cooled down to room temperature (step 3 in Figure 7.5). Recovery of the SME occurs by later increasing the temperature above  $T_g$ . Commonly two recovery processes have been used to study the SME, namely the constrained and the free end recovery. Twelve samples in total were programmed to be tested, three of each type C1.T1 and C1.T2 were programmed to test the constrained recovery and three of each type to test the free end recovery.

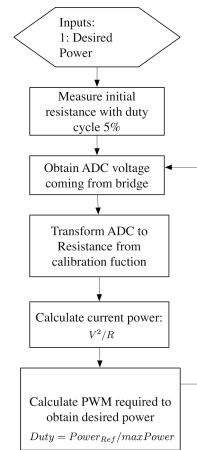
For all recovery processes, 4 watts was applied to each sample to activate the SME. The constrained recovery is defined as the method of activating the SME and record the recovery force by an instrumented actuator that constrains the recovery process. Figure 7.6a shows a sample being tested as its change in resistance and exerted force is being recorded. The free-end recovery is commonly used to determine the amount of strain that the sample has recovered and track the recovery process, specifically the recovery ratio, rate and time. Figure 7.6b shows a 3D printed sample programmed in the temporary shape at 90 degrees. Blue circles were placed in the middle of the sample to track the movement as it recovers. In house software was developed to detect the points of reference and the angle between the blue and orange lines shown in figure 7.6b. All data collection occurred at 30 fps.



(a)



(b)



(c)

Figure 7.3: Schematic modified from [6], where (a) is the design of the in-house built control unit where points A denote power input, SMPC denotes the connected sample at point B (WB), C is the signal amplifier, and D are the thermocouples. (b) Is the picture of the built control unit and (C) is the schematic of the control algorithm

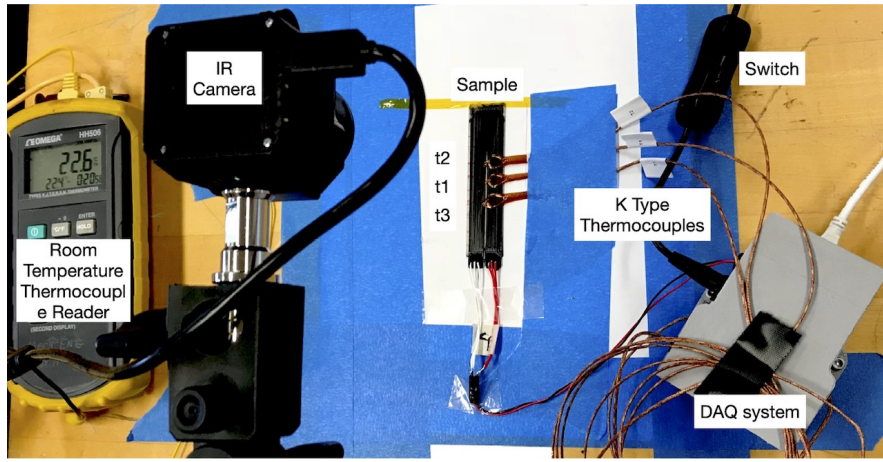


Figure 7.4: Experimental setup for heating characterization

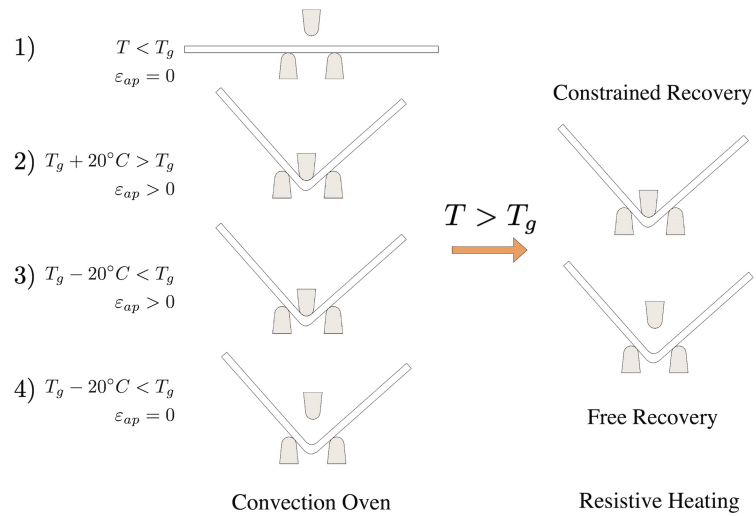
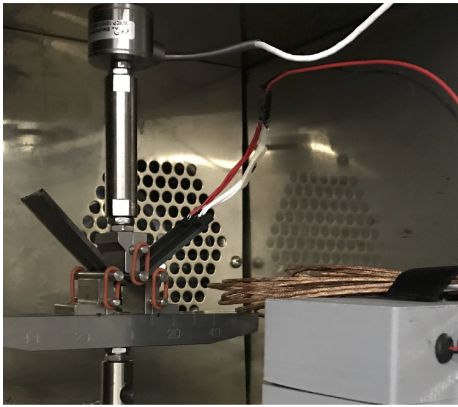
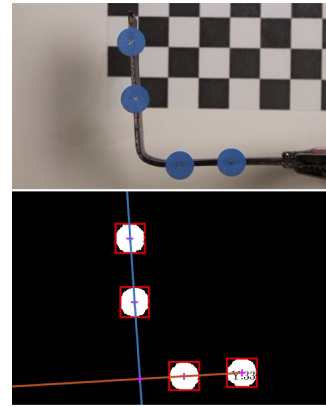


Figure 7.5: The programming process at the left (steps 1-4) and the two types of recovery at the right



(a)



(b)

Figure 7.6: (a) 3D printed SMPC sample programmed in the temporary shape and being activated to record its recovery force (b)3D printed SMPC sample programmed in the temporary shape and being activated, the software recognition of reference points to measure recovery angle and percentage its shown below

## 7.3 Results and Discussion

### 7.3.1 Material Characterization

#### TGA

Figure 7.7 shows the TGA result performed on the Graphene PLA material (GPLA). The figure shows an initial drop in weight due to moisture at  $\sim 100^\circ\text{C}$ , followed by a possible decomposition of carboxylic groups and release of  $\text{CO}_2$  at  $\sim 200^\circ\text{C}$  that leads to a second drop of 7.3% [24]. The matrix material PLA degrades at  $\sim 348^\circ\text{C}$  [32, 29]. However graphene is stable until  $\sim 700^\circ\text{C}$  [24], for which we can infer that the material had a particle weight percent content of about  $\sim 15\%$ . Because the thermal stability of GPLA drops at  $\sim 200^\circ\text{C}$ , it leaves a range between  $\sim 75 - 180^\circ\text{C}$  for the material to heat up. This shows that the proposed material is thermally stable within the necessary range of operation.

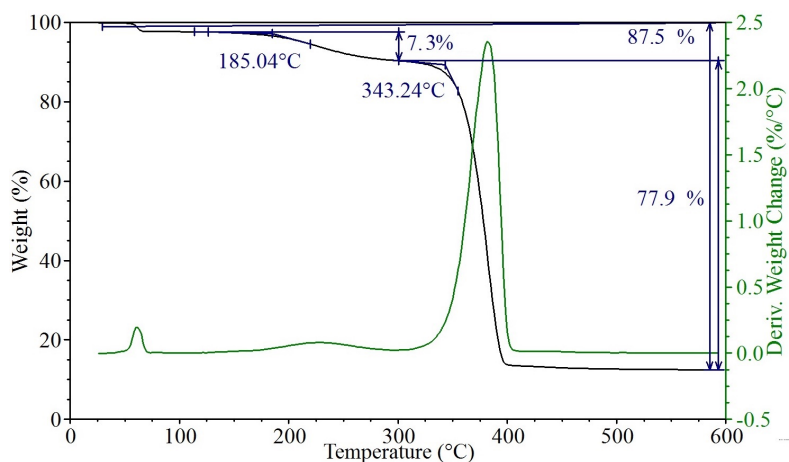


Figure 7.7: TGA of GPLA showing weight percentage drops

#### MDSC

The results of the MDSC are shown in Figure 7.8. SMP MM7520 showed a  $T_g$  of  $\sim 73.3^\circ\text{C}$  and GPLA a  $T_g$  of  $\sim 53.7^\circ\text{C}$ . This indicates that the GPLA will not hold back the motion of the SMPU when the SME has taken place. Melting point for GPLA is also shown to be much higher than the required temperature range, to keep the integrity of the sample, temperature must be kept below  $120^\circ\text{C}$ . GPLA did show crystallinity changes after  $\sim 140^\circ\text{C}$  which is much higher than the activation range and operating ranges of the material.

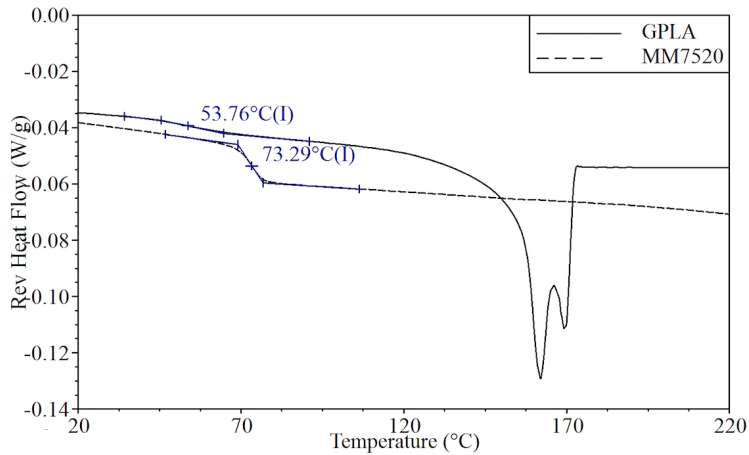


Figure 7.8: MDSC curves of SMP and GPLA for  $T_g$  characterization

### Sample Resistance

Samples' volumetric resistance was calculated and are presented in Figure 7.9. Volumetric resistance was obtained by measuring the total resistance across a thin surface of a material and multiplying it by the thickness of the 3D printed material.

- Configuration 1: A box plot of the samples' measurements are portrayed in Figure 7.9. The top and bottom of the blue boxes indicate the 25th and 75th percentile of the data. The mean values of each distribution is plotted with red crosses. There is no significant difference between measurements of samples type 1, 2 or 3. This finding suggests that printing more surrounding material does not affect the total volumetric resistance of the conductive material.
- Configuration 2: Sample resistances are plotted in Figure 7.9 with circles. All samples had similar values as expected, although they had different length and cross sectional areas. This proves that the manufacturing procedure is consistent and is not affected by changes in area or length.

The manufacturer's reference ( $0.6\Omega\text{-cm}$ ), and the batch filament measurement ( $0.37\Omega\text{-cm}$ ) are also shown on Figure 7.9. The discrepancy between sample measurements (averages of 0.29, 0.28 and  $0.29\Omega\text{-cm}$  for type T1, T2 and T3 respectively) and batch and manufacturer's reported volumetric resistance could possibly be attributed to voids in the 3D printed structure. Nevertheless, the initial measurements were all within the same range, this shows that the process is repeatable and consistent.

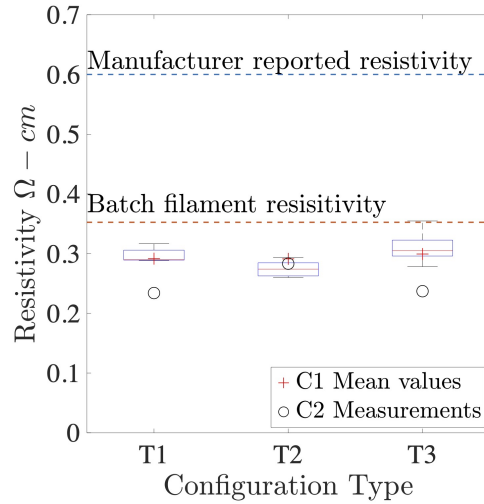


Figure 7.9: Plot of obtained volume resistance values for configuration 1 and 2

### Sample Heating

Following from section 7.2.4, here we focus the discussion on the three main points: 1) the steady state temperature that samples reach with respect to different power inputs. 2) The speed at which temperature dissipates and 3) the cyclic heating behaviour. The legend on each of the following graphs shows the power input followed by the cycle number ( $c$ ). For instance, 2W c3 denominates a heating curve obtained by applying 2 Watts after the third heating cycle.

The first row of Figure 7.10a shows the temperature readings with respect to time in the left axis and resistance readings with respect to time in the right axis. Heating of samples followed a first order system when heating. After the application of 2 Watts, the samples reached a steady temperatures of 55, 55 and 50°C for samples C1.T1, C1.T2 and C1.T3, respectively after three cycles. The steady state temperature decrease from C1.T1 to C1.T3 is attributed to the sample dimensions since there is more surrounding SMPU (or insulating material). When applying 4 Watts to the three types of samples C1.T1 reached  $\approx 95^\circ C$  at the 10 minute mark, while sample C1.T2 reached  $\approx 85^\circ C$  and C1.T3  $\approx 75^\circ C$ . In the same manner when applying 6 Watts, samples C1.T1 reached approximately 110°C. When applying a higher power much care needs to be taken since the temperature reading at the top of the sample (surrounding SMP) does not reflect the temperature reading of the inside GPLA core, which is expected to be much higher. This was the case when applying 6 Watts to the thicker samples (C1.T2 and C1.T3). Experiments were stopped after heating the 7 minute mark due to potential damage of the equipment by high currents due to the material reaching degradation temperatures.

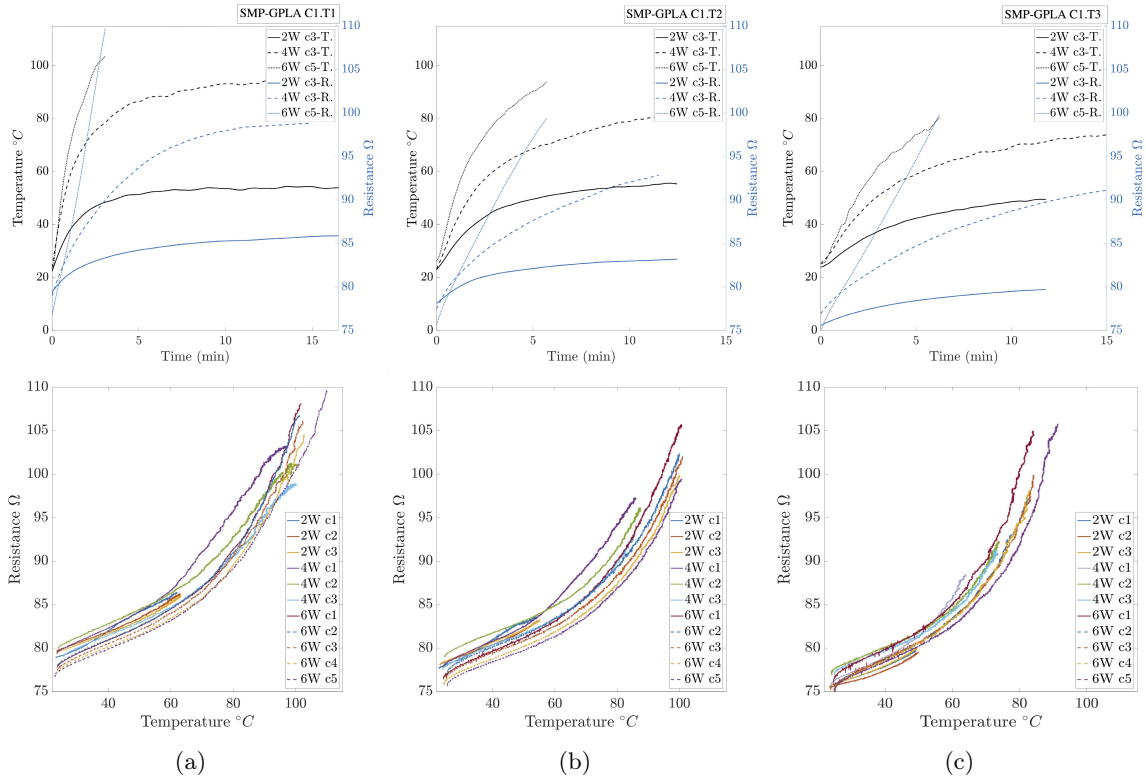


Figure 7.10: Data representation is shown for samples (a) C1.T1-S1, (b) C1.T2-S2 and (c) C1.T3-S1. On the first row, representation curves of sample transient heating with respect to power input are shown. At the bottom row, curves of resistance changes with respect to temperature readings can be seen.

The right hand axis of Figure 7.10a shows the total resistance readings, they also followed a first order curve with respect to time. Resistance readings are shown in the graph for the heating cycles 3 and 5. Initial resistance readings dropped with increase in power supply wattage (i.e 2, 4 and 6 Watts), this could be attributed to possible melting and cooling done previously which may have eliminated initial voids in the conductive 3D printed structure.

On the bottom of Figure 7.10a, 7.10b and 7.10c, the relationships of resistance with respect to temperature can be observed. Notice that resistance measurements become nonlinear starting at  $40^{\circ}\text{C}$ . This could be due to the beginning of the glass transition temperature,  $T_g$ , range where the layers of the 3D printed GPLA start to fuse. After the second cycle, the non-linearity was not observed. Furthermore, resistance readings are shown to be linear for 2 Watt cycles and the beginning of the 4 Watts cycles, suggesting that as long as the GPLA keeps its structural integrity the sample will display linear resistance readings until it hits  $T_g$ . Nevertheless, for the

proposed application, higher temperatures can be achieved and a nonlinear resistance would not be of disadvantage to the proposed system since it can be compensated with a robust control system. From the obtained temperature with respect to power input, it is evident that a more efficient temperature control could be conducted.

The temperature distribution was also investigated for all samples. Figure 7.11a shows infrared pictures at different points in time after the application of 2,4 and 6 watts to samples C1.T1, C1.T2, and C1.T3, respectively. The images presented are the temperature distribution when the sample has hit the activation temperature or very close to ( $75^{\circ}C$ ). Heating homogeneity decreases with sample thickness, this is obvious when a comparison between the application of 6 Watts to C1.T1 and C1.T3 is done. Sample C1.T3 shows distinct separate conducting lines, while it is unnoticeable for C1.T1. Notice that a heating point at the change in direction of the heating element can be seen. Although this was encountered, future change in geometry at the ends could prevent thermal concentrations. Nevertheless for this study, the heating characterization is taken from the middle section.

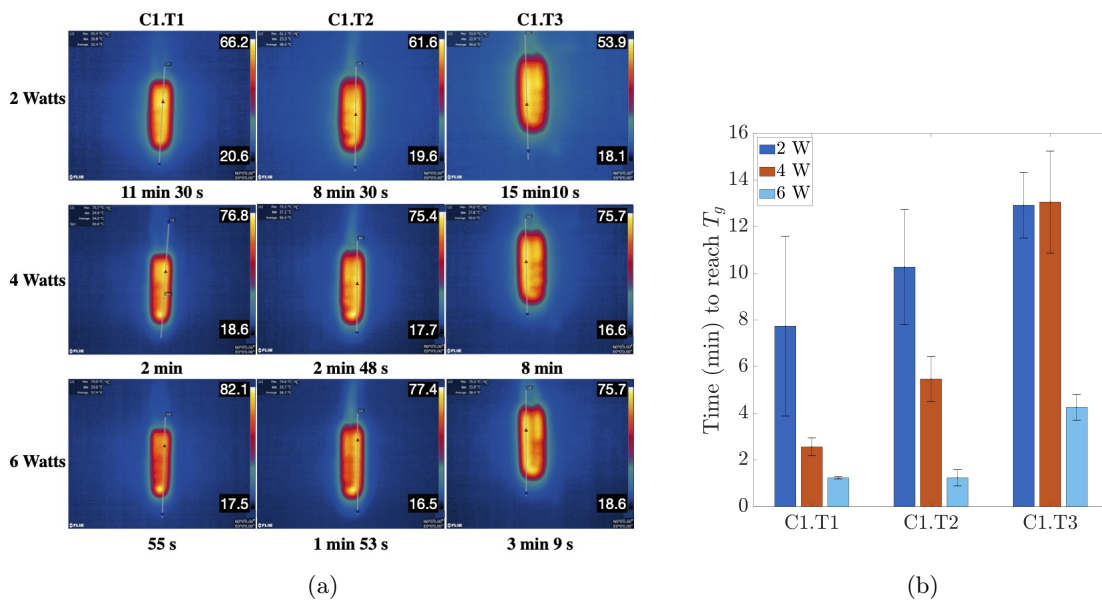


Figure 7.11: (a) Heat distribution presented by samples C1.T1,C1.T2,C1.T3 when they reach the activation temperature  $T_g$  ( $75^{\circ}C$ ) and (b) bar graph showing time to reach activation for all collected samples

A collection of all times to reach activation times was collected and can be seen in Figure 7.11b. Notice that the standard deviation of the application of 2 Watts is quite high, this could possibly be due to the fact that there are still voids in the system and the material has not fused completely

yet. Furthermore it could be mostly due to a low power supply which is more affected by room conditions. A general increase in activation time was observed with increase of surrounding SMPU thickness, which is to be expected due to heat dissipation within the material. However, a clear decrease in activation time with higher power input is observed. Hence, an important way to effectively improve activation time is to decrease the SMPU layer height and activate right away with a high power input and later control the required power to achieve an outside temperature of  $T_g$ . For C1.T3, application of 2W and 4W heating times were similar, although the tests were repeated a number of times, as indicated with the standard deviation bars in the figure, is clear this breaks the trend seen in the other specimen types and we acknowledge that this may require some further investigation in the future.

### 7.3.2 Shape Memory Effect

All the presented data has been shown with the purpose of characterizing and for future design of the optimal 3D printed SMPC that can be activated in out-of-laboratory conditions. Since the main objective of the present study is to activate the SME, two tests were conducted: the constrained and free end recovery. For both tests, samples C1.T1 and C1.T2 were tested. Samples C1.T3 were tested but no meaningful data was extracted since the thickness of these samples do not allow for a homogeneous heating and constrain the bending capability of the composites.

A sample of the programming cycle can be observed in Figure 7.12a; the graph shows the programming of sample C1.T1. It can be seen that the temperature increases for programming (application of strain) and cooling after for shape setting. Once the samples have been programmed, a constrained activation via resistive heating was carried out for both sample types. It is to be noted that the more SMPU the sample contains, the greater the recovery force will be as observed by Figure 7.12b. Figure 7.12b is a two axis graph, the recovery force is shown at the left and the changes in resistance at the right. The Figure shows approximately twice the recovery force for sample C1.T2 in contrast to sample C1.T1. In the figure, the resistance per sample is similar for both samples and the change in resistance is consistent with respect to the proportional expected recovery. Notice that the resistance converges to a value, this is due to the change in temperature occurred, since no changes due to strain happened due to the nature of the test. For the proposed sample sizes, the maximum recovery force observed for samples C1.T1 and C1.T2 were  $0.95 \pm 0.18 N$  and  $1.83 \pm 0.73 N$ , respectively. The time to reach peak force for samples C1.T1 and C1.T2 were  $43 \pm 25.6 s$  and  $75 \pm 41 s$ . Consistently Type 1 samples (C1.T1) showed recovery force peak faster than Type 2 samples.

Some of the observed problems during the recovery process were spikes in resistance when samples were not heated properly, this phenomena was mostly observed for samples that were thicker

(C1.T2), therefore suggesting that this is possibly due to a GPLA breakage during programming and eventual connection when actuation occurs. To avoid mentioned problems, small layers of graphene can be kept inserted inside a small SMPU unit cell (similar to C1.T1), this will allow for homogeneous heating. Spikes produced in resistance are a problem that occurs when programming by the conventional method but programming from inside out (Joule heating) would immediately repair this problem.

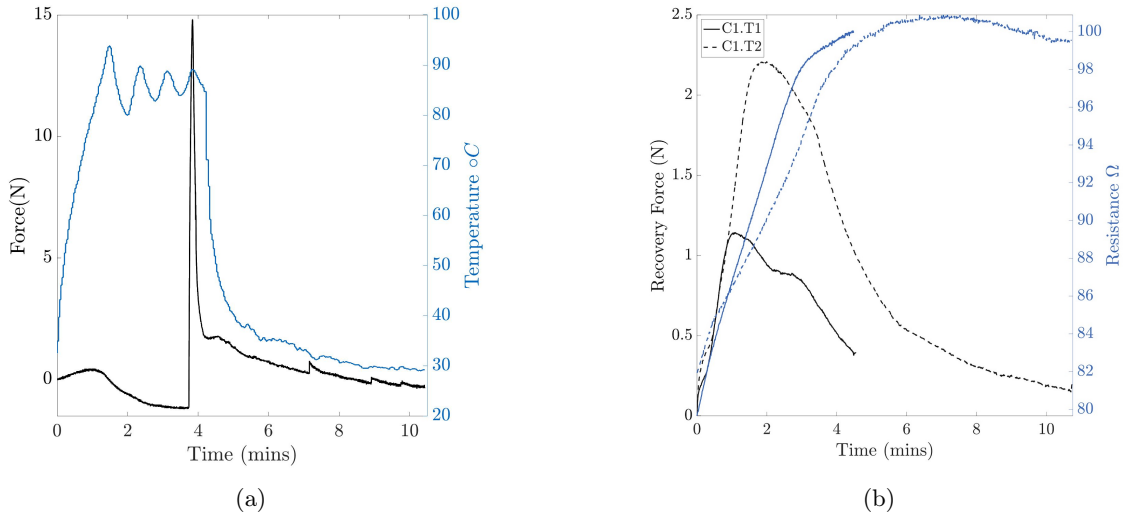


Figure 7.12: (a) Shape memory programming cycle by increased ambient temperature (b) Sample activation C1.T1 and C1.T2 via resistive heating with 4 Watts

Perhaps the most interesting part of this paper and what brings everything that has been developed together are the results of the free recovery tests, which are a primary indicator of the performance of the proposed smart composite. An SMPC (C1.T1) being activated in a free end recovery mode and can be observed in Figure 7.13a. In the figure, hotter spots can be observed, specifically at the bent parts of the sample. This is expected since the conductive material is stretched at this point and therefore resistance at the bent angle increases. Figure 7.13b is graph with two axis. It shows the recovery angle at the left axis and the recorded resistance changes at the right axis. Resistance measurements were collected in real time as the sample recovered. Sample curves of the recovery process are shown in Figure 7.13b. A general sharp steady increase in recovery angle was observed for type 1 samples, while type 2 samples showed a slow recovery with pauses which is attributed to the slow heat dissipation from within the sample. The total maximum recovery percentage obtained for the three samples was in average  $95.95 \pm 3.40$  for type 1 samples and  $62.74 \pm 24.02$  for samples type 2. Generally it was observed that type 1 samples had a higher recovery rate of  $1.84 \pm 0.31\%/s$  for type 1 samples and  $0.73 \pm 0.54\%/s$  for samples type 2. The

data agrees with the expected heat dissipation logic, since it takes longer times for thicker samples to reach activation temperatures.

Sample resistance curves with respect to time can be observed in Figure 7.13b at the right axis. The trends in the data initially suggest that an increase in resistance is mainly produced by the temperature increase until it peaks and then strain recovery happens at its maximum rate, causing resistance to sharply drop. This was a trend constantly observed in all tested samples. A higher drop in resistance occurs for C1.T2 than C1.T1, due to its greater thickness which produces higher deformations. Note that the developed control unit always supplied 4 Watts, therefore it regulates the applied voltage to the system by PWM. For C1.T1 a later significant increase in resistance suggests a recovery of the composite to its original position, while a permanent deformation is observed from C1.T2 and is reflected in the resistance readings. Furthermore the decrease in resistance appears in time when the recovery angle has over-passed half of the recovery angle percentage. With these results, resistance changes of the proposed smart self-sensing SMPC can be used to predict changes in strain and temperature. The proposed technology could be used as a sensor or actuator.

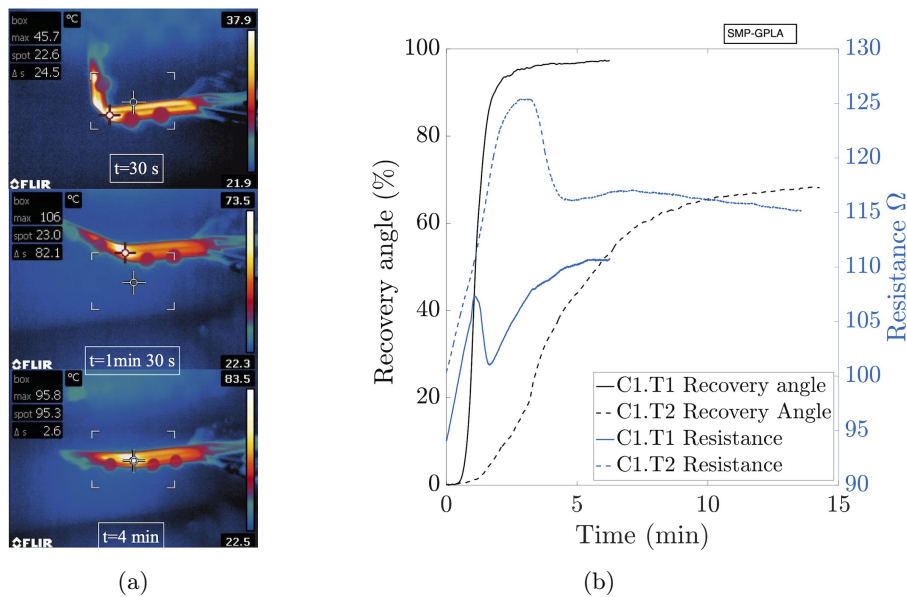


Figure 7.13: (a) Picture of sample C1.T1 recovering while 4 Watts are applied to the sample. (b) Graph of recovery angle percentage and resistance readings after the application of 4 Watts

The development of this material is part of an ongoing work, in which a future description of resistance with respect to strain will be characterized to form self-sensing SMPC materials.

## 7.4 Conclusions and Recommendations

The present work proposes an SMPC which is made of two different materials, a resistive thermoplastic material (GPLA) and a thermoplastic SMP. Both materials were 3D printed using an EBAM type desktop printer to design a composite for future applications as sensors or actuators. With a power input, the composite can be activated (SME) and give feedback information based on the resistance measurements. These resistance measurements can be correlated to strain and temperature changes experienced by the structure. The mentioned abilities makes the composite a self-sensing material. The proposed composite material can revolutionize the way we see actuators because they can be potentially prototyped in any intricate desired shape.

With the design and manufacture of a control unit to supply a constant power regardless of possible changes in resistance due to temperature or strain. The design of the control unit may be used with different conductive materials with few minor changes such as the resistances on the WB. Attempts in the literature to describe conductive materials have omitted this valuable step when characterizing a new proposed smart shape changing material.

To determine the required input power to reach steady state temperatures and provoke activation three different power inputs were proven i.e. 2, 4, 6 Watts. A transient description of temperature and resistance was obtained for different unit cell configurations. As expected, the unit cell with the thinner amount of surrounding SMPC heated up faster. This has a direct correlation in the activation of the shape memory effect, particularly in the free end recovery tests. A thicker surrounding matrix impedes a fast recovery due to the slowness of the heat dissipation. This constrains the total amount of recovery that the material can undergo. However, it is necessary to use the most SMP surrounding matrix to achieve high recovery forces. As such, the authors recommend that layers of thin unit cells may be stacked together in the thickness direction to produce any desired shape and achieve high recovery forces.

An optimization of the surrounding matrix with respect to heating material is part of an ongoing investigation. The authors are focusing on characterizing the behaviour of GPLA polymer with respect to strain in a future publication. The authors have also considered possible improvements on the composite by addition of particles to improve the material recovery rate and force. This can be achieved by modifying the SMPU matrix with particles such as cellulose nanocrystals. Better bond between the conductive material and the SMPU could be achieved by in house manufacturing a Graphene-SMPU composite and replacing the GPLA material used in this study while 3D printing the surrounding material of pure SMPU matrix. The great versatility of this technology can allow for different material alterations which can be used in a variety of potential applications.

## 7.5 References

- [1] P R Buckley, G H McKinley, T S Wilson, W Small, W J Benett, J P Bearinger, M W McElfresh, and D J Maitland. Inductively Heated Shape Memory Polymer for the Magnetic Actuation of Medical Devices. *IEEE Transactions on Biomedical Engineering*, 53(10):2075–2083, 2006.
- [2] Hong-Mei Chen, Lin Wang, and Shao-Bing Zhou. Recent Progress in Shape Memory Polymers for Biomedical Applications. *Chinese Journal of Polymer Science (English Edition)*, 36(8):905–917, August 2018.
- [3] Eleonora D’Elia, Hanaë Said Ahmed, Ezra Feilden, and Eduardo Saiz. Electrically-responsive graphene-based shape-memory composites. *Applied Materials Today*, 15:185–191, June 2019.
- [4] I T Garces, S Aslanzadeh, and Ayranci C. Boluk, Y. Cellulose nanocrystals (CNC) reinforced shape memory polyurethane ribbons for future biomedical applications and design. *Journal of Thermoplastic Composites*, 4(74003):089270571880633, October 2018.
- [5] I T Garces and C. Ayranci. A view into additive manufactured electro-active reinforced smart composite structures. *Manufacturing Letters*, 16:1–5, April 2018.
- [6] I T Garces and C. Ayranci. Additive manufactured electroactive shape memory polymer composites. In *Twenty Second International Conference on Composite Materials*. MCI, August 2019.
- [7] Irina T Garces, Samira Aslanzadeh, Yaman Boluk, and C. Ayranci. Effect of Moisture on Shape Memory Polyurethane Polymers for Extrusion-Based Additive Manufacturing. *Materials*, 12(2):244, January 2019.
- [8] Julien Gardan. Smart materials in additive manufacturing: state of the art and trends. *Virtual and Physical Prototyping*, 14(1):1–18, January 2019.
- [9] Xiaobo Gong, Liwu Liu, Yanju Liu, and Jinsong Leng. An electrical-heating and self-sensing shape memory polymer composite incorporated with carbon fiber felt. *Smart Materials and Structures*, 25(3):035036, March 2016.
- [10] Jahan Zeb Gul, Memoon Sajid, Muhammad Muqeet Rehman, Ghayas Uddin Siddiqui, Imran Shah, Kyung-Hwan Kim, Jae-Wook Lee, and Kyung Hyun Choi. 3D printing for soft robotics – a review. *Science and Technology of Advanced Materials*, 19(1):0–0, March 2018.
- [11] I Sedat Gunes, Guillermo A Jimenez, and Sadhan C Jana. Carbonaceous fillers for shape memory actuation of polyurethane composites by resistive heating. *Carbon*, 47(4):981–997, April 2009.

- [12] W. M. Huang, B. Yang, Y. Zhao, and Z. Ding. Thermo-moisture responsive polyurethane shape-memory polymer and composites: A review. *Journal of Materials Chemistry*, 20(17):3367–3381, June 2010.
- [13] H U Jinlian. *Shape memory polymers and textiles*. Woodhead Publishing Limited, Hong Kong Polytechnic University, Kowloon, Hong Kong, January 2007.
- [14] Hyunhyub Ko and Ali Javey. Smart Actuators and Adhesives for Reconfigurable Matter. *Accounts of Chemical Research*, 50(4):691–702, March 2017.
- [15] Xiao Kuang, Devin J Roach, Jiangtao Wu, Craig M Hamel, Zhen Ding, Tiejun Wang, Martin L Dunn, and Hang Jerry Qi. Advances in 4D Printing: Materials and Applications. *Advanced Functional Materials*, 29(2), January 2019.
- [16] Xin Lan, Yanju Liu, Haibao Lv, Xiaohua Wang, Jinsong Leng, and Shanyi Du. Fiber reinforced shape-memory polymer composite and its application in a deployable hinge. *Smart Materials and Structures*, 18(2):024002, April 2009.
- [17] Andreas Lendlein and Oliver E C Gould. Reprogrammable recovery and actuation behaviour of shape-memory polymers. *Nature Reviews Materials*, pages 1–18, January 2019.
- [18] Jinsong Leng and Shanyi Du. *Shape-Memory Polymers and Multifunctional Composites*. CRC Press, May 2010.
- [19] Yanju Liu, Haibao Lv, Xin Lan, Jinsong Leng, and Shanyi Du. Review of electro-active shape-memory polymer composite. *Composites Science and Technology*, 69(13):2064–2068, October 2009.
- [20] Xiaoang Ma. Bending of a polyurethane based shape memory polymer: modeling and experiment . June 2018.
- [21] Patrick T Mather, Xiaofan Luo, and Ingrid A Rousseau. Shape Memory Polymer Research. *Annual Review of Materials Research*, 39:445–471, August 2009.
- [22] Harper Meng and Guoqiang Li. A review of stimuli-responsive shape memory polymer composites. *Polymer (United Kingdom)*, 54(9):2199–2221, April 2013.
- [23] Charles L Moore and Hugh A Bruck. A fundamental investigation into large strain recovery of one-way shape memory alloy wires embedded in flexible polyurethanes. *Smart Materials and Structures*, 11(1):130–139, February 2002.
- [24] F Najafi and M Rajabi. Thermal gravity analysis for the study of stability of graphene oxide-glycine nanocomposites. *International Nano Letters*, 5(4):187–190, May 2015.

- [25] Debdatta Ratna and J Karger-Kocsis. Recent advances in shape memory polymers and composites: a review. *Journal of Materials Science*, 43(1):254–269, 2008.
- [26] Janice J Song, Quan Chen, and Hani E Naguib. Constitutive modeling and experimental validation of the thermo-mechanical response of a shape memory composite containing shape memory alloy fibers and shape memory polymer matrix. *Journal of Intelligent Material Systems and Structures*, 27(5):625–641, March 2015.
- [27] Jiefeng Sun and Jianguo Zhao. An Adaptive Walking Robot With Reconfigurable Mechanisms Using Shape Morphing Joints. *IEEE Robotics and Automation Letters*, 4(2):724–731, April 2019.
- [28] L Sun, W. M. Huang, Z. Ding, Y. Zhao, C C Wang, H Purnawali, and C Tang. Stimulus-responsive shape memory materials: A review. *Materials and Design*, 33(1):577–640, January 2012.
- [29] Hitachi High Tech. Thermal analysis of polylactic acid. pages 1–4, February 2013.
- [30] Jorge Villacres, David Nobes, and C. Ayranci. Additive Manufacturing of Shape Memory Polymers: Effects of print orientation and infill percentage on mechanical properties. *Rapid Prototyping Journal*, 24(4):744–751, 2018.
- [31] Xin Wang, John Sparkman, and Jihua Gou. Electrical actuation and shape memory behavior of polyurethane composites incorporated with printed carbon nanotube layers. *Composites Science and Technology*, 141:8–15, March 2017.
- [32] Mu-Hoe Yang and Yeuh-Hui Lin. Measurement and Simulation of Thermal Stability of Poly(Lactic Acid) by Thermogravimetric Analysis. *Journal of Testing and Evaluation*, 37(4):364–370, July 2009.
- [33] Yang Yang, Yonghua Chen, Ying Wei, and Yingtian Li. 3D printing of shape memory polymer for functional part fabrication. *International Journal of Advanced Manufacturing Technology*, 84(9-12):2079–2095, June 2016.
- [34] Wei Zhang, Fenghua Zhang, Xin Lan, Jinsong Leng, Amanda S Wu, Taylor M Bryson, Chase Cotton, Bohong Gu, Baozhong Sun, and Tsu-Wei Chou. Shape memory behavior and recovery force of 4D printed textile functional composites. *Composites Science and Technology*, 160:224–230, May 2018.

# Chapter 8

## Conclusions

Shape Memory Polymers are smart materials that are able to store a temporary shape and recover their original shape upon the application of a stimulus. Particularly thermal-sensitive shape memory polymers are the most commonly studied materials since an increase in temperature can easily activate their shape memory effect. These materials offer advantages over traditional actuators as they are lightweight and do not require a need for fasteners or mechanical components to achieve movement. Furthermore, a wide range of complex mobility can be achieved. In order to have a better fundamental understanding of SMPs and accomplish engineering applications, the following is required: 1) a study on the effect of ambient conditions and processability of shape memory polymers, 2) a transient model for bending, 3) a flexible production technique for producing parts with these materials, and 4) a controlled field activation. These will form pioneering stepping stones in the broader use of SMPs for engineering applications.

As such, this thesis contributes to the field on these four objectives. A thorough material characterization and selection of a material that can withstand ambient conditions to ensure material performance and processability for extrusion-based additive manufacturing of complex shapes was done. Later, a transient model for bending, which has an easy to understand formulation and ease of application, was developed and verified. A hybrid material based on an additive manufacturing technique is demonstrated for manufacturing SMPs and SMPC materials using a one-step process with embedded activation elements that can also be used as sensors. Finally, a thorough study on controlled field activation of these SMPC materials was conducted. The proposed composite is made of a conductive thermoplastic embedded in the SMP. Hence, the composite can be activated via resistive heating. Since a controlled activation is required for many engineering applications, a circuit and a closed-loop temperature control were designed. Furthermore, this composite showed

sensing capabilities in strain and temperature, which were studied in this thesis. This work proposes studying the material, modelling, activation, control and sensing of smart multifunctional shape-memory materials to link scientific knowledge to real-life engineering applications. More specific details of the thesis and related conclusions are as follows:

- A modelling review has been presented in this work, a general explanation of the most common modelling techniques were discussed and put forward. From this exhaustive review, a need for simple models for first stage design are acknowledged to be required to start a broader use of SMPs in engineering applications. As a result, this study focused on the formulation, application and validation of a model for bending applications. The model captures the overall transient behaviour of the polymer during recovery, and provides with valuable predictions for design. A method to obtain material parameters from Dynamic Mechanical Analysis data was also proposed to obtain the material parameter behaviour with respect to temperature and by using this technique, reduce usual experimentation time. This model is simple in formulation and application, and although much of the behaviour is captured, there are still improvements to be made to better predict the results of the experimental data. This model is easily adaptable to implement embedded heating elements. Hence, this model is a stepping stone towards the development and further capturing of the behaviour of shape memory polymers under bending for first stage design.
- The study on the moisture effects on two types of shape memory polymers was done. The results showed that the TP shape memory polymer with higher hard to soft segment ratio produces higher moisture trapping which causes a difficulty to 3D print the material via extrusion based additive manufacturing. On the other hand, the material with lower high to soft segment ratio is highly affected by bonded water which causes the material to plasticize and lose stiffness. A material with higher high to soft segment ratio and therefore higher  $T_g$  was chosen for this thesis due to its ability to resist hydrogen bonding and therefore plasticization. This material is therefore more resilient to ambient conditions.
- Following the exhaustive literature review of the techniques and advances of additive manufacturing of shape memory polymer composites, the area of additive manufacturing of self-actuated and self-sensing SMPCs was identified. The review also highlights research possibilities in the 3D of SMPs and 4D printing to obtain shape change. Hence, an investigation of the activation of 3D printing conductive shape memory polymer composites via joule heating was done. The exploration of the printing feasibility and activation showed promising results. The proposed composites showed potential to be used in many applications such as sports' equipment, self-deployable and self-folding structures, among others.
- A work on the exploration of the multifunctionality of a 3D printed conductive composite was

proposed. An apparatus to activate and measure resistance was developed. The equipment can regulate power input regardless of the changes within the material due to strain or temperature. This work provides the first control approach to shape memory polymers. The sensing capability of temperature and changes in strain was studied by measuring resistance. The technology showed great potential to be used in many applications such self-sensing actuators.

## 8.1 Recommendations for Future Work

Further work is needed to overcome the limitations identified in this thesis.

- The study of the moisture effect on shape memory polymers was comprehensive; and, it highlighted potential need for further improvement. The printability of the materials affected by moisture was only qualitatively described. Quantitative description with respect to time is required to ensure optimal printing conditions. Another area that was observed but was not addressed is the moisture swelling caused on the material. Such a study could potentially be crucial to keep the dimensional integrity of the material after printing.
- The modelling review work on this thesis is based on SMPs. However, a section on SMPCs will be included for publication since many more functionalities of the material can be obtained when using SMPCs.
- Although the proposed model in this thesis is demonstrated to have many advantages, there is still room for improvement, and further studies need to be made. Firstly, the model's cooling procedure must be further studied and described to identify if there is a change in material properties between the pre-programming stage and the end of the cooling process. For this, a microstructural study needs to be conducted since the crystallinity of the material may change the initial viscoelastic properties.

Additionally, in this work, the heat transfer within the material is not considered due to the thin specimen assumption. A correction of for activation time could be implemented by a study of heat transfer. This would allow a better prediction of when the SMP's mobility begins.

This model was designed and thought to capture the general behaviour trend of the material. The present conditions and assumptions are made for the increase in temperature by convection. However, a feature like the implementation of joule heating to the shape memory polymer on the model could be easily achievable by considering the heat transfer in the  $y$  direction of the beam. Hence, a temperature with respect to  $y$  and time can be obtained and implemented on the model. Specifically, a model for the technology proposed in this thesis

is still necessary, that is one that accounts for multimaterial printing and heat transfer for embedded heating material.

A use of a phase change model to convert the present model to a hybrid model could potentially bring better approximations, although a tradeoff should be made between complexity and applicability for engineering design.

- Further work needs to be performed in the area of activation and sensing properties of the conductive shape memory polymer composite proposed. A complete characterization of the sensing element with respect to the temperature needs to be completed. A detailed correlation between stress and strain has been preliminarily studied and presented in conference proceedings, but a thorough description is still to be performed. Characterization of the printing parameters and their effect on the temperature profile and the effect on the strain need to be developed, since anisotropy may occur due to the intrinsic manufacturing properties.

Classical laminate plate theory could be potentially used to design laminate like structures of a shape memory polymer matrix and use conductive reinforcing printed lines. This could improve the stiffness and overall strength of the composites.

Furthermore, by utilizing two different materials, one conductive PLA based, and a polyurethane shape memory polymer as a matrix, induced stress could be implemented during the 3D printing process to produce "direct 4D printing" and hence, eliminate the programming method of the composite.

The proposed technology is a stepping stone to many long-term new and exciting projects. Some of the proposed projects include the fabrication and development of a 3D printed kayak, which could be programmed into a compressed shape for ease of transportation. This technology could also induce the development of moisture sensors by taking advantage of the material swelling and or the shape memory effect activated by a decrease of the glass transition temperature due to moisture. Small robotic actuators like the legs of a crawling robot could potentially be the next step in the proposed technology. This application is particularly interesting, since the robot dynamics may be changed by merely changing the leg's geometry.

# References

- [1] Shweta Agarwala, Guo Liang Goh, Guo Dong Goh, Vishwesh Dikshit, and Wai Yee Yeong. *Chapter 10 - 3D and 4D printing of polymer/CNTs-based conductive composites*. Elsevier Inc., 2020.
- [2] Saeed Akbari, Amir Hosein Sakhaei, Kavin Kowsari, Bill Yang, Ahmad Serjouei, Zhang Yuanfang, and Qi Ge. Enhanced multimaterial 4D printing with active hinges. *Smart Materials and Structures*, 27(6):065027–16, May 2018.
- [3] Javed Alam, Aslam Khan, Manawwer Alam, and Raja Mohan. Electroactive Shape Memory Property of a Cu-decorated CNT Dispersed PLA/ESO Nanocomposite. *Materials*, 8(9):6391–6400, September 2015.
- [4] Daniel R Aldrich, C. Ayranci, and D. S Nobes. OSM-Classic : An optical imaging technique for accurately determining strain. *SoftwareX*, 6:225–230, August 2017.
- [5] Byoungkwon An, Hsiang-Yun Wu, Teng Zhang, Lining Yao, Ye Tao, Jianzhe Gu, Tingyu Cheng, Xiang 'Anthony Chen, Xiaoxiao Zhang, Wei Zhao, Youngwook Do, and Shigeo Takahashi. Thermorph : Democratizing 4D Printing of Self-Folding Materials and Interfaces. In *the 2018 CHI Conference*, pages 1–12, New York, New York, USA, 2018. ACM Press.
- [6] Soo Chan An, Eunsongyi Lee, Chang Hyun Lee, Hoon Yeub Jeong, Taek Sun Kwon, Jeong Hae Lee, and Young Chul Jun. Sharp Fano Resonance and Spectral Collapse in Stimuli-Responsive Photonic Structures. *Advanced Optical Materials*, 7(5):1801206–8, December 2018.
- [7] Jean-Claude André. *From Additive Manufacturing to 3D/4D Printing 2*. Current Techniques, Improvements and their Limitations. John Wiley & Sons, November 2017.
- [8] Xinling Ao, Deyan Kong, Ziyang Zhang, and Xinli Xiao. Enhancing recovery speed and anti-wear capability of high-temperature shape memory polymer with modified boron nitride nanoparticles. *Journal of Materials Science*, 55(10):4292–4302, December 2019.

- [9] D I Arun, P Chakravarthy, B S Girish, K S Santhosh Kumar, and B Santhosh. Experimental and Monte Carlo simulation studies on percolation behaviour of a shape memory polyurethane carbon black nanocomposite. *Smart Materials and Structures*, 28(5):055010, April 2019.
- [10] Z August, G Ostrander, and J Michasiow J. Recent developments in automated fiber placement of thermoplastic composites. In *SAMPE 2013*, Long Beach, 2013. SAMPE 2013, Education Green Sky.
- [11] F Auricchio, A Reali, and U Stefanelli. A three-dimensional model describing stress-induced solid phase transformation with permanent inelasticity. *International Journal of Plasticity*, 23(2):207–226, February 2007.
- [12] Ferdinando Auricchio and Lorenza Petrini. A three-dimensional model describing stress-temperature induced solid phase transformations: solution algorithm and boundary value problems. *International Journal for Numerical Methods in Engineering*, 61(6):807–836, October 2004.
- [13] C Azra, C J G Plummer, and J A E Manson. Tailoring the time-dependent recovery of shape memory polymers. In Nakhiah C Goulbourne and Zoubeida Ounaies, editors, *SPIE Smart Structures and Materials + Nondestructive Evaluation and Health Monitoring*, pages 834212–9. SPIE, March 2012.
- [14] G Baer, T S Wilson, D L Matthews, and D J Maitland. Shape-memory behavior of thermally stimulated polyurethane for medical applications. *Journal of Applied Polymer Science*, 103(6):3882–3892, 2006.
- [15] M Baghani, R Naghdabadi Journal of Intelligent, and 2012. A constitutive model for shape memory polymers with application to torsion of prismatic bars. *journals.sagepub.com*, 23(2):107–116, February 2012.
- [16] M Baghani, H Mohammadi, and R Naghdabadi. An analytical solution for shape-memory-polymer Euler-Bernoulli beams under bending. *International Journal of Mechanical Sciences*, 84:84–90, January 2014.
- [17] Anna B Baker, Simon R G Bates, Thomas M Llewellyn-Jones, Laurie P B Valori, Michael P M Dicker, and Richard S Trask. 4D printing with robust thermoplastic polyurethane hydrogel-elastomer trilayers. *Materials and Design*, 163(C):107544, February 2019.
- [18] Olaniyi A Balogun and Changki Mo. Shape memory polymers - Energy method superposition constitutive modeling. In *ASME 2014 Conference on Smart Materials, Adaptive Structures and Intelligent Systems, SMASIS 2014*. Washington State University Tri-Cities, Richland, United States, January 2014.

- [19] Olaniyi A Balogun and Changki Mo. Shape memory polymers - Viscoelastic thermomechanical constitutive modeling. In *ASME 2014 Conference on Smart Materials, Adaptive Structures and Intelligent Systems, SMASIS 2014*. Washington State University Tri-Cities, Richland, United States, January 2014.
- [20] Silvestro Barbarino, Onur Bilgen, Rafic M Ajaj, Michael I Friswell, and Daniel J Inman. A review of morphing aircraft. *Journal of Intelligent Material Systems and Structures*, 22(9):823–877, June 2011.
- [21] G Barot and I J Rao. Constitutive modeling of the mechanics associated with crystallizable shape memory polymers. *Zeitschrift für angewandte Mathematik und Physik*, 57(4):652–681, March 2006.
- [22] G Barot, I J Rao, and K R Rajagopal. A thermodynamic framework for the modeling of crystallizable shape memory polymers. *International Journal of Engineering Science*, 46(4):325–351, April 2008.
- [23] Sajad Razavi Bazaz, Omid Rouhi, Mohammad Amin Raoufi, Fatemeh Ejeian, Mohsen Asadnia, Dayong Jin, and Majid Ebrahimi Warkiani. 3D Printing of Inertial Microfluidic Devices. *Nature Publishing Group*, pages 1–14, March 2020.
- [24] Marc Behl and Andreas Lendlein. Shape-memory polymers. *Materials Today*, April 2007.
- [25] Murat Bengisu and Marinella Ferrara. *Materials that Move*. Smart Materials, Intelligent Design. Springer, April 2018.
- [26] Prahar M Bhatt, Max Peralta, Hugh A Bruck, and Satyandra K Gupta. Robot Assisted Additive Manufacturing of Thin Multifunctional Structures. In *ASME 2018 13th International Manufacturing Science and Engineering Conference*, pages 1–10. American Society of Mechanical Engineers, September 2018.
- [27] A Bhattacharyya and H Tobushi. Analysis of the isothermal mechanical response of a shape memory polymer rheological model. *Polymer Engineering & Science*, 40(12):2498–2510, December 2000.
- [28] Rahul Bhattacharyya, Claudio Di Leo, Christian Floerkemeier, Sanjay Sarma, and Lallit Anand. RFID tag antenna based temperature sensing using shape memory polymer actuation. In *Proceedings of IEEE Sensors*, pages 2363–2368. Massachusetts Institute of Technology, Cambridge, United States, IEEE, December 2010.
- [29] H Bikas, P Stavropoulos, and G Chryssolouris. Additive manufacturing methods and modelling approaches: a critical review. *The International Journal of Advanced Manufacturing Technology*, 83(1-4):389–405, July 2015.

- [30] Paolo Blasi, Susan S D'Souza, Francesca Selmin, and Patrick P DeLuca. Plasticizing effect of water on poly(lactide-co-glycolide). *Journal of Controlled Release*, 108(1):1–9, November 2005.
- [31] M Bodaghi, A R Damanpack, and W H Liao. Self-expanding/shrinking structures by 4D printing. *Smart Materials and Structures*, 25(10):105034–16, October 2016.
- [32] M Bodaghi and W H Liao. 4D printed tunable mechanical metamaterials with shape memory operations. *Smart Materials and Structures*, 28(4):045019–16, March 2019.
- [33] R Bouaziz, F Roger, and K Prashantha. Thermo-mechanical modeling of semi-crystalline thermoplastic shape memory polymer under large strain. *Smart Materials and Structures*, 26(5):055009, April 2017.
- [34] M C Boyce and E M Arruda. Constitutive models of rubber elasticity: A review. *Rubber Chemistry and Technology*, 73(3):504–523, January 2000.
- [35] Pinar Boyraz, Gundula Runge, and Annika Raatz. An overview of novel actuators for soft robotics. *Actuators*, 7(3), September 2018.
- [36] H A Bruck, C L Moore III, and T M Valentine. Bending actuation in polyurethanes with a symmetrically graded distribution of one-way shape memory alloy wires. *Experimental Mechanics*, 44(1):62–70, 2004.
- [37] C M Brunette, S L Hsu, and W J MackKnight. Hydrogen-Bonding Properties of Hard-Segment Model Compounds in Polyurethane Block Copolymers. *Macromolecules*, 15(1):71–77, 1982.
- [38] P R Buckley, G H McKinley, T S Wilson, W Small, W J Benett, J P Bearinger, M W McElfresh, and D J Maitland. Inductively Heated Shape Memory Polymer for the Magnetic Actuation of Medical Devices. *IEEE Transactions on Biomedical Engineering*, 53(10):2075–2083, 2006.
- [39] John Carrell, Garrett Gruss, and Elizabeth Gomez. Four-dimensional printing using fused-deposition modeling: a review. *Rapid Prototyping Journal*, ahead-of-print(ahead-of-print):155–15, January 2020.
- [40] Hong-Mei Chen, Lin Wang, and Shao-Bing Zhou. Recent Progress in Shape Memory Polymers for Biomedical Applications. *Chinese Journal of Polymer Science (English Edition)*, 36(8):905–917, August 2018.
- [41] Jianguo Chen, Liwu Liu, Yanju Liu, and Jinsong Leng. Thermoviscoelastic shape memory behavior for epoxy-shape memory polymer. *Smart Materials and Structures*, 23(5):055025, May 2014.

- [42] Kaijuan Chen, Xiao Kuang, Vincent Li, Guozheng Kang, and H Jerry Qi. Fabrication of tough epoxy with shape memory effects by UV-assisted direct-ink write printing. *Soft Matter*, 14(10):1879–1886, 2018.
- [43] Shaojun Chen, Jinlian Hu, Chun-wah Yuen, and Laikuen Chan. Novel moisture-sensitive shape memory polyurethanes containing pyridine moieties. *Additive Manufacturing*, 50(19):4424–4428, September 2009.
- [44] Shaojun Chen, Jinlian Hu, and Haitao Zhuo. Properties and mechanism of two-way shape memory polyurethane composites. *Composites Science and Technology*, 70(10):1437–1443, September 2010.
- [45] Shaojun Chen, Shixin Yang, Ziyu Li, Shiwei Xu, Hongming Yuan, Shiguo Chen, and Zhaochuan Ge. Electroactive two-way shape memory polymer laminates. *Polymer Composites*, 36(3):439–444, January 2015.
- [46] Tian Chen and Kristina Shea. An Autonomous Programmable Actuator and Shape Reconfigurable Structures Using Bistability and Shape Memory Polymers. *3D Printing and Additive Manufacturing*, 5(2):91–101, June 2018.
- [47] Xiang Chen and Thao D Nguyen. Influence of thermoviscoelastic properties and loading conditions on the recovery performance of shape memory polymers. *Mechanics of Materials*, 43(3):127–138, March 2011.
- [48] Yi-Chao Chen and Dimitris C Lagoudas. A constitutive theory for shape memory polymers. Part I. *Journal of the Mechanics and Physics of Solids*, 56(5):1752–1765, May 2008.
- [49] Yi-Chao Chen and Dimitris C Lagoudas. A constitutive theory for shape memory polymers. Part II. *Journal of the Mechanics and Physics of Solids*, 56(5):1766–1778, May 2008.
- [50] Yu Chen, Irina Tatiana Garces, Tian Tang, and C. Ayranci. Cellulose nanocrystals reinforced shape memory polymer cardiovascular stent. *Rapid Prototyping Journal*, ahead-of-print(ahead-of-print):19, December 2020.
- [51] Li Chong, Seeram Ramakrishna, and Sunpreet Singh. A review of digital manufacturing-based hybrid additive manufacturing processes. *International Journal Advanced Manufacturing Technology*, pages 1–20, February 2018.
- [52] Yu Ying Clarrisa Choong, Saeed Maleksaeedi, Hengky Eng, Suzhu Yu, Jun Wei, and Pei-Chen Su. High speed 4D printing of shape memory polymers with nanosilica. *Applied Materials Today*, 18:100515, March 2020.
- [53] Brett G Compton and Jennifer A Lewis. 3D-Printing of Lightweight Cellular Composites. *Advanced Materials*, 26(34):5930–5935, June 2014.

- [54] Sergio Conti, Martin Lenz, and Martin Rumpf. Hysteresis in magnetic shape memory composites: Modeling and simulation. *Journal of the Mechanics and Physics of Solids*, 89(C):272–286, April 2016.
- [55] Fangda Cui, Swapnil Moon, and I Rao. Modeling the Viscoelastic Behavior of Amorphous Shape Memory Polymers at an Elevated Temperature. *Fluids*, 1(4):15, December 2016.
- [56] Xihua Cui, Jianwen Chen, Yutian Zhu, and Wei Jiang. Natural sunlight-actuated shape memory materials with reversible shape change and self-healing abilities based on carbon nanotubes filled conductive polymer composites. *Chemical Engineering Journal*, 382:122823, February 2020.
- [57] S C Daminabo, S Goel, S A Grammatikos, H Y Nezhad, and V K Thakur. Fused deposition modeling-based additive manufacturing (3D printing): techniques for polymer material systems. *Materials Today Chemistry*, 16:100248, June 2020.
- [58] Eleonora D’Elia, Hanaë Said Ahmed, Ezra Feilden, and Eduardo Saiz. Electrically-responsive graphene-based shape-memory composites. *Applied Materials Today*, 15:185–191, June 2019.
- [59] Massimo Di Nicolantonio, Emilio Rossi, and Paride Stella. Generative Design for Printable Mass Customization Jewelry Products. In *Advances in Additive Manufacturing, Modeling Systems and 3D Prototyping*, pages 143–152. Springer, Cham, Cham, July 2019.
- [60] Julie Diani, Pierre Gilormini, Carole Frédy, and Ingrid Rousseau. Predicting thermal shape memory of crosslinked polymer networks from linear viscoelasticity. *International Journal of Solids and Structures*, 49(5):793–799, March 2012.
- [61] Julie Diani, Yiping Liu, and Ken Gall. Finite strain 3D thermoviscoelastic constitutive model for shape memory polymers. *Polymer Engineering & Science*, 46(4):486–492, 2006.
- [62] Andrés Díaz Lantada. Systematic Development Strategy for Smart Devices Based on Shape-Memory Polymers. *Polymers*, 9(12):496–19, December 2017.
- [63] Zhen Ding, Chao Yuan, Xirui Peng, Tiejun Wang, H Jerry Qi, and Martin L Dunn. Direct 4D printing via active composite materials. *Science Advances*, 3(4):e1602890–8, April 2017.
- [64] N J Distefano and K S Pister. On the identification problem for thermorheologically simple materials. *Acta Mechanica*, 13(3-4):179–190, September 1972.
- [65] Jiri George Drobny. *Handbook of Thermoplastic Elastomers*. PDL/Plastics Design Library. William Andrew, 2007.
- [66] Fei-Peng Du, En-Zhou Ye, Wen Yang, Tian-Han Shen, Chak-Yin Tang, Xiao-Lin Xie, Xing-Ping Zhou, and Wing-Cheung Law. Electroactive shape memory polymer based on optimized

- multi-walled carbon nanotubes/polyvinyl alcohol nanocomposites. *COMPOSITES PART B*, 68(C):170–175, January 2015.
- [67] M D Ediger. Spatially heterogeneous dynamics in supercooled liquids. *Annual review of physical chemistry*, 51:99–128, 2000.
- [68] Hengky Eng, Saeed Maleksaeedi, Suzhu Yu, Yu Ying Clarrisa Choong, Florencia Edith Wiria, Ruihua Eugene Kheng, Jun Wei, Pei-Chen Su, and Huijun Phoebe Tham. Development of CNTs-filled photopolymer for projection stereolithography. *Rapid Prototyping Journal*, 23(1):129–136, January 2017.
- [69] C Q Fang, H Y Sun, and J P Gu. Application of Fractional Calculus Methods to Viscoelastic Response of Amorphous Shape Memory Polymers. *Journal of Mechanics*, 31(4):427–432, January 2015.
- [70] M Fejos and G Romhány. Shape memory characteristics of woven glass fibre fabric reinforced epoxy composite in flexure. *Journal of Reinforced . . .*, 2012.
- [71] Márta Fejős, Kolos Molnár, and József Karger-Kocsis. Epoxy/Polycaprolactone Systems with Triple-Shape Memory Effect: Electrospun Nanoweb with and without Graphene Versus Co-Continuous Morphology. *Materials*, 6(10):4489–4504, October 2013.
- [72] S Felton, M Tolley, E Demaine, D Rus, and R Wood. A method for building self-folding machines. *Science*, 345(6):644–646, August 2014.
- [73] S Felton, M Tolley, E Demaine, D Rus, and R Wood. A method for building self-folding machines. *Science*, 345(6):644–646, August 2014.
- [74] S Felton, M Tolley, E Demaine, D Rus, and R Wood. Applied origami. A method for building self-folding machines. *Science*, 345(6197):644–646, August 2014.
- [75] S M Felton, K P Becker, D M Aukes, and R J Wood. Self-folding with shape memory composites at the millimeter scale. *Journal of Micromechanics and Microengineering*, 25(8):085004, August 2015.
- [76] Samuel M Felton, Michael T Tolley, ByungHyun Shin, Cagdas D Onal, Erik D Demaine, Daniela Rus, and Robert J Wood. Self-folding with shape memory composites. *Soft Matter*, 9(32):7688–8, 2013.
- [77] Bradley Finnigan, Darren Martin, Peter Halley, Rowan Truss, and Kayleen Campbell. Morphology and properties of thermoplastic polyurethane nanocomposites incorporating hydrophilic layered silicates. *Additive Manufacturing*, 45(7):2249–2260, March 2004.

- [78] Felix Franks. *Water Science Reviews 3: Volume 3*. Water Dynamics. Cambridge University Press, Cambridge, October 1988.
- [79] I T Garces, S Aslanzadeh, and Ayranci C. Boluk, Y. Cellulose nanocrystals (CNC) reinforced shape memory polyurethane ribbons for future biomedical applications and design. *Journal of Thermoplastic Composites*, 4(74003):089270571880633, October 2018.
- [80] I T Garces and C. Ayranci. A view into additive manufactured electro-active reinforced smart composite structures. *Manufacturing Letters*, 16:1–5, April 2018.
- [81] I T Garces and C. Ayranci. Additive manufactured electroactive shape memory polymer composites. In *Twenty Second International Conference on Composite Materials*. MCI, August 2019.
- [82] I T Garces and C. Ayranci. Active control of 4D prints: Towards 4D printed reliable actuators and sensors. *Sensors and Actuators, A: Physical*, 301:111717, January 2020.
- [83] I T Garces and C. Ayranci. Advances in additive manufacturing of shape memory polymer composites, January 2021.
- [84] Irina T Garces, Samira Aslanzadeh, Yaman Boluk, and C. Ayranci. Effect of Moisture on Shape Memory Polyurethane Polymers for Extrusion-Based Additive Manufacturing. *Materials*, 12(2):244, January 2019.
- [85] Carlos A Garcia Rosales, Mario F Garcia Duarte, Hoejin Kim, Luis Chavez, Deidra Hodges, Paras Mandal, Yirong Lin, and Tzu-Liang Bill Tseng. 3D printing of shape memory polymer (SMP)/carbon black (CB) nanocomposites with electro-responsive toughness enhancement. *Materials Research Express*, 5(6):065704–10, June 2018.
- [86] Julien Gardan. Smart materials in additive manufacturing: state of the art and trends. *Virtual and Physical Prototyping*, 14(1):1–18, January 2019.
- [87] Qi Ge, Conner K Dunn, H Jerry Qi, and Martin L Dunn. Active origami by 4D printing. *Smart Materials and Structures*, 23(9):094007–16, August 2014.
- [88] Qi Ge, H Jerry Qi, and Martin L Dunn. Active materials by four-dimension printing. *Applied Physics Letters*, 103(1):131901, September 2013.
- [89] Qi Ge, Amir Hosein Sakhaei, Howon Lee, Conner K Dunn, Nicholas X Fang, and Martin L Dunn. Multimaterial 4D Printing with Tailorable Shape Memory Polymers. *Nature Publishing Group*, 6:31110, August 2016.
- [90] Qi Ge, Kai Yu, Yifu Ding, and H Jerry Qi. Prediction of temperature-dependent free recovery behaviors of amorphous shape memory polymers. *Soft Matter*, 8:11098–, 2012.

- [91] P Ghosh, J N Reddy, and A R Srinivasa. Development and implementation of a beam theory model for shape memory polymers. *International Journal of Solids and Structures*, 50(3-4):595–608, February 2013.
- [92] Pierre Gilormini and Julie Diani. On modeling shape memory polymers as thermoelastic two-phase composite materials. *Comptes Rendus Mécanique*, 340(4-5):338–348, April 2012.
- [93] Guo Liang Goh, Shweta Agarwala, and Wai Yee Yeong. Directed and On-Demand Alignment of Carbon Nanotube: A Review toward 3D Printing of Electronics. *Advanced Materials Interfaces*, 6(4):1801318–29, January 2019.
- [94] Xiaobo Gong, Liwu Liu, Yanju Liu, and Jinsong Leng. An electrical-heating and self-sensing shape memory polymer composite incorporated with carbon fiber felt. *Smart Materials and Structures*, 25(3):035036, March 2016.
- [95] Jianping Gu, Jinsong Leng, and Huiyu Sun. A constitutive model for amorphous shape memory polymers based on thermodynamics with internal state variables. *Mechanics of Materials*, 111:1–14, August 2017.
- [96] Jahan Zeb Gul, Memoon Sajid, Muhammad Muqet Rehman, Ghayas Uddin Siddiqui, Imran Shah, Kyung-Hwan Kim, Jae-Wook Lee, and Kyung Hyun Choi. 3D printing for soft robotics – a review. *Science and Technology of Advanced Materials*, 19(1):0–0, March 2018.
- [97] I Sedat Gunes, Guillermo A Jimenez, and Sadhan C Jana. Carbonaceous fillers for shape memory actuation of polyurethane composites by resistive heating. *Carbon*, 47(4):981–997, April 2009.
- [98] Jianming Guo, Jingbiao Liu, Zhenqing Wang, Xiaofu He, Lifeng Hu, Liyong Tong, and Xiaojun Tang. A thermodynamics viscoelastic constitutive model for shape memory polymers. *Journal of Alloys and Compounds*, 705:146–155, May 2017.
- [99] Xiaogang Guo, Liwu Liu, Yanju Liu, Bo Zhou, and Jinsong Leng. Constitutive model for a stress- and thermal-induced phase transition in a shape memory polymer. *Smart Materials and Structures*, 23(10):105019, October 2014.
- [100] Xiaogang Guo, Liwu Liu, Bo Zhou, Yanju Liu, and Jinsong Leng. Influence of strain rates on the mechanical behaviors of shape memory polymer. *Smart Materials and Structures*, 24(9):095009, September 2015.
- [101] Xiaogang Guo, Liwu Liu, Bo Zhou, Yanju Liu, and Jinsong Leng. Constitutive model for shape memory polymer based on the viscoelasticity and phase transition theories. *Journal of Intelligent Material Systems and Structures*, 27(3):314–323, February 2016.

- [102] Martin D Hager, Stefan Bode, Christine Weber, and Ulrich S Schubert. Shape memory polymers: Past, present and future developments. *Progress in Polymer Science*, 49-50:3–33, October 2015.
- [103] B C Hancock and G Zografi. The Relationship Between the Glass-Transition Temperature and the Water-Content of Amorphous Pharmaceutical Solids. *Pharmaceutical Research*, 11(4):471–477, April 1994.
- [104] Christopher J Hansen. 3D and 4D printing of nanomaterials: Processing considerations for reliable printed nanocomposites. In *3D and 4D Printing of Polymer Nanocomposite Materials*, pages 25–44. Elsevier, 2020.
- [105] T Hatakeyama, K Nakamura, and H Hatakeyama. Determination of bound water content in polymers by DTA, DSC and TG. *Thermochimica Acta*, 123:153–161, 1988.
- [106] S Hayashi. Shape memory polyurethane elastomer molded article, September 1992.
- [107] A Herrera-Gómez, G Velázquez-Cruz, and M O Martín-Polo. Analysis of the water bound to a polymer matrix by infrared spectroscopy. *Journal of Applied Physics*, 89(10):5431–8, 2001.
- [108] Lindsey Hines, Veaceslav Arabagi, and Metin Sitti. Shape Memory Polymer-Based Flexure Stiffness Control in a Miniature Flapping-Wing Robot. *IEEE Transactions on Robotics*, 28(4):987–990.
- [109] Suong V Hoa and Xiao Cai. Twisted composite structures made by 4D printing method. *Composite Structures*, 238:111883, April 2020.
- [110] Alina-Maria Holban and Alexandru Grumezescu. *Materials for Biomedical Engineering: Nanobiomaterials in Tissue Engineering*. Elsevier, March 2019.
- [111] Seok Jin Hong, Woong-Ryeol Yu, and Ji Ho Youk. Two-way shape memory behavior of shape memory polyurethanes with a bias load. *Smart Materials and Structures*, 19(3):035022, March 2010.
- [112] Seok Jin Hong, Woong-Ryeol Yu, Ji Ho Youk, and Yang Rae Cho. Polyurethane smart fiber with shape memory function: Experimental characterization and constitutive modelling. *Fibers and Polymers*, 8(4):377–385, 2007.
- [113] G F Hu, A R Damanpack, M Bodaghi, and W H Liao. Increasing dimension of structures by 4D printing shape memory polymers via fused deposition modeling. *Smart Materials and Structures*, 26(1):125023, December 2017.

- [114] Jin Lian Hu, Feng Long Ji, and Yuen Wah Wong. Dependency of the shape memory properties of a polyurethane upon thermomechanical cyclic conditions. *Polymer International*, 54(3):600–605, 2005.
- [115] Jinlian Hu, Yong Zhu, Huahua Huang, and Jing Lu. Recent advances in shape-memory polymers: Structure, mechanism, functionality, modeling and applications. *Progress in Polymer Science*, 37(12):1720–1763, December 2012.
- [116] Dechuan Hua, Xiaoqin Zhang, Zhongying Ji, Changyou Yan, Bo Yu, Yuandong Li, Xiaolong Wang, and Feng Zhou. 3D printing of shape changing composites for constructing flexible paper-based photothermal bilayer actuators. *J. Mater. Chem. C*, 6(8):2123–2131, 2018.
- [117] W. M. Huang, B. Yang, L An, C. Li, and Y S Chan. Water-driven programmable polyurethane shape memory polymer: Demonstration and mechanism. *Applied Physics Letters*, 86(11):1–3, March 2005.
- [118] W. M. Huang, B. Yang, Y. Zhao, and Z. Ding. Thermo-moisture responsive polyurethane shape-memory polymer and composites: A review. *Journal of Materials Chemistry*, 20(17):3367–3381, June 2010.
- [119] Wei Min Fu Yong Qing Yang Bin Huang. Polyurethane Shape Memory Polymers. pages 1–374, October 2011.
- [120] Yong Huang, W Yang, and Bin Fu. Effects of Moisture on Electrically Conductive Polyurethane Shape Memory Polymers. In *Future of Polyurethane Shape Memory Polymers*, pages 93–116. CRC Press, December 2011.
- [121] Marta Invernizzi, Stefano Turri, Marinella Levi, and Raffaella Suriano. 4D printed thermally activated self-healing and shape memory polycaprolactone-based polymers. *European Polymer Journal*, 101:169–176, April 2018.
- [122] Danish Iqbal and Muhammad Samiullah. Photo-Responsive Shape-Memory and Shape-Changing Liquid-Crystal Polymer Networks. *Materials*, 6(1):116–142, January 2013.
- [123] Chetan S Jarali, S Raja, and A R Upadhya. Constitutive modeling of SMA SMP multifunctional high performance smart adaptive shape memory composite. *Smart Materials and Structures*, 19(10):105029–10, September 2010.
- [124] H M Jeong, J B Lee, S Y Lee, and B K Kim. Shape memory polyurethane containing mesogenic moiety. *Journal of Materials Science*, 35(2):279–283, 2000.
- [125] F L Ji, J L Hu, and J P Han. Shape memory polyurethane-ureas based on isophorone diisocyanate. *High Performance Polymers*, 23(3):177–187, June 2011.

- [126] Bingcong Jian, Frédéric Demoly, Yicha Zhang, and Samuel Gomes. Towards a Design Framework for Multifunctional Shape Memory Polymer Based Product in the Era of 4D Printing. In *ASME 2018 Conference on Smart Materials, Adaptive Structures and Intelligent Systems*, pages 1–13. American Society of Mechanical Engineers, November 2018.
- [127] Hong-Yang Jiang and Annette M Schmidt. Shape-Memory Polymers and Multifunctional Composites. pages 1–43, May 2010.
- [128] H U Jinlian. *Shape memory polymers and textiles*. Woodhead Publishing Limited, Hong Kong Polytechnic University, Kowloon, Hong Kong, January 2007.
- [129] C S Jithin, S Balasivanandha Prabu, and Ramachandran Velmurugan. Development of Shape Memory Alloy Polymer Composite and Influence of Material Parameters on Shape Memory. *Applied Mechanics and Materials*, 592-594:158–163, July 2014.
- [130] Joanne Teoh, Jia An, Xiaofan Feng, Yue Zhao, Chee Chua, and Yong Liu. Design and 4D Printing of Cross-Folded Origami Structures: A Preliminary Investigation. *Materials*, 11(3):376–27, March 2018.
- [131] Cagri Ayranci Jorge Villacres, David Nobes. Additive manufacturing of shape memory polymers: Effect of print orientation and infill percentage on shape memory recovery properties. *Rapid Prototyping Journal*, June 2020.
- [132] Seno Jose, Jinu Jacob George, Suchart Siengchin, and Jyotishkumar Parameswaranpillai. Introduction to Shape-Memory Polymers, Polymer Blends and Composites: State of the Art, Opportunities, New Challenges and Future Outlook. In *Shape Memory Polymers, Blends and Composites*, pages 1–19. Springer, Singapore, Singapore, 2020.
- [133] Siddharth Joshi, Krishna Rawat, Karunakaran C, Vasudevan Rajamohan, Arun Tom Mathew, Krzysztof Koziol, Vijay Kumar Thakur, and Balan A S S. 4D printing of materials for the future: Opportunities and challenges. *Applied Materials Today*, 18:100490–22, March 2020.
- [134] Lukas Kačergis, Rytis Mitkus, and Michael Sinapius. Influence of fused deposition modeling process parameters on the transformation of 4D printed morphing structures. *Smart Materials and Structures*, 28(10):105042–10, September 2019.
- [135] Minkyu Kang, Youngjun Pyo, Joon young Jang, Yunchan Park, Yeon-Ho Son, MyungChan Choi, Joo wan Ha, Young-Wook Chang, and Caroline Sunyong Lee. Design of a shape memory composite(SMC) using 4D printing technology. *Sensors and Actuators, A: Physical*, 283:187–195, November 2018.
- [136] Nand Jee Kanu, Eva Gupta, Umesh Kumar Vates, and Gyanendra Kumar Singh. Self-healing composites:A state of the art review. *Composites Part A*, 121:474–486, June 2019.

- [137] Kamal K Kar. *Composite materials: processing, applications, characterizations*. Landolt-Börnstein. SpringerMaterials fundamentals. Springer, Berlin, 2017.
- [138] Ayesha Kausar. Review on Technological Significance of Photoactive, Electroactive, pH-sensitive, Water-active, and Thermoresponsive Polyurethane Materials. *Polymer-Plastics Technology and Engineering*, 56(6):606–616, October 2016.
- [139] Brett E Kelly, Indrasen Bhattacharya, Hossein Heidari, Maxim Shusteff, Christopher M Spadaccini, and Hayden K Taylor. Volumetric additive manufacturing via tomographic reconstruction. *Science*, 363(6431):1075–1079, March 2019.
- [140] Hossein Ali Khonakdar, Seyed Hassan Jafari, Sorour Rasouli, Jalil Morshedian, and Hossein Abedini. Investigation and Modeling of Temperature Dependence Recovery Behavior of Shape-Memory Crosslinked Polyethylene. *Macromolecular Theory and Simulations*, 16(1):43–52, January 2007.
- [141] Zhong Xun Khoo, Joanne Ee Mei Teoh, Yong Liu, Chee Kai Chua, Shoufeng Yang, Jia An, Kah Fai Leong, and Wai Yee Yeong. 3D printing of smart materials: A review on recent progresses in 4D printing. *Virtual and Physical Prototyping*, 10(3):103–122, September 2015.
- [142] Mohammad Reza Khosravani and Tamara Reinicke. 3D-printed sensors: Current progress and future challenges. *Sensors and Actuators, A: Physical*, 305:111916, April 2020.
- [143] Byung Chul Kim, Paul M Weaver, and Kevin Potter. Manufacturing characteristics of the continuous tow shearing method for manufacturing of variable angle tow composites. *Composites Part A*, 61(C):141–151, June 2014.
- [144] Ju Hyun Kim, Tae Jin Kang, and Woong-Ryeol Yu. Thermo-mechanical constitutive modeling of shape memory polyurethanes using a phenomenological approach. *International Journal of Plasticity*, 26(2):204–218, February 2010.
- [145] Taeyoung Kim and Yong-Gu Lee. Shape transformable bifurcated stents. *Nature Publishing Group*, 8(1):13911, September 2018.
- [146] Yoonho Kim, Hyunwoo Yuk, Ruike Zhao, Shawn A Chester, and Xuanhe Zhao. Printing ferromagnetic domains for untethered fast-transforming soft materials. *Nature*, 558(7709):274–279, June 2018.
- [147] Hyunhyub Ko and Ali Javey. Smart Actuators and Adhesives for Reconfigurable Matter. *Accounts of Chemical Research*, 50(4):691–702, March 2017.
- [148] Dimitri Kokkinis, Manuel Schaffner, and Andr eacute R Studart. Multimaterial magnetically assisted 3D printing of composite materials. *Nature Communications*, pages 1–10, April 2019.

- [149] Fabian Kranert, Jana Budde, Philipp Neef, Robert Bernhard, Marius Lammers, Katharina Rettschlag, Tobias Grabe, Andreas Wienke, Jörg Neumann, Henning Wiche, Volker Wesling, Henning Ahlers, Roland Lachmayer, and Dietmar Kracht. 3D-printed, low-cost, lightweight optomechanics for a compact, low-power solid-state amplifier system. In Alexei L Glebov and Paul O Leisher, editors, *Components and Packaging for Laser Systems VI*, pages 4–13. SPIE, March 2020.
- [150] Xiao Kuang, Kaijuan Chen, Conner K Dunn, Jiangtao Wu, Vincent C F Li, and H Jerry Qi. 3D Printing of Highly Stretchable, Shape-Memory, and Self-Healing Elastomer toward Novel 4D Printing. *ACS Applied Materials & Interfaces*, 10(8):7381–7388, February 2018.
- [151] Xiao Kuang, Devin J Roach, Jiangtao Wu, Craig M Hamel, Zhen Ding, Tiejun Wang, Martin L Dunn, and Hang Jerry Qi. Advances in 4D Printing: Materials and Applications. *Advanced Functional Materials*, 29(2), January 2019.
- [152] Ruvini S Kularatne, Hyun Kim, Jennifer M Boothby, and Taylor H Ware. Liquid crystal elastomer actuators: Synthesis, alignment, and applications. *Journal of Polymer Science Part B: Polymer Physics*, 55(5):395–411, January 2017.
- [153] Xin Lan, Yanju Liu, Jinsong Leng, and Shanyi Du. Thermomechanical behavior of fiber reinforced shape memory polymer composite. In *International Conference on Smart Materials and Nanotechnology in Engineering*, pages 64235R–8. SPIE, December 2007.
- [154] Xin Lan, Yanju Liu, Haibao Lv, Xiaohua Wang, Jinsong Leng, and Shanyi Du. Fiber reinforced shape-memory polymer composite and its application in a deployable hinge. *Smart Materials and Structures*, 18(2):024002, April 2009.
- [155] S Lashgari, M Karrabi, I Ghasemi, H Azizi, M Messori, and K Paderni. Shape memory nanocomposite of poly(L-lactic acid)/graphene nanoplatelets triggered by infrared light and thermal heating. *Express Polymer Letters*, 10(4):349–359, 2016.
- [156] A Le Duigou, M Castro, R Bevan, and N Martin. 3D printing of wood fibre biocomposites: From mechanical to actuation functionality. *Materials and Design*, 96(C):106–114, April 2016.
- [157] Louis Laberge Lebel, Brahim Aissa, My Ali El Khakani, and Daniel Therriault. Ultraviolet-Assisted Direct-Write Fabrication of Carbon Nanotube/Polymer Nanocomposite Microcoils. *Advanced Materials*, 22(5):592–596, February 2010.
- [158] S Leclercq and C LExcellent. A general macroscopic description of the thermomechanical behavior of shape memory alloys. *Journal of the Mechanics and Physics of Solids*, 44(6):953–980, 1996.

- [159] Amelia Yilin Lee, Jia An, and Chee Kai Chua. Two-Way 4D Printing: A Review on the Reversibility of 3D-Printed Shape Memory Materials. *Engineering*, 3(5):663–674, October 2017.
- [160] E H Lee, American Society of Mechanical Engineers, and STANFORD UNIV CALIF DEPT OF APPLIED MECHANICS. *Elastic-plastic Deformation at Finite Strains*. 1968.
- [161] Ming Lei, Zhen Chen, Haibao Lu, and Kai Yu. Recent progress in shape memory polymer composites: methods, properties, applications and prospects. *Nanotechnology Reviews*, 8(1):327–351, November 2019.
- [162] Ming Lei, Kai Yu, Haibao Lu, and H Jerry Qi. Influence of structural relaxation on thermomechanical and shape memory performances of amorphous polymers. *Additive Manufacturing*, 109:216–228, January 2017.
- [163] Steven K Leist, Dajing Gao, Richard Chiou, and Jack Zhou. Investigating the shape memory properties of 4D printed polylactic acid (PLA) and the concept of 4D printing onto nylon fabrics for the creation of smart textiles. *Virtual and Physical Prototyping*, 12(4):290–300, July 2017.
- [164] Andreas Lendlein, Marc Behl, Bernhard Hiebl, and Christian Wischke. Shape-memory polymers as a technology platform for biomedical applications. *Expert Review of Medical Devices*, 7(3):357–379, May 2010.
- [165] Andreas Lendlein and Oliver E C Gould. Reprogrammable recovery and actuation behaviour of shape-memory polymers. *Nature Reviews Materials*, pages 1–18, January 2019.
- [166] Andreas Lendlein and Steffen Kelch. *Shape-Memory Polymers*. John Wiley & Sons, Inc., Hoboken, NJ, USA, 2002.
- [167] Jinsong Leng and Shanyi Du. *Shape-Memory Polymers and Multifunctional Composites*. CRC Press, May 2010.
- [168] Jinsong Leng, Xin Lan, Yanju Liu, and Shanyi Du. Electroactive thermoset shape memory polymer nanocomposite filled with nanocarbon powders. *Smart Materials and Structures*, 18(7):074003–8, June 2009.
- [169] Jinsong Leng, Xin Lan, Yanju Liu, and Shanyi Du. Shape-memory polymers and their composites: Stimulus methods and applications. *Progress in Materials Science*, 56(7):1077–1135, September 2011.
- [170] Jinsong Leng, Haibao Lu, and Shanyi Du. *Multifunctional Shape-Memory Polymers and Actuation Methods*. CRC Press, Boca Raton, 2010.

- [171] Jinsong Leng, Kai Yu, Jian Sun, and Yanju Liu. Deployable morphing structure based on shape memory polymer. *Aircraft Engineering and Aerospace Technology*, 87(3):218–223, January 2015.
- [172] Jennifer A Lewis, James E Smay, John Stuecker, and Joseph Cesarano. Direct Ink Writing of Three-Dimensional Ceramic Structures. *Journal of the American Ceramic Society*, 89(12):3599–3609, December 2006.
- [173] Christian LExcellent, Pauline Butaud, Emmanuel Folt te, and Morvan Ouisse. A Review of Shape Memory Polymers Thermomechanical Modelling: Analysis in the Frequency Domain. In *Advances in Shape Memory Materials*, pages 57–80. Springer International Publishing, Cham, March 2017.
- [174] Guoqiang Li. *Self-Healing Composites: Shape Memory Polymer Based Structures*. John Wiley & Sons Ltd, Chichester, United Kingdom, November 2014.
- [175] Guoqiang Li and Anqi Wang. Cold, warm, and hot programming of shape memory polymers. *Journal of Polymer Science Part B: Polymer Physics*, 54(14):1319–1339, March 2016.
- [176] Guoqiang Li and Wei Xu. Thermomechanical behavior of thermoset shape memory polymer programmed by cold-compression: Testing and constitutive modeling. *Journal of the Mechanics and Physics of Solids*, 59(6):1231–1250, June 2011.
- [177] Xiaofeng Li, Liancai Wang, Ziyang Zhang, Deyan Kong, Xinling Ao, and Xinli Xiao. Electroactive High-Temperature Shape Memory Polymers with High Recovery Stress Induced by Ground Carbon Fibers. *Macromolecular Chemistry and Physics*, 220(17):1900164–8, September 2019.
- [178] YueJia Li, Fenghua Zhang, Yanju Liu, and Jinsong Leng. 4D printed shape memory polymers and their structures for biomedical applications. *Science China Technological Sciences*, 63(4):545–560, February 2020.
- [179] Zhenghong Li, Haibao Lu, Yongtao Yao, and Long Lin. Thermomechanical performance and shape recovery behaviour of shape memory polymer nanocomposite incorporated with hexagonal boron nitride. *Pigment & Resin Technology*, 46(1):79–83, January 2017.
- [180] Fei Liang, Jihua Gou, He Shen, Yunjun Xu, and Bob Mabbott. Carbon fiber reinforced shape memory nanocomposites incorporated with highly conductive carbon nanopaper for electro actuation. In *ASME 2013 Conference on Smart Materials, Adaptive Structures and Intelligent Systems, SMASIS 2013*. University of Central Florida, Orlando, United States, January 2013.
- [181] Chya-Yan Liaw and Murat Guvendiren. Current and emerging applications of 3D printing in medicine. *Biofabrication*, 9(2):024102–, June 2017.

- [182] Samuel Clark Ligon, Robert Liska, Jürgen Stampfl, Matthias Gurr, and Rolf Mülhaupt. Polymers for 3D Printing and Customized Additive Manufacturing. *Chemical Reviews*, 117(15):10212–10290, July 2017.
- [183] Chutiwat Likitaporn, Phattarin Mora, Sunan Tiptipakorn, and Sarawut Rimdusit. Recovery stress enhancement in shape memory composites from silicon carbide whisker-filled benzoxazine-epoxy polymer alloy. *Journal of Intelligent Material Systems and Structures*, 29(3):388–396, May 2017.
- [184] J R Lin and L W Chen. Shape-memorized crosslinked ester-type polyurethane and its mechanical viscoelastic model. *Journal of Applied Polymer Science*, 73(7):1305–1319, 1999.
- [185] J R Lin and L W Chen. The mechanical-viscoelastic model and WLF relationship in shape memorized linear ether-type polyurethanes. *Journal of Polymer Research*, 6(1):35–40, January 1999.
- [186] C Liu, H Qin, and P T Mather. Review of progress in shape-memory polymers. *Journal of Materials Chemistry*, 17(16):1543, 2007.
- [187] Changdeng Liu, Seung B Chun, Patrick T Mather, Lei Zheng, Elisabeth H Haley, and E Bryan Coughlin. Chemically cross-linked polycyclooctene: Synthesis, characterization, and shape memory behavior. *Macromolecules*, 35(27):9868–9874, December 2002.
- [188] Wenbo Liu, Nan Wu, and Kishore Pochiraju. Shape recovery characteristics of SiC/C/PLA composite filaments and 3D printed parts. *Composites Part A*, 108:1–11, May 2018.
- [189] Yang Liu, Fenghua Zhang, Jinsong Leng, Kun Fu, X Lucas Lu, Liyun Wang, Chase Cotton, Baozhong Sun, Bohong Gu, and Tsu-Wei Chou. Remotely and Sequentially Controlled Actuation of Electroactivated Carbon Nanotube/Shape Memory Polymer Composites. *Advanced Materials Technologies*, 4(12):1900600–8, November 2019.
- [190] Yang Liu, Wei Zhang, Fenghua Zhang, Xin Lan, Jinsong Leng, Shuang Liu, Xinqiao Jia, Chase Cotton, Baozhong Sun, Bohong Gu, and Tsu-Wei Chou. Shape memory behavior and recovery force of 4D printed laminated Miura-origami structures subjected to compressive loading. *COMPOSITES PART B*, 153:233–242, November 2018.
- [191] Yang Liu, Wei Zhang, Fenghua Zhang, Jinsong Leng, Shaopeng Pei, Liyun Wang, Xinqiao Jia, Chase Cotton, Baozhong Sun, and Tsu-Wei Chou. Microstructural design for enhanced shape memory behavior of 4D printed composites based on carbon nanotube/poly(lactic acid) filament. *Composites Science and Technology*, 181:107692, September 2019.

- [192] Yanju Liu, Haiyang Du, Liwu Liu, and Jinsong Leng. Shape memory polymers and their composites in aerospace applications: a review. *Smart Materials and Structures*, 23(2):023001, February 2014.
- [193] Yanju Liu, Haibao Lv, Xin Lan, Jinsong Leng, and Shanyi Du. Review of electro-active shape-memory polymer composite. *Composites Science and Technology*, 69(13):2064–2068, October 2009.
- [194] Ye Liu, Ying Li, Guang Yang, Xiaotong Zheng, and Shaobing Zhou. Multi-Stimulus-Responsive Shape-Memory Polymer Nanocomposite Network Cross-Linked by Cellulose Nanocrystals. *ACS Applied Materials & Interfaces*, 7(7):4118–4126, February 2015.
- [195] Ying Liu, Julie K Boyles, Jan Genzer, and Michael D Dickey. Self-folding of polymer sheets using local light absorption. *Soft Matter*, 8(6):1764–1769, 2012.
- [196] Yiping Liu, Ken Gall, Martin L Dunn, Alan R Greenberg, and Julie Diani. Thermomechanics of shape memory polymers: Uniaxial experiments and constitutive modeling. *International Journal of Plasticity*, 22(2):279–313, February 2006.
- [197] F J Lockett. *Nonlinear viscoelastic solids*. London, New York, Academic Press, 1972.
- [198] Kevin N Long, Martin L Dunn, and H Jerry Qi. Mechanics of soft active materials with phase evolution. *International Journal of Plasticity*, 26(4):603–616, April 2010.
- [199] Amit J Lopes, Mireya A Perez, David Espalin, and Ryan B Wicker. Comparison of ranking models to evaluate desktop 3D printers in a growing market. *Additive Manufacturing*, 35:101291, May 2020.
- [200] Ze-Xian Low, Yen Thien Chua, Brian Michael Ray, Davide Mattia, Ian Saxley Metcalfe, and Darrell Alec Patterson. Perspective on 3D printing of separation membranes and comparison to related unconventional fabrication techniques. *Journal of Membrane Science*, 523(C):596–613, February 2017.
- [201] Haibao Lu, Yongtao Yao, and Long Lin. Carbon-based reinforcement in shape-memory polymer composite for electrical actuation. *Pigment & Resin Technology*, 43(1):26–34, December 2013.
- [202] Hongsheng Luo, Zhiwei Li, Guobin Yi, Xihong Zu, Huan Wang, Yunjia Wang, Hailiang Huang, Jiwen Hu, Zhenfei Liang, and Benbin Zhong. Electro-responsive silver nanowire-shape memory polymer composites. *Materials Letters*, 134(C):172–175, November 2014.
- [203] Son Thai Ly and Joo Yong Kim. 4D printing – fused deposition modeling printing with thermal-responsive shape memory polymers. *International Journal of Precision Engineering and Manufacturing-Green Technology*, 4(3):267–272, July 2017.

- [204] Xiaoang Ma. Bending of a polyurethane based shape memory polymer: modeling and experiment . June 2018.
- [205] Russell W Mailen, Michael D Dickey, Jan Genzer, and Mohammed A Zikry. A fully coupled thermo-viscoelastic finite element model for self-folding shape memory polymer sheets. *Journal of Polymer Science Part B: Polymer Physics*, 55(16):1207–1219, May 2017.
- [206] Sirisala Mamatha, Papiya Biswas, Pandu Ramavath, Dibakar Das, and Roy Johnson. 3D printing of complex shaped alumina parts. *Ceramics International*, 44(16):19278–19281, November 2018.
- [207] Yiqi Mao, Zhen Ding, Chao Yuan, Shigang Ai, Michael Isakov, Jiangtao Wu, Tiejun Wang, Martin L Dunn, and H Jerry Qi. 3D Printed Reversible Shape Changing Components with Stimuli Responsive Materials. *Nature Publishing Group*, 6(1):24761, April 2016.
- [208] Yiqi Mao, Kai Yu, Michael S Isakov, Jiangtao Wu, Martin L Dunn, and H Jerry Qi. Sequential Self-Folding Structures by 3D Printed Digital Shape Memory Polymers. *Nature Publishing Group*, 5(1):13616–12, September 2015.
- [209] American Society for Testing and Materials. *ISO and IEC selected standards for the plastics industry*. Astm Intl, 1996.
- [210] Patrick T Mather, Xiaofan Luo, and Ingrid A Rousseau. Shape Memory Polymer Research. *Annual Review of Materials Research*, 39:445–471, August 2009.
- [211] Amber J W McClung, Gyaneshwar P Tandon, and Jeffery W Baur. Deformation rate-, hold time-, and cycle-dependent shape-memory performance of Veriflex-E resin. *Mechanics of Time-Dependent Materials*, 17(1):39–52, February 2013.
- [212] Joselle M McCracken, Brian R Donovan, and Timothy J White. Materials as Machines. *Advanced Materials*, 1060202:1906564–48, March 2020.
- [213] Marlon Meier, Kim Hua Tan, Ming K Lim, and Leanne Chung. Unlocking innovation in the sport industry through additive manufacturing. *Business Process Management Journal*, 25(3):456–475, June 2019.
- [214] Stephen Kirwa Melly, Liwu Liu, Yanju Liu, and Jinsong Leng. Active composites based on shape memory polymers: overview, fabrication methods, applications, and future prospects. *Journal of Materials Science*, pages 1–77, May 2020.
- [215] Kevin P Menard. *Dynamic Mechanical Analysis. A Practical Introduction*, Second Edition. CRC Press, May 2008.

- [216] Harper Meng and Guoqiang Li. A review of stimuli-responsive shape memory polymer composites. *Polymer (United Kingdom)*, 54(9):2199–2221, April 2013.
- [217] Qinghao Meng, Jinlian Hu, KaiChiu Ho, Fenglong Ji, and Shaojun Chen. The Shape Memory Properties of Biodegradable Chitosan/Poly(l-lactide) Composites. *Journal of Polymers and the Environment*, 17(3):212–224, October 2009.
- [218] J Dyana Merline, C P Reghunadhan Nair, C Gouri, G G Bandyopadhyay, and K N Ninan. Polyether polyurethanes: Synthesis, characterization, and thermoresponsive shape memory properties. *Journal of Applied Polymer Science*, 107(6):4082–4092, 2007.
- [219] Shida Miao, Nathan Castro, Margaret Nowicki, Lang Xia, Haitao Cui, Xuan Zhou, Wei Zhu, Se-jun Lee, Kausik Sarkar, Giovanni Vozzi, Yasuhiko Tabata, John Fisher, and Lijie Grace Zhang. 4D printing of polymeric materials for tissue and organ regeneration. *Materials Today*, 20(10):577–591, December 2017.
- [220] Simone Micalizzi, Andrés Díaz Lantada, and Carmelo De Maria. Shape-memory actuators manufactured by dual extrusion multimaterial 3d printing of conductive and non-conductive filaments. *Smart Materials and Structures*, 28(10):105025–13, September 2019.
- [221] A Mitchell, U Lafont, M Holyńska, and C Semprimoschnig. Additive manufacturing — A review of 4D printing and future applications. *Additive Manufacturing*, 24:606–626, December 2018.
- [222] Farhang Momeni, Seyed M Mehdi Hassani N, Xun Liu, and Jun Ni. A review of 4D printing. *Materials and Design*, 122(C):42–79, May 2017.
- [223] Milad Momtaz, Mohammad Razavi-Nouri, and Mehdi Barikani. Effect of block ratio and strain amplitude on thermal, structural, and shape memory properties of segmented polycaprolactone-based polyurethanes. *Journal of Materials Science*, 49:7575–7584, November 2014.
- [224] Charles L Moore and Hugh A Bruck. A fundamental investigation into large strain recovery of one-way shape memory alloy wires embedded in flexible polyurethanes. *Smart Materials and Structures*, 11(1):130–139, February 2002.
- [225] Jalil Morshedian, Hossein A Khonakdar, and Sorour Rasouli. Modeling of Shape Memory Induction and Recovery in Heat-Shrinkable Polymers. *Macromolecular Theory and Simulations*, 14(7):428–434, August 2005.
- [226] Ziad Mourni, Wael Zaki, and Quoc Son Nguyen. Theoretical and numerical modeling of solid-solid phase change: Application to the description of the thermomechanical behavior of shape memory alloys. *International Journal of Plasticity*, 24(4):614–645, April 2008.

- [227] Quanyi Mu, Conner K Dunn, Lei Wang, Martin L Dunn, H Jerry Qi, and Tiejun Wang. Thermal cure effects on electromechanical properties of conductive wires by direct ink write for 4D printing and soft machines. *Smart Materials and Structures*, 26(4):045008–14, February 2017.
- [228] Tong Mu, Liwu Liu, Xin Lan, Yanju Liu, and Jinsong Leng. Shape memory polymers for composites. *Composites Science and Technology*, 160:169–198, May 2018.
- [229] F Najafi and M Rajabi. Thermal gravity analysis for the study of stability of graphene oxide-glycine nanocomposites. *International Nano Letters*, 5(4):187–190, May 2015.
- [230] Seokwoo Nam and Eujin Pei. A taxonomy of shape-changing behavior for 4D printed parts using shape-memory polymers. *Progress in Additive Manufacturing*, 4(2):167–184, March 2019.
- [231] L De Nardo, S Bertoldi, M C Tanzi, H J Haugen, and S Far. Shape memory polymer cellular solid design for medical applications. *Smart Materials and Structures*, 20(3):035004–6, February 2011.
- [232] Robin M Neville, Jianguo Chen, Xiaogang Guo, Fenghua Zhang, Wenxin Wang, Yousef Dobah, Fabrizio Scarpa, Jinsong Leng, and Hua-Xin Peng. A Kirigami shape memory polymer honeycomb concept for deployment. *Smart Materials and Structures*, 26(5):05LT03, April 2017.
- [233] Wei Long Ng, Jia Min Lee, Miaomiao Zhou, Yi-Wen Chen, Kai-Xing Alvin Lee, Wai Yee Yeong, and Yu-Fang Shen. Vat polymerization-based bioprinting—process, materials, applications and regulatory challenges. *Biofabrication*, 12(2):022001–23, April 2020.
- [234] T D Ngo, A Kashani, G Imbalzano, KTQ Nguyen Composites Part B, and 2018. Additive manufacturing (3D printing): A review of materials, methods, applications and challenges. *Sensors and Actuators A:Physical*, 143:172–196, June 2018.
- [235] Thao D Nguyen, H Jerry Qi, Francisco Castro, and Kevin N Long. A thermoviscoelastic model for amorphous shape memory polymers: Incorporating structural and stress relaxation. *Journal of the Mechanics and Physics of Solids*, 56(9):2792–2814, 2008.
- [236] Thao D Nguyen, Christopher M Yakacki, Parth D Brahmhatt, and Matthew L Chambers. Modeling the relaxation mechanisms of amorphous shape memory polymers. *Advanced materials (Deerfield Beach, Fla.)*, 22(31):3411–3423, August 2010.
- [237] Qing-Qing Ni, Chun-sheng Zhang, Yaqin Fu, Guangze Dai, and Teruo Kimura. Shape memory effect and mechanical properties of carbon nanotube/shape memory polymer nanocomposites. *Composite Structures*, 81(2):176–184, November 2007.

- [238] Neri Oxman. Variable property rapid prototyping. *Virtual and Physical Prototyping*, 6(1):3–31, March 2011.
- [239] Cem Ozan, Wouter Van Der Zee, Martin Brudy, and Justin Vinson. Mechanical Modeling of Shape Memory Polyurethane Foam for Application as a Sand Management Solution. In *SPE Annual Technical Conference and Exhibition*. Society of Petroleum Engineers, 2011.
- [240] Mahyar Panahi-Sarmad, Mahbod Abrisham, Mina Noroozi, Arian Amirikiai, Parham Dehghan, Vahabodin Goodarzi, and Benjamin Zahiri. Deep focusing on the role of microstructures in shape memory properties of polymer composites: A critical review. *European Polymer Journal*, 117:280–303, August 2019.
- [241] Haedong Park, Philip Harrison, Zaoyang Guo, Myoung-Gue Lee, and Woong-Ryeol Yu. Three-dimensional constitutive model for shape memory polymers using multiplicative decomposition of the deformation gradient and shape memory strains. *Mechanics of Materials*, 93:43–62, October 2015.
- [242] Martin Pastor. Simple particle tracking, matlab central file exchange.
- [243] Devendra Patil and Gangbing Song. A review of shape memory material’s applications in the offshore oil and gas industry. *Smart Materials and Structures*, 26(9):093002–18, August 2017.
- [244] Zhiqiang Pei, Yang Yang, Qiaomei Chen, Eugene M Terentjev, Yen Wei, and Yan Ji. Mouldable liquid-crystalline elastomer actuators with exchangeable covalent bonds. *Nature Materials*, pages 1–6, January 2013.
- [245] D M Phillips and J W Baur. A microvascular method for thermal activation and deactivation of shape memory polymers. *Journal of Intelligent Material Systems and Structures*, 24(10):1233–1244, 2013.
- [246] E A Pieczyska, M Staszczak, M Maj, K Kowalczyk-Gajewska, K Golasiński, M Cristea, H Tobushi, and S Hayashi. Investigation of thermomechanical couplings, strain localization and shape memory properties in a shape memory polymer subjected to loading at various strain rates. *Smart Materials and Structures*, 25(8):085002, August 2016.
- [247] Elzbieta Alicja Pieczyska, Michal Maj, Katarzyna Kowalczyk-Gajewska, Maria Staszczak, Leszek Urbanski, Hisaaki Tobushi, Shunichi Hayashi, and Mariana Cristea. Mechanical and Infrared Thermography Analysis of Shape Memory Polyurethane. *Journal of Materials Engineering and Performance*, 23(7):2553–2560, April 2014.
- [248] A Pilipovic, P Raos, M Sercer Tehnicki Vjesnik, and 2011. Experimental Testing of Quality of Polymer Parts Produced by Laminated Object Manufacturing- LOM. *Technical Gazette*, 18, 2011.

- [249] A C Pinho, C S Buga, and A P Piedade. The chemistry behind 4D printing. *Applied Materials Today*, 19:100611, March 2020.
- [250] Giovanni Postiglione, Gabriele Natale, Gianmarco Griffini, Marinella Levi, and Stefano Turri. Conductive 3D microstructures by direct 3D printing of polymer/carbon nanotube nanocomposites via liquid deposition modeling. *Composites Part A*, 76(C):110–114, September 2015.
- [251] H J Qi and M C Boyce. Stress-strain behavior of thermoplastic polyurethanes. *Mechanics of Materials*, 37(8):817–839, August 2005.
- [252] H Jerry Qi, Thao D Nguyen, Francisco Castro, Christopher M Yakacki, and Robin Shandas. Finite deformation thermo-mechanical behavior of thermally induced shape memory polymers. *Journal of the Mechanics and Physics of Solids*, 56(5):1730–1751, May 2008.
- [253] Xiaodong Qi, Hao Xiu, Yuan Wei, Yan Zhou, Yilan Guo, Rui Huang, Hongwei Bai, and Qiang Fu. Enhanced shape memory property of polylactide/thermoplastic poly(ether)urethane composites via carbon black self-networking induced co-continuous structure. *Composites Science and Technology*, 139:8–16, February 2017.
- [254] Abishera Ravichandra Rajkumar and Kumar Shanmugam. Additive manufacturing-enabled shape transformations via FFF 4D printing. *Journal of Materials Research*, 33(24):4362–4376, December 2018.
- [255] Prasansha Rastogi and Balasubramanian Kandasubramanian. Breakthrough in the printing tactics for stimuli-responsive materials: 4D printing. *Chemical Engineering Journal*, 366:264–304, June 2019.
- [256] Debdatta Ratna and J Karger-Kocsis. Recent advances in shape memory polymers and composites: a review. *Journal of Materials Science*, 43(1):254–269, 2008.
- [257] S G Rauscher. Testing and analysis of shape-memory polymers for morphing aircraft skin application. 2008.
- [258] Dan Raviv, Wei Zhao, Carrie McKnelly, Athina Papadopoulou, Achuta Kadambi, Boxin Shi, Shai Hirsch, Daniel Dikovsky, Michael Zyacki, Carlos Olguin, Ramesh Raskar, and Skylar Tibbits. Active Printed Materials for Complex Self-Evolving Deformations. *Nature Publishing Group*, 4(1):153–8, December 2014.
- [259] S Reese, M Böl, and D Christ. Finite element-based multi-phase modelling of shape memory polymer stents. *Computer Methods in Applied Mechanics and Engineering*, 199(21-22):1276–1286, April 2010.

- [260] H K Reimschuessel. Relationships on the effect of water on glass transition temperature and young's modulus of nylon 6. *Journal of Polymer Science: Polymer Chemistry Edition*, 16(6):1229–1236, June 1978.
- [261] Du Ren, Yujie Chen, Senlin Yang, Hua Li, Hafeez Ur Rehman, and Hezhou Liu. Fast and Efficient Electric-Triggered Self-Healing Shape Memory of CNTs@rGO Enhanced PCLPLA Copolymer. *Macromolecular Chemistry and Physics*, 220(21):1900281–8, September 2019.
- [262] Kailiang Ren, Robert S Bortolin, and Q M Zhang. An investigation of a thermally steerable electroactive polymer/shape memory polymer hybrid actuator. *Applied Physics Letters*, 108(6):062901–6, February 2016.
- [263] D A Roberson, D Espalin, and R B Wicker. 3D printer selection: A decision-making evaluation and ranking model. *Virtual and Physical Prototyping*, 8(3):201–212, October 2013.
- [264] Jennifer N Rodriguez, Cheng Zhu, Eric B Duoss, Thomas S Wilson, Christopher M Spadacini, and James P Lewicki. Shape-morphing composites with designed micro-architectures. *Nature Publishing Group*, pages 1–10, June 2016.
- [265] A A Rogovoy and O S Stolbova. Modeling the behaviour of shape memory materials under large deformations. *IOP Conference Series: Materials Science and Engineering*, 208(1):012036–, June 2017.
- [266] Stian Romberg, Christopher Hershey, John Lindahl, William Carter, Brett Compton, and Vlastimil Kunc. Large-scale Additive Manufacturing of Highly Exothermic Reactive Polymer Systems. In *SAMPE 2013 - Education & Green Sky*. SAMPE, April 2019.
- [267] Jonathan Rossiter and Sina Sareh. Kirigami design and fabrication for biomimetic robotics. In Akhlesh Lakhtakia, editor, *SPIE Smart Structures and Materials + Nondestructive Evaluation and Health Monitoring*, pages 90550G–9. SPIE, March 2014.
- [268] Ingrid A Rousseau and Tao Xie. Shape memory epoxy: Composition, structure, properties and shape memory performances. *Journal of Materials Chemistry*, 20(17):3431–3441, June 2010.
- [269] Ela Sachyani Keneth, Rama Lieberman, Matthew Rednor, Giulia Scalet, Ferdinando Auricchio, and Shlomo Magdassi. Multi-Material 3D Printed Shape Memory Polymer with Tunable Melting and Glass Transition Temperature Activated by Heat or Light. *Polymers*, 12(3):710–12, March 2020.
- [270] Kishor Kumar Sadasivuni, Kalim Deshmukh, and Mariam AlAli AlMaadeed. *3D and 4D Printing of Polymer Nanocomposite Materials*. Processes, Applications, and Challenges. Elsevier, October 2019.

- [271] Takenobu Sakai, Takayuki Tao, and Satoshi Somiya. Estimation of creep and recovery behavior of a shape memory polymer. *Mechanics of Time-Dependent Materials*, 19(4):569–579, November 2015.
- [272] A I Salimon, F S Senatov, V A Kalyaev, and A M Korsunsky. *Chapter 6 - Shape memory polymer blends and composites for 3D and 4D printing applications*. Elsevier Inc., 2020.
- [273] David Santiago, Francesc Ferrando, and Silvia De la Flor. Influence of holding time on shape recovery in a polyurethane shape-memory polymer. In *Journal of Materials Engineering and Performance*, pages 2567–2573. Universitat Rovira i Virgili, Tarragona, Spain, January 2014.
- [274] G Scalet, F Auricchio, E Bonetti, L Castellani, D Ferri, M Pachera, and F Scavello. An experimental, theoretical and numerical investigation of shape memory polymers. *International Journal of Plasticity*, 67:127–147, April 2015.
- [275] Christian Schuh, Kerstin Schuh, Maria C Lechmann, Louis Garnier, and Arno Kraft. Shape-Memory Properties of Segmented Polymers Containing Aramid Hard Segments and Polycaprolactone Soft Segments. *Polymers*, 2(2):71–85, June 2010.
- [276] Xinxin Shen, Baoxian Jia, Hanxing Zhao, Xing Yang, and Zhengxian Liu. Study on 3D printing process of continuous carbon fiber reinforced shape memory polymer composites. *IOP Conference Series: Materials Science and Engineering*, 563:022029–8, July 2019.
- [277] MD Nahin Islam Shiblee, Kumkum Ahmed, Masaru Kawakami, and Hidemitsu Furukawa. 4D Printing of Shape-Memory Hydrogels for Soft-Robotic Functions. *Advanced Materials Technologies*, 4(8):1900071–10, June 2019.
- [278] Ming-You Shie, Yu-Fang Shen, Suryani Dyah Astuti, Alvin Kai-Xing Lee, Shu-Hsien Lin, Ni Luh Bella Dwijaksara, and Yi-Wen Chen. Review of Polymeric Materials in 4D Printing Biomedical Applications. *Polymers*, 11(11):1864–17, November 2019.
- [279] Ward Small, Patrick R Buckley, Thomas S Wilson, William J Benett, Jonathan Hartman, David Saloner, and Duncan J Maitland. Shape memory polymer stent with expandable foam: a new concept for endovascular embolization of fusiform aneurysms. *IEEE Transactions on Biomedical Engineering*, 54(6 Pt 2):1157–1160, June 2007.
- [280] Ward Small IV, Pooja Singhal, Thomas S Wilson, and Duncan J Maitland. Biomedical applications of thermally activated shape memory polymers. *Journal of Materials Chemistry*, 20(17):3356–11, 2010.
- [281] Witold Sokolowski, Annick Metcalfe, Shunichi Hayashi, L’Hocine Yahia, and Jean Raymond. Medical applications of shape memory polymers. In *Biomedical Materials*, pages S23–S27. Jet

- Propulsion Laboratory, California Institute of Technology, Pasadena, United States, March 2007.
- [282] Janice J Song, Quan Chen, and Hani E Naguib. Constitutive modeling and experimental validation of the thermo-mechanical response of a shape memory composite containing shape memory alloy fibers and shape memory polymer matrix. *Journal of Intelligent Material Systems and Structures*, 27(5):625–641, March 2015.
- [283] V Srivastava. *large-deformation thermo-mechanically coupled elastic-viscoplastic theory for amorphous polymers: modeling of micro-scale forming and the shape memory phenomenon*. PhD thesis, Massachusetts Institute of Technology, 2010.
- [284] Vikas Srivastava, Shawn A Chester, Nicoli M Ames, and Lallit Anand. A thermo-mechanically-coupled large-deformation theory for amorphous polymers in a temperature range which spans their glass transition. *International Journal of Plasticity*, 26(8):1138–1182, August 2010.
- [285] Vikas Srivastava, Shawn A Chester, and Lallit Anand. Thermally actuated shape-memory polymers: Experiments, theory, and numerical simulations. *Journal of the Mechanics and Physics of Solids*, 58(8):1100–1124, August 2010.
- [286] Panagiotis Stavropoulos and Panagis Foteinopoulos. Modelling of additive manufacturing processes: a review and classification. *Manufacturing Review*, 5:2–26, March 2018.
- [287] Andrew Stevenson. Effect of crystallization on the mechanical properties of elastomers under large deformations. In *American Society of Mechanical Engineers, Applied Mechanics Division, AMD*, volume 203, pages 1–8, Materials Engineering Research Lab, Ltd, 1995.
- [288] M Straubel, J Block, M Sinapius, and C Hüne. Deployable composite booms for various gossamer space structures. *arc.aiaa.org*, 468:107, June 2012.
- [289] Jian Sun, Qinghua Guan, Yanju Liu, and Jinsong Leng. Morphing aircraft based on smart materials and structures: A state-of-the-art review. *Journal of Intelligent Material Systems and Structures*, 27(17):2289–2312, July 2016.
- [290] Jiefeng Sun and Jianguo Zhao. An Adaptive Walking Robot With Reconfigurable Mechanisms Using Shape Morphing Joints. *IEEE Robotics and Automation Letters*, 4(2):724–731, April 2019.
- [291] Ke Sun, Teng-Sing Wei, Bok Yeop Ahn, Jung Yoon Seo, Shen J Dillon, and Jennifer A Lewis. 3D Printing of Interdigitated Li-Ion Microbattery Architectures. *Advanced Materials*, 25(33):4539–4543, June 2013.

- [292] L Sun, W M Huang, Z Ding, Y Zhao, C C Wang, H Purnawali, and C Tang. Stimulus-responsive shape memory materials: A review. *Materials and Design*, 33(1):577–640, January 2012.
- [293] L Sun, W. M. Huang, Z. Ding, Y. Zhao, C C Wang, H Purnawali, and C Tang. Stimulus-responsive shape memory materials: A review. *Materials and Design*, 33(1):577–640, January 2012.
- [294] Yu-Chen Sun, Yimei Wan, Ryan Nam, Marco Chu, and Hani E Naguib. 4D-printed hybrids with localized shape memory behaviour: Implementation in a functionally graded structure. *Scientific Reports*, 9(1):18754, December 2019.
- [295] James Utama Surjadi, Libo Gao, Huifeng Du, Xiang Li, Xiang Xiong, Nicholas Xuanlai Fang, and Yang Lu. Mechanical Metamaterials and Their Engineering Applications. *Advanced Engineering Materials*, 21(3):1800864, December 2018.
- [296] T Takahashi, N Hayashi, and S Hayashi. Structure and properties of shape-memory polyurethane block copolymers. *Journal of Applied Polymer Science*, 60(7):1061–1069, 1996.
- [297] Lin Tan, Lu Gan, Jinlian Hu, Yong Zhu, and Jianping Han. Functional shape memory composite nanofibers with graphene oxide filler. *Composites Part A*, 76(C):115–123, September 2015.
- [298] Junkun Tang, Yan Zhou, Liqiang Wan, and Farong Huang. Automatically Programmable Shape-Memory Polymers Based on Asymmetric Swelling of Bilayer Structures. *Macromolecular Rapid Communications*, 39(9):1800039–7, March 2018.
- [299] Hitachi High Tech. Thermal analysis of polylactic acid. pages 1–4, February 2013.
- [300] SMP Technologies. SMP technologies.
- [301] Suman Thakur and Niranjana Karak. Bio-based tough hyperbranched polyurethane–graphene oxide nanocomposites as advanced shape memory materials. *RSC Advances*, 3(24):9476–7, 2013.
- [302] C Thill, J Etches, I Bond, K Potter, and P Weaver. Morphing skins. *Aeronautical Journal*, 112(1129):117–139, January 2008.
- [303] S Tibbits. The emergence of “4D printing”. TED, TED, 2013.
- [304] H Tobushi, T Hashimoto, S Hayashi, and E Yamada. Thermomechanical constitutive modeling in shape memory polymer of polyurethane series. *Journal of Intelligent Material Systems and Structures*, 8(8):711–718, August 1997.

- [305] H Tobushi, T Hashimoto, N Ito, S Hayashi, and E Yamada. Shape Fixity and Shape Recovery in a Film of Shape Memory Polymer of Polyurethane Series. *Journal of Intelligent Material Systems and Structures*, 9(2):127–136, 1998.
- [306] H Tobushi, S Hayashi, K Hoshio, and N Miwa. Influence of strain-holding conditions on shape recovery and secondary-shape forming in polyurethane-shape memory polymer. *Smart Materials and Structures*, 15(4):1033–1038, August 2006.
- [307] Hisaaki Tobushi, Syunichi Hayashi, Kazumasa Hoshio, and Yoshihiro Ejiri. Shape recovery and irrecoverable strain control in polyurethane shape-memory polymer. *Science and Technology of Advanced Materials*, 9(1):015009, January 2008.
- [308] Hisaaki Tobushi, Kayo Okumura, Shunichi Hayashi, and Norimitsu Ito. Thermomechanical constitutive model of shape memory polymer. *Mechanics of Materials*, 33(10):545–554, October 2001.
- [309] Michael T Tolley, Samuel M Felton, Shuhei Miyashita, Lily Xu, ByungHyun Shin, Monica Zhou, Daniela Rus, and Robert J Wood. Self-folding shape memory laminates for automated fabrication. In *IEEE International Conference on Intelligent Robots and Systems*, pages 4931–4936. Harvard University, Cambridge, United States, IEEE, December 2013.
- [310] Antoniya Toncheva, Farid Khelifa, Yoann Paint, Michel Voué, Pierre Lambert, Philippe Dubois, and Jean-Marie Raquez. Fast IR-Actuated Shape-Memory Polymers Using in Situ Silver Nanoparticle-Grafted Cellulose Nanocrystals. *ACS Applied Materials & Interfaces*, 10(35):29933–29942, September 2018.
- [311] A Q Tool. Viscosity and the Extraordinary Heat Effects in Glass. *Journal of Research of the National Bureau of Standards*, 37(2):73–90, 1946.
- [312] Takuya Umedachi, Vishesh Vikas, and Barry A Trimmer. Highly deformable 3-D printed soft robot generating inching and crawling locomotions with variable friction legs. *2013 IEEE/RSJ International Conference on Intelligent Robots and Systems*, pages 4590–4595, November 2013.
- [313] Suong Van Hoa. Development of composite springs using 4D printing method. *Composite Structures*, 210:869–876, February 2019.
- [314] Jorge Villacres, David Nobes, and C. Ayranci. Additive Manufacturing of Shape Memory Polymers: Effects of print orientation and infill percentage on mechanical properties. *Rapid Prototyping Journal*, 24(4):744–751, 2018.
- [315] Brent L Volk, Dimitris C Lagoudas, and Yi-Chao Chen. Analysis of the finite deformation response of shape memory polymers: II. 1D calibration and numerical implementation of a

- finite deformation, thermoelastic model. *Smart Materials and Structures*, 19(7):075006–12, May 2010.
- [316] Brent L Volk, Dimitris C Lagoudas, and Duncan J Maitland. Characterizing and modeling the free recovery and constrained recovery behavior of a polyurethane shape memory polymer. *Smart Materials and Structures*, 20(9):094004, 2011.
- [317] Xue Wan, Fenghua Zhang, Yanju Liu, and Jinsong Leng. CNT-based electro-responsive shape memory functionalized 3D printed nanocomposites for liquid sensors. *Carbon*, 155:77–87, December 2019.
- [318] Anqi Wang, Guoqiang Li, and Harper Meng. Strain rate effect on the thermomechanical behavior of a thermoset shape memory polymer. *Smart Materials and Structures*, 22(8):085033, August 2013.
- [319] Kaojin Wang, Satu Strandman, and X X Zhu. A mini review: Shape memory polymers for biomedical applications. *Frontiers of Chemical Science and Engineering*, 11(2):143–153, April 2017.
- [320] Qingrui Wang, Xiaoyong Tian, Lan Huang, Dichen Li, Andrei V Malakhov, and Alexander N Polilov. Programmable morphing composites with embedded continuous fibers by 4D printing. *Materials and Design*, 155(C):404–413, October 2018.
- [321] Wei Wang, Hugo Rodrigue, Hyung-Il Kim, Min-Woo Han, and Sung-Hoon Ahn. Soft composite hinge actuator and application to compliant robotic gripper. *Composites Part B: Engineering*, 98:397–405, August 2016.
- [322] Wenshou Wang, Peng Ping, Xuesi Chen, and Xiabin Jing. Biodegradable polyurethane based on random copolymer of L-lactide and  $\epsilon$ -caprolactone and its shape-memory property. *Journal of Applied Polymer Science*, 104(6):4182–4187, 2007.
- [323] Wenxin Wang, Yanju Liu, and Jinsong Leng. Recent developments in shape memory polymer nanocomposites: Actuation methods and mechanisms. *Coordination Chemistry Reviews*, 320–321:38–52, August 2016.
- [324] Xiaodong Wang, Haibao Lu, Xiaojuan Shi, Kai Yu, and Yong Qing Fu. A thermomechanical model of multi-shape memory effect for amorphous polymer with tunable segment compositions. *Composites Part B: Engineering*, 160:298–305, March 2019.
- [325] Xin Wang, John Sparkman, and Jihua Gou. Electrical actuation and shape memory behavior of polyurethane composites incorporated with printed carbon nanotube layers. *Composites Science and Technology*, 141:8–15, March 2017.

- [326] Z D Wang, D F Li, Z Y Xiong, and R N Chang. Modeling thermomechanical behaviors of shape memory polymer. *Journal of Applied Polymer Science*, 113(1):651–656, July 2009.
- [327] Zhaojing Wang, Pan Li, and Yuxi Jia. Predicting shape memory characteristics of polyurethane in three-point bending deformation. *Polymers for Advanced Technologies*, 25(10):1130–1134, January 2014.
- [328] Hongqiu Wei, Xavier Cauchy, Ivonne Otero Navas, Yahya Abderrafai, Kambiz Chizari, Utandaraman Sundararaj, Yanju Liu, Jinsong Leng, and Daniel Therriault. Direct 3D Printing of Hybrid Nanofiber-Based Nanocomposites for Highly Conductive and Shape Memory Applications. *ACS Applied Materials & Interfaces*, 11(27):24523–24532, July 2019.
- [329] Hongqiu Wei, Qiwei Zhang, Yongtao Yao, Liwu Liu, Yanju Liu, and Jinsong Leng. Direct-Write Fabrication of 4D Active Shape-Changing Structures Based on a Shape Memory Polymer and Its Nanocomposite. *ACS Applied Materials & Interfaces*, 9(1):876–883, January 2017.
- [330] Ten-Chin Wen, Ming-Sieng Wu, and Chien-Hsin Yang. Spectroscopic Investigations of Poly(oxypropylene)glycol-Based Waterborne Polyurethane Doped with Lithium Perchlorate. *Macromolecules*, 32(8):2712–2720, April 1999.
- [331] David Ian Wimpenny, Pulak M Pandey, and L Jyothish Kumar. *Advances in 3D Printing & Additive Manufacturing Technologies*. Springer, Singapore, August 2016.
- [332] P Wollants, J R Roos, and L Delaey. Thermally- and stress-induced thermoelastic martensitic transformations in the reference frame of equilibrium thermodynamics. *Progress in Materials Science*, 37(3):227–288, January 1993.
- [333] Y S Wong, Z H Stachurski, and S S Venkatraman. Modeling shape memory effect in uncrosslinked amorphous biodegradable polymer. *Polymer*, 52(3):874–880, February 2011.
- [334] Jiangtao Wu, Chao Yuan, Zhen Ding, Michael Isakov, Yiqi Mao, Tiejun Wang, Martin L Dunn, and H Jerry Qi. Multi-shape active composites by 3D printing of digital shape memory polymers. *Nature Publishing Group*, 6(1):773, April 2016.
- [335] Shuiliang Wu, Wensen Xu, G Prasath Balamurugan, Michael R Thompson, Kent E Nielsen, and Frank A Brandys. Recovery behaviour of shape memory polyurethane based laminates after thermoforming. *Smart Materials and Structures*, 26(1):115002, November 2017.
- [336] Xuelian Wu, Wei Huang, Yong Zhao, Zheng Ding, Cheng Tang, and Jiliang Zhang. Mechanisms of the Shape Memory Effect in Polymeric Materials. *Polymers*, 5(4):1169–1202, December 2013.

- [337] Rui Xiao, Jingkai Guo, and Thao D Nguyen. Modeling the multiple shape memory effect and temperature memory effect in amorphous polymers. *RSC Advances*, 5(1):416–423, 2015.
- [338] Rui Xiao and Thao D Nguyen. Thermo-mechanics of Amorphous Shape-memory Polymers. *Procedia IUTAM*, 12:154–161, 2015.
- [339] Rui Xiao, Christopher M Yakacki, Jingkai Guo, Carl P Frick, and Thao D Nguyen. A predictive parameter for the shape memory behavior of thermoplastic polymers. *Journal of Polymer Science Part B: Polymer Physics*, 54(14):1405–1414, January 2016.
- [340] Rui Xiao, Cheng Zhang, and Wei Min Huang. *Chapter Four. Programming of Shape-Memory Polymers: The Temperature Memory Effect and Triple/Multiple-Shape-Memory Effect in Polymers*. Elsevier Inc., 2017.
- [341] Xiaozhou Xin, Liwu Liu, Yanju Liu, and Jinsong Leng. Mechanical Models, Structures, and Applications of Shape-Memory Polymers and Their Composites. *Acta Mechanica Solida Sinica*, 32(5):535–565, June 2019.
- [342] Wei Xu, Ruoyu Zhang, Wei Liu, Jin Zhu, Xia Dong, Hongxia Guo, and Guo-Hua Hu. A Multiscale Investigation on the Mechanism of Shape Recovery for IPDI to PPDI Hard Segment Substitution in Polyurethane. *Macromolecules*, 49(16):5931–5944, 2016.
- [343] B. Yang. Influence of moisture in polyurethane shape memory polymers and their electrically conductive composites. 2007.
- [344] B. Yang, W. M. Huang, C. Li, C M Lee, and L Li. On the effects of moisture in a polyurethane shape memory polymer. *Smart Materials and Structures*, 13(1):191–195, February 2004.
- [345] B. Yang, W. M. Huang, C. Li, and L Li. Effects of moisture on the thermomechanical properties of a polyurethane shape memory polymer. *Polymer*, 47(4):1348–1356, January 2006.
- [346] B. Yang, W. M. Huang, C. Li, L Li, and J H Chor. Qualitative separation of the effects of carbon nano-powder and moisture on the glass transition temperature of polyurethane shape memory polymer. *Scripta Materialia*, 53(1):105–107, July 2005.
- [347] Gi Hoon Yang, Miji Yeo, Young Won Koo, and Geun Hyung Kim. 4D Bioprinting: Technological Advances in Biofabrication. *Macromolecular Bioscience*, 19(5):1800441–10, March 2019.
- [348] Hui Yang, Wan Ru Leow, Ting Wang, Juan Wang, Jiancan Yu, Ke He, Dianpeng Qi, Changjin Wan, and Xiaodong Chen. 3D Printed Photoresponsive Devices Based on Shape Memory Composites. *Advanced Materials*, 29(33):1701627–7, June 2017.

- [349] Mu-Hoe Yang and Yeuh-Hui Lin. Measurement and Simulation of Thermal Stability of Poly(Lactic Acid) by Thermogravimetric Analysis. *Journal of Testing and Evaluation*, 37(4):364–370, July 2009.
- [350] Pengfei Yang, Guangming Zhu, Xuelin Shen, Xiaogang Yan, and Jing Nie. Poly( $\epsilon$ -caprolactone)-based shape memory polymers crosslinked by polyhedral oligomeric silsesquioxane. *RSC Advances*, 6(93):90212–90219, January 2016.
- [351] Qianxi Yang and Guoqiang Li. Investigation into stress recovery behavior of shape memory polyurethane fiber. *Journal of Polymer Science Part B: Polymer Physics*, 52(21):1429–1440, November 2014.
- [352] Qianxi Yang and Guoqiang Li. Temperature and rate dependent thermomechanical modeling of shape memory polymers with physics based phase evolution law. *International Journal of Plasticity*, 80:168–186, May 2016.
- [353] Wen Guang Yang, Haibao Lu, Wei Min Huang, Hang Jerry Qi, Xue Lian Wu, and Ke Yuan Sun. Advanced shape memory technology to reshape product design, manufacturing and recycling. *Polymers*, 6(8):2287–2308, January 2014.
- [354] Yang Yang, Yonghua Chen, Ying Wei, and Yingtian Li. 3D printing of shape memory polymer for functional part fabrication. *International Journal of Advanced Manufacturing Technology*, 84(9-12):2079–2095, June 2016.
- [355] Brahim Yarali, Ali Taheri, and Mostafa Baghani. A comprehensive review on thermomechanical constitutive models for shape memory polymers. *Journal of Intelligent Material Systems . . .*, pages 1–41, May 2020.
- [356] Kenjiro Yazawa, Kana Ishida, Hiroyasu Masunaga, Takaaki Hikima, and Keiji Numata. Influence of Water Content on the  $\beta$ -Sheet Formation, Thermal Stability, Water Removal, and Mechanical Properties of Silk Materials. *Biomacromolecules*, 17(3):1057–1066, March 2016.
- [357] E Yilgor, I Yilgor, and E Yurtsever. Hydrogen bonding and polyurethane morphology. I. Quantum mechanical calculations of hydrogen bond energies and vibrational spectroscopy of model compounds. *Additive Manufacturing*, 43(24):6551–6559, November 2002.
- [358] Wang Yongkun, Zhu Guangming, Tang Yusheng, Liu Tingting, Xie Jianqiang, and Ren Fang. Short glass fiber reinforced radiation crosslinked shape memory SBS/LLDPE blends. *Journal of Applied Polymer Science*, 131(17):n/a–n/a, April 2014.
- [359] Kai Yu, Qi Ge, and H Jerry Qi. Effects of stretch induced softening to the free recovery behavior of shape memory polymer composites. *Polymer (United Kingdom)*, 55(23):5938–5947, November 2014.

- [360] Kai Yu, Qi Ge, and H Jerry Qi. Reduced time as a unified parameter determining fixity and free recovery of shape memory polymers. *Nature Communications*, 5:3066, 2014.
- [361] Kai Yu, Yanjiu Liu, and Jinsong Leng. Conductive Shape Memory Polymer Composite Incorporated with Hybrid Fillers: Electrical, Mechanical, and Shape Memory Properties. *Journal of Intelligent Material Systems and Structures*, 22(4):369–379, May 2011.
- [362] Kai Yu, Amber J W McClung, Gyaneshwar P Tandon, Jeffrey W Baur, and H Jerry Qi. A thermomechanical constitutive model for an epoxy based shape memory polymer and its parameter identifications. *Mechanics of Time-Dependent Materials*, 18(2):453–474, May 2014.
- [363] Kai Yu, David M Phillips, Jeffery W Baur, and H Jerry Qi. Analysis of shape-memory polymer composites with embedded microvascular system for fast thermal response. In *Journal of Composite Materials*, pages 1881–1893. The George W. Woodruff School of Mechanical Engineering, Atlanta, United States, January 2015.
- [364] Kai Yu, Alexander Ritchie, Yiqi Mao, Martin L Dunn, and H Jerry Qi. Controlled Sequential Shape Changing Components by 3D Printing of Shape Memory Polymer Multimaterials. *Procedia IUTAM*, 12:193–203, 2015.
- [365] Chao Yuan, Devin J Roach, Conner K Dunn, Quanyi Mu, Xiao Kuang, Christopher M Yakacki, T J Wang, Kai Yu, and H Jerry Qi. 3D printed reversible shape changing soft actuators assisted by liquid crystal elastomers. *Soft Matter*, 13(33):5558–5568, 2017.
- [366] Shangqin Yuan, Jiaming Bai, Chee Kai Chua, Kun Zhou, and Jun Wei. Characterization of Creeping and Shape Memory Effect in Laser Sintered Thermoplastic Polyurethane. *Journal of Computing and Information Science in Engineering*, 16(4):489–5, November 2016.
- [367] Shangqin Yuan, Fei Shen, Chee Kai Chua, and Kun Zhou. Polymeric composites for powder-based additive manufacturing: Materials and applications. *Progress in Polymer Science*, 91:141–168, April 2019.
- [368] Matt Zarek, Michael Layani, Shira Eliazar, Nicola Mansour, Ido Cooperstein, Efrat Shukrun, Atara Szlar, Daniel Cohn, and Shlomo Magdassi. 4D printing shape memory polymers for dynamic jewellery and fashionwear. *Virtual and Physical Prototyping*, 11(4):263–270, November 2016.
- [369] Matt Zarek, Nicola Mansour, Shir Shapira, and Daniel Cohn. 4D Printing of Shape Memory-Based Personalized Endoluminal Medical Devices. *Macromolecular Rapid Communications*, 38(2):1600628–6, December 2016.

- [370] Chengjun Zeng, Liwu Liu, Wenfeng Bian, Yanju Liu, and Jinsong Leng. 4D printed electro-induced continuous carbon fiber reinforced shape memory polymer composites with excellent bending resistance. *COMPOSITES PART B*, 194:108034, August 2020.
- [371] C Zhang. Computational study of hydrogen-bonding interactions in shape memory polymers. 2014.
- [372] Quan Zhang, Dong Yan, Kai Zhang, and Gengkai Hu. Pattern Transformation of Heat-Shrinkable Polymer by Three-Dimensional (3D) Printing Technique. *Nature Publishing Group*, 5:8936, March 2015.
- [373] Wei Zhang, Fenghua Zhang, Xin Lan, Jinsong Leng, Amanda S Wu, Taylor M Bryson, Chase Cotton, Bohong Gu, Baozhong Sun, and Tsu-Wei Chou. Shape memory behavior and recovery force of 4D printed textile functional composites. *Composites Science and Technology*, 160:224–230, May 2018.
- [374] Qian Zhao, H Jerry Qi, and Tao Xie. Recent progress in shape memory polymer: New behavior, enabling materials, and mechanistic understanding. *Progress in Polymer Science*, 49-50:79–120, October 2015.
- [375] Tingting Zhao, Ran Yu, Xinpan Li, Bing Cheng, Ying Zhang, Xin Yang, Xiaojuan Zhao, Yulei Zhao, and Wei Huang. 4D printing of shape memory polyurethane via stereolithography. *European Polymer Journal*, 101:120–126, April 2018.
- [376] L Zhu and R Pitchumani. Analysis of a process for curing composites by the use of embedded resistive heating elements. *Composites Science and Technology*, 60(14):2699–2712, November 2000.
- [377] Mingzhu Zhu, Mengying Xie, Xuanming Lu, Shima Okada, and Sadao Kawamura. A soft robotic finger with self-powered triboelectric curvature sensor based on multi-material 3D printing. *Nano Energy*, 73:104772, July 2020.
- [378] Yong Zhu, Jinlian Hu, Kwok-wing Yeung, Ka-fai Choi, Yeqiu Liu, and Haiming Liem. Effect of cationic group content on shape memory effect in segmented polyurethane cationomer. *Journal of Applied Polymer Science*, 103(1):545–556, January 2007.
- [379] Ali Zolfagharian, Akif Kaynak, and SY Khoo A. Pattern-driven 4D printing. *Sensors and Actuators A:Physical*, March 2018.
- [380] Ali Zolfagharian, Akif Kaynak, and Abbas Kouzani. Closed-loop 4D-printed soft robots. *Materials and Design*, December 2019.

# Appendices

## A.1 Permissions Related to Chapter 2

This section includes the Copyright permissions for Figure 2.5

## A.1.1 Figure 5

1/17/2021

RightsLink Printable License

### JOHN WILEY AND SONS LICENSE TERMS AND CONDITIONS

Jan 17, 2021

---

This Agreement between Irina Garces ("You") and John Wiley and Sons ("John Wiley and Sons") consists of your license details and the terms and conditions provided by John Wiley and Sons and Copyright Clearance Center.

License Number 4991530304404

License date Jan 17, 2021

Licensed  
Content  
Publisher John Wiley and Sons

Licensed  
Content  
Publication Advanced Materials

Licensed  
Content Title Modeling the Relaxation Mechanisms of Amorphous Shape Memory Polymers

Licensed  
Content Author Thao. D. Nguyen, Christopher M. Yakacki, Parth D. Brahmhatt, et al

Licensed  
Content Date Aug 4, 2010

Licensed  
Content Volume 22

Licensed  
Content Issue 31

Licensed  
Content Pages 13

<https://s100.copyright.com/AppDispatchServlet>

1/6

Type of use      Dissertation/Thesis

Requestor type      University/Academic

Format      Print and electronic

Portion      Figure/table

Number of figures/tables      1

Will you be translating?      No

Title      Shape Memory Polymers and Their Composites: Towards Field Applications via Production, Characterization and Modelling

Institution name      University of Alberta

Expected presentation date      Jan 2021

Portions      Figure 2

Requestor Location      Irina Garces  
Mechanical Engineering Building  
University of Alberta  
116 St & 85 Ave  
Edmonton, AB T6G 2R3  
Canada  
Attn: Irina T. Garces and Cagri Ayranci

Publisher Tax ID      EU826007151

Total      0.00 CAD

Terms and Conditions      243

**TERMS AND CONDITIONS**

## A.2 Permissions Related to Chapter 3

This section includes the Copyright permissions for Figure 4,5

## A.2.1 Figure 4

1/17/2021

RightsLink Printable License

### JOHN WILEY AND SONS LICENSE TERMS AND CONDITIONS

Jan 17, 2021

---

This Agreement between Irina Garces ("You") and John Wiley and Sons ("John Wiley and Sons") consists of your license details and the terms and conditions provided by John Wiley and Sons and Copyright Clearance Center.

License Number 4991500278252

License date Jan 17, 2021

Licensed  
Content  
Publisher John Wiley and Sons

Licensed  
Content  
Publication Advanced Materials

Licensed  
Content Title 3D Printed Photoresponsive Devices Based on Shape Memory Composites

Licensed  
Content Author Xiaodong Chen, Changjin Wan, Dianpeng Qi, et al

Licensed  
Content Date Jun 29, 2017

Licensed  
Content Volume 29

Licensed  
Content Issue 33

Licensed  
Content Pages 7

<https://s100.copyright.com/AppDispatchServlet>

1/6



## A.2.2 Figure 5

1/17/2021

RightsLink Printable License

### ELSEVIER LICENSE TERMS AND CONDITIONS

Jan 17, 2021

---

This Agreement between Irina Garces ("You") and Elsevier ("Elsevier") consists of your license details and the terms and conditions provided by Elsevier and Copyright Clearance Center.

License Number	4991510038706
License date	Jan 17, 2021
Licensed Content Publisher	Elsevier
Licensed Content Publication	Composites Science and Technology
Licensed Content Title	Microstructural design for enhanced shape memory behavior of 4D printed composites based on carbon nanotube/polylactic acid filament
Licensed Content Author	Yang Liu,Wei Zhang,Fenghua Zhang,Jinsong Leng,Shaopeng Pei,Liyun Wang,Xinqiao Jia,Chase Cotton,Baozhong Sun,Tsu-Wei Chou
Licensed Content Date	Sep 8, 2019
Licensed Content Volume	181
Licensed Content Issue	n/a
Licensed Content Pages	1
Start Page	107692

<https://s100.copyright.com/AppDispatchServlet>

1/8

End Page 0

Type of Use reuse in a thesis/dissertation

Portion figures/tables/illustrations

Number of figures/tables/illustrations 1

Format both print and electronic

Are you the author of this Elsevier article? No

Will you be translating? No

Title Shape Memory Polymers and Their Composites: Towards Field Applications via Production, Characterization and Modelling

Institution name University of Alberta

Expected presentation date Jan 2021

Portions Figure 3

Requestor Location Irina Garces  
Mechanical Engineering Building  
University of Alberta  
116 St & 85 Ave  
Edmonton, AB T6G 2R3  
Canada  
Attn: Irina T. Garces and Cagri Ayranci

Publisher Tax ID GB 494 6272 12

Total 0.00 CAD

Terms and Conditions

## A.2.3 Figure 7

**Direct-Write Fabrication of 4D Active Shape-Changing Structures Based on a Shape Memory Polymer and Its Nanocomposite**

**Author:** Hongqiu Wei, Qiwei Zhang, Yongtao Yao, et al  
**Publication:** Applied Materials  
**Publisher:** American Chemical Society  
**Date:** Jan 1, 2017

ACS Publications  
Most Trusted. Most Cited. Most Read.

Copyright © 2017, American Chemical Society

---

**PERMISSION/LICENSE IS GRANTED FOR YOUR ORDER AT NO CHARGE**

This type of permission/license, instead of the standard Terms & Conditions, is sent to you because no fee is being charged for your order. Please note the following:

- Permission is granted for your request in both print and electronic formats, and translations.
- If figures and/or tables were requested, they may be adapted or used in part.
- Please print this page for your records and send a copy of it to your publisher/graduate school.
- Appropriate credit for the requested material should be given as follows: "Reprinted (adapted) with permission from (COMPLETE REFERENCE CITATION). Copyright (YEAR) American Chemical Society." Insert appropriate information in place of the capitalized words.
- One-time permission is granted only for the use specified in your request. No additional uses are granted (such as derivative works or other editions). For any other uses, please submit a new request.

If credit is given to another source for the material you requested, permission must be obtained from that source.

[BACK](#) [CLOSE WINDOW](#)

Figure 1: Free Permission for Academic Purposes

## A.2.4 Figure 9

1/17/2021

RightsLink Printable License

### ELSEVIER LICENSE TERMS AND CONDITIONS

Jan 17, 2021

---

This Agreement between Irina Garces ("You") and Elsevier ("Elsevier") consists of your license details and the terms and conditions provided by Elsevier and Copyright Clearance Center.

License Number 4991511425839

License date Jan 17, 2021

Licensed Content  
Publisher Elsevier

Licensed Content  
Publication Composites Science and Technology

Licensed Content Title Electrical actuation and shape memory behavior of polyurethane composites incorporated with printed carbon nanotube layers

Licensed Content Author Xin Wang, John Sparkman, Jihua Gou

Licensed Content Date Mar 22, 2017

Licensed Content Volume 141

Licensed Content Issue n/a

Licensed Content Pages 8

Start Page 8

End Page 15

<https://s100.copyright.com/AppDispatchServlet>

1/8

Type of Use reuse in a thesis/dissertation

Portion figures/tables/illustrations

Number of figures/tables/illustrations 1

Format both print and electronic

Are you the author of this Elsevier article? No

Will you be translating? No

Title Shape Memory Polymers and Their Composites: Towards Field Applications via Production, Characterization and Modelling

Institution name University of Alberta

Expected presentation date Jan 2021

Portions Figure 1

Requestor Location  
Irina Garces  
Mechanical Engineering Building  
University of Alberta  
116 St & 85 Ave  
Edmonton, AB T6G 2R3  
Canada  
Attn: Irina T. Garces and Cagri Ayranci

Publisher Tax ID GB 494 6272 12

Total 0.00 CAD

Terms and Conditions

251

## INTRODUCTION

## A.2.5 Figure 10

1/17/2021

RightsLink Printable License

### ELSEVIER LICENSE TERMS AND CONDITIONS

Jan 17, 2021

---

This Agreement between Irina Garces ("You") and Elsevier ("Elsevier") consists of your license details and the terms and conditions provided by Elsevier and Copyright Clearance Center.

License Number	4991520130360
License date	Jan 17, 2021
Licensed Content Publisher	Elsevier
Licensed Content Publication	Materials & Design
Licensed Content Title	Programmable morphing composites with embedded continuous fibers by 4D printing
Licensed Content Author	Qingrui Wang,Xiaoyong Tian,Lan Huang,Dichen Li,Andrei V. Malakhov,Alexander N. Polilov
Licensed Content Date	Oct 5, 2018
Licensed Content Volume	155
Licensed Content Issue	n/a
Licensed Content Pages	10
Start Page	404
End Page	413

<https://s100.copyright.com/AppDispatchServlet>

1/8

Type of Use	reuse in a thesis/dissertation
Portion	figures/tables/illustrations
Number of figures/tables/illustrations	2
Format	both print and electronic
Are you the author of this Elsevier article?	No
Will you be translating?	No
Title	Shape Memory Polymers and Their Composites: Towards Field Applications via Production, Characterization and Modelling
Institution name	University of Alberta
Expected presentation date	Jan 2021
Portions	Figure 2 and 7
Requestor Location	Irina Garces Mechanical Engineering Building University of Alberta 116 St & 85 Ave Edmonton, AB T6G 2R3 Canada Attn: Irina T. Garces and Cagri Ayranci
Publisher Tax ID	GB 494 6272 12
Total	0.00 CAD
Terms and Conditions	253

## INTRODUCTION

## A.2.6 Figure 11

1/17/2021

RightsLink Printable License

### ELSEVIER LICENSE TERMS AND CONDITIONS

Jan 17, 2021

---

This Agreement between Irina Garces ("You") and Elsevier ("Elsevier") consists of your license details and the terms and conditions provided by Elsevier and Copyright Clearance Center.

License Number	4991520286268
License date	Jan 17, 2021
Licensed Content Publisher	Elsevier
Licensed Content Publication	Composite Structures
Licensed Content Title	Twisted composite structures made by 4D printing method
Licensed Content Author	Suong V. Hoa,Xiao Cai
Licensed Content Date	Apr 15, 2020
Licensed Content Volume	238
Licensed Content Issue	n/a
Licensed Content Pages	1
Start Page	111883
End Page	0

Type of Use reuse in a thesis/dissertation

Portion figures/tables/illustrations

Number of figures/tables/illustrations 2

Format both print and electronic

Are you the author of this Elsevier article? No

Will you be translating? No

Title Shape Memory Polymers and Their Composites: Towards Field Applications via Production, Characterization and Modelling

Institution name University of Alberta

Expected presentation date Jan 2021

Portions Figure 2 and 6

Requestor Location  
Irina Garces  
Mechanical Engineering Building  
University of Alberta  
116 St & 85 Ave  
Edmonton, AB T6G 2R3  
Canada  
Attn: Irina T. Garces and Cagri Ayranci

Publisher Tax ID GB 494 6272 12

Total 0.00 CAD

Terms and Conditions

255

## INTRODUCTION

## A.2.7 Figure 12

1/17/2021

RightsLink Printable License

### AIP PUBLISHING LICENSE TERMS AND CONDITIONS

Jan 17, 2021

---

This Agreement between Irina Garces ("You") and AIP Publishing ("AIP Publishing") consists of your license details and the terms and conditions provided by AIP Publishing and Copyright Clearance Center.

License Number 4991520536625

License date Jan 17, 2021

Licensed  
Content  
Publisher AIP Publishing

Licensed  
Content  
Publication Applied Physics Letters

Licensed  
Content Title Active materials by four-dimension printing

Licensed  
Content Author Qi Ge, H. Jerry Qi, Martin L. Dunn

Licensed  
Content Date Sep 23, 2013

Licensed  
Content Volume 103

Licensed  
Content Issue 13

Type of Use Thesis/Dissertation

Requestor type Student

Format Print and electronic

Portion Figure/Table

Number of figures/tables 2

Title Shape Memory Polymers and Their Composites: Towards Field Applications via Production, Characterization and Modelling

Institution name University of Alberta

Expected presentation date Jan 2021

Portions Figure 1 and 5

Requestor Location  
Irina Garces  
Mechanical Engineering Building  
University of Alberta  
116 St & 85 Ave  
Edmonton, AB T6G 2R3  
Canada  
Attn: Irina T. Garces and Cagri Ayranci

Total 0.00 CAD

#### Terms and Conditions

#### AIP Publishing -- Terms and Conditions: Permissions Uses

AIP Publishing hereby grants to you the non-exclusive right and license to use and/or distribute the Material according to the use specified in your order, on a one-time basis, for the specified term, with a maximum distribution equal to the number that you have ordered. Any links or other content accompanying the Material are not the subject of this license.

1. You agree to include the following copyright and permission notice with the reproduction of the Material: "Reprinted from [FULL CITATION], with the permission of AIP Publishing." For an article, the credit line and permission notice must be printed on the first page of the article or book chapter. For photographs, covers, or tables, the notice may appear with the Material, in a footnote, or in the reference list.

## B.3 Supplementary Information Related to Chapter 4

### DSC and FTIR

Sample measurements of DSC are reported on Figure 2 for MM4520 and MM7520. Samples were also verified via Modulated DSC, samples are similar to those found by the manufacturer.

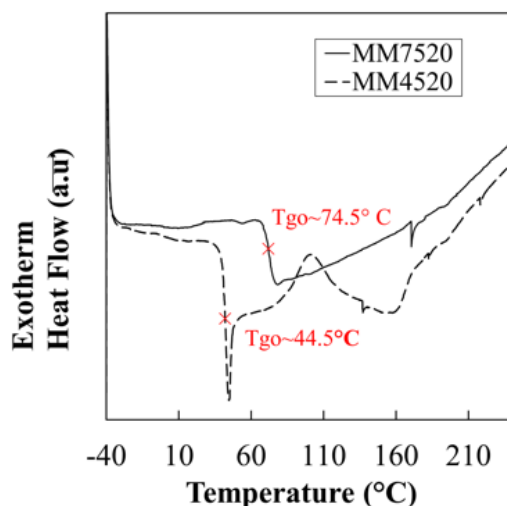


Figure 2: Examples of DSC measurement for MM4520 and MM7520

In Figure 3.a and b, hydrogen bonded groups appear as strong peaks while free groups appear as slight shoulders. Free groups for MM4520 and MM7520 appear in a wavenumber of 3400  $\text{cm}^{-1}$  and 3383  $\text{cm}^{-1}$  for N-H, respectively; and for free C=O appear approximately about 1724  $\text{cm}^{-1}$  and 1730  $\text{cm}^{-1}$  respectively. Similar studies have been performed on SMP MM3520 by Yang et al.<sup>1</sup>, and values found are in agreement to those discussed by the authors and other studies performed on thermoplastic polyurethanes<sup>2,3,4,5</sup>.

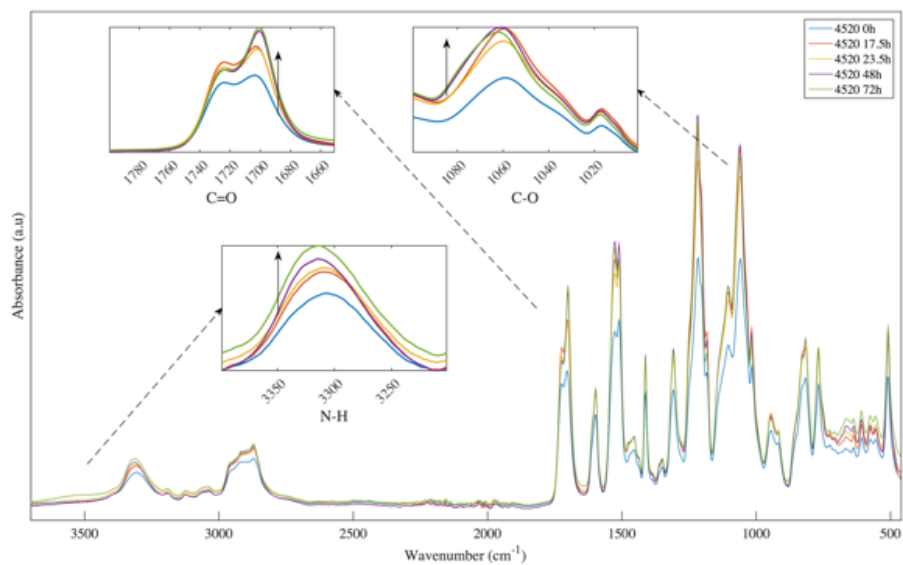
<sup>1</sup>Yang, B., Huang, W., Li, C., Lee, C., & Li, L. (2004). On the effects of moisture in a polyurethane shape memory polymer. *Smart Materials and Structures*, 13(1), 191–195.

<sup>2</sup>Wen, T.C., Wu, M.S., & Yang, C.H. (1999). Spectroscopic Investigations of Poly(oxypropylene)glycol-Based Waterborne Polyurethane Doped with Lithium Perchlorate. *Macromolecules*, 32(8), 2712–2720.

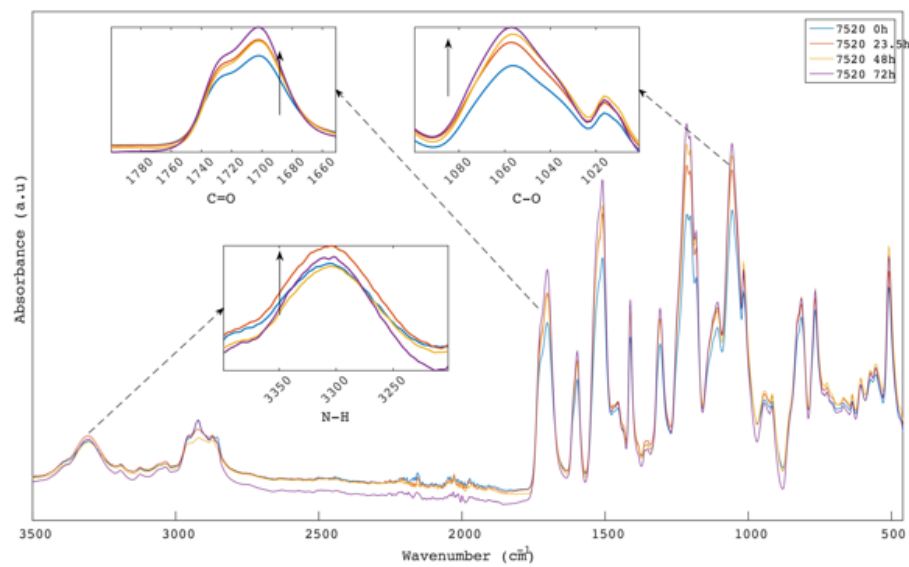
<sup>3</sup>Zhang, C. (2014). Computational study of hydrogen-bonding interactions in shape memory polymers. Hong Kong Polytechnic University.

<sup>4</sup>Brunette, C., Hsu, S., & MackKnight, W. (1982). Hydrogen-Bonding Properties of Hard-Segment Model Compounds in Polyurethane Block Copolymers. *Macromolecules*, 15(1), 71–77.

<sup>5</sup>Yilgor, E., Yilgor, I., & Yurtsever, E. (2002). Hydrogen bonding and polyurethane morphology. I. Quantum mechanical calculations of hydrogen bond energies and vibrational spectroscopy of model compounds. *Additive Manufacturing*, 43(24), 6551–6559.



(a)



(b)

Figure 3: FTIR spectra for (a) MM4520 and (b) MM7520 with zoomed in at different bonds

## B.4 Supplementary Information Related to Chapter 7

The equipment was calibrated by measuring several known resistances with the setup as seen in Figure 4a. The formula for a Wheatstone bridge is expressed according to equation 1, where  $V_g, G, V_s, R_s, R_2, R_3, R_4$  are the obtained voltage difference, the gain of the system, the supplied voltage, the sample resistance, and the three resistances of the bridge were set as  $1 \Omega, 5700 \Omega, 100 \Omega$ , respectively. Equation 2 can be reorganized to the form expressed in equation 2. Where  $c, e$  and  $d$  are the parameters estimated via a nonlinear least squares method. The values of the estimated parameters are presented in table 1. Curve fit and residuals is presented in figure 4b. The figure shows a maximum error in readings of  $\approx 1 \Omega$  when readings surpass  $\approx 150 \Omega$ . With this methodology, equation 2 was used to determine resistance values from voltage measurements.

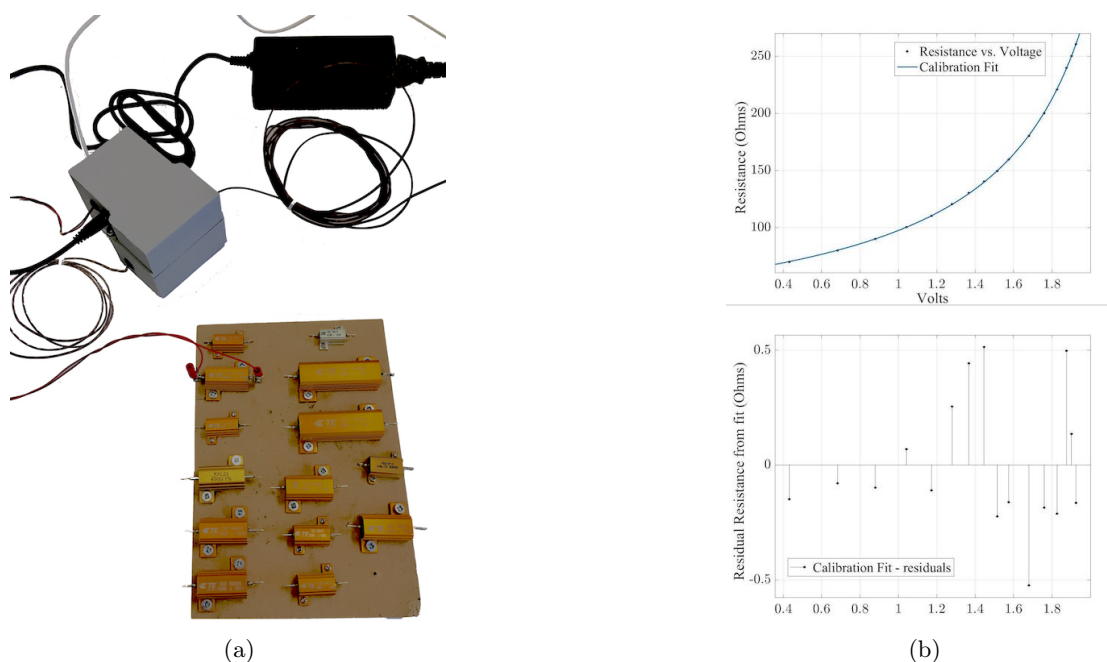


Figure 4: (a) In-house built control unit with resistances for calibration and (b) Calibration fit to resistance measurements with graph of residuals at the bottom

$$V_g = V_s \times \left( \frac{R_s}{R_s + R_2} - \frac{R_4}{R_3 + R_4} \right) \quad (1)$$

$$R_s = \frac{cV_g + e}{V_g + d} \quad (2)$$

Parameter	Calculated Reference value	Estimated
c	$R_2 = -1 \Omega$	-0.4966 $\Omega$
e	$c \times G\left(\frac{R_4 V_s}{R_3 + R_4}\right) = -142.00 \Omega - V$	-144 $\Omega - V$
d	$G\left(\frac{R_4 V_s}{R_3 + R_4} - V_s\right) = -2.49 V$	-2.481 V

Table 1: Estimated Parameters

## C.5 MATLAB CODE Related to Chapter 5

```

% %
% % %%Bending +SRR
% % Author: Irina Garces @ University of Alberta.
% % Description: Numerical solution for a thin SMP beam
% % |
% % | Input: Need to input the fits and values for the material
% % | parameters which were obtained from DMA data.
% % |
% % | Output: Deflection of the programming stage and recovery
% ratio
% % |
% % | Algorithm: Follow chapter equations on thesis (Chapter 5)
% % |
% % |
% % %%%%%%%%%%%%%%%%%%%%%%%%%%%%%%%%%%%%%%%%%%%%%%%%%%%%%%%%%%%%%%%%%%%%%%%%%
digits(32)
tic
clear all;
%close all;
clc;
digits(10)
set(groot, 'DefaultTextInterpreter', 'LaTeX');
set(groot, 'DefaultAxesTickLabelInterpreter', 'LaTeX');
set(groot, 'DefaultAxesFontName', 'LaTeX');
set(groot, 'DefaultLegendInterpreter', 'LaTeX');
set(groot, 'DefaultAxesFontSize',24);
set(groot, 'DefaultLineLineWidth', 4);
set(groot, 'DefaultFigureColor','w')
set(groot, 'DefaultAxesLineStyleOrder', '-|--|:|-.|--')
set(groot, 'Defaultfigurereposition',[500 500 600 600])
%%%%%%%%%%%%%%%%%%%%%%%%%%%%%%%%%%%%%%%%%%%%%%%%%%%%%%%%%%%%%%%%%%%%%%%%
%%%%%%%%%%%%%%%%%%%%%%%%%%%%%%%%%%%%%%%%%%%%%%%%%%%%%%%%%%%%%%%%%%%%%%%%
%%%%%%%%%%%%%%%%%%%%%%%%%%%%%%%%%%%%%%%%%%%%%%%%%%%%%%%%%%%%%%%%%%%%%%%%
%% MATERIAL PARAMETERS FOR ISOTHERMAL PROGRAMMING %%%%%%%%%%%%%%%%%%%%%%%%%%%%%%%%%%%%%%%%%%%%%%%%%%%%%%%%%%%%%%%%%%%%%%%%%
%%%%%%%%%%%%%%%%%%%%%%%%%%%%%%%%%%%%%%%%%%%%%%%%%%%%%%%%%%%%%%%%%%%%%%%%

E_g = 920.4;%846.9;
mu_g = 39.8147;%13.98;%12.18;%65.79;
lambda_g = 0.2214;%0.2214;%0.2214;%0.0271;%0.7128;
C_g = 0.066;%if using the fit 0.198
epsilon_l_g = 0.0015;

%fitted to programming and recovery
Tg=75;

%%%%%%%%%%%%%%%%%%%%%%%%%%%%%%%%%%%%%%%%%%%%%%%%%%%%%%%%%%%%%%%%%%%%%%%%
%%%%%%%%%%%%%%%%%%%%%%%%%%%%%%%%%%%%%%%%%%%%%%%%%%%%%%%%%%%%%%%%%%%%%%%%
%% TRANSIENT MATERIAL PROPERTIES %%%%%%%%%%%%%%%%%%%%%%%%%%%%%%%%%%%%%%%%%%%%%%%%%%%%%%%%%%%%%%%%%%%%%%%%%
%%%%%%%%%%%%%%%%%%%%%%%%%%%%%%%%%%%%%%%%%%%%%%%%%%%%%%%%%%%%%%%%%%%%%%%%
E_inf = 3.896e-14 ;%MPa
E_o = 2063 ;
ae = 0.2286 ;

% Latest Gaussian fit for lambda constrain starts at 1
a1l = 0.3099;
b1l = 84.24;
c1l = 13.81;
d1l = 0.01336;

```

```

au = 0.3361;
u_inf = 1; %cannot be less than 1
u_o = 1076;%1076

%%constants for gaussian distribution on mu
au1 = 104.9;
bu1 = 66.04;
cu1 = 8.635;

ac = 66.79;
bc = -0.07758;

ap = 0.4;
epsilon_l_0 = 0.0001; %0.0001
epsilon_l_inf = 0.002; %0.03;Model

%%%%%%%%%%%%%%%%%%%%%%%%%%%%%%%%%%%%%%%%%%%%%%%%%%%%%%%%%%%%%%%%%%%%%%%%
count = 2;
r = 2;
s = 2;
%dimension of the beam
%40*12*3 mm
L = 40;% distance between two supports

bm(1) = 12.695; % width of the beam Sample 1
hm(1) = 2.883; % height of the beam (all measured dimensions)

bm(2) = 12.636; % width of the beam Sample 2
hm(2) = 2.827; % height of the beam (all measured dimensions)

bm(3) = 12.563; % width of the beam Sample 3
hm(3) = 2.843; % height of the beam (all measured dimensions)

bm(4) = 12.642; % width of the beam Sample 4
hm(4) = 2.7576; % height of the beam (all measured dimensions)

bm(5) = 12.556; % width of the beam Sample 5
hm(5) = 2.9082; % height of the beam (all measured dimensions)

bm(6) = 12.611; % HR 0.4 Sample 1 width of the beam
hm(6) = 2.886; % HR 0.4 height of the beam (all measured dimensions)

bm(7) = 12.584; % HR 0.4 Sample 2 width of the beam
hm(7) = 2.756; % HR 0.4 height of the beam (all measured dimensions)

bm(8) = 12.638; % HR 0.4 Sample 3 width of the beam
hm(8) = 2.853; % HR 0.4 height of the beam (all measured dimensions)

bm(9) = 12.652; % HR 0.4 Sample 4 width of the beam
hm(9) = 2.719; % HR 0.4 height of the beam (all measured dimensions)

bm(10) = 12.602; % HR 0.4 Sample 5 width of the beam
hm(10) = 2.801; % HR 0.4 height of the beam (all measured dimensions)

b=bm(count);
h=hm(count);

```

```

I = b*(h^3)/12;    % inertia moment
%%%%%%%%%%%%%%%%%%%%%%%%%%%%%%%%%%%%%%%%%%%%%%%%%%%%%%%%%%%%%%%%%%%%%%%%

%%the original point of x is in the left end of the beam and only left
%%half of the beam is considered

dx = L/2/10;      % x step
x = 0:dx:(L/2);   % discrete x along beam span direction
x = x';           % for the multiply of load history that will be used to moment
num_x = length(x);

dt = 0.003;       % time step
t = 0:dt:7;       % discrete time
num_t = length(t);

dy = (h/2)/1000;  % y step
y = 0:dy:(h/2);  % discrete y along the height of the beam
num_y = length(y);

P_rate = 1;       % load_rate(N/second)
P = P_rate*t;     % applied load
M = x*P/2;        % moment (N*mm) (x*t dimension)
%%%%%%%%%%%%%%%%%%%%%%%%%%%%%%%%%%%%%%%%%%%%%%%%%%%%%%%%%%%%%%%%%%%%%%%%

kappa = zeros(num_x,num_t);    % curvature,initial condition assume to be zero
sigma = zeros(num_x,num_t,num_y); % stress,initial condition assume to be zero
c1 = zeros(1,num_t);
w = zeros(num_x,num_t);
delta = zeros(1,num_t);
epsilon_c_dot = zeros(num_x,num_t,num_y);
epsilon = zeros(num_x,num_t,num_y);
epsilon_e = zeros(num_x,num_t,num_y);
epsilon_c = zeros(num_x,num_t,num_y);
Adm = zeros(num_x,num_t,num_y);
Bdm = zeros(num_x,num_t,num_y);
Cdm = zeros(num_x,num_t,num_y);

epsilon_c_tau= zeros(num_x,1,num_y);
mu_EFF = zeros(num_x,num_t,num_y);
lambda_EFF = zeros(num_x,num_t,num_y);
epsilon_EFF = zeros(num_x,num_t,num_y);
flag1 = zeros(num_x,num_t,num_y);
flag2 = zeros(num_x,num_t,num_y);
flag3 = zeros(num_x,num_t,num_y);
E = zeros(1,num_t);
lambda = zeros(1,num_t);
mu = zeros(1,num_t);
epsilon_l = zeros(num_t,1);
C = zeros(1,num_t);
mu_eff = zeros(1,num_t);
lambda_eff = zeros(1,num_t);
epsilon_eff = zeros(1,num_t);
A_integral = zeros(num_x,num_t);
B_integral = zeros(num_x,num_t);
C_integral = zeros(num_x,num_t);
%%%%%%%%%%%%%%%%%%%%%%%%%%%%%%%%%%%%%%%%%%%%%%%%%%%%%%%%%%%%%%%%%%%%%%%%
%%%%%%%%%%%%%%%%%%%%%%%%%%%%%%%%%%%%%%%%%%%%%%%%%%%%%%%%%%%%%%%%%%%%%%%%

```

```

%PROGRAMING:

Tl = 75;
Q = 0;

for q = 1:num_x

    for n = 1:(num_t-1)

        E(n) = E_g;
        lambda(n) = lambda_g;
        mu(n) = mu_g;
        epsilon_l(n) = epsilon_l_g;
        C(n) = C_g;
        mu_eff(n) = mu(n)/(1-((mu(n)*C(n))/(lambda(n)*E(n)))); % effective viscosity (MPa*s)
        lambda_eff(n) = lambda(n)/(1-C(n)); % effective retardation time(s)
        epsilon_eff(n) = -1*(C(n)*epsilon_l(n))/(1-C(n)); % effective epsilons

        for m = 1:num_y

            epsilon(q,n,m) = kappa(q,n)*((m-1)*dy); %get strain along y direction at one time point

            if n>1
                sigma(q,n,m) = E(n-1)*epsilon(q,n,m)+sigma(q,n-1,m)*(1-E(n-1))*dt/mu_EFF(q,n-1,m)+epsilon(q,n-1,m)*(E(n-1)*dt/lambda_EFF(q,n-1,m)-E(n-1))*dt/mu_EFF(q,n-1,m)-epsilon_eff(q,n-1,m)*dt*E(n-1)/lambda_EFF(q,n-1,m);
            else
                sigma(q,n,m) = 0;
            end

            epsilon_e(q,n,m) = sigma(q,n,m)/E(n);

            epsilon_c(q,n,m) = epsilon(q,n,m)-epsilon_e(q,n,m); % one dimension along y direction, this is creep strain

            if n>2
                epsilon_c_dot(q,n,m) = (epsilon_c(q,n,m)-epsilon_c(q,n-2,m))/(2*dt);
                epsilon_c_dot(q,n,m) = epsilon_c_dot(q,n,m)*0.05+epsilon_c_dot(q,n-1,m)*0.95;
            else
                epsilon_c_dot(q,n,m) = 0;
            end

            if epsilon_c_dot(q,n,m) > 0

```

```

if epsilon_c(q,n,m) < epsilon_l(n)
    mu_EFF(q,n,m) = mu(n);
    lambda_EFF(q,n,m) = lambda(n);
    epsilon_EFF(q,n,m) = 0;
    flag1(q,n,m)=1;

else

    mu_EFF(q,n,m) = mu_eff(n);
    lambda_EFF(q,n,m) = lambda_eff(n);
    epsilon_EFF(q,n,m) = epsilon_eff(n);
    flag2(q,n,m)=1;

end

else

    mu_EFF(q,n,m) = mu(n);
    lambda_EFF(q,n,m) = lambda(n);

    if epsilon_c_tau(q,1,m) == 0
        epsilon_EFF(q,n,m) = 0;
    else

epsilon_EFFatTau(q,1,m);%C(n)*(epsilon_cr(m)-epsilon_l(n));
        epsilon_EFF(q,n,m) = C(n)*(epsilon_c_tau(q,1,m)-epsilon_l(n)); %C
    end

    flag3(q,n,m)=1;

end

%Calculating dM % this assumes constrained recovery
Adm(q,n,m) = (1/mu_EFF(q,n,m))*(sigma(q,n,m)*y(m));
Bdm(q,n,m) = (1/lambda_EFF(q,n,m))*kappa(q,n)*y(m)^2;
Cdm(q,n,m) = (1/lambda_EFF(q,n,m))*epsilon_EFF(q,n,m)*y(m);

end

A_integral(q,n) = trapz(y,Adm(q,n,:));
B_integral(q,n) = trapz(y,Bdm(q,n,:));
C_integral(q,n) = trapz(y,Cdm(q,n,:));

kappa(q,n+1) = kappa(q,n)+(1/(E(n)*I))*(M(q,n+1)-M(q,n))+(2*b*dt/I)*C
(A_integral(q,n)-B_integral(q,n)+C_integral(q,n));

end

end

for u = 1:num_t
    c1(u) = x\kappa(:,u);
end

%get deflection w along x and deflection at mid-span delta

```

```

for v = 1:num_t
    w(:,v) = (c1(v)*x.^3)/6-L^2*c1(v)*x/8;
    delta(1,v) = c1(v)*L^3/24;
end

figure(1);
hold on
plot(t,delta)
hold on
yyaxis right
hold on
plot(t,Tl+Q*t*dt)
ylabel('Temperature ($^{\circ}$C$)', 'Interpreter', 'latex');

yyaxis left
ylim([0 3])
xlabel('Time(s)')
ylabel('deflection at midspan (mm)')
hold on
drawbrace([0, 2.4], [5.7, 2.4], 10, 'Color', 'k')
hold on
drawbrace([5.7, 2.4], [7, 2.4], 10, 'Color', 'k')
hold on

text(2.7,2.6,sprintf('R 1', 'FontSize',40))
text(6.2,2.6,sprintf('R 2', 'FontSize',40))

Maxdelta = max(delta);

figure(1)

filename = sprintf('/Users/Irina/Dropbox/Paper for model/DATA/SRF_DATA/With data
selection/dpn_SRF_0.%d/SRF_0.%d.%d.csv',r,r,s);

data = csvread(filename);
t_exp=data(:,2);
disp=data(:,4);
Load=data(:,5);
Tcham=data(:,7);
Tcmd=data(:,9);

findval(1) = 267.2;%0.2 Sample 1
findval(2) = 266.9;%0.2 Sample 2
findval(3) = 265.6;%0.2 Sample 3
findval(4) = 268.6;%0.2 Sample 4
findval(5) = 266.3;%0.2 Sample 5

findval(6) = 265.2; %0.4 Sample 1
findval(7) = 267.1; %0.4 Sample 2
findval(8) = 265.1; %0.4 Sample 3
findval(9) = 256.9; %0.4 Sample 4
findval(10) = 271.5;%0.4 Sample 5

[val,idx]=min(abs(t_exp-findval(count)));
ini_t=t_exp(idx);

```

```

range = 160;

hold on
yyaxis left

delta_exp =-disp(idx:idx+range);
Maxdelta_exp = max(delta_exp);
plot(t_exp(idx:idx+range)-findval(count),(-disp(idx:idx+range)))
% experimental = resample((-disp(idx:idx+range)),141,161);
% R_s(count) = rsquare(experimental',delta);

xlim([0 7])
% text(1.5,1,sprintf('$R^2=%.5f$',R_s(count)),'FontSize',20)

ylabel('Displacement (mm)')
xlabel('Time (s)')
yyaxis right
%plot(t_exp(idx:idx+range)-findval,Tcham(idx:idx+range))
legend('Model Programming','Experimental Programming',↵
'Interpreter','latex','location','northwest');

%%%%%%%%%%%%%%%%%%%%%%%%%%%%%%%%%%%%%%%%%%%%%%%%%%%%%%%%%%%%%%%%%%%%%%%%
%%%%%%%%%%%%%%%%%%%%%%%%%%%%%%%%%%%%%%%%%%%%%%%%%%%%%%%%%%%%%%%%%%%%%%%%
figure(2)
scatter(t,flag1(end,:),end)
hold on
scatter(t,flag2(end,:),end)
hold on
scatter(t,flag3(end,:),end)
hold on
legend('Reg1','Reg2','Reg3','Interpreter','Latex');

figure(3)

yyaxis left
plot(t,epsilon(end,:),end)
hold on
plot(t,epsilon_e(end,:),end)
hold on
plot(t,epsilon_c(end,:),end)
hold on
plot(t,epsilon_l)
hold on
plot(t,ones(size(t))*epsilon_c_tau(end,1,end),'k')
hold on
plot(t,epsilon_EFF(end,:),end),'g')
ylabel('$\epsilon$', 'Interpreter', 'latex');

yyaxis right

plot(t,smooth(epsilon_c_dot(end,:),end))
hold on

xlabel('Time (s)', 'Interpreter', 'latex');
ylabel('$\dot{\epsilon}$', 'Interpreter', 'latex');

```

```

legend('$\epsilon(L/2,t,h/2)$', '$\epsilon_e(L/2,t,h/2)$', '$\epsilon_c(L/2,t,
h/2)$', '$\epsilon_L(t)$', '$\epsilon_c(L/2,\tau,h/2)$', '$\epsilon_{s_
{EFF}}$', 'Interpreter', 'Latex');

figure(4)
plot(t, kappa(end,:))

figure(5)
plot(t, epsilon(end,:,end))

figure(6)
plot(A_integral(end,:))
hold on
plot(B_integral(end,:))
hold on
plot(C_integral(end,:))
hold on
%

figure(7)

plot(t, mu_EFF(end,:,end))
hold on
plot(t, mu_EFF(end,:,500))
hold on
plot(t, mu_EFF(end,:,1))

figure(8)

plot(y, squeeze(mu_EFF(end,end-1,:)))
hold on
plot(y, squeeze(mu_EFF(end,50,:)))
hold on
plot(y, squeeze(mu_EFF(end,10,:)))
hold on

figure(9)

plot(t, sigma(end,:,end))

figure(10)
stress=squeeze(sigma(end,end-1,:));
plot(stress,(1:num_y)*dy)
hold on
plot(t, 3*P(end,:)*40/(2*b*h^2))
ylabel('Stress (MPa)')
xlabel('Time (s)')
legend('Viscoelastic Model', 'Linear Beam Model',
'Interpreter', 'latex', 'location', 'northwest');

%-----
% RECOVERY RATIO
%-----
% Initial conditions:

epsilon_c_tau = epsilon_c(:,end-1,:);

```

```

Tl = 55;

clear C_integral B_integral A_integral mu lambda C E epsilon_l mu_EFF lambda_EFF
epsilon_s_EFF

dtr = dt;          % time step
tr = 0:dtr:150;

%WLF Material variables
mu_inf = (4.292e-09);
mu_o = 112.6;
au = 0.3315;

l_o = 0.01492 ;
l_inf = 0.3406;
al = 0.248;

for Q=0.6:0.6:0.6

% discrete time

num_tr = length(tr);
kappa_r = kappa(:,end);
epsilon_r = zeros(num_x,num_tr-1,num_y);
epsilon_r(:,1,:) = epsilon(:,end-1,:);

sigma_r = zeros(num_x,num_tr,num_y); % stress,initial condition assume to be zero
M_r = zeros(num_x,num_tr);
E = zeros(num_tr,1);
epsilon_l = zeros(num_tr,1);
lambda = zeros(num_tr,1);
mu_eff_fit = zeros(num_tr-1,1);
mu = zeros(num_tr,1);
C = zeros(num_tr,1);
mu_eff_r = zeros(num_tr,1);
lambda_eff_r = zeros(num_tr,1);
epsilon_s_eff_r = zeros(num_tr,1);
epsilon_cr_dot = zeros(num_x,num_tr,num_y);
flag1 = zeros(num_x,num_tr,num_y);
flag2 = zeros(num_x,num_tr,num_y);
flag3 = zeros(num_x,num_tr,num_y);
flag4 = zeros(num_x,num_tr,num_y);
epsilon_cr_plot = zeros(num_x,num_tr,num_y);
epsilon_e = zeros(num_x,num_tr,num_y);
epsilon_cr = zeros(num_x,num_tr,num_y);
Adm = zeros(num_x,num_tr);
Bdm = zeros(num_x,num_tr);
Cdm = zeros(num_x,num_tr);
A_integral = zeros(num_x,num_tr);
B_integral = zeros(num_x,num_tr);
C_integral = zeros(num_x,num_tr);

mu_EFF = zeros(num_x,num_tr,num_y);
lambda_EFF = zeros(num_x,num_tr,num_y);
epsilon_s_EFF = zeros(num_x,num_tr,num_y);

for q = 1:num_x

```

```

for n = 1:(num_tr-1)
    T(n) = Tl+Q*n*dtr;
    if T(n)<=82
        T(n) = Tl+Q*n*dtr;
    else
        T(n)=82;
    end
    E(n) = (E_inf*exp(-ae*Tg)+E_o*exp(-ae*T(n)))/(exp(-ae*Tg)+exp(-ae*T(n)));
    lambda(n) = a1l*exp(-((T(n)-b1l)/c1l).^2)+d1l; % gaussian lambda
    mu(n) = au1*exp(-((T(n)-bu1)/cu1)^2); %from Es modulus gaussian
    epsilon_l(n)=(epsilon_l_inf*exp(-ap*Tg)+epsilon_l_0*exp(-ap*T(n)))/(exp(-ap*Tg)+exp(-ap*T(n)));
    if T(n)< 55
        C(n) = 0.97;
    else
        C(n) = ac*exp(bc.*T(n));
    end
    mu_eff_r(n) = (mu(n)/(1-((mu(n)*C(n))/(lambda(n)*E(n))))); % effective
viscosity (MPa*s)
    lambda_eff_r(n) = lambda(n)/(1-C(n)); % effective retardation time(s)
    epsilon_eff_r(n) = -1*(C(n)*epsilon_l(n))/(1-C(n)); % effective epsilon

    for m = 1:num_y
        epsilon_r(q,n,m) = kappa_r(q,n)*((m-1)*dy); %get strain along y
direction at one time point
        if n>1
            sigma_r(q,n,m) = E(n-1)*epsilon_r(q,n,m)+sigma_r(q,n-1,m)*(1-((E(n-1)
*dtr)/mu_EFF(q,n-1,m)))+epsilon_r(q,n-1,m)*((E(n-1)*dtr/lambda_EFF(q,n-1,m))-E(n-1))...
            -((epsilon_eff_r(q,n-1,m)*dtr*E(n-1))/lambda_EFF(q,n-1,m));
        else
            sigma_r(q,n,m) = 0;
        end
        epsilon_e(q,n,m) = sigma_r(q,n,m)/E(n);
        epsilon_cr(q,n,m) = epsilon_r(q,n,m)-epsilon_e(q,n,m); % one dimension
along y direction, this is creep strain

        if n<=2
            epsilon_cr_dot(q,n,m)=0;
        end
    end
end

```

```

else
epsilon_cr_dot(q,n,m) = (epsilon_cr(q,n,m)-epsilon_cr(q,n-2,m))/(2*dtr);
epsilon_cr_dot(q,n,m) = epsilon_cr_dot(q,n,m)*0.05+epsilon_cr_dot(q,n-1,
m)*0.95;

end

if epsilon_cr_dot(q,n,m)>0
if epsilon_cr(q,n,m)< epsilon_l(n)
mu_EFF(q,n,m) = mu(n);
lambda_EFF(q,n,m) = lambda(n);
epsilons_EFF(q,n,m) = 0;
flag1(q,n,m)=1;

else

mu_EFF(q,n,m) = mu_eff_r(n);
lambda_EFF(q,n,m) = lambda_eff_r(n);
epsilons_EFF(q,n,m) = epsilons_eff_r(n);
flag2(q,n,m)=1;

end

else

mu_EFF(q,n,m) = mu(n);
lambda_EFF(q,n,m) = lambda(n);
epsilons_EFF(q,n,m) = C(n)*(epsilon_c_tau(q,1,m)-epsilon_l(n));

flag3(q,n,m)=1;

end

%Calculating dM % this assumes constrained recovery
Adm(q,n,m) = (1/mu_EFF(q,n,m))*(sigma_r(q,n,m)*y(m));
Bdm(q,n,m) = (1/lambda_EFF(q,n,m))*kappa_r(q,n)*y(m)^2;
Cdm(q,n,m) = (1/lambda_EFF(q,n,m))*epsilons_EFF(q,n,m)*y(m);

end

A_integral(q,n) = trapz(y,Adm(q,n,:));
B_integral(q,n) = trapz(y,Bdm(q,n,:));
C_integral(q,n) = trapz(y,Cdm(q,n,:));

kappa_r(q,n+1) = kappa_r(q,n)+(2*b*dt/I)*(A_integral(q,n)-B_integral(q,n)
+C_integral(q,n));

end

end

```

```

for u = 1:num_tr
    c1_r(u) = x\kappa_r(:,u);
end

%get deflection w along x and deflection at mid-span delta
for v = 1:num_tr
    w(:,v) = c1_r(v)*x.^3/6-L^2*c1_r(v)*x/8;
    delta_r(1,v) = c1_r(v)*L^3/24;
end

figure(10)

yyaxis left
plot(tr(1:end-1),epsilon_r(end,:,end))
hold on
plot(tr,epsilon_e(end,:,end))
hold on
plot(tr,epsilon_cr (end,:,end))
hold on
plot(tr,epsilon_l)
hold on
plot(tr,ones(size(tr))*epsilon_c_tau(end,1,end), 'k')
hold on
plot(tr,epsilons_EFF(end,:,end), 'g')
ylabel('$\epsilon$', 'Interpreter', 'latex');

yyaxis right

plot(tr,smooth(epsilon_cr_dot(end,:,end)))
hold on

xlabel('Time (s)', 'Interpreter', 'latex');
ylabel('$\dot{\epsilon}$', 'Interpreter', 'latex');

legend('$\epsilon(L/2,t,h/2)$', '$\epsilon_e(L/2,t,h/2)$', '$\epsilon_c(L/2,t,h/2)$', '$\epsilon_L(t)$', '$\epsilon_c(L/2,\tau,h/2)$', '$\epsilon_{s\_EFF}$', 'Interpreter', 'Latex');

figure(11)
plot(tr(1:end-1),epsilon_r (end,:,end))
hold on
plot(tr(1:end-1),epsilon_r (end,:,500))
hold on
plot(tr(1:end-1),epsilon_r (end,:,1))

legend('$y=h/2$', '$y=h/4$', '$y=0.05$ (mm)', 'Interpreter', 'Latex');
xlabel('Time (s)', 'Interpreter', 'latex');
ylabel('$\epsilon$', 'Interpreter', 'latex');

figure(12)
plot(tr,epsilon_cr (end,:,end))
hold on

```

```
plot(tr,epsilon_cr (end,:,500))
hold on
plot(tr,epsilon_cr (end,:,1))
hold on
legend('$y=h/2$', '$y=h/4$', '$y=0.05$ (mm)$', 'Interpreter', 'Latex');
xlabel('Time (s)', 'Interpreter', 'latex');
ylabel('$\varepsilon_c$', 'Interpreter', 'latex');
```

```
figure(15)
scatter(tr,flag1(end,:,end))
hold on
scatter(tr,flag2(end,:,end))
hold on
scatter(tr,flag3(end,:,end))
hold on
legend('Reg1', 'Reg2', 'Reg3', 'Interpreter', 'Latex');
```

```
figure(13);
yyaxis left
plot(tr,delta_r)
hold on
ylabel('Deflection at midspan (mm)');
hold on
yyaxis right
plot(tr(1:end-1),T);
hold on
ylabel('Temperature ( $^{\circ}$ C)', 'Interpreter', 'latex');
xlabel('Time(s)')
```

```
figure(14);
Rr=(delta(end)-delta_r)*100/(delta(end));
yyaxis left
hold on
plot(tr,Rr)
xlabel('Time(s)');
ylabel('Recovery Ratio (\%)', 'Interpreter', 'latex');
hold on
yyaxis right
hold on
plot(tr(1:end-1),T)
ylabel('Temperature ( $^{\circ}$ C)', 'Interpreter', 'latex');
hold on
```

```
end
```

```

% %
% % %%Bending +SRF
% % Author: Irina Garces @ University of Alberta.
% % Description: Numerical solution for a thin SMP beam
% %
% % |
% % |      Input:  Need to input the fits and values for the material
% % |              parameters which were obtained from DMA data.
% % |
% % |      Output: Deflection of the programming stage and recovery force
% % |
% % |      Algorithm: Follow chapter equations on thesis (Chapter 5)
% % |
% % %%%%%%%%%%%%%%%%%%%%%%%%%%%%%%%%%%%%%%%%%%%%%%%%%%%%%%%%%%%%%%%%%%%%%%%%%
digits(32)
tic
clear all;
close all;
clc;
digits(10)
set(groot, 'DefaultTextInterpreter', 'LaTeX');
set(groot, 'DefaultAxesTickLabelInterpreter', 'LaTeX');
set(groot, 'DefaultAxesFontName', 'LaTeX');
set(groot, 'DefaultLegendInterpreter', 'LaTeX');
set(groot, 'DefaultAxesFontSize',24);
set(groot, 'DefaultLineLineWidth', 4);
set(groot, 'DefaultFigureColor','w')
set(groot, 'DefaultAxesLineStyleOrder','-|--:|-.|--')
set(groot, 'Defaultfigureposition',[500 500 600 600])
%%%%%%%%%%%%%%%%%%%%%%%%%%%%%%%%%%%%%%%%%%%%%%%%%%%%%%%%%%%%%%%%%%%%%%%%
%%%% MATERIAL PARAMETERS FOR ISOTHERMAL PROGRAMMING %%%
E_g = 920.4;%846.9;
mu_g = 39.8147;%13.98;%12.18;%65.79;
lambda_g = 0.2214;%0.2214;%0.2214;%0.0271;%0.7128;
C_g = 0.066;%if using the fit 0.198
epsilon_l_g = 0.0015;

%fitted to programming and recovery
Tg=75;

%%%%%%%%%%%%%%%%%%%%%%%%%%%%%%%%%%%%%%%%%%%%%%%%%%%%%%%%%%%%%%%%%%%%%%%%
%%%% TRANSIENT MATERIAL PROPERTIES %%%
E_inf = 3.896e-14 ;%MPa
E_o = 2063 ;
ae = 0.2286 ;

% Latest Gaussian fit for lambda constrain starts at 1
a1l = 0.3099;
b1l = 84.24;
c1l = 13.81;
d1l = 0.01336;

au = 0.3361;
u_inf = 1; %cannot be less than 1
u_o = 1076;%1076

```

```
%%constants for gaussian distribution on mu
au1 = 104.9;
bu1 = 66.04;
cu1 = 8.635;

ac = 66.79;
bc = 0.07758;

ap = 0.4;
epsilon_l_0 = 0.0001; %0.0001
epsilon_l_inf = 0.002; %0.03;Model

%
%%%%%%%%%%%%%%%%%%%%%%%%%%%%%%%%%%%%%%%%%%%%%%%%%%%%%%%%%%%%%%%%%%%%%%%%
count = 2;
r = 2;
s = 2;
%dimension of the beam
%40*12*3 mm
L = 40;% distance between two supports

bm(1) = 12.695; % width of the beam Sample 1
hm(1) = 2.883; % height of the beam (all measured dimensions)

bm(2) = 12.636; % width of the beam Sample 2
hm(2) = 2.827; % height of the beam (all measured dimensions)

bm(3) = 12.563; % width of the beam Sample 3
hm(3) = 2.843; % height of the beam (all measured dimensions)

bm(4) = 12.642; % width of the beam Sample 4
hm(4) = 2.7576; % height of the beam (all measured dimensions)

bm(5) = 12.556; % width of the beam Sample 5
hm(5) = 2.9082; % height of the beam (all measured dimensions)

bm(6) = 12.611; % HR 0.4 Sample 1 width of the beam
hm(6) = 2.886; % HR 0.4 height of the beam (all measured dimensions)

bm(7) = 12.584; % HR 0.4 Sample 2 width of the beam
hm(7) = 2.756; % HR 0.4 height of the beam (all measured dimensions)

bm(8) = 12.638; % HR 0.4 Sample 3 width of the beam
hm(8) = 2.853; % HR 0.4 height of the beam (all measured dimensions)

bm(9) = 12.652; % HR 0.4 Sample 4 width of the beam
hm(9) = 2.719; % HR 0.4 height of the beam (all measured dimensions)

bm(10) = 12.602; % HR 0.4 Sample 5 width of the beam
hm(10) = 2.801; % HR 0.4 height of the beam (all measured dimensions)

b=bm(count);
h=hm(count);

I = b*(h^3)/12; % inertia moment
%%%%%%%%%%%%%%%%%%%%%%%%%%%%%%%%%%%%%%%%%%%%%%%%%%%%%%%%%%%%%%%%%%%%%%%%
```

```

%%the original point of x is in the left end of the beam and only left
%%half of the beam is considered

dx = L/2/10;      % x step
x = 0:dx:(L/2);  % discrete x along beam span direction
x = x';          % for the multiply of load history that will be used to moment
num_x = length(x);

dt = 0.001;      % time step
t = 0:dt:7;      % discrete time
num_t = length(t);

dy = (h/2)/1000; % y step
y = 0:dy:(h/2); % discrete y along the height of the beam
num_y = length(y);

P_rate = 1;      % load_rate(N/second)
P = P_rate*t;    % applied load
M = x*P/2;       % moment (N*mm) (x*t dimension)
%%%%%%%%%%%%%%%%%%%%%%%%%%%%%%%%%%%%%%%%%%%%%%%%%%%%%%%%%%%%%%%%%%%%%%%%

%Variable initialization
kappa = zeros(num_x,num_t); % curvature,initial condition assume to be zero
sigma = zeros(num_x,num_t,num_y); % stress,initial condition assume to be zero
c1 = zeros(1,num_t);
w = zeros(num_x,num_t);
delta = zeros(1,num_t);
epsilon_c_dot = zeros(num_x,num_t,num_y);
epsilon = zeros(num_x,num_t,num_y);
epsilon_e = zeros(num_x,num_t,num_y);
epsilon_c = zeros(num_x,num_t,num_y);
Adm = zeros(num_x,num_t,num_y);
Bdm = zeros(num_x,num_t,num_y);
Cdm = zeros(num_x,num_t,num_y);
epsilon_c_tau= zeros(num_x,1,num_y);

%Material Parameters initialization
E = zeros(1,num_t);
lambda = zeros(1,num_t);
mu = zeros(1,num_t);
epsilon_l = zeros(num_t,1);
C = zeros(1,num_t);
mu_eff = zeros(1,num_t);
lambda_eff = zeros(1,num_t);
epsilon_eff = zeros(1,num_t);
mu_EFF = zeros(num_x,num_t,num_y);
lambda_EFF = zeros(num_x,num_t,num_y);
epsilon_EFF = zeros(num_x,num_t,num_y);

flag1 = zeros(num_x,num_t,num_y);
flag2 = zeros(num_x,num_t,num_y);
flag3= zeros(num_x,num_t,num_y);

A_integral = zeros(num_x,num_t);
B_integral = zeros(num_x,num_t);

```

```

C_integral = zeros(num_x,num_t);
%=====
%PROGRAMING:
%-----

Tl = 75;
Q = 0;

for q = 1:num_x
    for n = 1:(num_t-1)
        E(n) = E_g;
        lambda(n) = lambda_g;
        mu(n) = mu_g;
        epsilon_l(n) = epsilon_l_g;
        C(n) = C_g;
        mu_eff(n) = mu(n)/(1-((mu(n)*C(n))/(lambda(n)*E(n))));
        lambda_eff(n) = lambda(n)/(1-C(n));
        epsilons_eff(n) = -1*(C(n)*epsilon_l(n))/(1-C(n));

        for m = 1:num_y
            epsilon(q,n,m) = kappa(q,n)*((m-1)*dy); %get strain along y direction
at one time point

            if n>1
                epsilon(q,n,m) = epsilon(q,n,m)*0.1+epsilon(q,n-1,m)*0.9;
            end

            if n>1
                sigma(q,n,m) = E(n)*epsilon(q,n,m)+sigma(q,n-1,m)*(1-E(n-1)*dt/mu_EFF
(q,n-1,m))+epsilon(q,n-1,m)*(E(n-1)*dt/lambda_EFF(q,n-1,m)-E(n-1))...
-epsilons_EFF(q,n-1,m)*dt*E(n-1)/lambda_EFF(q,n-1,m);
            else
                sigma(q,n,m) = 0;
            end

            epsilon_e(q,n,m) = sigma(q,n,m)/E(n);

            epsilon_c(q,n,m) = epsilon(q,n,m)-epsilon_e(q,n,m);

            if n>1
                epsilon_c_dot(q,n,m) = (epsilon_c(q,n,m)-epsilon_c(q,n-1,m))/(dt);
                epsilon_c_dot(q,n,m) = epsilon_c_dot(q,n,m)*0.05+epsilon_c_dot(q,n-1,
m)*0.95;
            else
                epsilon_c_dot(q,n,m) = 0;
            end

            if epsilon_c_dot(q,n,m) > 0

                if epsilon_c(q,n,m) < epsilon_l(n)
                    mu_EFF(q,n,m) = mu(n);
                    lambda_EFF(q,n,m) = lambda(n);
                    epsilons_EFF(q,n,m) = 0;
                    flag1(q,n,m)=1;
                end
            end
        end
    end
end

```

```

else
    mu_EFF(q,n,m) = mu_eff(n);
    lambda_EFF(q,n,m) = lambda_eff(n);
    epsilons_EFF(q,n,m) = epsilons_eff(n);
    flag2(q,n,m)=1;
end
else
    mu_EFF(q,n,m) = mu(n);
    lambda_EFF(q,n,m) = lambda(n);
    if epsilon_c_tau(q,1,m) == 0
        epsilons_EFF(q,n,m) = 0;
    else
        epsilons_EFF(q,n,m) = C(n)*(epsilon_c_tau(q,1,m)-epsilon_l(n));
    end
    flag3(q,n,m)=1;
end

%Calculating dM % this assumes constrained recovery
Adm(q,n,m) = (1/mu_EFF(q,n,m))*(sigma(q,n,m)*y(m));
Bdm(q,n,m) = (1/lambda_EFF(q,n,m))*kappa(q,n)*y(m)^2;
Cdm(q,n,m) = (1/lambda_EFF(q,n,m))*epsilons_EFF(q,n,m)*y(m);

end
A_integral(q,n) = trapz(y,Adm(q,n,:));
B_integral(q,n) = trapz(y,Bdm(q,n,:));
C_integral(q,n) = trapz(y,Cdm(q,n,:));

kappa(q,n+1) = kappa(q,n)+(1/(E(n)*I))*(M(q,n+1)-M(q,n))+(2*b*dt/I)*C
(A_integral(q,n)-B_integral(q,n)+C_integral(q,n));

end
end
for u = 1:num_t
    c1(u) = x\kappa(:,u);
end

%Deflection w along x and deflection at mid-span delta
for v = 1:num_t
    w(:,v) = (c1(v)*x.^3)/6-L^2*c1(v)*x/8;
    delta(1,v) = c1(v)*L^3/24;
end

figure(1);

```

```

hold on
    plot(t,delta)
hold on
yyaxis right
hold on
    plot(t,Tl+Q*t*dt)
    ylabel('Temperature ( $\text{C}$ )','Interpreter','latex');
yyaxis left
ylim([0 3])
xlabel('Time(s)')
ylabel('deflection at midspan (mm)')

findval(1) = 267.2;%0.2 Sample 1
findval(2) = 266.9;%0.2 Sample 2
findval(3) = 265.6;%0.2 Sample 3
findval(4) = 268.6;%0.2 Sample 4
findval(5) = 266.3;%0.2 Sample 5

findval(6) = 265.2; %0.4 Sample 1
findval(7) = 267.1; %0.4 Sample 2
findval(8) = 265.1; %0.4 Sample 3
findval(9) = 256.9; %0.4 Sample 4
findval(10) = 271.5;%0.4 Sample 5

[val,idx]=min(abs(t_exp-findval(count)));
ini_t=t_exp(idx);
range = 160;

hold on
%yyaxis left

delta_exp =-disp(idx:idx+range);
Maxdelta_exp = max(delta_exp);
plot(t_exp(idx:idx+range)-findval(count),(-disp(idx:idx+range)))
xlim([0 7])
ylabel('Displacement (mm)')
xlabel('Time (s)')
%yyaxis right
legend('Model Programming','Experimental Programming',
'Interpreter','latex','location','northwest');
hold on

%-----

figure(2)
scatter(t,flag1(end,:),end)
hold on
scatter(t,flag2(end,:),end)
hold on
scatter(t,flag3(end,:),end)
hold on
legend('Reg1','Reg2','Reg1','Reg3','Interpreter','Latex');
hold on

figure(3)
yyaxis left

```

```

plot(t,epsilon (end,:,end))
hold on
plot(t,epsilon_e(end,:,end))
hold on
plot(t,epsilon_c (end,:,end))
hold on
plot(t,epsilon_l)
hold on
plot(t,epsilons_EFF(end,:,end),'g')
ylabel('\epsilon','Interpreter','latex');

yyaxis right

plot(t,smooth(epsilon_c_dot(end,:,end)))
hold on
xlabel('Time (s)','Interpreter','latex');
ylabel('\dot{\varepsilon}','Interpreter','latex');
legend('\epsilon(L/2,t,h/2)','\epsilon_e(L/2,t,h/2)','\epsilon_c(L/2,t,h/2)','\epsilon_l(t)','\epsilon_{s_{EFF}}','Interpreter','Latex');

%-----

figure(4)

plot(t,sigma(end,:,end))

%=====
% RECOVERY STRESS
%=====
for Q=0.2:0.2:0.4

clear T C_integral B_integral A_integral mu lambda C E epsilon_l mu_EFF lambda_EFF
epsilons_EFF epsilon_e

dtr = 0.01; % time step could be different for programming
tr = 0:dtr:250;
num_tr = length(tr);

Tl = 55;
T = zeros(num_tr,1);
epsilon_c_tau = epsilon_c(:,end-1,:);

% Recovery initial conditions
kappa_r = ones(num_x,num_tr).*kappa(:,end-1);
epsilon_r = zeros(num_x,num_tr,num_y);
epsilon_r(:,1,:) = epsilon(:,end-1,:);
sigma_r = zeros(num_x,num_tr,num_y); % stress,initial condition assume to be zero
M_r = zeros(num_x,num_tr);

%Material paramters initialization
E = zeros(num_tr,1);
epsilon_l = zeros(num_tr,1);
lambda = zeros(num_tr,1);
mu = zeros(num_tr,1);
C = zeros(num_tr,1);
mu_eff_r = zeros(num_tr,1);
lambda_eff_r = zeros(num_tr,1);
epsilons_eff_r = zeros(num_tr,1);

```

```

mu_EFF = zeros(num_x,num_tr,num_y);
lambda_EFF = zeros(num_x,num_tr,num_y);
epsilons_EFF = zeros(num_x,num_tr,num_y);

%WLF Material variables

mu_inf = (4.292e-09);
mu_o = 112.6;
au = 0.3315;

l_o = 0.01492 ;
l_inf = 0.3406;
al = 0.248;

%Variable initialization

epsilon_cr_dot = zeros(num_x,num_tr,num_y);
epsilon_e = zeros(num_x,num_tr,num_y);
epsilon_cr = zeros(num_x,num_tr,num_y);
flag1 = zeros(num_x,num_tr,num_y);
flag2 = zeros(num_x,num_tr,num_y);
flag3 = zeros(num_x,num_tr,num_y);
flag4 = zeros(num_x,num_tr,num_y);
Adm = zeros(num_x,num_tr);
Bdm = zeros(num_x,num_tr);
Cdm = zeros(num_x,num_tr);
A_integral = zeros(num_x,num_tr);
B_integral = zeros(num_x,num_tr);
C_integral = zeros(num_x,num_tr);

for q = 1:num_x
    for n = 1:(num_tr-1)
        T(n) = Tl+Q*n*dtr;
        if T(n)<=82
            T(n) = Tl+Q*n*dtr;
        else
            T(n)=82;
        end
        E(n) = (E_inf*exp(-ae*Tg)+E_o*exp(-ae*T(n)))/(exp(-ae*Tg)+exp(-ae*T(n)));
        lambda(n) = a1l*exp(-((T(n)-b1l)/c1l).^2)+d1l; % gaussian lambda
        mu(n) = au1*exp(-((T(n)-bu1)/cu1)^2); %from Es modulus gaussian
        epsilon_l(n)=(epsilon_l_inf*exp(-ap*Tg)+epsilon_l_0*exp(-ap*T(n)))/(exp(-ap*Tg)+exp(-ap*T(n)));

        if T(n)< 55
            C(n) = 0.97;
        else
            C(n) = ac*exp(-bc.*T(n));
        end
    end
end

```

```

if n>1
    C(n) = C(n)*0.1+C(n-1)*0.9;
end

mu_eff_r(n) = mu(n)/(1-((mu(n)*(C(n)))/(lambda(n)*E(n))));
lambda_eff_r(n) = lambda(n)/(1-C(n));

epsilons_eff_r(n) = -1*(C(n)*epsilon_l(n))/(1-C(n));

for m = 1:num_y
    epsilon_r(q,n,m) = kappa_r(q,n)*((m-1)*dy);

    if n>1
        epsilon_r(q,n,m) = epsilon_r(q,n,m)*0.1+epsilon_r(q,n-1,m)*0.9;
    end

    if n>1
        as = E(n)*epsilon_r(q,n,m);
        bs = sigma_r(q,n-1,m)*(1-E(n-1)*dtr/mu_EFF(q,n-1,m));
        cs = epsilon_r(q,n-1,m)*(E(n-1)*dtr/lambda_EFF(q,n-1,m)-E(n-1));
        ds = -epsilons_EFF(q,n-1,m)*dtr*E(n-1)/lambda_EFF(q,n-1,m);
        sigma_r(q,n,m) = as+bs+cs+ds;
    else
        sigma_r(q,n,m) = 0;
    end

    epsilon_e(q,n,m) = sigma_r(q,n,m)/E(n);
    epsilon_cr(q,n,m) = epsilon_r(q,n,m)-epsilon_e(q,n,m); % one dimension
along y direction, this is creep strain

    if n<=2
        epsilon_cr_dot(q,n,m)=0;

    else
        epsilon_cr_dot(q,n,m) = (epsilon_cr(q,n,m)-epsilon_cr(q,n-2,m))/(2*dtr);
        epsilon_cr_dot(q,n,m) = epsilon_cr_dot(q,n,m)*0.001+epsilon_cr_dot(q,n-1,
m)*0.999;

        epsilons_EFF(q,n,m) = epsilons_EFF(q,n,m)*0.5+epsilons_EFF(q,n-1,m)*0.5;
    end

    if epsilon_cr_dot(q,n,m)>0
        if epsilon_cr(q,n,m)< epsilon_l(n)
            mu_EFF(q,n,m) = mu(n);
            lambda_EFF(q,n,m) = lambda(n);
            epsilons_EFF(q,n,m) = 0;
            flag1(q,n,m)=1;
        else
            mu_EFF(q,n,m) = mu_eff_r(n);
            lambda_EFF(q,n,m) = lambda_eff_r(n);

```

```

        epsilons_EFF(q,n,m) = epsilons_eff_r(n);
        flag2(q,n,m)=1;

    end

else
    mu_EFF(q,n,m) = mu(n);
    lambda_EFF(q,n,m) = lambda(n);
    epsilons_EFF(q,n,m) = C(n)*(epsilon_c_tau(q,1,m)-epsilon_l(n));
    flag3(q,n,m)=1;
end

%Calculating dM % this assumes constrained recovery
Adm(q,n,m) = 2*b*(1-(E(n)*dtr/mu_EFF(q,n,m)))*sigma_r(q,n,m)*y(m);
Bdm(q,n,m) = (2*b*dtr*E(n)/lambda_EFF(q,n,m))*kappa_r(q,n,m)*y(m)^2;
Cdm(q,n,m) = (2*b*E(n)*dtr/lambda_EFF(q,n,m))*epsilons_EFF(q,n,m)*y(m);
end

A_integral_r = trapz(Adm(q,n,:)*dy);
B_integral_r = trapz(Bdm(q,n,:)*dy);
C_integral_r = trapz(Cdm(q,n,:)*dy);

M_r(q,n+1) = A_integral_r+B_integral_r-C_integral_r;
end
end
P_r = 4*M_r(end,:)/(L);

figure(5)
yyaxis left
plot(tr,P_r)
ylabel('$Force$ (N)','Interpreter','latex');
xlabel('Time (s)','Interpreter','latex');
hold on

yyaxis right
plot(tr,T)
hold on
ylabel('$Temperature$ (^{\circ}C$)','Interpreter','latex');
end

%-----
figure(6)

yyaxis left
plot(tr(1:end),epsilon_r(end, :,end))
hold on
plot(tr(1:end),epsilon_e(end, :,end))
hold on
plot(tr(1:end),epsilon_cr(end, :,end))
hold on
plot(tr(1:end),epsilon_l)

```

```
hold on
plot(tr,ones(size(tr))*epsilon_c_tau(end,1,end),'k')
hold on
plot(tr,epsilons_EFF(end,:,end),'g')

yyaxis right
plot(tr,smooth(epsilon_cr_dot(end,:,end)))
hold on
xlabel('Time (s)','Interpreter','latex');
ylabel('\dot{\varepsilon}','Interpreter','latex');
legend('\epsilon(L/2,t,h/2)','\epsilon_e(L/2,t,h/2)','\epsilon_c(L/2,t,
h/2)','\epsilon_l(t)','\epsilon_c(L/2,\tau,h/2)','\epsilon_{s_
{EFF}}','Interpreter','Latex');

%-----

figure(7)
scatter(tr,flag1(end,:,end))
hold on
scatter(tr,flag2(end,:,end))
hold on
scatter(tr,flag3(end,:,end))
hold on
legend('Reg1','Reg2','Reg3','Interpreter','Latex');
```